17th International Symposium on Ice
Saint Petersburg, Russia, 21 - 25 June 2004
International Association of Hydraulic Engineering and Research

NUMERICAL ALGORITHMS AND PROGRAM COMPLEX FOR FLOW AND DYNAMICS SIMULATION OF ICE-THERMAL PROCESSES IN OPEN RESERVOIRS

V.A.Prokofyev[1]

ABSTRACT

There are presented two numerical algorithms: 2D and 3D ones to calculate flow dynamics, heat transmission and ice cover formation. Both algorithms are conservative and use the finite volume method for discretization. The first of them (2D) is made on the Saint-Venant equations system added by the heat transmission equation averaged by depth. The vertical temperature profile is approximated by the polynomial of the 2-nd degree that allows to determine more precisely heat fluxes on the bottom and on the free surface. The model takes into account the possibility of forming the ice cover on the water surface and the presence of snow on the ice cover. The numerical algorithm is made on the base of the Hancock/MUSCL explicit scheme of the second order of the precision by space and time and can be used for the calculation process in the presence of island and changes of the coast line. The second algorithm (3D) is made on three-dimensional system of hydro-dynamics and heat transmission equations. It envisages to set up a boundary condition like "cap" on the free surface. In this algorithm the unknowns are approximated by the flow depth using *sine*- and *cosine*-Fourier series, and the decision of discrete analogues is obtained on the base of the semi-implicit method SIMPLER. Leonard scheme is used to obtain the second order by plane coordinates.

INTRODUCTION

The calculation of the ice cover thickness and polynya dimensions is necessary, e.g., in such tasks as heat calculations of reservoirs-coolers, simulation the ice situation in tail water of hydro-nodes. The presence of the ice cover on the water surface considerably changes the processes of heat-mass transmission in open reservoirs. From one side the flow pattern is changing because the ice changes the tangential stress on the water surface: friction, wind load. From the other side the ice changes heat fluxes: diffusive transmission by the vertical as well as heat exchange with the atmosphere are changing. The task of ice cover dynamics simulation can be divided into three component parts: the calculation of the flow hydro-dynamics under ice, heat transmission simulation and

[1] The B.E. Vedeneev All-Russian Research Institute of Hydraulic Engineering (VNIIG), Gzhatskaya str., 21, St.Petersburg, Russia, Phone/Fax: (812) 535-67-45; E-mail: Prok@Hydro.vniig.ru

heat exchange simulation on the boundary of the water surface with the atmosphere taking into account the possibility of ice formation and melting. At that this task has to be solved namely at unsteady setting taking into account the dynamics of weather factors changing: air temperature, wind velocity and direction, air humidity, precipitation intensity, cloudiness and so on. Unsteadiness imposes strict demands on the efficiency of the used numerical method especially if the task is solved in three-dimensional (3D) setting. There is a number of different approaches to solve the task with the majority of which are based on one-dimensional [1] or plane (2D) [2-4] setting.

2D and 3D algorithms given in this work are made up on the method of the finite volume that allows to create numerical diagrams conservative by mass and pulse [5-7]. For the tasks connected with unsteady heat transmission the conservatism of the numerical diagram is an obligatory condition.

Plane (2D) Model of Hydro-Dynamics and Heat Transmission

The divergent form of the 2-D system of the shallow water equations for viscous liquid and for heat transmission in Cartesian coordinate system (x,y) is the following [8]:

$$\frac{\partial \mathbf{Q}}{\partial t}+\frac{\partial \mathbf{E}}{\partial x}+\frac{\partial \mathbf{G}}{\partial y}=\mathbf{S}\ , \tag{1}$$

where the vector of variables, fluxes and sources is written as

$$\mathbf{Q}=\begin{bmatrix} h \\ hu \\ hv \\ hT \end{bmatrix};\quad \mathbf{E}=\begin{bmatrix} hu \\ hu^2+gh^2/2 \\ huv \\ huT+h\gamma_T\,\partial T/\partial x \end{bmatrix};\quad \mathbf{G}=\begin{bmatrix} hv \\ huv \\ hu^2+gh^2/2 \\ hvT+h\gamma_T\,\partial T/\partial y \end{bmatrix};$$

$$\mathbf{S}=\begin{bmatrix} \Phi \\ ghS_{0x}-S_{fx}+hfv+\tau_x/\rho+h\gamma\nabla^2 u \\ ghS_{0y}-S_{fy}-hfu+\tau_y/\rho+h\gamma\nabla^2 v \\ \rho c\left(\Theta_\Phi+\Theta_{bot}+\Theta_S\right) \end{bmatrix}.$$

Here: g – free fall acceleration; h – water depth; u and v – components of the vector **U** averaged by the velocity depth in Cartesian coordinate system; S_{0x}, S_{0y} – components of the bottom slope; $f=1{,}458\times10^{-4}\sin(\varphi)$ – Coriolis parameter, φ – geographical latitude; τ_x, τ_y – components of the wind tangential stress on the free surface; ρ – water density, c – its specific heat; ∇^2 – Laplace operator; Φ – mass source; T – water temperature average by depth; γ_T – coefficient of temperature conductivity in the horizontal direction including turbulent and disperse components. The components of the friction force vector on the bottom can be determined by Manning formulae:

$$S_{fx}=C_f(h)hu|\mathbf{U}|\ ;\quad S_{fy}=C_f(h)hv|\mathbf{U}|\ ;\quad |\mathbf{U}|=\sqrt{u^2+v^2}\ ;\quad C_f(h)=\frac{gn^2}{h^{4/3}}\ . \tag{2}$$

If there is ice cover the roughness coefficient n is calculated by the formula [9]:

$$n = \left(n_{bot}^{3/2} + n_{ice}^{3/2} \right)^{2/3},$$

where n_{bot} and n_{ice} – roughness coefficients of the bottom and the lower surface of ice correspondingly. For the open water surface $n=n_{bot}$.

The coefficient of turbulent viscosity γ averaged by the depth can be determined, for example, by Prandtle formula with turbulence scale choice according to [8]:

$$\gamma = \frac{1}{4}\kappa U_* h \quad , \quad U_* = |\mathrm{U}|\sqrt{hC_f(h)} \quad , \tag{3}$$

where Carman constant $\kappa = 0{,}41$.

Besides in the equations (1) there are used the following notations for heat fluxes. Θ_Φ – the heat flux specified by mass sources:

$$\Theta_\Phi = T\Phi/(\rho c), \quad \Phi < 0 - \text{ for water input;}$$

$\Theta_\Phi = T_{out}\Phi/(\rho c)$, $\Phi > 0 -$ for water output with water temperature T_{out}.

Θ_{bot} – heat flux from the reservoir bottom towards the water determined according to the recommendations [10]; Θ_S – heat flux towards the water from the side of its boundary with the ice [1]:

$$\Theta_S = \Theta_{ice} = -2640\ (T - T_0)|\mathbf{U}|,$$

or with the atmosphere (for the open water surface):

$$\Theta_S = \Theta_A = \Psi_{SUN} + \Psi_{VP} + \Psi_K + \Psi_{IK} \quad . \tag{4}$$

Here the temperature of the lower ice surface is taken equal to the temperature of water freezing T_0. The fluxes of the right part of (4) are connected correspondingly with solar radiation, evaporation from the surface, convective heat exchange with the atmosphere, infrared radiation from the surface. These fluxes are determined according to the recommendations [1,10,11], at that the heat consumption for evaporation Ψ_{VP} is calculated either by Carpenter formula [11] or by Braslavsky-Nurgaliev formula [1,10]. If on the water surface there is bare ice or ice covered with snow the heat flux of their boundary with the atmosphere Θ_A is still include four components in itself – see (4), however the flux Ψ_{SUN} is calculated for the albedo of the ice or snow surface and also Ψ_{VP} and Ψ_K are determined in another way [1]. To determine heat fluxes Ψ_{VP}, Ψ_K and Ψ_{IK} it is necessary to know the temperature on the surface adjoining the atmosphere T_S:

$$T_S = T_0 + \Theta_A R_T \quad . \tag{5}$$

Here R_T – heat resistance of the ice layer of h_{ice} thickness covered with the snow layer of h_{sn} thickness:

$$R_T = h_{ice}/\lambda_{ice} + h_{sn}/\lambda_{sn} \quad , \tag{6}$$

where λ_{ice} – the coefficients of its conductivity of ice and snow correspondingly. Calculation of the surface temperature T_S and determination of heat fluxes (4) demand not complicated iterative procedure [2], for example, the method of bisection.

In plane model to obtain the condition of ice forming and melting on the water surface it is necessary to connect the water temperature T average by the depth with the surface temperature T_S. Approximation of the temperature vertical profile by the polynomial of the 2-nd degree is the most simple method. Using boundary conditions for the heat

fluxes on the bottom and on the free surface we can determine two of the three coefficients of this polynomial and obtain:

$$T_S = T + \frac{h\Theta_{ice}}{3\lambda_S} - \frac{h\Theta_{bot}}{6\lambda_{bot}} \quad , \tag{7}$$

where h – water depth; λ_S and λ_{bot} – the coefficients of the water turbulent heat conductivity by the vertical near the free surface and the bottom correspondingly. The similar approach but applied to the velocity profile by the depth and also based on the approximation of the polynomial of the 2-nd degree and the calculations of two coefficients of this polynomial according to the boundary conditions on the bottom and on the free surface are described in [12]. This method is quite perspective to expand the possibilities of the plane model without dimension increasing of the discrete analogue. Let's note that in the relation (7) the heat flux on the water surface is calculated under the condition that the ice layer has already been formed that is why it is logically to take the coefficients λ_S, λ_{bot} when there is ice. In the most simple case they can be taken identical and can be determined by the recommendations [10]:

$$\lambda_S = \lambda_{bot} = 1{,}163h\sqrt{1296000\left|\mathbf{U}\right|^2} + 0{,}52h + 0{,}6 \quad . \tag{8}$$

Comparing the temperature T_S in every surface point with T_0 we can determine whether ice forming or melting is happening at the moment. If the ice has already been formed the increment of its thickness during the time interval Δt is

$$\Delta h_{ice} = \Delta t \frac{\Theta_{ice} - \Theta_A}{\alpha\rho_{ice}} \quad , \tag{9}$$

where α – the specific heat of ice melting, ρ_{ice} – its density. Let's note that the condition (7) with the parameters (8) is used only on the ice cover edge as the condition of ice forming and melting. The parameters Θ_{ice}, λ_S и λ_{bot} can be specified at model calibration because they can be another than the parameters under the ice surface having been formed far from the ice field edge. Because of these parameters it depends how much average by the depth water temperatures under the ice cover can exceed T_0 and the dimension of the polynya.

The coefficient of the water temperature conductivity in the horizontal plane is calculated by the formula similar to Van-Rein one [8] but with additional summand:

$$\gamma_T = a\kappa U_* h + \gamma_0 \quad . \tag{10}$$

Two free parameters in the formula (10) were left for the possibility to calibrate the model: the multiplier a calibrates the turbulence scale, and the addend γ_0 must take into account the contribution of wind waving into diffusive heat transmission. The calculations given below were carried out at a = 1/4, as also in [8], $\gamma_0 = 10$ m^2/s.

The numerical algorithm for solving the equations system (1) represents the explicit two-step (Predictor-Corrector) Hancock method being a variation of Runge-Kutt method by time for the hyperbolic equations system [5-7, 13]. Using the technology of MUSCL-reconstruction (Monotone Upwind Scheme for Conservation Laws) for physical variables it provides the 2-nd order of precision by space and time [7]. This algorithm was realized on the regular curvilinear quadrangular grid of finite volumes (FV) – Fig. 1a. This does not restrict the field of its application because at using the technique

of continuous calculation [13-15] on this grid there can be fulfilled the calculations multiply connected areas, for example, for reservoirs with islands, for arbitrary configurations including the configurations changing in time. In this work there was used the modification of the finite volume method permitting comparatively simple to increase boundary approximation precision at using the curvilinear quadrangular or *regular Cartesian* grid. The method consists of "trimming" a part of the area and edge lengths of FV by the boundary line (Fig. 1b) instead of using the entire (for Cartesian grid – rectangular) FV with the step approximation of the boundary. The outlook of this approach is indicated in [5] and in the description of the well-known software *"STAR-CD"* accessed through *Internet*.

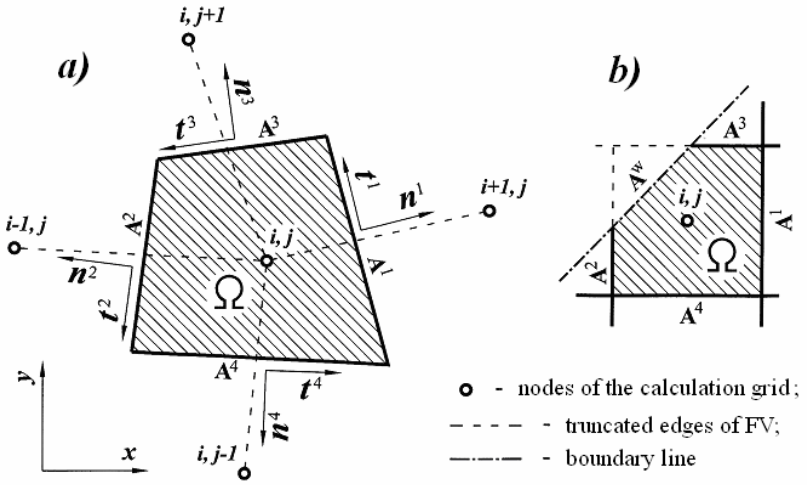

Fig. 1. Finite volumes on the regular grid:
a – position of the nodes, normals and tangents to the edges;
b – "truncated" finite volume near the boundary

The algorithm is described quite in detail in the works [13,15,16] that is why here we will pay our attention only to its peculiarities applying to the task of heat transmission and ice formation on the water surface. The record of heat fluxes for the discrete analogue of the heat transmission equation was carried out by Roe scheme – all necessary formulas are given in [8], or by Lax-Friedrichs, HLLE, CIR schemes – see [7,13].The discrete analogue of the heat transmission equation in the absence of the outer heat exchange has to correspond to the simple decision – constant temperature preservation in the reservoir at any bottom shape and flow conditions. It also relates to the case when the water with the same temperature as in the reservoir is dropped into the reservoir. That is why this discrete analogue must be entirely transferred into the discrete analogue of the mass transmission equation (equation of continuity) at substitution in it the uniform field of temperatures. A simple example: you can not write mass fluxes in the form, let's say as HLLE, using at that the writing of heat fluxes in Roe form. By the author's opinion the writing of all fluxes (mass, pulses, heat) in HLLE form provides the most precision in conjunction with calculation efficiency.

The algorithm stability is provided by fulfilling Curant-Friedrichs-Levi condition which, taking into account viscosity γ and temperature conductivity γ_T in the center of FV, is written as (see Fig. 1a):

$$\Delta t < Cr \Big/ \max_{i,j} \left\{ \frac{1}{\Omega} \sum_{k=1}^{4} A^k \left[\frac{\max\left(\left|s_L^k\right|,\ \left|s_R^k\right|\right)}{2} + \frac{\max(\gamma, \gamma_T)}{(\mathbf{n}_k \cdot \mathbf{r}_k)} \right] \right\} \quad , \tag{11}$$

where $\mathbf{r}_k$ – the vector from the center of the finite volume up to the nearby (through the *k* edge) node; s_L, s_R – wave numbers at the left and at the right of the FV bound [13,15]. The Curant number *Cr* for all carried out calculations was chosen in the interval of 0,7-0,95.

Three Dimensional (3D) Model of Hydro-Dynamics and Heat Transmission

Within the frame of this report there is no possibility to describe in detail the 3-D model and semi-explicit algorithm SIMPLER that realizes the model. That is why this model, as also the 2-D model, is presented here schematically and the algorithm description can be found in the work [17,18]. Let's write the system of Reynolds nonstationary equations for the flow of incompressible liquid in the divergent form [19]:

$$\frac{\partial u}{\partial t} + \mathrm{div}(\mathbf{U}u) - \mathrm{div}(\gamma\, \mathrm{grad}\, u) = -\frac{1}{\rho}\frac{\partial P}{\partial x}\ ; \quad \frac{\partial v}{\partial t} + \mathrm{div}(\mathbf{U}v) - \mathrm{div}(\gamma\, \mathrm{grad}\, v) = -\frac{1}{\rho}\frac{\partial P}{\partial y}\ ; \tag{12}$$

$$\frac{\partial w}{\partial t} + \mathrm{div}(\mathbf{U}w) - \mathrm{div}(\gamma\, \mathrm{grad}\, w) = -\frac{1}{\rho}\frac{\partial P}{\partial z} + F_A\,; \quad \mathrm{div}\,\mathbf{U} = \frac{\partial u}{\partial x} + \frac{\partial v}{\partial z} + \frac{\partial w}{\partial z} = \Phi\,; \tag{13}$$

$$\frac{\partial T}{\partial t} + \mathrm{div}(\mathbf{U}T) - \frac{\partial(\gamma_T\, \mathrm{grad}\, T)}{\partial x} - \frac{\partial(\gamma_T\, \mathrm{grad}\, T)}{\partial y} - \frac{\partial(K_Z\, \mathrm{grad}\, T)}{\partial z} = \Theta\ . \tag{14}$$

Here: **U** – the flow velocity vector averaged by Reynolds method with the components *u*,*v*,*w*; Φ – mass source; Θ – heat source; *P* – pressure deviation from the hydrostatic pressure; $F_A = \beta g(T - \overline{T})$ – Archimedes force; β – thermal coefficient of volumetric expansion of water. Let's note that in widely used model of 2,5 dimension the equation for vertical component of the pulse (13) is not included at all, that is why the velocity component *w* is determined only on the base of the equation of continuity. Further we will consider that the slopes of the bottom and free surface are not great, so the normals for them are practically vertical. Let's pass from the coordinate *z* to the non-dimensional coordinate ξ that is equal to zero on the upper boundary of the near bottom logarithmic layer of the thickness σ, but on the free surface ξ=1. Let's present distribution of the velocity component, hydro-dynamic pressure and the temperature by the vertical coordinate ξ in every node of the diverse calculation grid of FV as *cosine*- and *sine*-Fourier series with the additional multiplier *f*(ξ):

$$u(\xi) = u_{wind}(\xi) + f(\xi)\sum_{m=0}^{M} u_m \cos(k_m \xi)\,; \quad v(\xi) = v_{wind}(\xi) + f(\xi)\sum_{m=0}^{M} v_m \cos(k_m \xi)\,; \tag{15}$$

$$w(\xi) = \tilde{w}(\xi) + \sum_{m=1}^{M} w_m \sin(k_m \xi)\,; \qquad P(\xi) = \tilde{p}(\xi) + \sum_{m=0}^{M} p_m \cos(k_m \xi)\,; \tag{16}$$

$$T(\xi) = T_{flux}(\xi) + \sum_{m=0}^{M} t_m \cos(k_m \xi)\ . \tag{17}$$

In these expansions: *M* – the number of the last harmonic, $k_m = m\pi$ – wave numbers. Without the addends $\tilde{w}(\xi)$ and $\tilde{p}(\xi)$ the expansions of the velocity and pressure vertical

component (17) satisfy the uniform conditions in spite of the choice of the expansion coefficients w_m, p_m ("cap" condition). The logarithmic multiplier $f(\xi)$ in the expansion (16) allows to fulfill the boundary conditions on the bottom for the velocity vector components tangent to it at random choice of the expansion coefficients u_m, v_m. For this as the multiplier $f(\xi)$ and "wind" addend $u_{wind}(\xi)$ it should be taken, for example, the functions:

$$u_{wind} = \mu\xi^2 , \quad \mu = \tau_x/(2h\rho\gamma) ; \quad f(\xi) = \ln\frac{\xi h + \sigma}{c_s} - \frac{\xi^2 h}{2h + \sigma} , \qquad (18)$$

where c_S characterizes the size of bulges of the bottom roughness. The additional summand $T_{flux}(\xi)$ to the temperatures profile is made up like u_{wind} and serves to fulfill the boundary conditions for heat fluxes on the bottom and the free surface. Heat fluxes are calculated in the same way as in the 2-D model: see above. The addends $\tilde{w}(\xi)$ and $\tilde{p}(\xi)$ in (16) are used to correct the boundary conditions on the bottom if its slopes are considerable and determined according the previous iteration; for the horizontal bottom these addends are not necessary.

The coefficient of the vertical turbulent exchange K_Z is determined on the base of the turbulence "**k**"-model [20] and then corrects by the empirical formula taking into account the reduction of the vertical displacement in the area of the steady temperature stratification [21]:

$$K_Z = K_0(1 + \vartheta \mathrm{Ri})^{-p} , \quad \mathrm{Ri} = g\beta \frac{\partial T}{\partial z} \Big/ \left(\frac{\partial |\mathbf{U}|}{\partial z}\right)^2 ,$$

where ϑ = 0,3; p =1,5; Ri – Richardson number.
Substituting the expansions (15) – (17) into the original equations (12) – (14) after the integration by FV and by the coordinate ξ - according to the method of the weighted disparities, it is possible to get five-point discrete analogues [19,22] of the original equations the coefficients of which are the matrixes ($M \times M$). The algorithm of getting and solving such discrete analogous is described in [17,18] in more details. Leonard scheme is used to specify convective fluxes of the pulses through the edges of the finite volumes.

Using the expansions by the specially chosen basic functions (15) – (17) allows, even before the task "being in the plane" is solved, to provide fulfilling the boundary conditions on the bottom and on the free surface that simplifies solving the discrete analogue. As it is shown in [17] the interconnection between separate harmonics of the expansions (15) – (17) stipulated by the non-linearity of the task is not large and can be taken into account by iterations. It allows to split the task: first of all to solve the "plane" discrete analogue for the zero harmonic ($M=0$) and then – local (but not plane) systems of the linear algebraic equations connecting the rest harmonics inside FV. At planar dimensions of the calculation grid exceeding the flow depth a great number of iterations is not demanded at such splitting. This approach has got much in common with the approximation of the temperature vertical profile by the polynomial of the 2-nd degree in the 2-D model given above as well as with the work [12].

Let's note that even at M = 1 the suggested model has got more possibilities than the traditional model of the shallow water. With the same structure of the obtaining five-point discrete analogue it allows to calculate, for example, reciprocal-wind flows (there are different direction of flows at the bottom and on the surface) and to take into account the temperature profile by the depth in the 1-st approximation.

Software Realization

In the up to date software the realization of programs is the significant part and takes up to 90% of the program coding and labor intensity in developing software product as a whole. The software realization includes user interface, the procedures for preparing initial data, mechanism of interconnection with the in-built data base, graphic support and so on.

The realization of the calculation algorithm itself in the form of the program code is significantly more simple: it takes not more than 10% of labor intensity.

To realize the 2D model given above there has been developed the software for *MS Windows*. This software includes the unit for digitalizing the scanned topographic maps on the base of Delone triangulation with further transferring the marks of the site (or depth) on the calculation grid. Dimensions of the last one are limited only by the volume of the on-line storage: using PC there have been carried out the calculations on the grids with more than 2 billion cells (FV) that allows to describe in detail the relief of the site, bottom, the geometry of the engineering structures. All initial information is stored in data base (DB) built in the software, the DB was realized on the base of *InterBase-7.0*. In the interface of access to the tables of this DB there are facilities to control the correction of the inputting information, and great information volumes (for example, bottom maps) are stored in the form of references on their files. Graphic support is realized in the form of charts for control points (for example, temperatures, dynamics of ice thickness), color maps of the reservoir (for example, temperature fields with a plan of the ice cover), three-dimensional visualization of the water surface partially covered with ice and of the bottom with luminous effect on the base of *OpenGL*-graphics and so on. In the *process* of calculations (for detailed grids they can last about several hours) the user has got the possibility to follow the parameters of the flow and ice field in digital and chart form. Besides the information is stored in the files to be viewed and analyzed *after* the calculations, in particular, according to the calculations the software provides recording of “videos” in the format *AVI* with video-compression (2D and 3D) projections).

Calculation Examples

Testing of the presented here 2D and 3D hydrodynamics models on the base of analytical decisions and experimental data is given in the work [13 – 16] and [17,18] correspondingly. Let’s consider here only the application of these algorithms to two practical tasks connected with nonsteady heat transmission in open reservoirs and with ice cover forming on their surface.

The first example – plane simulation of hydro-ice-thermal mode of the reservoir-cooler situated in middle zone of Russia. For this object there were assigned bathymetry, meteorological data (daily), the dynamics of the thermal spillway. There were also carried out temperature measurements of water at water scoop and visual observations for the plane polynya shapes in the region of water-discharging and in the region of water scoop. The calculations were carrying out from the middle of September up to the 12-th of January: for this period the data of the observation on the site were quite full. The following model parameters were used at obtaining the results shown in Fig. 2. There was no information about the intensity of snowfall that is why the thickness of the snow cover was taken equal to a half of the thickness of the ice itself obtained in the process of calculation at the present moment. The surface heat exchange was calculated with the use of Braslavsky-Nurgaliev formula: Carpenter formula led to close results.

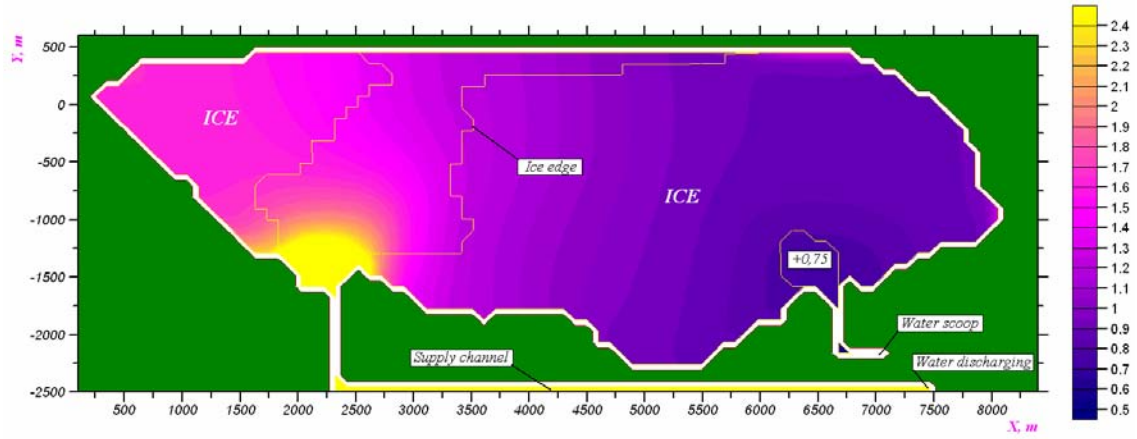

a)

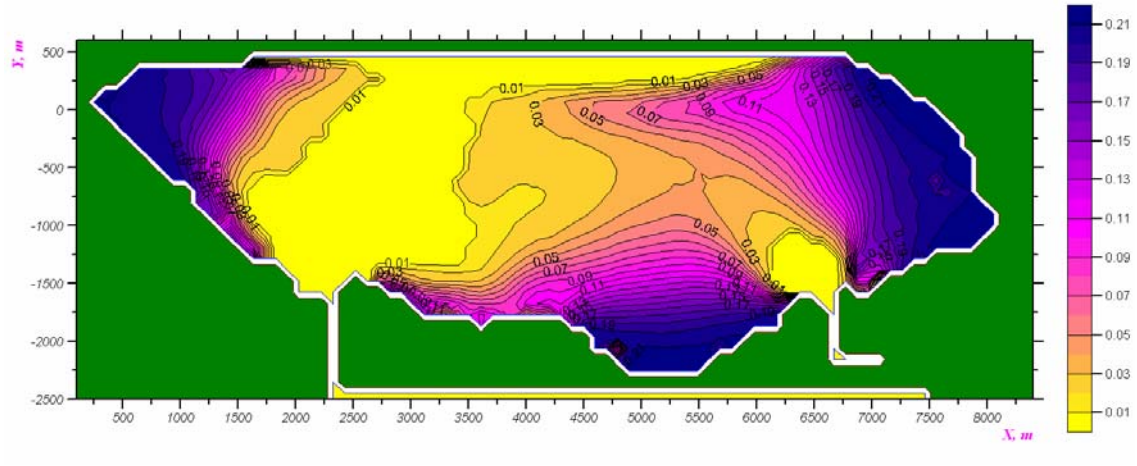

b)

Fig. 2. 2D-numerical simulation of hydro-ice-thermal mode of the reservoir-cooler (the date – 12-th of January): a – distribution of the temperatures averaged by the depth: in the yellow area the temperature changes from +15°C up to +2,5°C; b – ice cover thickness, in meters

Roughness coefficients: $n_{bot} = 0{,}023$; $n_{ice} = 0{,}015$ The coefficient of heat conductivity in the horizontal plane is determined by (10) with the empirical parameters values indicated above. It should be noted that the snow cover thickness significantly influence on the ice thickness: according to the results of the numerical experiments in the absence of the snow "fur" the ice thickness is nearly doubled in comparison with Fig. 2b because of abrupt heat exchange increasing with the atmosphere at negative temperatures. Heat exchange with the bottom also considerably influence on the ice situation in the reservoir and on the temperature distribution in it, but the role of the rest empirical parameters of the model is not so significant. As it can be seen from Fig. 1a the average water temperatures by depth under ice are in the range +0,7°…+1,7°C, and in the water scoop area they are of the order of +0,75°, at that there are forming the second polynya (small). It coincides with the observation data on the site, with polynya forming before water scoop stipulating by increasing the vertical heat exchange together with the flow velocity increasing: the empirical formula (10) includes the velocity module. The polynya shapes at water-dischaging (Fig. 2) is correlated with the data of visual observations.

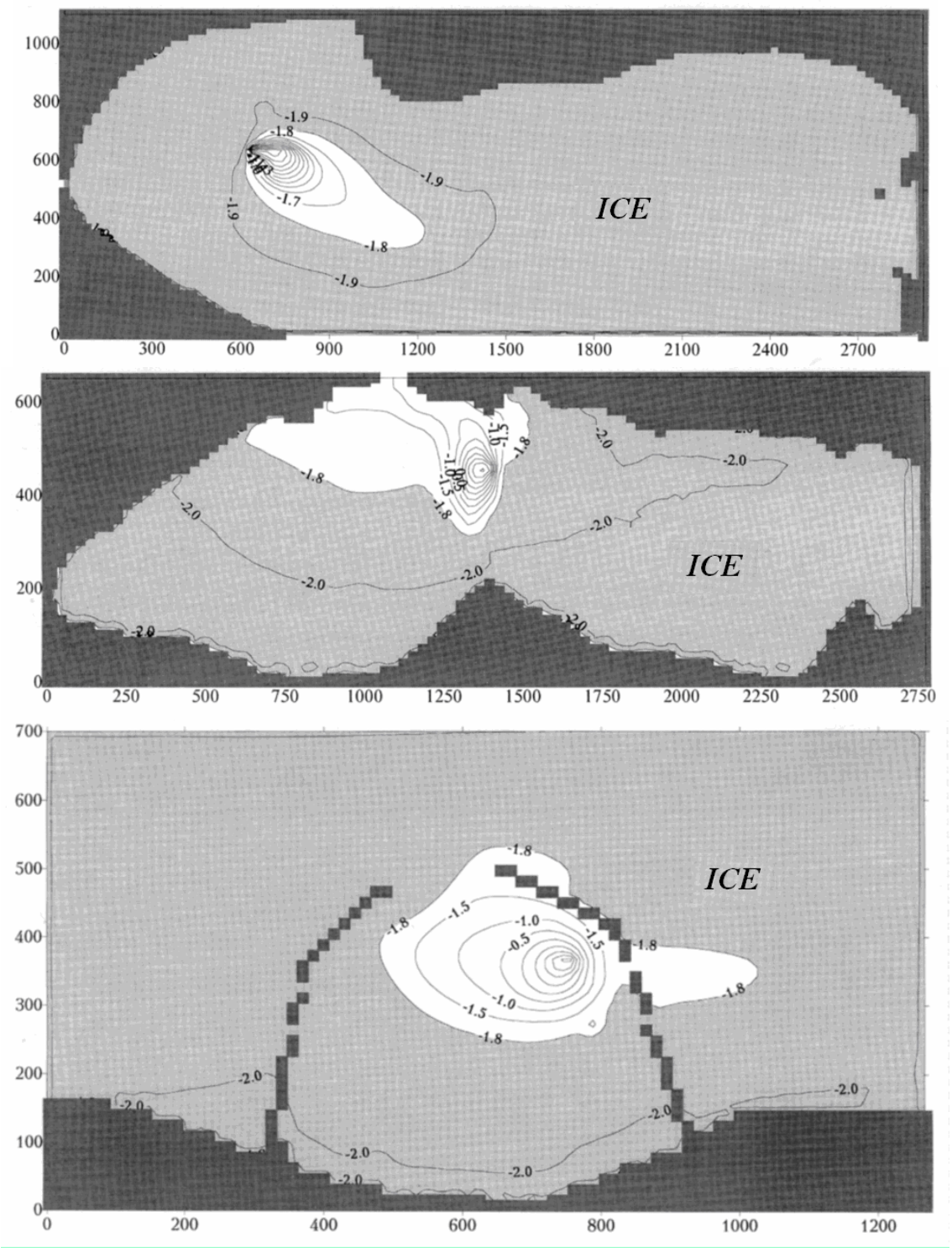

Fig. 3. 3D-modeling of temperatures (isotherms are shown in the upper layer) and ice situation in Pevek bay at working of the floating power unit: at NW wind of 11 m/s and air temperature –28° for different variants of the power units disposition:

- deep-water part of lagoon (above)
- in the region of artificial bottom deepening attaching to the bar (in the middle),
- in the partition of two concurrent piers with navigable passes (below)

Coincidence of temperatures distribution at water scoop obtained numerically and in conditions on the site is also good: it is presented for the given reservoir in the report of VNIIG authors group in another section of our Symposium. Temperature fields and ice cover thickness shown in Fig. 2 are far from the exhausting examples of visualization possibilities of the developed software.

The second example – the numerical 3D-modeling of the flow hydrodynamics and ice-thermal mode in coastal water area to substantiate the site of the floating power unit in Pevek bay. Fig. 3 shows the calculation results for three variants of power unit site for one of the time moments. Water freezing temperature T_0=1,8^{o}C. In this case there was used the 3D model with a number of harmonics by vertical of M=4 on the diverse grid of finite volumes 99x55. Water consumption of the power unit is 20 thousand m^3/h, temperature drop between the water scoop deepened on 4,5 m under the power unit floor and water-discharging (by its boards) is 12,4^{o}C, and the depth of the water area exceeded 8 m. Great volumes of circulating water leads in this case to appearing the ascending liquid flows noticeable against the background of natural sea streams and wind flows. The plane models and the models of 2,5 dimensions do not reproduce these flows because they do not take into account Archimedes force (temperature convection by the vertical).

CONCLUSIONS

In this work the mechanism of ice cover forming is considered in the most simple form: without taking into account shuga forming in water mass, freezing of ice fragments on the surface and mechanical influence of the wind on the forming ice. This approach allows to minimize a number of empirical parameters of the model and at the same time to get, for a number of practical tasks, quite reliable results about ice cover thickness, polynya dimensions, hydro-dynamics of the water flow under ice and temperature distribution in reservoirs and currents.

2D and 3D algorithms presented here use the approximation of the unknown by flow depth using the polynomial or, otherwise, basic functions. It allows to make up quite efficient numerical schemes to solve a great variety of practical tasks connected with the hydraulics of open flows where it is possible ice forming on the free surface: polynya dimensions modeling in tail water of hydro-nodes, calculation of reservoirs-cooler for winter conditions, forecast of ice conditions in water areas.

BIBLIOGRAPHY

1. Recommendations on Polynya Length Calculation in Tail Water of HPS, П-28-86, VNIIG.SPb, 1986.
2. Alexandrov I.Ya., Kvon V.I., Filatova T.N., Jukovskaya O.P. Mathematical Modeling of Ice-Thermal Mode at Great Heat Loads. *Meteorology and Hydrology*, 1992, N-2.
3. Vasilyev O.F., Bocharov O.B., Zinovyev A.G. Mathematical Modeling of Hydro-Thermal Modes in Deep Water Reservoirs. *Hydro-Technical Construction*, 1991, N-7.
4. Dmitriev N.V. Forming and Melting Ice Modeling in the Freshwater Reservoir. *Proceedings of CC of SD of the RAS.* Numerical Modeling in the Tasks of the Atmosphere, Ocean and Environment, edition 1, 1993.
5. Mingham C.G., Causon D.M. Calculation of unsteady bore diffraction using a high resolution finite volume method. *Journal of Hydraulic research*, 2000, vol. 38, №1.

6. Zhou J.G., Causon D.M., Ingram D.M., Mingham C.G. Numerical simulation of dam-break flows with high resolution finite volume method. *Proceeding of XXIX IAHR Congress*, Theme-E, Pekin, 2000.

7. Kulykovskiy A.G., Pogorelov N.V., Semenov A.Yu. Mathematical Problems of Numerical Solving of Hyperbolic System of Equations. M.: *Phizmatlit*, 2001. – 608p.

8. Zuhua C., Guangqian W., Zhishi W. Numerical solution of the two-dimensional unsteady depth-averadged flow and solute transport. *Proceeding of XXIX IAHR Congress*, Theme-E, Pekin, 2000.

9. Belokon P.M. Engineering Hydraulics of the Flow under the Ice Cover. M.-L.:*Gosenergoizdat*, 1950.

10. Recommendations on Heat Calculation of Reservoirs. П78-79. VNIIG. SPb, 1979.

11. Methodical Recommendations on Calculation of Reservoirs-Coolers of HPS. П33-75, VNIIG. SPb. 1976.

12. Girgidov A.D. Quasi-Three-Dimensional Model of Shallow Water. Izv. RAN. *Vodnie Resursy*, 1993, v. 20, N-1.

13. Prokofyev V.A. Consequences Modeling of Flood Influence on HTS Using the Method Hancock on the Regular Grid. Collected Articles, *Safety of Power Constructions*, ed. 11, NIIES, M.,:2003.

14. Klimovich V.I., Prokofyev V.A. Efficient Numerical Algorithms on the Base of the Finite Volume Method and Beam-Warming Scheme for Simulation Plane Breaking Flows with the Free Surface. *Izvestiya B.E. Vedeneev VNIIG*, v. 240, SPb, 2002.

15. Prokofyev V.A. Contemporary Numerical Schemes on the Base of Fininte Volume for Simulation Stormy Streams and Breaking Waves. *Hydrotechnical Construction*, 2002, N-7.

16. Prokofyev V.A. Using of Different Modifications of the Finite Volume Method for Simulation Open Flows. *Proceedings of the International Symposium IAHR "Hydraulic and Hydrological Aspects of Reliability and Safety of THS"*, C10, SPb, 2002 (CD-ROM).

17. Prokofyev V.A. Differential-Spectral Method of Three-Dimensional Flows. *Water Resources*, 1994, v. 21, N-3

18. Prokofyev V.A. Specifying the Shallow Water Model on the Base of Spectral Representation of the Velocity Profile by the Depth. *Izvestiya B.E. Vedeneev VNIIG*, v. 236, SPb, 2000.

19. Belov I.A., Isaev S.A., KorobkovZ.A. Tasks and Calculation Methods of Detachable Flows of Non-compressive Liquid. – L.: *Shipbuilding*, 1989, 256 p.

20. Voltzinger N.E., Klevanniy K.A., Pelinovskiy E.N. Longwave Dynamics of the Coastal Area. L.: *Gidrometeoizdat*, 1989.

21. K. Bouden. Physical Oceanography of Coastal Water: *Trasl. From Engl.* – M.: Mir, 1988, - 324 p.

22. Patankar S. Numerical Methods for Solving the Tasks of Heat Exchange and Dynamics of Liquids; Transl. From Engl. – M.: *Energoavtomizdat*, 1984, 152 p.

17th International Symposium on Ice
Saint Petersburg, Russia, 21 - 25 June 2004
International Association of Hydraulic Engineering and Research

RIVER ICE MODEL COUPLED HYDROLOGICAL MODELING IN THE LENA RIVER BASIN

X. Ma[1], T. Yasunari[1,2], T. Ohata[3,4] and Y. Fukushima[5]

ABSTRACT

This study applied a combined hydrological model designed for northern rivers to the Lena River basin, using daily routine meteorological data for the region from October 1986 to September 2000. The timing of flood rising and flood peak could be modeled for the selected hydrological station, which present the entire basin (at Kusur Station). In general, estimates of annual runoff were sufficient accurate (within 20 mm on average and 8.85 in percent) at Kusur. Since calculated annual runoffs were underestimate compared with observed values, an interpolation method that considers weather conditions and geographical feature would be requested to improve modeling accuracy.

INTRUDCTION

Runoff from Ob, Yenisei, Lena and Mackenzie rivers in Arctic region account for approximately 50 percent of the total freshwater input into the Arctic Ocean. On the other hand, over the past several decades, climate changes has altered terrestrial environment across the Arctic region. Changes in temperature and precipitation have slightly altered the hydrographs of Arctic rivers. Wetherald and Manabe (2002) predicted the continental hydrological changes associated with global warming. In the Arctic region, hydrological processes are dominated by snowmelt, river ice melt and the active permafrost layer, all of which are sensitive to environmental change. It is important, therefore, to understand these rivers' hydrological processes in order to evaluate land-sea-atmosphere interactions in the Arctic region. A modeling of the Lena River for one hydrological year has been

[1] Frontier Research System for Global Change, 3173-25 Showamachi, Kanazawa-ku, Yokohama 236-0001, Japan
[2] Hydrospheric Atmospheric Research Center, Nagoya University, Nagoya 464-8601, Japan
[3] Frontier Observational Research System for Global Change, 3173-25 Showa-machi, Kanazawa-ku, Yokohama 236-0001, Japan
[4] Institute of Low Temperature Science, Hokkaido University, Kita-19, Nishi-8, Kita-ku, Sapporo 060-0819, Japan
[5] Research Institute for Humanity and Nature, 335 Takashima-cho, Kamigyo-ku, Kyoto 602-0878, Japan

performed by Ma and Fukushima (2002). This paper presents long-term modeling results based on hydrometeorological data from 1986-2000 using a coupled hydrological model in the Lena River.

MODEL DESCRIPTION

In this study a combined hydrological model developed by Ma and Fukushima (2002) was used to examine cold region hydrological processes. The model is composed of four submodels: a one-dimensional soil-vegetation-atmosphere transfer (SVAT) model, a runoff formation model, a river routing model, and a river ice model. Fig. 1 shows a flowchart of the model. A brief description of each part is as follows.

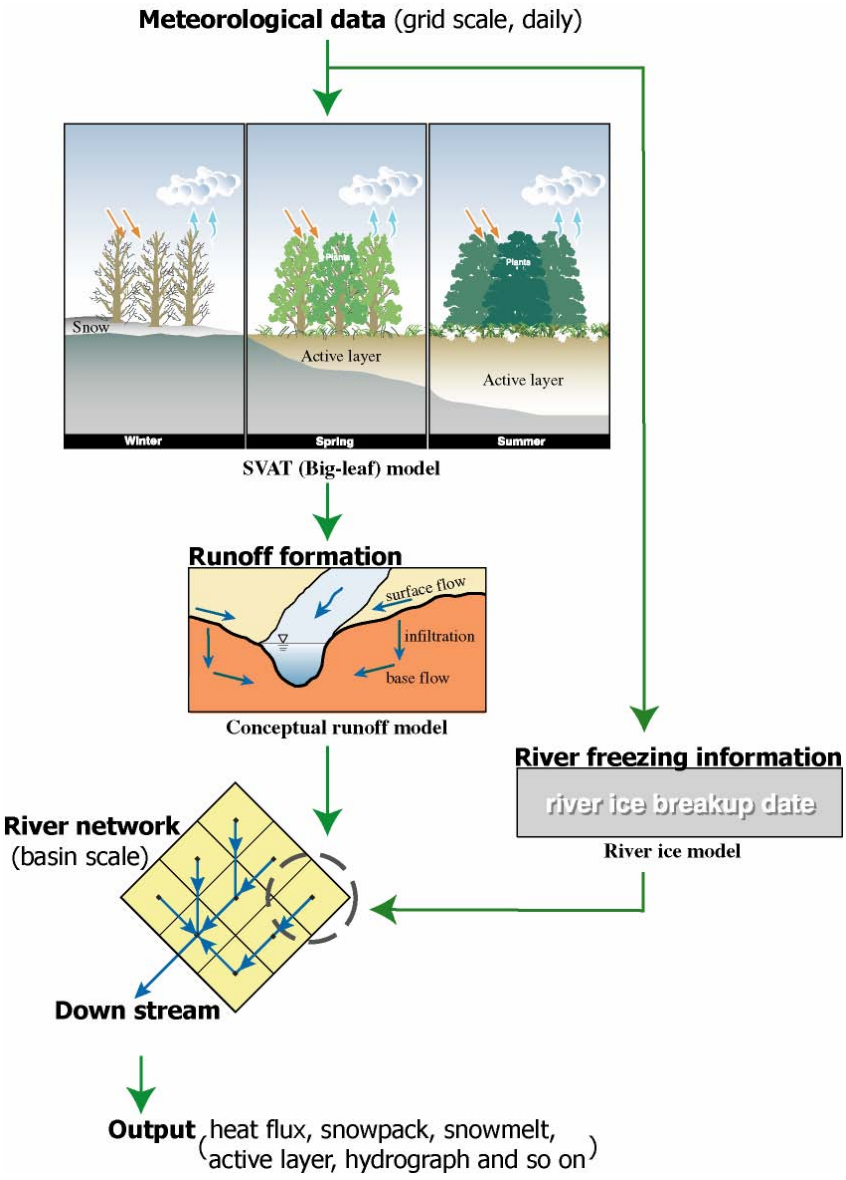

Fig. 1. Flowchart of the modeling system (Ma and Fukushima, 2000)

SVAT model

To represent soil-vegetation-atmosphere transfer (SVAT), a simple biosphere model was used. In the model, vegetation is described by a single-layer, big-leaf model; the soil layer is given as 6-m thick, which is considered the isothermal depth. The model provides estimates of latent and sensible heat fluxes between the land surface and atmosphere and thermal regimes in the soil layer under the assumptions that (a) the land surface is covered by snow in the snowfall season and by vegetation in the snow-free season; and (b) the lower boundary of the model is set at a depth of 6 m below the ground surface, and the soil temperature is equal to the annual air temperature at an observational height 2 m above the land surface. It was defined that the total amount of rainfall and snowmelt, minus the evapotranspiration, is the same as effective precipitation, which is an outputs of the SVAT model and is divided into four components in the runoff model, as mentioned later. The downward short-wave and long-wave radiations required by the SVAT model were estimated from sunshine duration data.

Heat fluxes on the land surface were determined by the Penman-Monteith method (Monteith, 1965). In the soil and snow layers, the thermal conductive processes were considered separately for different material zones. The soil layer and snowpack were subdivided at 0.01-m intervals in this study. An iterative process was used in the calculation and the value of convergence was set to 0.001^{o}C for the surface temperature difference between the last two estimated results.

Runoff model

The runoff formation for a grid was simulated using a runoff model (Ma *et al*., 2000) in consideration of the active layer depth. The total runoff for a grid is calculated using four reservoirs to give surface runoff and base runoff.

River-ice model

A simple method using accumulated degree-days was used to determine river-ice growth and decay processes. Here, it was assumed that (a) the river ice expands upwards when the air temperature is continuously below the freezing, and that the river-ice decay process begins when the growth process ends; (b) turbulent heat transfer between the water and ice is neglected; (c) there is no snow on the river ice, and (d) to simplify calculations, the surface temperature of the river ice equals the daily mean air temperature when required data are lacking.

River routing model

It was assumed that most of the runoff calculated from the runoff model is stored temporarily in the river while the river is fully frozen. Once the river ice breaks up, part of the stored runoff over a given depth is moved along the river with high velocity (Ma and Fukushima, 2002).

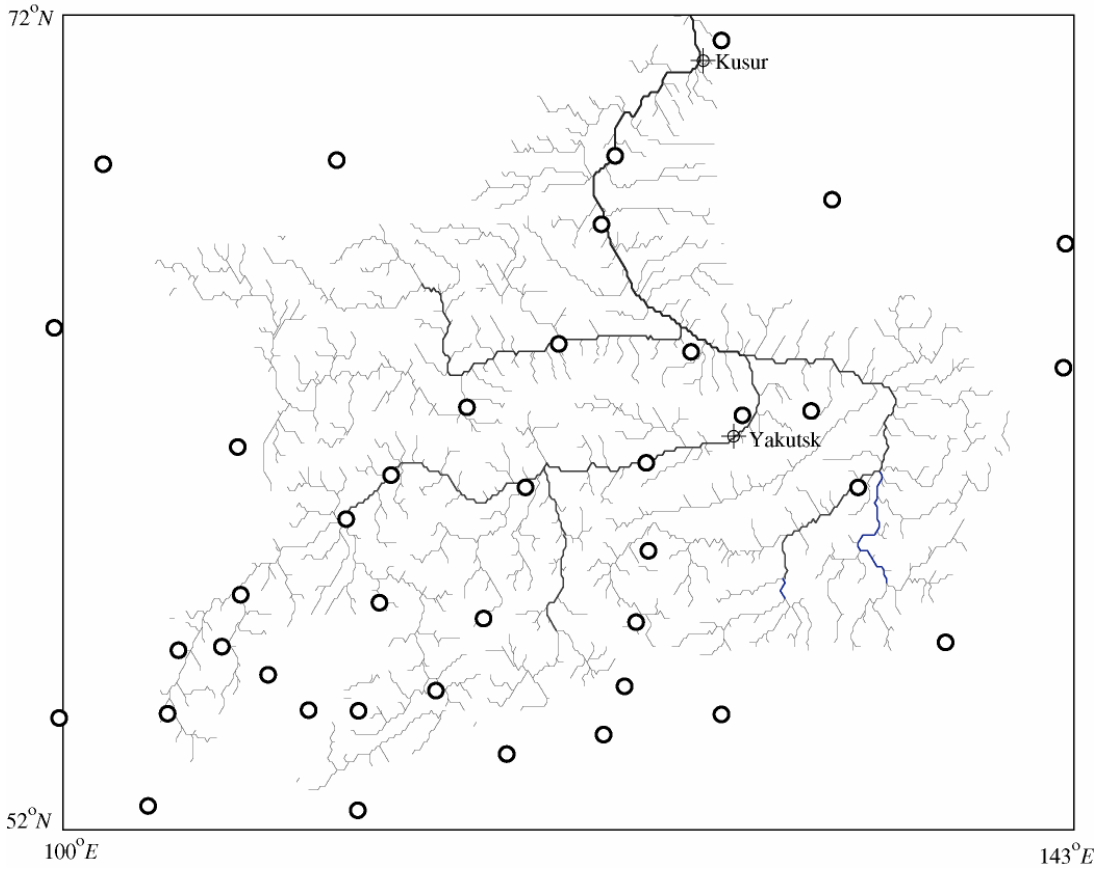

Fig. 2. Study area, showing the locations of hydrological stations (circle with plus), forty meteorological stations (circle) and the river network of the Lena River basin

APPLICATION AND RESULTS

Dataset The GAME project (GEWEX [Global Energy and Water Cycle Experiment] Asian Monsoon Experiment) has released a vast amount of data related to hydrology, meteorology, and climatology for study areas from Thailand to Siberia (http://www.hyarc.nagoya-u.ac.jp/game/). A meteorological dataset covering the Lena River basin from 1986-2000 is available from the GAME dataset (CD-ROM: GAME Dataset for the Water and Energy Cycle in Siberia, Version 1). Forty stations were selected for this study (Fig. 1). The record for each station included daily measurements of 13 items: mean air temperature ($°C$), maximum air temperature ($°C$), minimum temperature ($°C$), precipitation amount (mm), minimum relative air humidity (%), water vapor pressure (hPa), saturation deficit value, mean wind speed (m/s), maximum wind speed (m/s), total cloud amount, amount of low cloud, sea level atmospheric pressure (hPa), sunshine duration (hour), minimum land surface temperature ($°C$), snow depth (cm), and extent of snow coverage. The wind speed was measured at a 10-m height above the ground surface; other measurements were taken at 2 m. Station data were interpolated onto the entire basin using the inverse of the distance between each grid point and the nearest three gauges (Ma *et al.*, 2000). Although the geographical factors should be considered in such data reprocessing, only the temperature was corrected according to the

altitude, because no suitable method for incorporating geographic features has been found to date.

Two web sites provide discharge datasets for the Arctic region. One is R-ArcticNet (Version 3.0) of the University of New Hampshire (http://www.r-arcticnet.-sr.unh.edu/v3.0/index.html). Ten water supply regions (rivers) of the Arctic Ocean are monitored, and long-term monthly discharge data over those regions are archived (e.g., data on the Lena at Kusur covers the period 1934 to 2000). The other dataset is ArcticRIMS (A Regional, Integrated Hydrological Monitoring System for the Pan-Arctic Land Mass), also of the University of New Hampshire. Data on part of the Lean's daily discharge in recent years are available at this site. For example, the time series data for the Lena River's daily discharge at Kusur cover the period from 1st January 1978 to 31st December 2003.

Study area The study basin was established up to $72^{o}N$ near the hydrological station at Kusur, because the main river flow divides into several directions after that point.

The model was run directly from 1 October 1986 to 30 September 2000, or fourteen hydrological years, using parameter calibrated by Ma and Fukushima (2002).

Figure 3 shows results for the daily hydrograph (a), monthly hydrograph (b), and annual runoff amount (c) from 1986 to 2000 at Kusur. Comparison with the observed hydrograph for the same period reveals that the model performs well in reproducing the timing of flood rise and peak, and that in the first half of the study period (1987-1994) the estimated flood peak value was usually less than the observed flood peak; the largest error (4.1 mm) appears in spring 1989. However, a reverse of this situation appears in the latter period, as seen in Figure 3a. Although the estimated monthly hydrograph (Fig.3b) was well in agreement with the observation, the same problem as in daily hydrograph occurred. These results indicate that the model can represent seasonal variation at the station. The underestimate of annual runoff is about 20 mm in average (8.85 in percent), especially in first three years (1987,1988 and 1989) and the maximum underestimate value is 66.6 mm in 1988 (Fig.3c).

It is well known that snowmelt dominates runoff in northern river basins. To understand the variation of snowfall in a mountainous area (south of $60^{o}N$) in winter (October-April) was estimated from the model. Figure 4 shows the results. The average snowfall in the study period was 122 mm. Since 1994, snowfall has increased to a maximum of 146 mm in 2000. The figure shows the high correlation between snowfall and runoff. Years with heavy snowfall exceeding 120 mm (1988-1989, 1992, 1994-2000) also had heavy runoff in both the simulations and observations.

CONCLUSION

Long-term (1986-2000) hydrological modeling of the Lena River was conducted using routine, daily meteorological data, collected at forty stations covering the basin. The model was designed for a northern river basin. River-ice is particularly important in

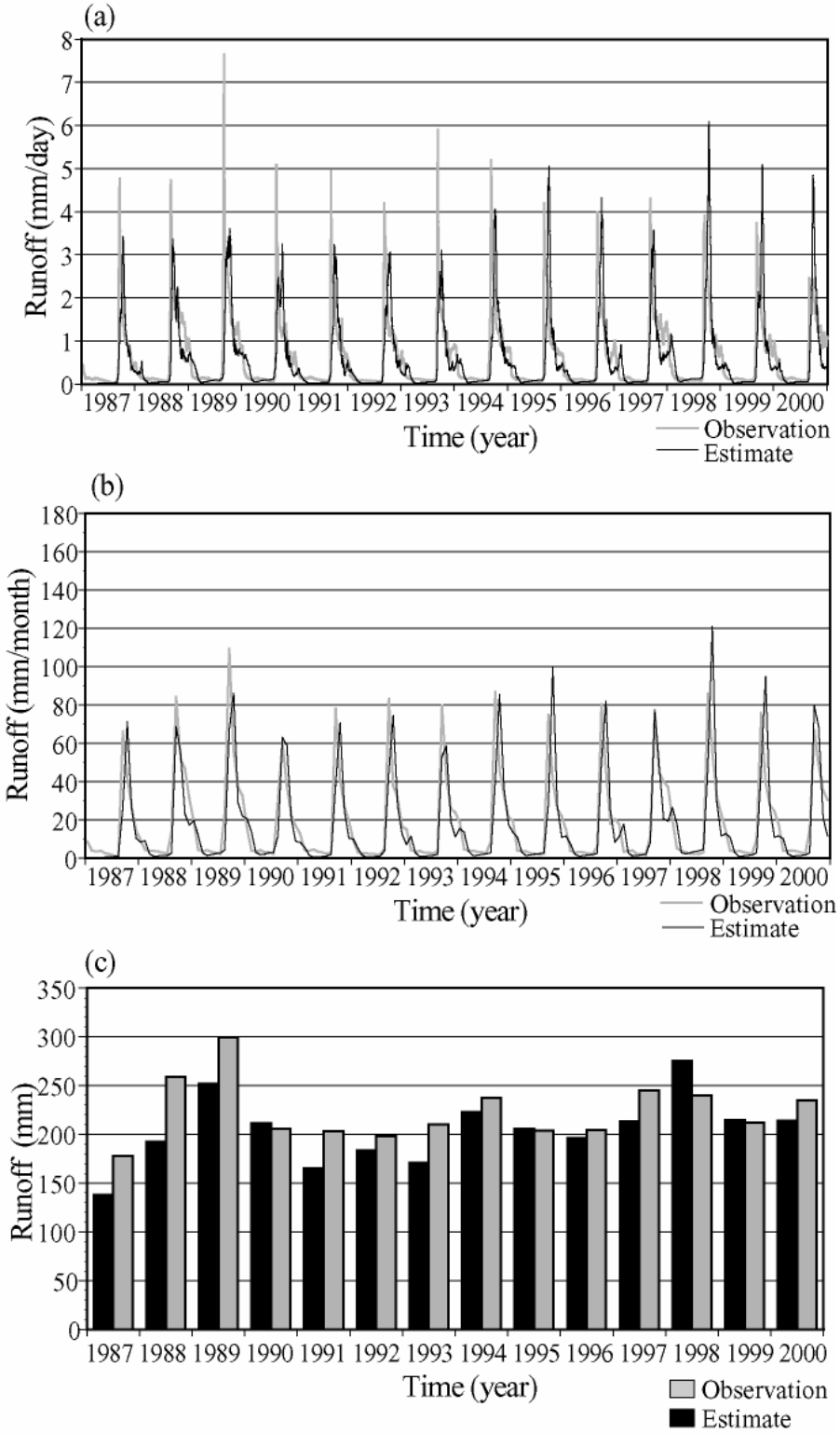

Fig. 3. Comparison between estimates and observed values at Kusur station on the Lena River: (a) daily runoff in the 1987-2000, (b) monthly runoff , and (c) annual runoff

simulated. Daily Lena River runoff at Kusur was well modeled, although there were differences between calculated and observed flood peak values. The model successfully presented snowmelt and break-up processes; it turned out well that the timing of flood rise and flood peak appearance generating in connection with both processes by it compared with the discharge data over the 14 years. In general, estimates of annual runoff were sufficient accurate, where the estimated and observed values of annual runoff at Kusur were 203.9 mm, and 223.7 mm, respectively. The annual error was within 20 mm on average; error was greatest in the period of June-September, and can be attributed to the underestimates of winter snowfall. Estimates might be improved by supplemental winter precipitation data in the future.

REFERENCES

Ma, X. and Fukushima, Y., 2002. A numerical model of the river freezing process and its application to the Lena River. *Hydrological Processes*, 16, 2131-2140.

Ma, X., Fukushima, Y., Hiyama, T., Hashimoto, T., Ohata, T., 2000. A macro-scale hydrological analysis of the Lena River basin. Hydrol. Process. 14, 639-651.

Monteith, J.L., 1965. Evaporation and environment. In: Fogg, G.E., (Ed.), The stage and movement of water in living organisms, *Symposia of the Society for Experimental Biology* 19, Cambridge University Press, Cambridge, pp. 205-234.

Wetherald, R.T., Manabe, S., 2002. Simulation of hydrologic changes associated with global warming. *Journal of Geophysical Research* 107, D19, ACL7-1-ACL7-15.

17th International Symposium on Ice
Saint Petersburg, Russia, 21 - 25 June 2004
International Association of Hydraulic Engineering and Research

THE COMPUTER MODEL OF FORMATION OF AN ICE JAM AT THE LENA RIVER

Belikov V.V.[1], Zaitsev A.A.[2]

ABSTRACT

The computer hydraulic model of formation of an ice jam levels on the rivers is considered in the reporting. The model is based on construction of a digital model of a relief with application of GIS-technologies and numerical solution of the equations of the Saint-Venant in a one-dimensional and two-dimensional schematization. The accounts of a disastrous jam of 2001 in region of city Lensk in Ykut region are conducted. The good concurrence to full-scale dates was obtained. A main outcome that by primary factors, defining an ice jam levels, are length of a jam and water discharge. Height of an ice dam in the basis of a jam is not the main reason of rise of a level of water. It allows to evaluate recurrence of a jam levels.

The jams of ice originating during rough ice moving on the large rivers, call of splashing down of territory and result in disastrous consequences. Per the last years are marked is anomalous high jam flood on the Vuychegda and the Lena rivers. The disastrous floods from jams of ice put enormous damage to economy. The huge losses were suffered by economy and population of Yakutia republic after a series of high-power vernal floods in region of cities Lensk, Olekminsk and Yakutsk. As have shown conducted researches existing of techniques of the prognosis of a jam floods are incomplete, owing to many factors of the phenomenon.

The problem was delivered to supply a guard of the occupied items from of a jam floods and other unfavorable effects caused by the rivers. For construction of levies and acceptance of other measures on prevention or minimization of consequences of floods it is required to have an operating information about probable levels and flooded areas of territory. The executed researches put by the purpose to supply account of levels of a jam flood and area of its distribution for a high water of 2001 to use the developed technique for the operating forecast for consequent years.

The research of the problem consists of development of the numerical method of the prognosis of floods caused by ice jams. It was selected the fragment of the Lena river in

[1] Scientific Research Institute of Energy Structures, Moscow
[2] Moscow State University of Environmental Engineering

region of city Lensk as an example. For operating account of floods caused by jams of ice, it is required to apply the calculate methods dependent on a limited gang of the factors, by selecting major from them. The solution of a problem is based on account of current with application of the one-dimensional and two-dimensional equations of the Saint-Venant. The work, conducted earlier on numerical simulation of water streams [1 – 4], have shown, that is possible to use the limited gang of parameters influencing to a solution, under condition of the careful description of the entry conditions. Therefore important block in a full solution of a problem is the construction of a detail digital model of a contour of a valley and channel of the river.

The modern technology of construction of a digital contour of relief assumes use of electronic topographical maps, navigational maps and measurements of depths of a channel with application of ultrasounds and systems of satellite positioning. The digital model of a contour of relief is based on outcomes of full-scale measurements of a modern channel obtained with the help of hardware-software equipment of a complex with satellite co-ordination [5] by Lena's team of the Moscow state university in 2001 –2002 at a 157-kilometer section of the Lena river. The site began approximately in 20 Km above on current from one city of Lensk in top about the Half Island and included places of formation of systematic jams, which call floods with disastrous consequences in city and neighboring settlements. There are a mouth parts of the rivers Muriy, Kantaika and Nuya, about islands Batamayskiy, Samnagas, Gluhoy and Tinnuy (fig.1). Channel of the river on all stretch no breaded and only on sites of the extension of a valley there are single islands and consolidated groups of islands. Low level flood plane is distributed by fragments. The extensions of a valley are characterized in development high level flood plane with separate fragments of terraces. The model of a contour of a valley is constructed by a vectorization of topographical maps and plans of large scale in absolute coordinates. It has allowed to synthesize vectorial maps and outcomes of full-scale measurements, by enumerating them in absolute high-altitude marks. The outcome of work is a digital model of a contour of the bottom of a valley. It is basis for construction of a computer model.

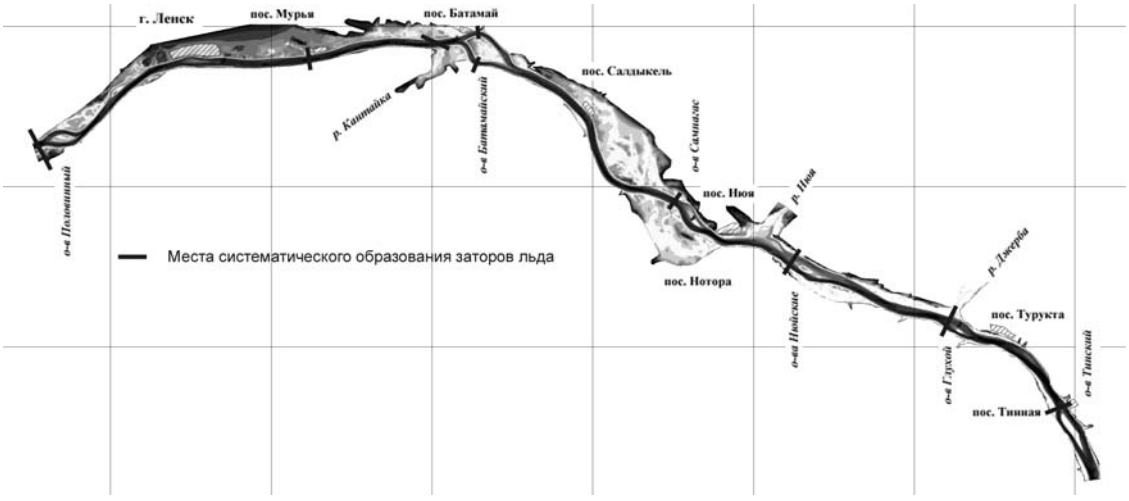

Fig. 1. Shem of the Lena River and the jam places

The bottom of the river is composed by pebble and gravel material. There are outputs of rocky breeds in the river. The analysis of the river bad processes [6] specifies absence of rearrangements of a base contour, which could be determined by existing methods. Therefore account of the river bad processes of strains in a hydraulic model was not conducted. The channel deep also does not call difficulties for navigation, therefore special dragging work on this section of the river were never conducted. The absence of the hydro technical work on recess of bottom cannot cause formation of jams of ice.

The accounts of current are conducted on one-dimensional and two-dimensional models. As boundary conditions the daily of water discharge on a hydrometric post Krestovskoe were used. It is located in 100 Km above on current of the river. On this section of the river the inflow of water is very small, on a comparison with volume of water of the Lena River. It was taken only in flow of the Nuy River, the discharge of water, which reach 2000 m^3/s. The discharge of a high water on the Nuy river passes always earlier, than on the Lena. During period of a high water on the Lena the discharge in the Nuy is reduced up to tens m^3/s. It on two orders is less than a volume of flow of the main river. The levels of waters used for calibration of a model and a selection of factors of a roughness, undertook on being available a hydrometric posts. The thickness of ice on a hydrometric post in winter period was taken into account.

The modern technique of realization of accounts because of equations of the Saint-Venant assumes semi-automatic construction of cross section of a channel and hybrid irregular settlement grids [7]. The settlement grids consist of triangular and four-coal cells. In consequent on special algorithms they automatically interpolate a contour in knots of a grid [8]. For region of city Lensk on a site by a valley of 150 km were constructed both only triangular, and special hybrid grids. The hybrid grids consist of curvilinear four-coal cells in a channel and triangular on cells (fig. 2). The pitch of a settlement grid has made for a channel 50 – 150 m, for flood plane 150 – 500 m. The accounts were conducted under the obvious scheme of disintegration of ruptures [9,10] and on implicit on time to the scheme [2,4,11].

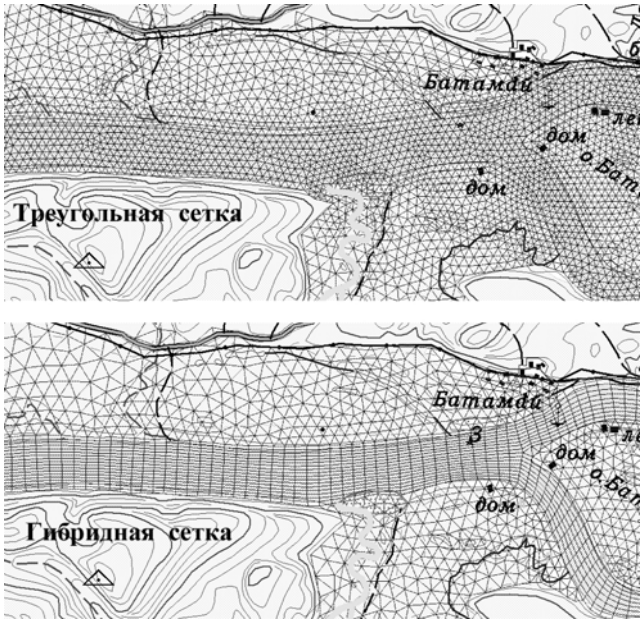

Fig. 2. The digital nets of the computer model

The outcomes of accounts under the implicit scheme have appeared more correct, than under the obvious scheme. Therefore further accounts were conducted under the implicit scheme disregarding of convective members and with factor of a roughness in a channel n=0.023, that corresponds to account under the implicit scheme with allowance for of convective members with *n=0.022* in a channel (0.042 – under ice), 0.050 – on a flood plane. The discharge of water was emulated in a range from 690 (for of ice coverage) up to 35000 m^3/s (it is anomalous high flow of spring period) for calibration of a model.

The calibration of a numerical hydraulic model was conducted with use of full-scale dates on discharges and levels of water for winter, spring (high water) and summer conditions. The accounts have shown good concurrence to measurements on post Lensk and satisfactory concurrence to measurements (within the limits of an exactitude of a measurement of discharges) on post Nuy. The consequent systematic accounts have allowed to continue a curve of communication of discharges and levels for free channel in a range of values, before not observed in full-scale conditions. Has appeared, that marks of a water surface in region Lensk even for want of discharges of rare security it is essential (on some meters) below, than repeatedly observed ice jam levels.

The accounts of an open stream have shown, that an existing channel of the river can to pass any natural discharge of water without flooding of valley practically. Therefore it seems, that the surface high level of valley is not flooded. So the urban quarters of city Lensk and some settlements were constructed on a surface the flood plane. Actually flood is observed very seldom, approximately time per 30 years. It is caused only by ice jams. Earlier it was supposed, that the special measures will not suppose formation of jams of ice. It was not justified in a consequence.

Following step of researches was simulation of a jam of 2001 in region of an island Batamay, when reducing to disastrous splashing down of the city Lensk. The discharge of water and levels on posts Krestovskiy, Lensk and Lensk were known. With application of a computer model were restored actual dynamics of growth of levels and destruction of a jam. The conveyance of a channel in region of a jam was appreciated. The formation of jams model in a one-dimensional schematization was offered by A.N.Militeev [12] more than 10 years ego. It allows to determine the most probably places of formation of jams on the river. In practice of a place of formation of jams are well known (fig. 1). A main problem is the determination of maximum height of a jam level in a specific place under condition of a known discharge of water, as it determines zones and intensity of flood.

Main postulates for want of modeling of a jam of ice are the following:

- the places of formation of jams known;
- the concentration of ice on the approach to a jam is known (this magnitude influences a velocity of distribution of an edge of a jam up on current);
- the velocity of traffic of ice in a jam is very small on a comparison with flow rate of water;
- factor of a roughness of ice in a jam known and is constant (total factor of a roughness is received in addition of factor of a roughness of an open stream and factor of a roughness for want of ice cover (coverage));

- maximum length of an ice field is known;
- time (date) of a beginning of formation of a jam and its destruction are known;
- on a considered site of the river a jam only one, but can form in different places of a site;
- the total discharge of water and ice on the source boundaries of settlement area are known.

With allowance for of listed above assumptions the one-dimensional mathematical model both program of account of formation and development of jams in region of city Lensk was developed. On this site 6 constants of places of jams are known (fig. 1). Because of digital model of a relief and with the help of especially of developed program for a site 95 cross sections of a channel and valley of the river were constructed. The cross sections are located on a distance about 1.5 Km from each other, with a pitch 25 m between verticals (on some cross sections the number of verticals reached 400).

Cross sections have formed the basis for construction of a one-dimensional mathematical model of current, which has allowed to expect passing high waters on a considered site, including formation of ice jams. The model is based on a numerical solution of the one-dimensional equations of the Saint-Venant on algorithm [1, 13] and is supplemented by an elementary model of increase of length of a jam depending on concentration of ice, approaching to a jam, and flow rate at a leading edge of a jam. Basic data for a model are:

- hydrograph in a first cross section, as which was accepted of the hydrograph of a post Krestovsky, with allowance for of lag channel, equal to 12 hours;
- hydrograph of the river Nuy (was set to constants: Q = 100 m^3/s);
- factor of concentration of ice in a first cross section (was accepted in a range 0,5 – 0,7);
- place of formation of a jam (one from four specific, since of an island Batamaisky);
- factors of a roughness (on Manning) the channels (n = 0,023) and flood plane of the river (n = 0,05) in a stream without ice (were determined by calibration of a model under the fact sheet);
- additional factor of a roughness of a jam (ice surface), which was determined on full-scale dates for winter conditions with allowance for adjustments on an increased roughness of ice in a jam (was accepted equal n = 0,03);
- maximum length of a jam (was accepted under the fact sheet or more);
- time of a beginning of formation and the destructions of a jam were accepted on actual approximate dates.

On the last boundary of a stream it was put the «not reflecting» boundary condition appropriate to relation between of discharges and levels accordance the equation of Shezy for known of slope of a water surface (was accepted I = 0,0001).

The simulation of an actual high water of a 2001 with known parameters has given maximum a jam level on a post Lensk, equal 171.8 m, that on 0.3 m there is less then actually level (fig. 3). Considering, that special «the adjustment» of parameters for want of it was not made, such concurrence is necessary to consider good. Dynamics of a modification of levels in time also is close to an actual picture. The longitudinal structures of a water surface with allowance for of jam for various instants on rise of a high water are represented in a fig. 3. It is necessary to take into account, that simultaneously with a jam in region of an island Batamay one more jam below on current from the river Nuy was derivate. Within the framework of a considered model has appeared possible to reproduce these jams as one continuous jam, and in this case designed levels in city Lensk have appeared above factual on 0,3 m.

Research of influence of height of a jam in point of its formation on levels at city Lensk also was conducted. For want of to height of an ice dam 4 m above maximum (for want of mode without ice) level of water in it point the level on a post Lensk was lifted all on 0,2 m (fig. 3). It specifies that in many cases (especially for want of to large length of a jam) height of a jam at a place of its formation does not render essential influence to levels of splashing down.

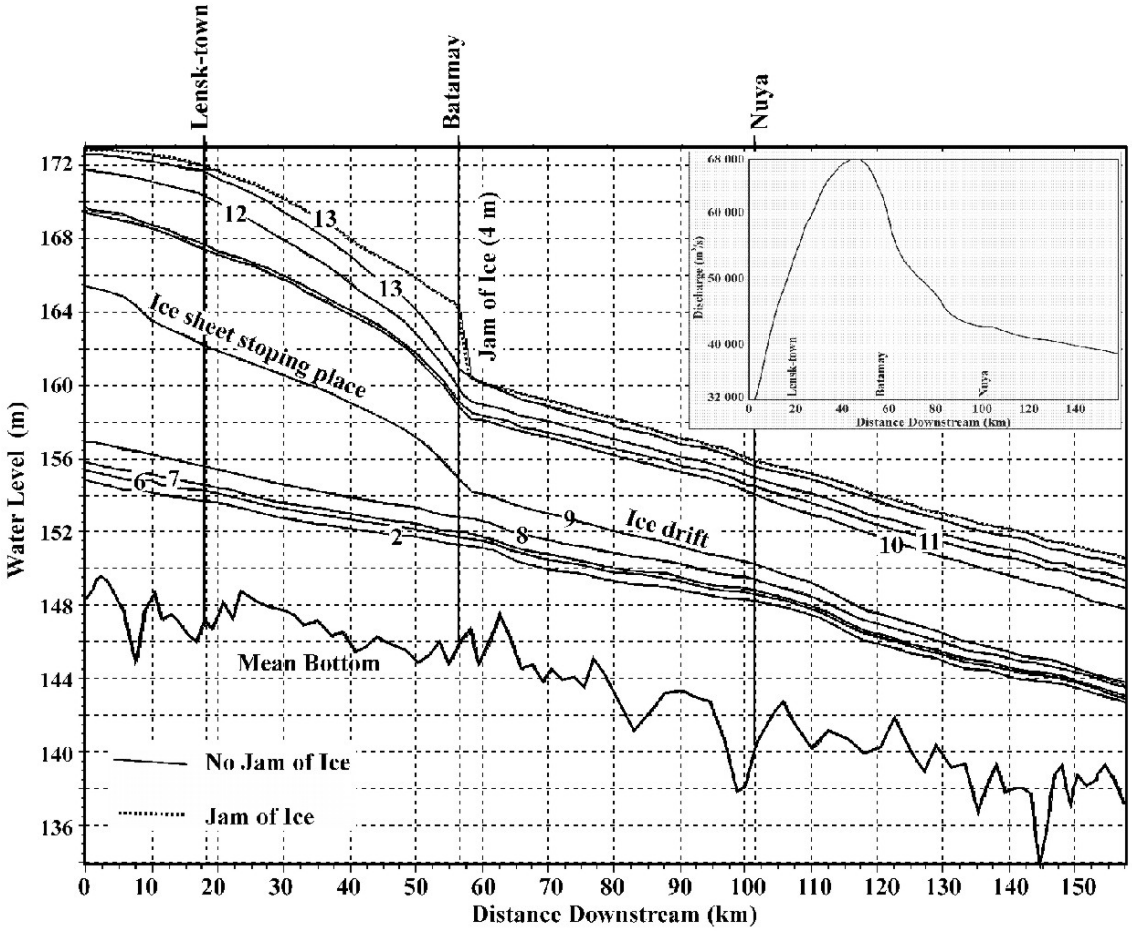

Fig. 3. Calculation of water table from the ice jam at the middle stream of the Lena River

The natural observing testify that the river is lower jam always on large stretch is free from ice. Therefore as a first approximation wave of break for want of destruction of a jam can be simulated by a usual image, numerically deciding the one-dimensional or two-dimensional equations of the Saint-Venant by usual methods [9, 10]. Such accounts are conducted for a Lena's jam 2001 in region of an island Batamay. The zones and depths of splashing down on a site of a valley below than jam by an expansion about 80 kms are obtained. For want of fast destruction of a jam there is a wave of break, the initial discharge of water in which reached 58000 m^3/s. It almost twice exceeds maximum discharge on the upper boundary. However this discharge fast flattening-out on length of a site and in time. Floating on a surface of water the ice should influences on parameters of a wave of break, especially near to it of front. This problem requires special researches. Most interesting for accounts and dangerous in practice a situation can be observed, if on the river some jams were derivate sequentially, and the wave, which has arisen for want of destruction on current of a jam, can reduce in destruction of underlying jams.

Under condition of the several sequentially located jams the accounts on a two-dimensional numerical model for construction of maximum zones of flood [2,3,11] were conducted. With some stock was accepted, that on a considered site the continuous jam was derivate, and the cost of water is equal 32000 m^3/s (maximum for period of a high water 2001). In such statement of a problem the levels of flooding in region of city Lensk have made 172,25 m, that is very close to observed significances. On other cross sections of a considered site of the river the levels, probably, are overestimated (so, in region Nuy approximately on 0,6 m) a little. The fragment of account of maximum depth of flood plane is represented in a fig. 4. For want of maximum development of a jam bottom of the valley appears flooded practically on all breadth, i.e. the levels of flooding are close to extremely high, that testifies to rare recurrence of a high water 2001. Alongside with determination of scale of flood the vectors of flow rates on the flooded territory are certain. It allows to define maximum strength on constructions, being available in a valley.

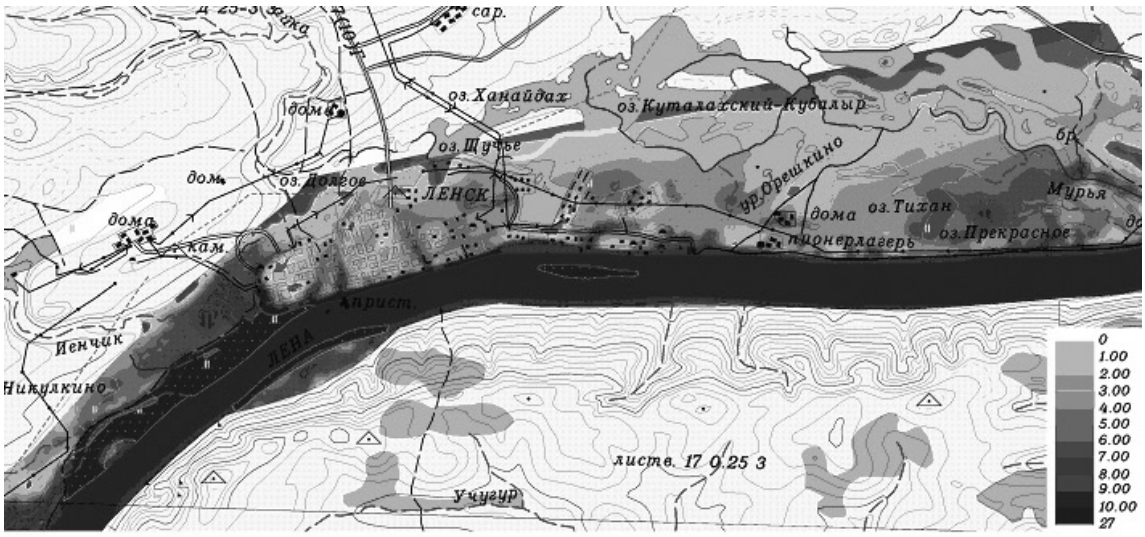

Fig. 4. Calculated of the flooded area from the ice jam

The conducted researches have allowed to uncover physics of process of flood in case of suspension of transition of an ice field and explain process of shaping is anomalous of high levels. They arise because of receipt of a large mass of water. Huge volume of water cannot be passed through a channel of the river owing to sharp increase of a roughness under a congestion of ice. Backwater forms, mainly, stopping ice, but not ice dam, as it was supposed earlier. The outcomes of a research envelop common regularities of shaping of flood from ice jams and can be applied for account of splashing down of territory on other rivers of Russia. Important for a successful solution of a problem the request of a maximum approximation of the accepted entry conditions to an actual contour of territory, i.e. creation of an adequate digital model of a contour of a channel and valley is. The boundary conditions can lean on an existing dates of observations at hydrology posts. The perfecting of a technique of account is possible by inclusion of actual conditions of debacle and mechanical properties of ice. It will require additional full-scale observations and experiments; an amount which quality stills it is not enough.

REFERENS

1. Liyhter V.M., Militeev A.N. Hydraulic investigation by digital methods. *Vater Res.*, N3, 1981
2. Belikov V.V., Zaitsev A.A., Militeev A.N. The digital models cinematic structure of flow at the unerosion river channel. *Vater Res.*, 2001, V. 34, N6
3. Belikov V.V., Zaitsev A.A., Militeev A.N. The mathematical models of complicated channel of the big rivers. *Vater Res.*, 2002, V. 34, N6
4. Belikov V.V., Militeev A.N., Rodionov V.B. Two-layer model for flood computation in complicated channel system with erosion riverbed with floodplain. *Proc. Conf. «RIVER FLOW 2002»*, Bousmar&Zech (eds.),2002 Swets&Zeltinger, Lisse, ISBN 905809 509 6
5. Egorov V.F., Zaitsev A.A. Primenenie programno-apparatnogo compleksa I sputnikovogo coordinirovaniy pri provedenii izyskaniy na krupnyih rekah. In vol. “Sovremennoe sostoyanie vodnuih putey I problemy ruslovuih processov”. Moscow, Geography Facility MSU, 1999
6. Zaitsev A.A. Rol ledostava I vesennego ledohoda v processe formirovaniy rusla krupnoy reki. In vol. “Vodohoziaystvennue problemy ruslovedeniy”, Academiy vodohoziaystvennyh nauk. Moscow, 1994
7. Belikov V.V. Vyuchislitelnuiy complex TRIANA – generator setok treugolnuih conechnuyh elementov v proizvolnuih ploskih oblastiah. GosFAP USSR, P007705, 1984
8. Belikov V., Semenov A. Non-Sibsonian interpolation on arbitrary system of points in Euclidean space and adaptive isolines generation. Appl. Numer. Math. 32, № 4, 2000.
9. Belikov V.V., Semenov A.Yu. A Godunov’s Type Method Based on an Exact Solution to the Riemann Problem for the Shallow-Water Equations. // *Proc. 4 Eur. Comp. Fluid Dyn. Conf. (ECCOMAS 98).* WILEY, New York,1998.V.1, Part 1, pp.310-315.
10. Belikov V.V., Militeev A.N., Kochetkov V.V. Compleks program dliy rascheta voln proruiva “BOR”. Patent Russian agency. Official registration of soft N2001610638. Moscow. 2001
11. Belikov V.V., Militeev A.N. Compleks program dliy rascheta rechnuih techeniy “FLOOD”. *Patent Russian agency. Official registration of soft N20022610941*. Moscow. 2002
12. Zaitsev A.A., Militeev A.N. Ledovue zatory I ruslovue processy na reke Lene. In vol. “Bezopasnost energeticheskih soosugeniy”. Vol. 11. Moscov, 2003
13. Belikov V.V., Militeev A.N., Kochetkov V.V. Compleks program dliy rascheta techeniy v sisteme rusel (RIVER*). Patent Russian agency. Official registration of soft N2002610938*. Moscow. 2002

17th International Symposium on Ice
Saint Petersburg, Russia, 21 - 25 June 2004
International Association of Hydraulic Engineering and Research

ICE PHENOMENA ON THE RIVER AMUR

Verhoglydov A.A.[1], Debolsky V.K.[2], Kozlov D.V.[1]

ABSTRACT

The overwhelming majority of objects of the water industry of Russia are located in the territories, which are characterized by minus temperatures of the winter period. Taking the Amur river in the Khabarovsk area as an example it is possible to consider a number of typical problems arising on rivers in the winter time. The current programs make it possible to produce modeling of the most different processes occurring in waterways (reservoirs) and fulfil calculations with a rather high degree of adequacy. The good study and mastering of the regions where large bridges are located promote to the clarification of the situation. Basic difficulties during construction and especially reconstruction of main and strategic bridge structures are often connected with the choice of possible variants of arrangement of supports, location of navigation and ice passing spans. The most perspective way of solving this task can be development of independent mathematical models of the given section on the basis of software environment with further comparison of results and issuing final recommendations.

ICE SITUATION

Like the majority of rivers flowing in the latitudinal direction (from westward to eastward) the Amur is characterized by a complicated ice situation. As a result of location of the river whole length and most part of its large tributaries (Zeya, Bureya) on approximately the same latitude, ice formation in autumn and its weakening in spring take place almost simultaneously along the whole water way which causes scaled ice drifting and provokes ice mixing and jams in places with a constrained current. The situation becomes especially difficult during the years when ice on the tributaries breaks before it breaks on the Amur (1924, 1962, 1974).

For protection from floods (including winter floods) there were constructed protective dams which significantly reduced areas of flooding and underflooding ensuring a proper protection from summer monsoon floods. But during catastrophic rises of levels caused by ice phenomena there happen water overflows over protective structures which leads to arising of an extreme situation. Besides the direct danger to the life of people (there are known cases of people's death) this leads to the direct threat of arising

[1] Moscow State University of Environmental Engineering
[2] Water problem institute of the RAS, Moscow, Russian

of a man-caused catastrophe. A number of enterprises of the military defense industry including chemical armed forces, tank repairing plant, the largest city heat and power station operating on the solid fuel (coal) and some enterprises of wood working and food processing industry, dwelling regions get into the flooding and underflooding zone.

The main role in arising of such a situation is played by the following factors:

1. The transport reinforced concrete bridge of strategic significance located in the lower part of the city along the river current via the Amur river. The structure erected in the middle of the last year has protected supports placed close to each other (with a space of 18 – 30 meters) which provoke building-up of large ice areas, frazil, anchor ice causing powerful long-term jams (ice mixing). Sometimes during a whole winter period (from November to the end of May) there was an ice mixing created during first frosts.

2. A very strong branching of the Amur river before Khabarovsk. A lot of channels and arms of most different lengths and capacity create favorable conditions for hummocking of ice fields and formation of ice mound. During flood wave passing ice is accumulated in relatively narrow channels, it partially melts and washes, then it is taken away by the rising water into large streams (Kazakevich, Amurskaya, Pemzenskaya, Pryamaya, Beshenaya channels), then it moves as a single great mass downstream.

3. Low regulation of the Amur river and its tributaries. At present only the Zeyaskij hydrosystem functions, The Burejskaja Hydraulic Power Station is under construction now. However putting into operation of the latter station will not be able to significantly improve the situation. The general low level of the economic development of the region does not allow yet to speak about a possibility of creation of a cascade of hydraulic power stations on the Amur river, however similar projects exist.

From the above given factors the first two are acceptable for action. For today a bridge is the main and the only public transport artery connecting the river banks on the length of almost three hundred kilometers of its stream. Construction of a more acceptable structure which will be able to replace the bridge (for example, a suspension bridge) is an extremely expensive measure and it will be hardly implemented in the near future. The alternative to construction of a new bridge can be modernization of the existing one, carried out after a preliminary development of such a system of location of supports and ice-cutters which will make it possible for ice masses to pass with the least ice jams.

A possible solution variant of the transport problem during the bridge reconstruction can be using of the existing tunnel under the Amur river channel located downstream from the bridge (but within the city precincts).

The second factor also seems promising for development of measures on ensuring safety of the Khabarovsk agglomeration. With a purpose of minimizing the probability of flooding the city territory it was proposed to block the channels Pemzenskaya and Beshenaya by dams aiming at redistribution of the water flow and directing it into the prepared channel of the Amur river or to the unused territories. The existing hydraulic and mathematical models show the prospects of these researches as the ones which allow to reduce the probability of ice jams arising. Further investigations will permit to work out a system of blocking the flow excluding or minimizing the role of channels and arms in arising of the phenomena of ice jams and mixing on the Amur river.

The given above example characterizes the modern approach to the solution of the floods problem resulted from ice jams and mixing phenomena. For building a detailed and correct (valid) model of the processes taking place in this region it appears desirable to have a combination of several program products. Such a scheme will allow to decrease a possibility of logical and program mistakes, to compare results and what is especially important to use special packages in difficult cases.

DEVELOPMENT OF MATHEMATICAL MODELS

The current programs make it possible to produce modeling of the most different processes occurring in waterways (reservoirs) and fulfil calculations with a rather high degree of adequacy. From the whole program diversity there was accepted a graphic-analytical package HEC-RAS as the technically closest one for solving problems of ice jams and mixing phenomena on the Amur river. This product has been developed with the assistance of the USA Corps of military engineers in West Point which can to a great extent guarantee its high quality and excellent adequacy. HEC-RAS is an integrated program package of hydraulic calculations in which the user interacts with the system through the graphic interface of the user GUI – Graphical User Interface). The system is capable to fulfill calculations of curves of a free surface at steady or unsteady movements, some calculations on designing hydrotechnical structures, bridges availability of the ice cover in its different conditions.

The main purpose of the model development in the given electronic environment is a possibility of creating a connected picture of processes capable to change in time on the river Amur in a region of the Khabarovsk agglomeration of processes. At the same time there is both a possibility of forecasting possible ice difficulties and issuing correct hydrologic prognosis of development of events taking the influence on man's activity into consideration.

The input process of the environment data HEC-RAS is fulfilled at several separate stages, each of which is little dependent from the rest but is substantially necessary. There are the following basic technical stages of creation: inputting of the geometric data, inputting of the flow and boundary conditions data, fulfillment of hydraulic estimations.

Materials of the geometric data are put into the geometric data block providing communication of the data system of hydrotechnical structures (bridges, tubular structures, weirs) with the flow (scheme of the river system), data of the cross section etc.

In our case it was necessary to geometrically determine a section from the beginning of the Amur river branching to the arbitrary known cross section downstream from the bridge. A number of factors make this task difficult: heavy branching of the Amur river channel upstream above Khabarovsk, instability of geometric forms of waterways resulted from heavy treatment of the channel during floods passing and ice jams and mixing on the level rise, lack of cartographic materials and measuring data of depths in the river.

Possible ways of the problem solution can be considered as either purchasing of the commercial cartographic material which is connected with significant costs and does not fully guarantee the correctness of geometrical data even of the last year or usage of materials of the related industries. As for accuracy, frequency of innovations and

simplicity there were acknowledged maps of ships steering (pilot chart) as the best. Such a choice is conditioned also by a priori high authenticity of similar documents connected with their application in the field where any inaccuracy can become fatal.

A map fragment taken for consideration (scale 1:50000) covers a part of the length on 100 km above and 25 kilometers downstream relating to the section line of the hydropost of Khabarovsk. With its help there were determined water depths in different sections, axes of the proposed modeled hydraulic flows were chosen, necessary sections were built.

The obtained geometric data were put into the block of the geometric data of the hydraulic model HEC-RAS environment. When inputting the geometry data of the waterways roughness resulted from the presence of vegetation in the watered section was deliberately ignored. It can be justified by the fact that considerable speeds of current and ice masses passing are able to essentially change (decrease) roughness of the flood lands for very short periods of time. Roughness increase is also possible for a rather insignificant period of time (2…4 months) which is determined by reed vegetating time in flood lands.

Making profiles of the cross section is also extremely difficult – transformation of the channel sand bed takes place practically round the year which is caused by a complicated character of floods (monsoon and ice floods during snow melting), little connected or non-connected grounds of waterway channels and large squares of marshes (flooded) territories the roughness of which for every layer it is difficult to determine.

Especially difficult is modeling of the parts on which damming is made (Pemzenskaya and Beshenaya channels). Introduction of blocking elements into the settling hydrosystem of channels and watercourses can change the pattern of depths. At the same time it is not possible to consider such changes sufficient in order to speak about a complete or considerable correction of the picture.

The work with the navigation map resulted in establishment of the geometric model consisting of 26 connected with each other calculated sections determined by diameters. The accuracy of the created geometric model can be evaluated in plus – minus 0.1 meter and 5 meters across which is quite compared with the values of the channel annual transformation.

The next stage – input of the flow parameters – was carried out according to the data of hydrological year books and materials of some design organizations. The calculated year was taken as an average one relative to the water content, flow movement was taken as a settled one. The adoption of such a year was due to the convenience of the adjustment of programs. The data of the settled movement contain the following: the number of the estimated profile, parameters of the flow, boundary conditions for every section.

The ice cover was assigned in various alternatives of thickness (from 0.1 to 2.0 meters) and different states (though the possibility of modeling different ice forms in HEC-RAS is limited); besides, variants with non-simultaneous cleaning of the whole estimated section of a length of 125 kilometers from ice were considered. When assigning parameters of ice there was taken into consideration location of spillways of the Khabarovsk TETS (Thermo-Power Station) and industrial enterprises (a thiner ice was

accepted). In addition to it, a situation with a much earlier ice movement relative to the Amur river on the large tributary – the Ussuri river was taken into consideration.

The heaviest ice situation is formed according to the modeling data (as it is observed in nature) above the mentioned bridge via the Amur river.
In such cases the aim of mathematical modeling is creation of a stable software package fulfilling a scope of calculations sufficient for forecasting negative ice phenomena on the bridge structure (ice jams, mixing, damages of supports and ice cutters, wedging of ice etc.).

Development of bridge crossing on the rivers which are not enough studied from the point of view of glaciology and on the rivers with changeable ice environment can be simplified a little due to the possibility of forecasting the situation of passing the ice through the bridge spans. At the same time it is possible to obtain the necessary for calculation data long before the beginning of the bridge reconstruction by processing the data of weather observations, comparison with analogical structures on similar rivers of the same climatic area.

When creating similar programs at initial stages it is extremely desirable to use the formulas and theories proved by the time and engineering experience as an estimation basis which will allow to expect a general sufficient correctness of the obtained results. The most detailed and reliable method seems to be calculation of ice interaction with engineering structures, this method was worked out by K.N.Korzhavin in the middle of the last century. The basic calculation formula used when developing the program determines the dependence of the ice force of masses on the structure or its elements depending on the power of the ice cover. All this data can be directly or indirectly installed according to the data inquired by the program.

For modeling each situation a similar program package must inquire a number of parameters accessible for clarification of main components participating in consideration. This data can be united in four main big groups: parameters of the bridge, water, channel and ice. Calculation of the necessary values brings to the assignment of well-known basic parameters and choice of the arrangement scheme which ensures most favorable conditions. When projecting large objects it will be allowed to quickly and with low costs compare different variants of placement of supports, forms and attack angle of ice cutters heads and ice protective structures. Reduction of labor and time on fulfillment of the comparison analysis will make it possible to consider a big number of variants and choose the optimal one on a technical plane.

Data transfer from the hydraulic model HEC-RAS environment to the working windows of the estimation program of the ice passing through bridge crossings is preliminarily carried out manually which is laborious and provokes involuntary mistakes caused by man's factor. Extremely desirable seems development and creation of the program-mediator capable to automatically draw out the necessary data from exit files of model HEC-RAS and transfer them into the corresponding input data cells of the program of bridges calculations. Such improvement demands an access to the roots of the HEC-RAS file environment and it is still technically difficult.

The obtained program "symbiosis" allows to solve rather difficult engineering tasks not accessible for solving each component separately (though each program is autonomous and can be successfully used separately). It is clear that the output data of the program complex needs checking and verification with natural data, the geometric model must

be periodically clarified (ideally – twice a year), the hydrology and hydrothermics data can be corrected when putting HES into operation. Further ways of perfection are seen in reduction of the operator's role in the package work, in more accuracy.

The most important moment is testing of the issued by programs forecasts by real events taking place during implementation of those actions (in particular final crossing of the channels Pemzenskaya and Beshenaya by overflowing dams which were modeled in an electronic way.

The obtained for the given moment results allow to present a movement of water levels at different scenarios of crossing the channel and canals by both hydraulic structures and ice masses during ice mixing. It can be said that the implemented actions on installation of dams in Pemzenskaya and Beshenaya channels and forming a bottom deepening slot on the main channel will solve one of the main tasks (improvement of water supply in Khabarovsk) but they do not remove ice problems on the river from the agenda. And the complicated ice situation on this section of the river is created not only by the bridge crossing but also by the most intricate pattern of the waterway channel which provokes an unpredictable character of movement and deformations of ice masses. Thus the final aim of the performed researches is the development of such a scheme of man's impact on the Amur river in the line of Khabarovsk (dams, bottom deepening slots, recommendations of the bridge reconstruction) which could take the complexity and changeability of channel's forms into account.

17th International Symposium on Ice
Saint Petersburg, Russia, 21 - 25 June 2004
International Association of Hydraulic Engineering and Research

TWO-DIMENSIONAL MODEL OF RIVER-ICE PROCESSES USING BOUNDARY-FITTED COORDINATE

Mao Zeyu[1], Zhang Lei[1], Yue Guangxi[2]

ABSTRACT

River ice is natural phenomena in the northern of China under specific conditions of meteorology, geomorphology and hydraulics. The ice-related problems often makes the function and management of structures or channels very difficult. In this paper a two-dimensional river-ice numerical model under boundary-fitted coordinate is developed to accurately simulate complicated boundary condition. The numerical model consists of hydraulics model, flow temperature model, frazil-ice distribution model, and ice transportation under ice cover. MacCormack scheme is used to solve the equations. The model is validated with field data on the Hequ Section of Yellow River.

INTRODUCTION

The river-ice evolution is influenced by river hydraulics, thermodynamics, geomorphology and freezing, etc (Mao and Wu etal., 2002). Characteristic of flow in natural rivers are more complicated compared to that in straight channel, especially in meandering river. The one-dimensional model is only applicable for straight channel. It is well known that hydraulic conditions affect significantly ice condition, and the meander of river makes it impossible to use rectangular Cartesian coordinates to deal with complex geometric boundaries accurately. Boundary-fitted-coordinate (BFC in shortened form) is a kind of curvilinear coordinate, and can represent accurately the actual boundary. By means of BFC, the solution can be conducted on the fixed rectangular perpendicular grids, Fig.1. In this paper, two-dimensional numerical model of river-ice using BFC is developed, including models of river hydraulics, ice transport, thermal and freezing. The basic procedure is illustrated in Fig.2.

[1] Supported by Tsinghua University Research Foundation (No. JC2002006). Department of Hydraulic Engineering, Tsinghua University, Beijing 100084, China; E-mail address:maozeyu@tsinghua.edu.cn
[2] Department of Thermal Engineering, Tsinghua University, Beijing 100084, China

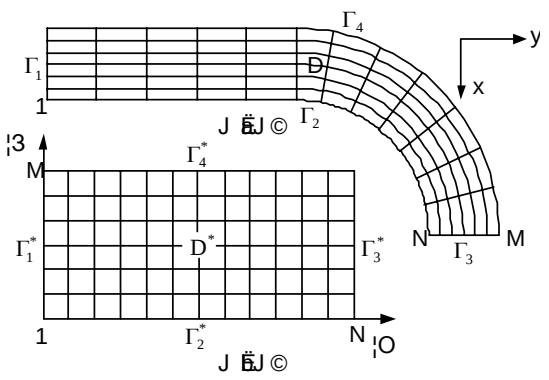

Fig. 1. (x-y) domain and (ξ – η) domain

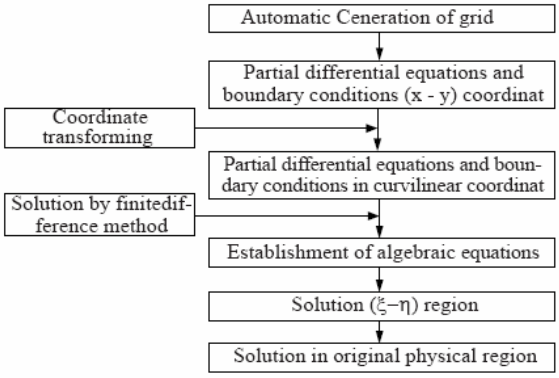

Fig. 2. Procedure for BFC method

RIVER-ICE TWO-DIMENSIONAL MODEL

The two-dimensional shallow water equations in conservational form in terms of water depth h, unit discharge q_x and q_y are used. Considering resistance under ice cover, the two-dimensional governing equations for unsteady flow can be written as (Wang, 1999)

$$\frac{\partial h}{\partial t}+\frac{\partial q_x}{\partial x}+\frac{\partial q_y}{\partial y}=0\ ; \tag{1}$$

$$\frac{\partial q_x}{\partial t}+\frac{\partial}{\partial x}\left(\frac{q_x^{\,2}}{h}+\frac{gh^2}{2}\right)+\frac{\partial}{\partial y}\left(\frac{q_x q_y}{h}\right)=hb_x^{'}-gh\frac{\rho_i}{\rho}\frac{\partial h_i}{\partial x}=b_x\ ; \tag{2}$$

$$\frac{\partial q_y}{\partial t}+\frac{\partial}{\partial x}\left(\frac{q_x q_y}{h}\right)+\frac{\partial}{\partial y}\left(\frac{q_y^{\,2}}{h}+\frac{gh^2}{2}\right)=hb_y^{'}-gh\frac{\rho_i}{\rho}\frac{\partial h_i}{\partial y}=b_y\,, \tag{3}$$

in which ρ, ρ_i=density of water and ice respectively,; h = water depth; h_i = ice-cover thickness; u and v are velocity components in x- and y-direction respectively. The conservative discrete scheme is applied ensuring no conservative error occurs (Wu, 2002). For without ice-cover and with ice-cover cases respectively:

$$b_x^{'}=-\frac{1}{\rho}\frac{\partial p_a}{\partial x}-g\frac{\partial z_b}{\partial x}+\frac{\tau_{ax}-\tau_{bx}}{\rho h}+F_{bx}\qquad b_y^{'}=-\frac{1}{\rho}\frac{\partial p_a}{\partial y}-g\frac{\partial z_b}{\partial y}+\frac{\tau_{ay}-\tau_{by}}{\rho h}+F_{by}\,,$$

$$b_x^{'}=-\frac{1}{\rho}\frac{\partial p_a}{\partial x}-g\frac{\partial z_b}{\partial x}-\frac{\tau_{ix}-\tau_{bx}}{\rho h}+F_{bx}\qquad b_y^{'}=-\frac{1}{\rho}\frac{\partial p_a}{\partial x}-g\frac{\partial z_b}{\partial x}-\frac{\tau_{ix}-\tau_{bx}}{\rho h}+F_{by}\,,$$

in which p_a= surface air pressure; z_b = bed elevation; $\vec{\tau}_b$ = bed resistance; $\vec{\tau}_i$ = ice-cover underside resistance; $\vec{\tau}_a$ = wind shear stress; $\vec{F}_b$ = Coriolis force. From the Chezy' formula, the resistance at the riverbed can be written as:

$$\tau_{bx}=\frac{\rho g n_b^2\sqrt{u^2+v^2}}{h^{1/3}}u\qquad \tau_{by}=\frac{\rho g n_b^2\sqrt{u^2+v^2}}{h^{1/3}}v\ . \tag{4}$$

If an ice cover presents, the composite resistances are respectively:

$$\tau_{ix} + \tau_{bx} = \frac{\rho g n_C^2 \sqrt{u^2 + v^2}}{h^{1/3}} u \quad \tau_{iy} + \tau_{by} = \frac{\rho g n_C^2 \sqrt{u^2 + v^2}}{h^{1/3}} v, \tag{5}$$

where, n_b=bed roughness; n_c=composite Manning's roughness. In this paper, the composite Manning's coefficent is taken to be (Mao and Ma, 2002)

$$n_C = \left(\frac{P_b n_b^{3/2} + P_i n_i^{3/2}}{P} \right)^{2/3}. \tag{6}$$

Water temperature can be expressed as a two-dimensional convection-diffusion equation in terms of conservation of thermal energy:

$$\begin{aligned} &\frac{\partial}{\partial t}(\rho C_P A T) + \frac{\partial}{\partial x}(Q \rho C_P T) + \frac{\partial}{\partial y}(Q \rho C_P T) = \\ &= \frac{\partial}{\partial x}\left(A E_x \rho C_P \frac{\partial T}{\partial x} \right) + \frac{\partial}{\partial y}\left(A E_y \rho C_P \frac{\partial T}{\partial y} \right) + B \Sigma S, \end{aligned} \tag{7}$$

where T = water temperature; C_p= specific heat of water; A = area; B = surface width; E_x, E_y are dispersion coefficient in x- and y-direction respectively; $\sum S$ = net heat flux from water to air, per unit surface area of flow. Assuming $E_x = E_y = E$ and Q remaining constant, the above equation can be re-written as

$$\frac{\partial T}{\partial t} + u \frac{\partial T}{\partial x} + v \frac{\partial T}{\partial y} = E \left(\frac{\partial^2 T}{\partial x^2} + \frac{\partial^2 T}{\partial y^2} \right) + \frac{B}{\rho C_P A} \Sigma S. \tag{8}$$

The equations for surface and suspended ice are respectively (Lal and Shen, 1991)

$$\frac{\partial C_S}{\partial t} + u \frac{\partial C_S}{\partial x} + v \frac{\partial C_S}{\partial y} = -\frac{B}{\rho_i L_i A} \sum S + \frac{\alpha}{A} \left(1 - \frac{V_z}{u_i} \right) C_C; \tag{9}$$

$$\frac{\partial C_c}{\partial t} + u \frac{\partial C_C}{\partial x} + v \frac{\partial C_C}{\partial y} = -\frac{B}{\rho_i L_i A} \sum S - \frac{\alpha}{A} \left(1 - \frac{V_z}{u_i} \right) C_C, \tag{10}$$

where, C_s = surface-ice volumetric concentration; C_c = suspended ice volumetric concentration; L_i = latent heat of water fusion; α = an empirical coefficient quantifying the rate of supply to the surface ice from suspended frazil ice (Wu, 2002) ; u_i = buoyant velocity; V_z = vertical component of current turbulence. From the mass conservation of surface ice at the leading edge, the rate of ice-cover progression of leading edge is (Lal and Shen, 1991):

$$V_P = \frac{Q_S^i - Q_u}{B_0 t_i (1 - e_j) - (Q_S^i - Q_u)/V_{SCP}}, \tag{11}$$

where V_p = progression rate; e_j = overall porosity of ice cover; Q_u = volumetric rate of ice swept at the leading edge; Q_S^i = volumetric rate of surface-ice discharge; B_0 = top

open-water width; t_i = initial ice-cover thickness; V_{scp}= average velocity of the incoming surface ice. The node-isolation method is applied in computation of the progression of each leading grid point. For the hydraulic-thickening mode, the changes in ice thickness are calculated based upon the calculation at each node. The ice transport capacity is formulated according to the following relationship

$$\phi = 5.487\left(\Theta - \Theta_C\right)^{1.5} \tag{12}$$

in which ϕ = dimensionless ice transport capacity; Θ = dimensionless flow strength; Θ_C = dimensionless critical shear stress.

BOUNDARY-FITTED-COORDINATE SYSTEM

The boundary on x – y is transformed into ξ–η by coordinate transformation, Fig.3. Solution of the elliptical partial-differential equations results in ξ = ξ(x, y), η=η(x,y),

$$\frac{\partial^2\xi}{\partial x^2} + \frac{\partial^2\xi}{\partial y^2} = P(\xi,\eta) \qquad \frac{\partial^2\eta}{\partial x^2} + \frac{\partial^2\mu}{\partial y^2} = Q(\xi,\eta) \tag{13}$$

and satisfying Dirichlet boundary condition:

$$\Gamma_1:\begin{pmatrix}\xi\\ \eta\end{pmatrix}=\begin{pmatrix}\xi=1\\ \eta_1=(x,y)\end{pmatrix} \qquad \Gamma_2:\begin{pmatrix}\xi\\ \eta\end{pmatrix}=\begin{pmatrix}\xi_1(x,y)\\ \eta_2=1\end{pmatrix}$$

$$\Gamma_3:\begin{pmatrix}\xi\\ \eta\end{pmatrix}=\begin{pmatrix}\xi=N\\ \eta_2=(x,y)\end{pmatrix} \qquad \Gamma_4:\begin{pmatrix}\xi\\ \eta\end{pmatrix}=\begin{pmatrix}\xi_2(x,y)\\ \eta=M\end{pmatrix}.$$

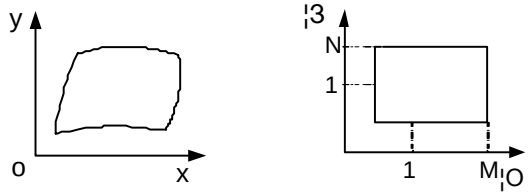

a) b)

Fig. 3. Transformation of BFC method

By selecting proper functions of P and Q the curvilinear grids at x-y can be transformed into uniform rectangular grids at ξ – η. The procedure of BFC includes arrangement of grid points along boundaries on x-y in terms of requirements, and numerical solution of the following equations:

$$\alpha x_{\xi\xi} - 2\beta x_{\xi\eta} + \gamma x_{\eta\eta} + J^2(P x_\xi + Q x_\eta) = 0; \tag{14}$$

$$\alpha y_{\xi\xi} - 2\beta y_{\xi\eta} + \gamma y_{\eta\eta} + J^2(P y_\xi + Q y_\eta) = 0, \tag{15}$$

in which $\alpha = x_\eta^2 + y_\eta^2$, $\beta = x_\xi x_\eta + y_\xi y_\eta$, $\gamma = x^2 + y_\xi^2$, $J = x_\xi y_\eta - x_\eta y_\xi$.

TRANSFORMATION AND COMPUTATION OF BASIC EQUATIONS

Let $\xi_x = \xi_x \cdot J$, $\xi_y = \xi_y \cdot J$, $\overline{\eta}_x = \eta_x \cdot J$, $\overline{\eta}_y = \eta_y \cdot J$, $u_\xi = u\xi_x + v\xi_y$, $v_\eta = u\overline{\eta}_x + v\overline{\eta}_y$, $q_\xi = q_x\xi_x + q_v\xi_y$, $q_\eta = q_x\overline{\eta}_x + q_y\overline{\eta}_y$, in which u_ξ and are velocities in ξ and η directions respectively. The governing equations under BFC can be deduced through coordinate transformation of equations (1) – (3):

$$\frac{\partial h}{\partial t} + \frac{1}{J}\frac{\partial q_\xi}{\partial \xi} + \frac{1}{J}\frac{\partial q_\eta}{\partial \eta} = 0\ , \tag{16}$$

$$\frac{\partial q_x}{\partial t} + \frac{1}{J}\frac{\partial}{\partial \xi}\left(\frac{q_x q_\xi}{h} + \overline{\xi}_x \frac{gh^2}{2}\right) + \frac{1}{J}\frac{\partial}{\partial \eta}\left(\frac{q_x q_\eta}{h} + \overline{\eta}_x \frac{gh^2}{2}\right) = b_x\,, \tag{17}$$

$$\frac{\partial q_y}{\partial t} + \frac{1}{J}\frac{\partial}{\partial \xi}\left(\frac{q_x q_\xi}{h} + \overline{\xi}_y \frac{gh^2}{2}\right) + \frac{1}{J}\frac{\partial}{\partial \eta}\left(\frac{q_y q_\eta}{h} + \overline{\eta}_y \frac{gh^2}{2}\right) = b_y\,. \tag{18}$$

The boundary conditions can be expressed as $A\varphi + B\partial\varphi/\partial n = C$ with A, B, and C given, $\partial\varphi/\partial n$ is normal derivative at boundary, φ is any variable desired, gradient of function f is $\nabla f = \left(f_\xi \xi_x + f_\eta \eta_x\right)\vec{i} + \left(f_\xi \xi_y + f_\eta \eta_y\right)\vec{j}$. The transformation equations of boundary conditions can be obtained as:

$$\frac{\partial \varphi}{\partial n^{(\xi)}} = \frac{1}{J\sqrt{q_{11}}}\left(q_{11}\frac{\partial \varphi}{\partial \xi} + q_{12}\frac{\partial \varphi}{\partial \eta}\right)\ \ \frac{\partial \varphi}{\partial n^{(\eta)}} = \frac{1}{J\sqrt{q_{22}}}\left(q_{12}\frac{\partial \varphi}{\partial \xi} + q_{22}\frac{\partial \varphi}{\partial \eta}\right)\ , \tag{19}$$

in which: $q_{11} = \overline{\xi}_x{}^2 + \overline{\xi}_y{}^2 = x_\eta{}^2 + y_\eta{}^2 = \alpha$ $q_{12} = \overline{\xi}_x\overline{\eta}_x + \overline{\xi}_y\overline{\eta}_y = -\beta$ $q_{22} = \overline{\eta}_x{}^2 + \overline{\eta}_y{}^2 = \gamma$.

As illustrated in Fig.4, ABCD is control volume, (i, j) is control node, $\Delta\xi\Delta\eta$ is control area. Let $U = \left(h, \mathrm{q_x}, \mathrm{q_y}\right)^T$, $F = \left(q_x, \mathrm{q_x^2}/h + gh^2/2, \mathrm{q_x}q_y/h\right)^T$,

$G = \left(q_y, \mathrm{q_x}q_y/h, \mathrm{q_y^2}/h + gh^2/2\right)^T$, then equations (16) – (18) give:

$$U_{i,j}^{n+1} = U_{i,j}^{n} - \left(\frac{\Delta t}{\Delta\xi\,\Delta\eta}\right)\left(H_{AB} + H_{BC} + H_{CD} + H_{DA}\right)\ , \tag{20}$$

where $H_{AB} = F_{AB}\Delta\eta$, $H_{BC} = G_{BC}\Delta\xi$, $H_{CD} = -F_{CD}\Delta\eta$, $H_{DA} = H_{DA}\Delta\xi$. The two-step MacCormack scheme is used with stagger difference scheme. Boundary conditions include incoming flow, outflow and non-penetrable wall condition $\vec{u}\cdot\vec{n} = 0$.

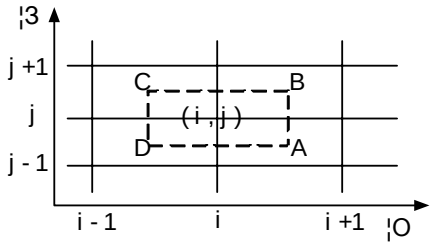

Fig. 4. Discrete scheme

Similarly, the governing equations of two-dimensional water temperature, surface and frazil ice under BFC can be deduced:

$$\frac{\partial T}{\partial t}+\frac{1}{J}[\frac{\partial(u_\xi T)}{\partial \xi}+\frac{\partial(v_\eta T)}{\partial \eta}]-\frac{1}{J}\frac{\partial}{\partial \xi}\{\frac{\Gamma}{J}[q_{11}\frac{\partial T}{\partial \xi}+q_{12}\frac{\partial T}{\partial \eta}]\}- \\ -\frac{1}{J}\frac{\partial}{\partial \eta}\{\frac{\Gamma}{J}[q_{12}\frac{\partial T}{\partial \xi}+q_{22}\frac{\partial T}{\partial \eta}]\}=\frac{B}{\rho C_P A}\Sigma S; \tag{21}$$

$$\frac{\partial C_S}{\partial t}+\frac{1}{J}[\frac{\partial(u_\xi C_S)}{\partial \xi}+\frac{\partial(v_\eta C_S)}{\partial \eta}]-\frac{1}{J}\frac{\partial}{\partial \xi}\{\frac{\Gamma}{J}[q_{11}\frac{\partial C_S}{\partial \xi}+q_{12}\frac{\partial C_S}{\partial \eta}]\}- \\ -\frac{1}{J}\frac{\partial}{\partial \eta}\{\frac{\Gamma}{J}[q_{12}\frac{\partial C_S}{\partial \xi}+q_{22}\frac{\partial C_S}{\partial \eta}]\}=-\frac{B}{\rho_i L_i A}\Sigma S+\frac{\alpha}{\mathrm{A}}(1-\frac{V_z}{u_i})\,\mathrm{C_C}, \tag{22}$$

$$\frac{\partial C_C}{\partial t}+\frac{1}{J}[\frac{\partial(u_\xi C_C)}{\partial \xi}+\frac{\partial(v_\eta C_C)}{\partial \eta}]-\frac{1}{J}\frac{\partial}{\partial \xi}\{\frac{\Gamma}{J}[q_{11}\frac{\partial C_C}{\partial \xi}+q_{12}\frac{\partial C_C}{\partial \eta}]\}- \\ -\frac{1}{J}\frac{\partial}{\partial \eta}\{\frac{\Gamma}{J}[q_{12}\frac{\partial C_C}{\partial \xi}+q_{22}\frac{\partial C_C}{\partial \eta}]\}=-\frac{B}{\rho_i L_i A}\Sigma S-\frac{\alpha}{\mathrm{A}}(1-\frac{V_z}{u_i})\,\mathrm{C_C}. \tag{23}$$

MODEL TEST

The observations of Hequ reach from Yingzhantan to Yumiao with length of 56 km in Yellow River is used to validate the numerical model, Fig.5 – Fig.10. The simulated duration is three days from 8 am of Nov.26 to 8 am of Nov.29 in 1986, with time-step of 900 s. Boundary conditions are flow upstream and water-level downstream. The section-averaged simulations are presented in order to compare with field observations.

From Fig.5, it can be seen that during ice-cover progression ice-cover thickness changes due to the ice transport under ice cover. Fig.6 gives the comparison of variation of the position of leading edge with time. Comparison of water level between computations and observations are shown in Fig.7 and Fig.8, respectively, with the maximum discrepancy of less than 0.3m. Comparison of water-level variation at different time is shown in Fig.9. It is obvious that water level at the leading edge increases as ice-cover advances. The influence of two progression modes on water level is shown in Fig.10.

CONCLUSIONS

To accurately simulate the complicated boundary in natural rivers, a two-dimensional numerical model of river-ice processes under BFC is developed. The MacCormack scheme is used to solve the transformed equations. The model is validated by the field observation and satisfactory results are achieved.

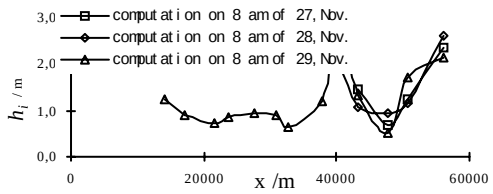

Fig. 5. Ice cover thickness variation

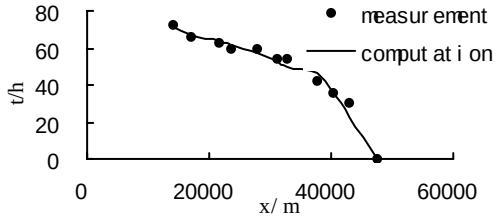

Fig. 6. Leading edge of ice cover

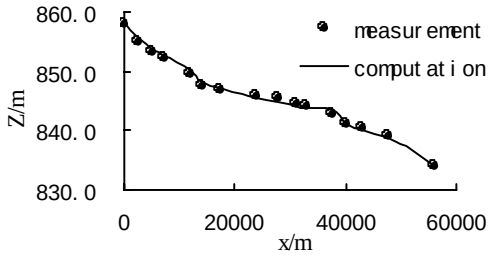

Fig. 7. Water level variation(8am, 28.Nov)

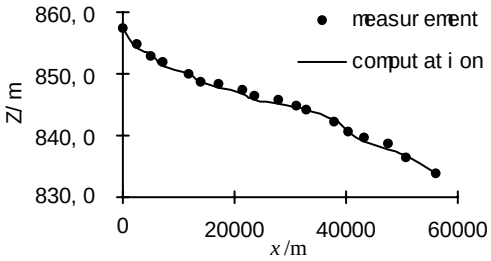

Fig. 8. Water level variation (8am, 29.Nov)

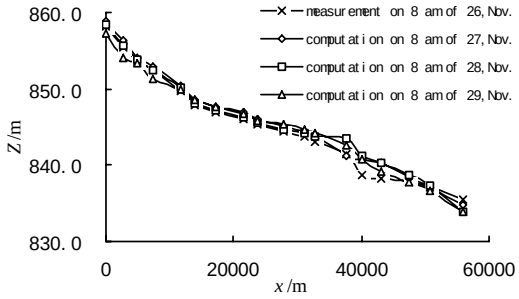

Fig.9. Water level variation at different time

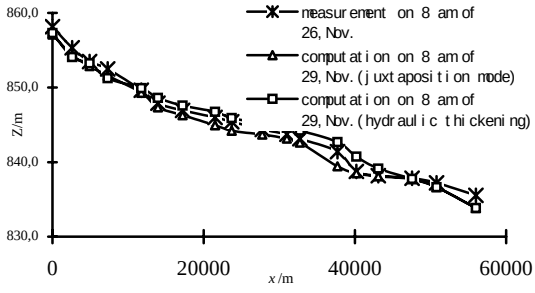

Fig. 10. Water level variation in two modes

REFERENCES

Lal A. M. W. and Shen H. T.: A mathematical model for river ice processes[J], *Journal of hydraulic engineering*, ASCE, 117(7), 1991.

Mao Zeyu, Ma Jiming , She Yuntong, Hydraulic resistance of ice-covered river, *Journal of Hydraulic Engineering* , No.5, 2002, 59-64.(in Chinese)

Mao Zeyu, Wu Jianjiang and She Yuntong. River ice process, *Journal of Hydroelectric Engineering*, No.1, 2002, 153-161 (in Chinese)

Wu Jianjiang, Ice processes mechanics and numerical simulation of ice jam and frazil ice evolution, *Ms thesis, Tsinghua University*, 2002.(in Chinese)

Wang Yongtian, Numerical simulation of river ice and analysis of ice characteristics, *Ph.D. theses, Tsinghua University*, 1999. (in Chinese)

17th International Symposium on Ice
Saint Petersburg, Russia, 21 - 25 June 2004
International Association of Hydraulic Engineering and Research

ANALYSIS AND SIMULATION OF SEA ICE DRAFT PROFILE ON OKHOTSK SEA COAST OF HOKKAIDO

Shinji Kioka[1], Yasuji Yamamoto[1], Daisuke Honma[1]
Mitsuhiro Sakikawa[2] and Shigeki Sakai[3]

ABSTRACT

Sea ice surveys were conducted along the Okhotsk Sea coast of Hokkaido, Japan using a bottom-mounted IPS and ADCP. We quantitatively analyzed the draft and the bottom unevenness of sea ice. The purpose was to mainly acquire inputs or boundary conditions needed to forecast the range of oil spreading under sea ice. The collected observation data (distance vs. draft) were analyzed by *discrete wavelet transform* and by l*ocally stationary AR model*. We suggested that the complicated sea ice draft profile or bottom unevenness that is non-Gaussian and has non-stationary characteristics could be represented using only typical normalized spectrum and variance of sea ice draft that indirectly reflects non-stationary characteristics of sea ice draft. We also found significant amplitude of bottom unevenness elevation were roughly proportional to standard deviation of sea ice draft (its ratio: 3.6), which means we could describe the bottom unevenness elevation of sea ice intuitively and visually using the standard deviation.

INTRODUCTION

The Okhotsk Sea coast of Hokkaido is known as the southern limit of sea ice, which forms in high-latitude waters and arrives at Hokkaido between January and March every year. When designing and constructing offshore/coastal structures, pipelines and other underwater and buried structures or winter navigation through pack ice, interaction with sea ice must be fully taken into consideration. It is also necessary to acquire information on the ice draft profile or plane unevenness of ice bottom in advance for oil spill contingency plans such as prediction of the range of oil spreading under an ice cover or recovery of oil in ice-infested waters. In particular, with the recent progress of oil and natural gas development along the Sakhalin continental shelf, transport of oil and natural gas to Japan by pipelines and vessels as well as accompanying oil spills or other accidents are expected in the future. Increased understanding of ice conditions in Okhotsk Sea coast of Hokkaido and other engineering studies concerning the above issues will therefore be

[1] Port and harbor eng. division, Civil Engineering Research Institute of Hokkaido, Hiragishi 1-3-1-34, Toyohira-ku, Sapporo, 062-8602, Japan
[2] Hokkaido regional development bureau, N-2, W-2, Sapporo, 060-8511, Japan
[3] Iwate University, 3-18-8 Ueda, Morioka, Iwate, 020-8550 JAPAN, N-13 W-8, Sapporo 060-8628, Japan

increasingly necessary in the future. Because hardly any field observations are available in Okhotsk Sea coast of Hokkaido, we have conducted sea ice surveys using IPS (Ice Profiling Sonar) since 2000. In 2001, ADCP (Acoustic Doppler Current Profiler) was added to the survey to focus primarily on drift characteristics of pack ice and to provide a means to change the temporal IPS data set to spatial data set. Theories and survey methods of these measuring instruments were detailed by Sakikawa et al. (2002), Belliveau et al. (1989) and Birch et al. (1999). Some of the survey results including the characteristics of sea ice drift have already been reported (Sakikawa et al., 2002; Yamamoto et al., 2002, Yamamoto et al., 2003). Furthermore, sea ice surveys using the same measuring instruments (IPS and ADCP) have been conducted in the northeastern part of Sakhalin (Birch et al.; 1999).

This study quantitatively analyzed the bottom unevenness (roughness) or draft profile of sea ice using spectrum analysis (locally stationary AR model) and time-frequency analysis (Discrete Wavelet Transformation). We examined methods for representing typical unevenness characteristics of the sea ice bottom, methods that can produce input for simulation of ice draft profile or the bottom unevenness.

SURVEY AND ICE DRAFT PROFILE [Yamamoto et al., 2002]

The observation site was 2.4 km off the coast of Mombetsu, Hokkaido. An Acoustic Doppler Current Profiler (ADCP) and an Ice Profiling Sonar (IPS) were installed at a depth of 18 m for continuous observation of the draft and drift speed/direction of sea ice passing over the observation equipment. Detailed observation methods were described by Sakikawa et al. (2002) and Yamamoto et al. (2002).

Figure 1 shows a nominal locus of sea ice drift between February 8 and 19, 2001, when sea ice existed. Note that this figure constitutes a simple coordinate based on sea ice drift direction and velocity data at one fixed location, instead of an essential locus of sea ice motion [Yamamoto et al., 2002]. Sea ice mainly moved southward along the coast during this period. Figure 2 indicates sea ice draft during the same period, i.e., draft vis-à-vis the distance of sea ice drift, which can be regarded as the ice draft profile. It shows that about 180 km of an ice draft profile was traced during this period.

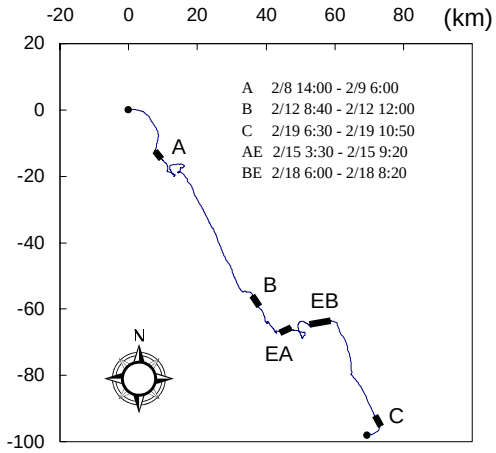

Fig. 1. Nominal locus of sea ice drift (Feb. 8-19, 2001) [Yamamoto et al.,2002]

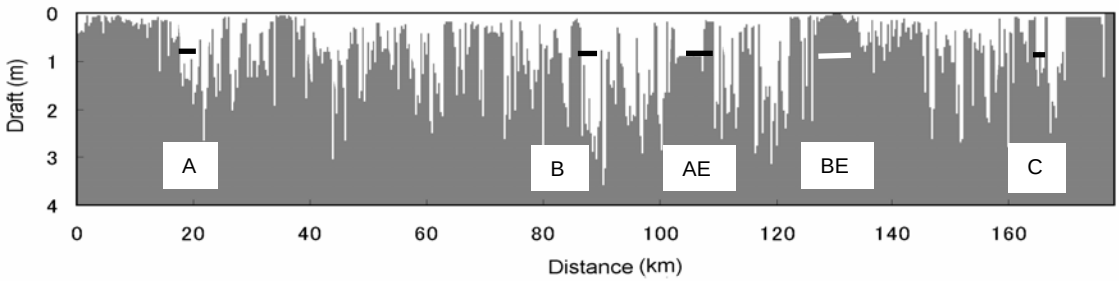

Fig. 2. Underside profile observed between February 8 and 19, 2001 [Yamamoto.et al.,2002]

ANALYSIS TARGETS AND NON-STATIONARY CHARACTERISTICS OF SEA ICE BOTTOM UNEVENNESS

When the sea ice bottom unevenness is represented as a waveform, it is important to determine whether this waveform has non-stationary characteristics. The decision whether to take into account non-stationary characteristics depends on the scale for which calculation is to be performed (e.g., calculation region for oil spill spread under the sea ice). If the scale is too small relative to the obtained data length, non-stationary characteristics may need to be taken into account. It would be desirable to incorporate the properties of level ice areas and open sea areas (where no sea ice exists), and the effects of travel direction on waveform characteristics. However, we do not have sufficient information on these factors to accurately analyze their effects. This study focuses on a section of sea ice bottom unevenness exhibiting macro-scale unevenness, selected from areas where the waveforms show that the prominent direction of sea ice drifts is southeast. Excluded areas are those where sea ices are rotating, or where they are drifting almost perpendicular to the prominent direction of sea ice drifts. The data were divided according to the basic span (1200 m) for the locally stationary AR model (presented in a later section). For each basic span, sections whose average draft is less than 10 cm are considered to be open water and are therefore excluded.

ANALYSIS BY DISCRETE WAVELET TRANSFORMATION

We conducted time (distance)-frequency (wave number) analysis of draft data by wavelet analysis. We omit the details of the algorithm of this method, and only briefly present the concept behind it. The wavelet $\Psi(x)$ is a unit for localizing a section of the signal $f(x)$. The wavelet transform assigns a value to each localized part of the signal. Wavelet transform is defined by Eq.1, which is produced by convolution integration using the wavelet and the signal.

$$W_\Psi f(b,a) = \int_{-\infty}^{\infty} \frac{1}{\sqrt{|a|}} \Psi\left(\frac{x-b}{a}\right) f(x)dx. \qquad (1)$$

Figure 3 shows translation (horizontal shift by b) and scaling (divided by a for compression) of "mother wavelet" for the transformation. The translated and scaled mother wavelet is compared with the original to find how closely they correspond. In the figure, $1/a$ and b denote the frequency of the localized section and its location on the time axis, respectively.

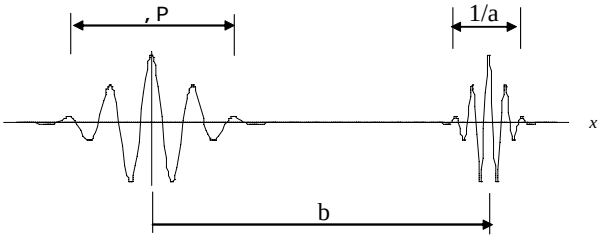

Fig. 3. Mother wavelet and translate

$d_k^{(j)}$, the discrete wavelet transformation function, can be discretized by integers j and k as $(b, 1/a) = (2^{-j}k, 2^j)$. When this is substituted into Equation (1), the equation is transformed as follows:

$$d_k^{(j)} = W_\Psi f(b,a) = 2^j \int^{\infty} \Psi(2^j x - k) f(x)dx. \qquad (2)$$

The wavelet and decomposition algo-

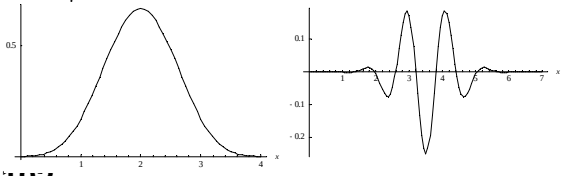

Fig.4. Scaling function (4th order B- spline) (the left Fig.) and mother wavelet (the right Fig.)

rithm is derived from the two-scale relationships that satisfy the scaling function. Using this algorithm, Equation (2) is sequentially calculated according to j, which denotes the level of decomposition.

The 4th order *B-spline* is chosen as the scaling function, from which the mother wavelet can be derived (Figure 4).

Figure 5 shows the calculated values of $d_k^{(j)}$. When j is small, $d_k^{(j)}$ represents the energy of low-frequency components. The graph of $j = 0$ shows the original signals (draft data). The horizontal axis represents distance. The wave number k is denoted as $k = 2^j k_N$, using the Nyquist frequency k_N (0.167 cycle/m in this case). The figures of $j = -1$ to -5 seem to show the strong energies of many signals whose wavelengths range between 12 m and 192 m. From looking at the distance axis, it is clear that the frequency changes over time, and therefore that the signals are non-stationary. As stated above, the distance/region for which calculation is to be performed determines whether the non-stationary characteristics need to be taken into account. However, the distribution of energy with respect to time (distance) seems to be almost the same at each level. That is to say, with respect distance, although there are local differences in the average power (variance) of the waveform, the frequency characteristics are likely to be similar. For practical application, the base spectrum can be set to survey the patterns of the power changes over a certain distance (time).

In this section, the characteristics of waveforms have been analyzed with respect to distance (time) and wave number (frequency) on a visual basis, using the wavelet transform. In the next section, we take a different approach for quantification.

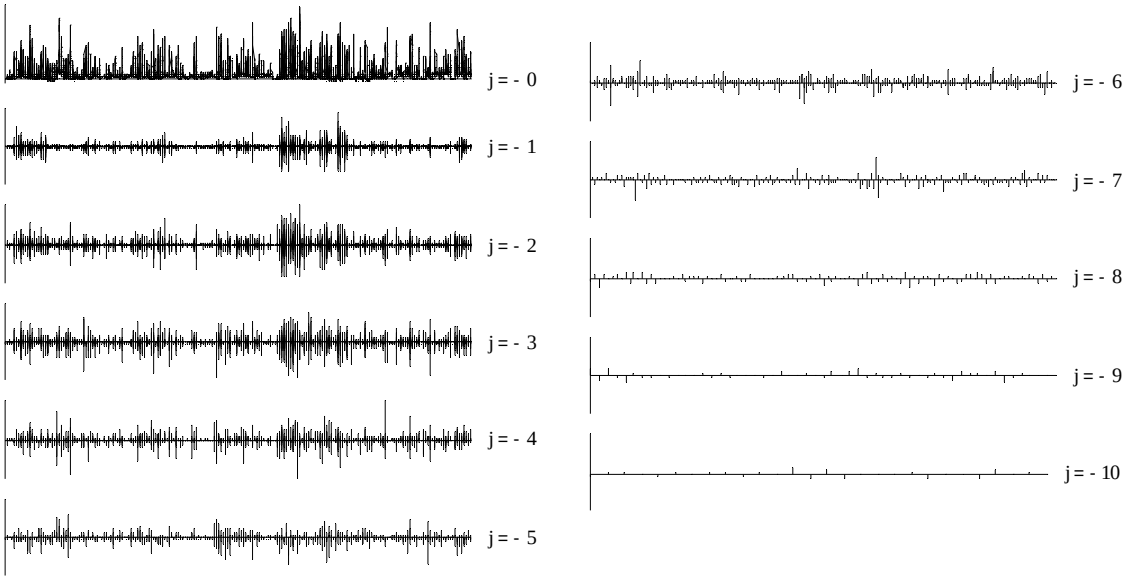

Fig. 5. Time-frequency analysis of sea ice draft by wavelet transform

ANALYSIS BY LOCALLY STATIONARY AUTOREGRESSIVE (AR) MODEL

The locally stationary autoregressive (AR) model is applicable for non-stationary analysis. The algorithm for this model is essentially the same as that of the MEM method: The time (distance) axis is divided into base spans (1.2 km). After the model is applied to these

basic spans, the base spans with similar characteristics are combined. Akaike's Information Criterion (AIC) is the standard for determining similarity. Base spans, including combined ones, are regarded as stationary sections, since the waveform is assumed to be stationary in each base span. Figure 6 shows the results of the analysis in which the locally stationary AR model is applied. The vertical axis shows wave number spectra, which is normalized by dividing the spectrum density by the variance of the draft depth, which is the 0-th moment of the spectrum. The other two axes are the wave number *k* (cycle/m) and distance (km). In this case, there are 66 stationary sections. The figure shows that the normalized spectra of the stationary sections tend to be similar. From a practical view points, we can assume that although the average power (variance of draft depth) of each section is different, the spectrum characteristics of the sections are similar, and their normalized spectra can be assumed identical. This result roughly agrees with that in the previous result using wavelet transform. Meanwhile, no significant relationship can be found between the normalized spectrum and the variance. For practical application of this method, the typical normalized spectrum as well as the range of the variance and its frequency distribution should be estimated, which is a very straightforward process. The typical normalized spectrum (hereinafter, "typical spectrum") is defined as the ensemble averages of the normalized spectra of the stationary sections (Figure 8). The spectrum is proportional to the inverse of the square of the wave number. Figure 7 shows the non-normalized spectra of each section. The two bold lines represent the spectra of the greatest and smallest values of variance of the stationary sections multiplied by the typical normalized spectrum. The figure indicates that the curves of the non-normalized spectra of each stationary section behave in a similar manner, although they deviate in a certain range. As shown in Figure 6, dividing those non-normalized spectra with the variance greatly reduces the deviations.

The bold curves, representing the spectra of greatest and smallest values of the variance of the stationary sections multiplied by the typical normalized value, cover the range of the original non-normalized spectra, thereby validating the concept of this model.

The discussion above assumes normality of data (Gaussian process). However, the actual distribution has the skewness. It is not proper to apply the spectra in their current form to various statistical estimates. When applying these spectra to simulation of the ice draft profile and bottom unevenness, improvements to this method or employment of another method is necessary. The non-Gaussian model and other models have been therefore proposed. Here, we attempt to normalize our data as much as possible. The generally known data transformation method that includes logarithmic transformation is a *Box-Cox transformation*, which is given by the following formula:

$$z_n = \begin{cases} \lambda^{-1}\left(y_n{}^{\lambda} - 1\right) & \lambda \neq 0 \\ \log y_n & \lambda = 0 \end{cases}, \tag{3}$$

λ is a variable parameter that is selected such that the value of AIC is minimized when the transformed data are assumed to follow normal distribution. The value of λ is –0.1

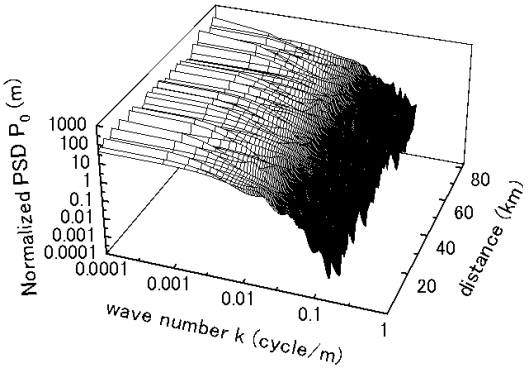

Fig. 6. Normalized power spectra in sections (spans) considered locally stationary by the locally stationary AR model

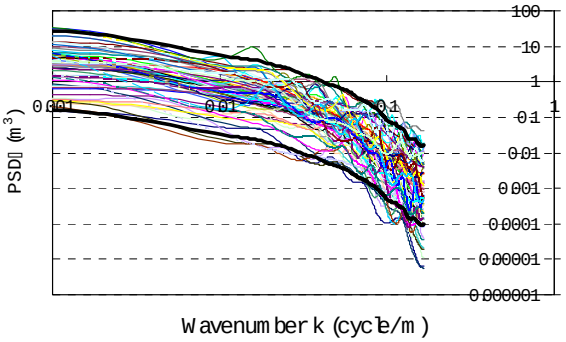

Fig. 7. Range of non-normalized power spectra in stationary spans compared with the typical normalized spectra (bold lines)

if this rule is strictly applied. However, we chose 0 for convenience, which means employment of logarithmic transformation. The data to which logarithmic transformation is applied are analyzed by the method explained above. Figure 8 shows the typical normalized spectrum of the data (dotted line). This spectrum is also not very different from that before the transformation, even though the frequency range is slightly smaller. This spectrum is proportional to the inverse of the square of the wave number, which agrees with the previous results. The average wavelength is 81 m. All these results are similar to those presented in Figures 6 and 7, including the above-mentioned statement: “The average power of each section is different. However, the spectrum characteristics of the sections are similar, and their normalized spectra can be assumed to be identical.” In practice, the unevenness characteristics of the non-stationary undersurface of sea ice can be represented by the typical normalized spectrum and the variance (standard deviation) that indirectly reflects non-stationary characteristics of the sea ice draft.

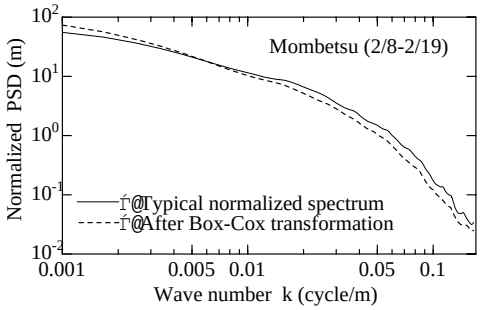

Fig. 8. The typical normalized spectrums, with and without logarithmic transformation on the sea ice draft profile

RELATIONSHIPS BETWEEN THE AVERAGE VALUE AND STANDARD DEVIATION OF SEA ICE DRAFT AND BETWEEN THE SIGNIFICANT AMPLITUDE OF BOTTOM UNEVENNESS ELEVATION AND STANDARD DEVIATION OF SEA ICE DRAFT

For development of a simulation method of sea ice draft or bottom unevenness, the variance (standard deviation) is a key factor. Therefore, we discuss the basic characteristics and range of variance (standard deviation) in advance. Figure 9 presents average values and standard deviations of the data. Each data point on the figure represents a result in each stationary section. The straight line in the figure indicates that the average value is equal to the standard deviation. In fact it means the relationship between the average value and standard deviation of the population when the initial variates follow an

exponential distribution. The number of samples is not large for any section, but the figure shows that they are distributed around the straight line. This suggests that the draft data follow a roughly exponential distribution.

It would be useful to describe the unevenness elevation of sea ice intuitively and visually using the standard deviation. The significant ocean wave height (highest one-third wave) is though to the height that we subjectively perceive as the average wave height. Following this idea, this section discusses the relationship between the significant amplitude of bottom unevenness elevation of sea ice and the standard deviation of the ice draft, a value that is a parameter of unevenness. The ocean wave height distribution is defined by the zero-upcrossing method, but if the original water surface fluctuation is Gaussian, it is theoretically a Rayleigh distribution. In this case, the significant wave height is four times the standard deviation of the original water surface fluctuation. The fluctuation of sea ice draft is not Gaussian, but it roughly conforms to exponential distribution or logarithmic normal distribution with strong skewness. This fluctuation also has non-stationary characteristics, so logical analysis is difficult for this case. Thus, for each section considered locally stationary above mentioned, the zero-upcrossing method was employed to calculate the amplitude (Figure 10). The figure shows that the standard deviation and the significant amplitude are roughly proportional. The slope is about 3.6, which means that the standard deviation multiplied by 3.6 would give a subjective the unevenness elevation. In fact, the significant amplitude of the unevenness calculated in this method represented a subjective of the unevenness elevation in most of the sections.

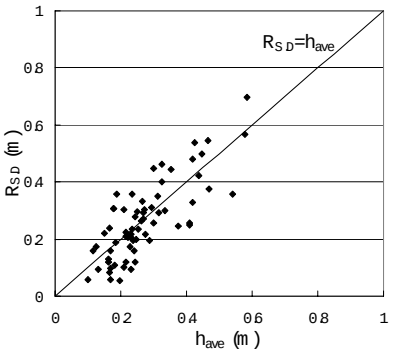

Fig. 9. Average values (h_{ave}) and standard deviations ($R_{S.D}$) of ice draft in locally stationary sections

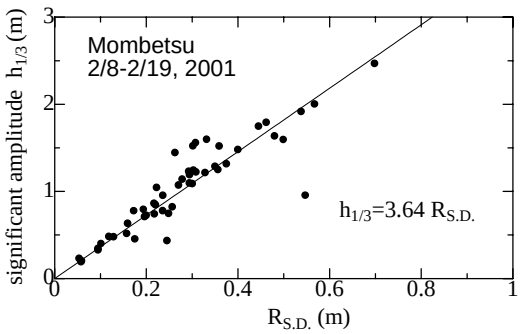

Fig. 10. Standard deviations ($R_{S.D}$) vs. significant amplitudes of sea ice draft in locally stationary sections

SIMULATION OF DRAFT PROFILE AND BOTTOM UNEVENNESS OF SEA ICE

The information provided thus far can be input into simulation of draft profile and bottom unevenness of sea ice. The fundamental simulation method has been outlined (Yamamoto et al., 2003). For the simulation, we applied input/output relations of linear response system. We then were able to simulate ice draft profile and plane unevenness of sea ice bottom using abovementioned typical normalized spectrum and variance. But, in that case, we calculated logarithm of the profile or unevenness using the typical normalized spectrum obtained from transformed data, and inverse transform (exp()) was eventually performed. The advantages of this method are these: 1) the resultant logarithmic values can be considered Gaussian and 2) the final outputs are always non-negative values. We will report a more developed and generic method than the current method for another

publication.

CONCLUSIONS

In this study, we quantitatively analyzed draft and bottom unevenness of sea ice. The purpose was to acquire inputs or boundary conditions needed to forecast the spread of oil spilled under sea ice, as well as for estimating ice loads acting when sea ice interacts with a structure. The results are as follows:

- The collected observation data (distance vs. draft) were analyzed by discrete wavelet transform (for distance – wave number analysis) and by locally stationary AR model. The results indicate that non-stationary characteristics may need to be considered, depending on the scale concerned. The average power (variance of draft depth) differs along distance axis (for each section), but the spectrum characteristics are similar. The normalized spectrum is roughly the same for each section considered locally stationary.
- From the results obtained in 1) above, we described the estimation method of a typical normalized spectrum. This also suggests that the complicated sea ice draft profile or bottom unevenness that is non-Gaussian and has non-stationary characteristics can be represented using only the typical normalized spectrum and variance (standard deviation) of sea ice draft. Also, thereby, we can easily simulate an ice draft profile and bottom unevenness using them.
- We found that significant amplitude of bottom unevenness elevation were roughly proportional to standard deviation of sea ice draft (its ratio: 3.6), which means we could describe the bottom unevenness elevation of sea ice intuitively and visually using the standard deviation.

We will continue to collect sea ice draft data, and especially, we need to get more information about distribution and range of the variance that indirectly reflects non-stationary characteristics of the sea ice draft. We also have to collect information on cross-sectional shapes from various angles and spatial profile.

REFERENCES

Belliveau, D.J., Budgen, G.L. and Melrose, S.G.K. Measurement of sea ice motion using bottom mounted Acoustic Doppler Current Profilers. *Sea Technology* (1989).

Birch, R., Fissel, D., Melling, H., Vaudrey, K., Schaudt, K., Heideman, J. and Lamb, W. Ice Profiling Sonar. *Sea Technology-Arcticle on Sahalin Ice Project* (1999).

SakikawA, M., Yamamoto, Y., and Honma, D. Underside Profile of Sea Ice on the Okhotsk Coast. In *Proceedings of the 17th International Symposium on Okhotsk Sea & Sea Ice*, Mombetsu, Japan (2002) 163–167.

Yamamoto, Y., Sakikawa, M., Honma, D. and Kioka, S. Underside profile and drift characteristics of sea ice on the Japanese Coast of Okhotsk Sea, *Proc. of the 16th International Symposium on Ice*, Dunedin, New Zealand (2002) Vol. II, 399-406.

Yamamoto, Y., Kioka, S., Sakikawa, M., Honma, D. Sea Ice Draft Profile on Okhotsk Sea Coast of Hokkaido, *Proc. of the 13th International Offshore and Polar Engineering Conference (ISOPE)*, Honolulu, USA (2003) Vol. I, 439-444.

17th International Symposium on Ice
Saint Petersburg, Russia, 21 - 25 June 2004
International Association of Hydraulic Engineering and Research

AN ORIENTED THICKNESS DISTRIBUTION FOR SEA ICE

Max D. Coon[1], Gerald S. Knoke[2], Douglas C. Echert[3], and Robert S. Pritchard[4]

ABSTRACT

This paper describes the kinematics and ice-thickness redistribution of pack ice while accounting for lead and ridge orientations. The pack ice deformations are described in terms of velocity discontinuities rather than invariants, allowing direct interpretation of open-water production and ridging. This description of pack ice allows an oriented ice-thickness distribution to account for the growth and ridging of ice in refrozen leads. Results of simple model calculations for ice-thickness redistribution appear reasonable. Results for kinematics indicate that most of the apparent scatter in isotropic calculations of open-water production can be explained by accounting for lead orientation.

INTRODUCTION

In polar regions, the sea-ice cover acts as a barrier between the atmosphere and the ocean, curtailing the transfer of thermal and mechanical energy as well as curtailing mass transport. The large-scale motion of the pack ice creates a small amount of open water, in the form of leads. In the Arctic winter and spring, leads are linear features often several hundred kilometers long. As these leads close and shear, rafted ice, pressure ridges, shear ridges, and rubble are created along these same linear features. SAR ice motion products show active leads as linear slip-lines in the pack ice (Stern et al., 1995). For convenience, all of these linear features will be referred to as leads. In this paper, the term 'lead' indicates a lead system that has a direction.

An ice dynamics model that assumes isotropy in the ice cover can adequately characterize an ice cover in the absence of leads, e.g., summer/autumn ice with multi-year floes surrounded on all sides by open water or thin ice. However, once a lead forms, the ice becomes anisotropic and is best described by a model that accounts for this property. Careful modeling of leads in sea ice is important not only because leads provide the opportunity for the heat exchange necessary for ice production, but also because the re-

[1] NorthWest Research Associates, Inc., Bellevue, WA, USA
[2] Energy International, Inc., Bellevue, WA, USA
[3] Skip Echert Web Associates, Renton, WA, USA
[4] IceCasting Inc., San Rafael, CA, USA

frozen lead ice controls the ice dynamics through its strength (Coon et al., 1992).

The architecture for a new large-scale anisotropic constitutive law intended for use in a sea-ice dynamics model has been presented by Coon et al. (1992, 1998). This architecture accounts directly for refrozen lead systems in pack ice strength with an anisotropic failure surface. This constitutive law has sub-scale simulation that allows for the inclusion of phenomena such as ridging, rafting, buckling, and fractures on the behavior of the ice. The oriented thickness distribution for sea ice presented here is intended to complete the architecture set forth by Coon et al. (1998). Pritchard (1998) demonstrated the behavior of an anisotropic elastic-plastic constitutive law with examples using an idealized deformation history. Therefore, in this paper, we will describe the formulation of the model and not its implementation.

In order to account for lead and ridge orientation for pack ice, Coon et al. (1992, 1998) introduces two types of ice:

- *Isotropic* ice is consolidated multi-year and thick first-year ice. Much of it is the jointed ice described above; *isotropic* ice is assumed rigid in this paper.
- *Oriented* ice includes open water, new ice, nilas, young ice, first-year ice, rafted ice, and ridged ice that occurs in long, narrow features. These features are assumed linear for (grid, element, or cell) scales of 5 to 100 km. All pack ice deformations are assumed to occur in the *oriented* ice. In addition, the linearity assumption implies that a shearing deformation of a lead does not cause rafting or ridging of the oriented ice and does not cause any failure of the *isotropic* ice.

ICE-THICKNESS REDISTRIBUTION

Subfreezing temperatures will cause *oriented* ice to form in leads, and ice deformations will cause a distribution of ice thickness within these leads. The distribution of ice thickness at each lead orientation can be described much as Thorndike et al. (1975) described the distribution of ice thickness, and Pritchard (1998) described the distribution of ice thickness in an anisotropic model. Figure 1 illustrates how to characterize these ice-thickness distributions, assuming *isotropic* ice has one ice-thickness category and *oriented* ice has four ice-thickness categories in two lead systems. The thickest *oriented* ice category may be thicker than the isotropic ice.

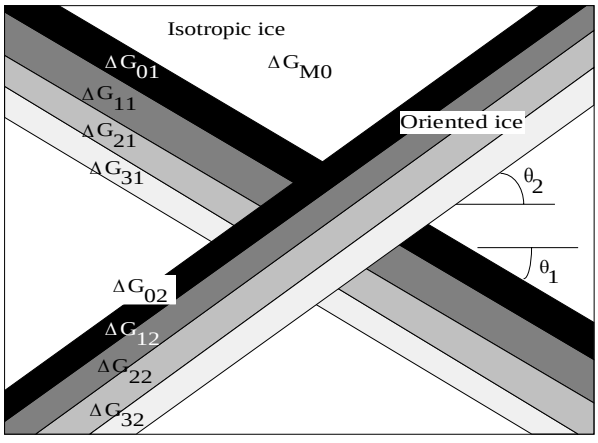

Fig. 1. Ice thickness distribution includes ice in each slip-line direction and the isotropic ice

The refrozen lead ice is assumed to be homogeneous (within each ice-thickness category). In addition, the leads are assumed straight so that a shearing deformation of the lead deforms neither *isotropic* ice nor *oriented* ice. Four ice-thickness categories are associated with each lead direction, applying the term 'oriented thickness distribution' to distinguish it from the usual (isotropic) ice-thickness distributions (e.g., Thorndike et al., 1975).

Based on Pritchard and Coon (1981), the mathematical equations and calculation procedures for the ice-thickness distribution with four ice-thickness categories in each lead have been developed.

RESULTS OF MODEL CALCULATIONS

The behavior of these ice-thickness redistribution equations is illustrated by a simple example for one lead; the results are shown in Figure 2. In this example, a cell of pack ice initially has only ice in the thickest category (white). At an air temperature of -40° C, the lead area fraction increases steadily at the rate of 10^{-5} s^{-1} for two days, then closes steadily at the same rate for two days. Initially, the open-water area fraction (black) increases rapidly at the same rate for two days. The open-water area fraction (black) increases rapidly at the expense of the thickest category. Gradually, freezing moves ice from the open-water category to the thin-ice category (dark gray). During closing, the open-water ice-thickness category is rafted into the thin-ice category. When the open-water category is fully consumed, the thin-ice category is ridged into the medium-ice category (light gray). When the thin-ice category is consumed, the medium-ice category is ridged into the thick-ice category (white).

Open-water production using the anisotropic model was compared to open-water production using the usual isotropic models. Isotropic models approximate the open-water production as a single function of the ratio of the stretching invariants (Thorndike et al., 1975; Stern et al., 1995).

Stern et al. (1995) shows considerable scatter in the opening found from 342 strips of SAR data for which the time interval was three days when compared with three isotropic functions, including Equation (12). They explained the scatter in the data as "measurement error". Here it is suggested that accounting for lead orientation may explain much of the apparent scatter.

Based on the actions of one or two lead systems, families of curves were generated for opening as a function of Θ with a fixed angle between two lead systems of 34° (angle from Cunningham et al., 1994). These results are applicable over all scales for which the leads are linear, e.g., from 5 to 100 km; these results are therefore comparable to a SAR pixel or an entire SAR strip.

The total stretching is the sum of N lead stretching contributions rotated to the reference coordinate system:

$$D_{xx} = \sum_{j=1}^{N}\left[\left(\frac{\partial V}{\partial \eta}\right)_j\left(\frac{1}{2}-\frac{1}{2}\cos 2\theta_j\right)+\left(\frac{\partial U}{\partial \eta}\right)_j\left(-\frac{1}{2}\sin 2\theta_j\right)\right];$$

$$D_{yy} = \sum_{j=1}^{N} \left[\left(\frac{\partial V}{\partial \eta} \right)_j \left(\frac{1}{2} + \frac{1}{2} \cos 2\theta_j \right) + \left(\frac{\partial U}{\partial \eta} \right)_j \left(\frac{1}{2} \sin 2\theta_j \right) \right] \; ; \qquad (1)$$

$$D_{xy} = \sum_{j=1}^{N} \left[\left(\frac{\partial V}{\partial \eta} \right)_j \left(-\frac{1}{2} \sin 2\theta_j \right) + \left(\frac{\partial U}{\partial \eta} \right)_j \left(\frac{1}{2} \cos 2\theta_j \right) \right],$$

where D_{xx}, D_{xy}, and D_{yy} are components of plastic stretching, and the velocities (UV) correspond to the lead direction (θ_j).

Applying Equation (1) to the case of two leads at an angle to each other can be used to demonstrate that any stretching can be accomplished from opening, closing, and shearing the two leads.

The open-water production is calculated directly from the positive values of $\left(\frac{\partial V}{\partial \eta} \right)_j$:

Lead 1 opening with Lead 2 closing: $\frac{Opening}{|D|} = \frac{\left(\frac{\partial V}{\partial \eta} \right)_1}{|D|}$. (2)

Both leads opening: $\frac{Opening}{|D|} = \frac{\left(\frac{\partial V}{\partial \eta} \right)_1 + \left(\frac{\partial V}{\partial \eta} \right)_2}{|D|}$. (3)

Figure 2 shows that open-water production depends strongly on the presence of lead systems. Figure 3 shows curves on which the ratio of lead-2 opening velocity to lead-1 opening velocity is varied over a wide range. The curve corresponding to the opening function is shown for reference as Thorndike (1975). The case in which only lead 1 is active and opening is shown. Only a limited range of values for Θ are possible because the stretching parallel to the lead is zero. The case in which lead 1 is opening and shearing to the right along with lead 2 closing with no shear passes close to the Thorndike (1975) case. The case in which lead 1 is opening and shearing to the left along with lead 2 closing with no shear produces large values of opening. Such large values of opening can occur only until lead 2 is closed, which, depending upon the rates involved, may take hours or days. This limitation suggests that the reduced scatter, seen by Stern at al. when they considered only the more active scenes, results from closing the second lead during the 3-day period.

The results of these calculations indicate that the apparent scatter in open-water production can be explained by accounting for lead orientation. There is no longer the one-to-one mapping of stretching to open-water production as there is with an isotropic model. Additional constraints imposed by the relations between stress, stretching, and the corresponding plastic failure surface, however, may provide bounds on the opening not seen in these figures.

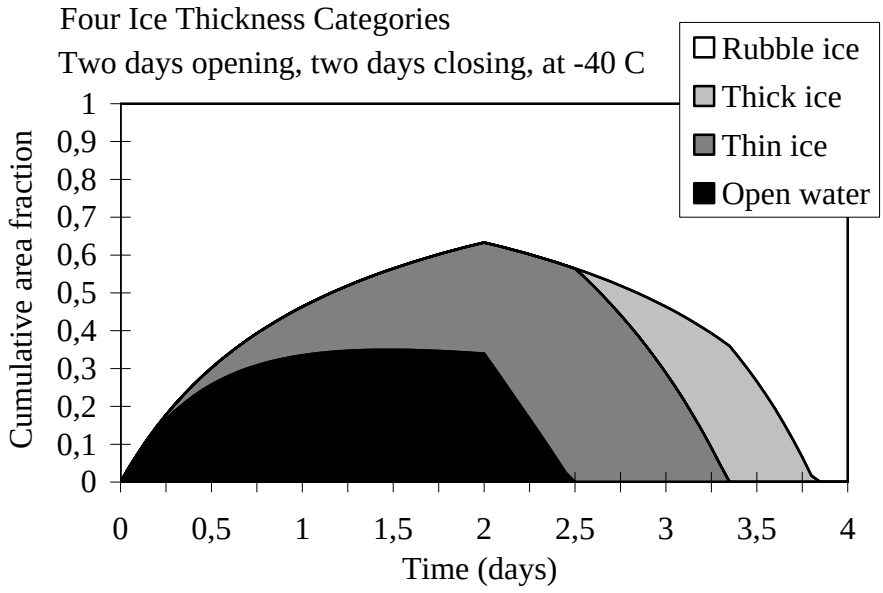

Fig. 2. Redistribution of ice thickness expressed as area fractions for four ice-thickness categories

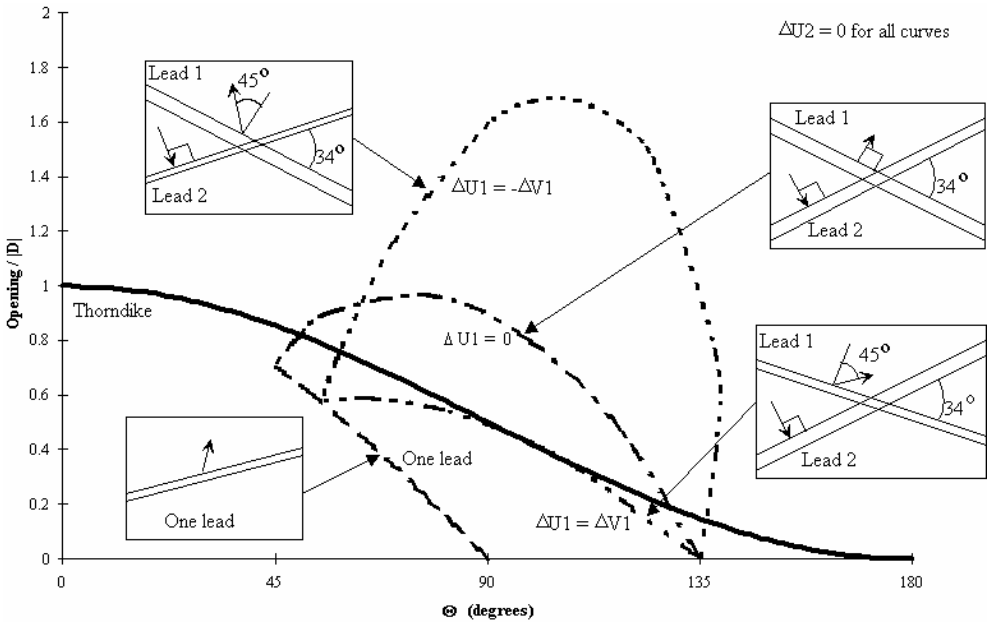

Fig. 3. Accounting for lead orientation results in families of curves for opening. Failure of isotropic ice falls on the curve for one active lead. The three higher loops result from varying the closing of the second lead for three values of the shear to opening ratio for the first lead

CONCLUSIONS

A formulation for pack ice kinematics and an *oriented* ice-thickness distribution that accounts for the orientation of existing leads and ridges has been developed. We concluded that:

1. The plastic deformations of pack ice can be expressed as the sum of contributions from the active leads and ridges.

2. The opening/closing of individual lead/ridge systems can be used to directly redistribute the ice thickness.
3. The apparent scatter in isotropic calculation of open-water production can be explained by accounting for lead orientation.

This oriented thickness distribution will be appropriate to complete the architecture of the anisotropic elastic-plastic sea ice mechanics constitutive law introduced by Coon et al. (1998).

ACKNOWLEDGMENTS

The NWRA authors gratefully acknowledge the National Aeronautics and Space Administration (under Contract Number NASW-4701) and the Office of Naval Research (under Contract Numbers N00014-92-C-0027 and N00014-96-C-0096) for funding this work. RSP gratefully acknowledges the Office of Naval Research (under Contract Numbers N00014-94-C-0215, N00014-96-C-0174, and N00014-98-C-0180) for funding this work.

REFERENCES

Coon, M. D., D. C. Echert, and G. S. Knoke, Pack ice anisotropic, constitutive model, *in IAHR 92, Proceedings of the 11th International Symposium on Ice*, p. 1188, Banff, Alberta, Canada, 1992.

Coon, M. D., G. S. Knoke, D. C. Echert, and R. S. Pritchard, The architecture of an anisotropic elastic-plastic sea ice mechanics constitutive law, *Journal of Geophysical Research*, Vol. 103, pp. 21,915–21, 925, 1998.

Cunningham, G. F., R. Kwok, and J. Banfield, Ice lead orientation characteristics in the winter Beaufort Sea, *in Proceedings of the International Geoscience and Remote Sensing Symposium*, Pasadena, CA, August, pp. 1747–1749, 1994.

Pritchard, R. S., Ice conditions on an anisotropic sea ice dynamics models, *International Journal of Offshore and Polar Engineering*, Vol. 8, No. 1, pp. 9-15. 1998.

Pritchard, R. S., and M. D. Coon, Canadian Beaufort Sea ice characterization, in POAC'81, *Proceedings of the Sixth International Conference on Port and Ocean Engineering under Arctic Conditions*, pp. 609-618, Université Laval, Quebec, Canada, 1981.

Stern, H. L., D. A. Rothrock, and R. Kwok, Open-water production in Arctic sea ice: satellite measurements and model parameterizations, *Journal of Geophysical Research*, Vol. 100, No. C10, pp. 20,601–612, 1995.

Thorndike, A. S., D. A. Rothrock, G. A. Maykut, and R. Colony, The thickness distribution of sea ice, *Journal of Geophysical Research*, Vol. 80, No. 33, November 20, pp. 4501-4513, 1975.

17th International Symposium on Ice
Saint Petersburg, Russia, 21 - 25 June 2004
International Association of Hydraulic Engineering and Research

THE APPLICATION OF PIV TO MEASUREMENT OF SEA ICE

Sun Hequan, Shen Yongming and Qiu Dahong[1]

ABSTRACT
The motion of sea ice has a great effect on winter navigation, oil field exploration in the Bohai Sea, and it is very important to measure the ice drift accurately and efficiently. Radar imagery has been used for sea ice monitoring and forecasting. Combining with the radar imagery and Particle Image Velocimetry (PIV), full field measurement of sea ice drift around the platform can be obtained, which is specified in detail in this paper. The theory and implementation of cross-correlation in PIV are presented briefly in the paper, including the filtering method to modify the invalid vectors, and some motion maps by cross-correlation are provided. Furthermore, the comparison with traditional tracing method is conducted in the paper to show deeply the validity of the application of PIV.

1. INTRODUCTION
In winter, freezing of sea occurs in the Bohai Sea and the north of the Yellow Sea in China. The sea ice drift has a great effect on the navigation of ships, the oil field exploration and the safety of the harbor structures and oil platform in the Bohai Sea. It is very important to monitor and forecast the sea ice drift. There are some practical methods to observe the sea ice motion including SAR facility (Kwok et al 1990), satellite passive microwave imagery and drift buoy (Kwok et al 1998, Meier et al 2001), marine radar imagery (Sun 1999, Yue et al 2000), airborne remote sensing (Zhang 1996) and so on. The marine radar imagery has been applied well to measure the sea ice around the oil platform in the Bohai Sea (Sun 1999, Yue et al 2000), since measurement in local area can be conducted with low cost.

Through the radar images, the growth and drift of the sea ice near the platform can be analyzed. In traditional way, the motion of sea ice can be obtained by tracing the sea ice's drifting trajectory in radar images. The radar system can be utilized to detect the sea ice in a local sea area, which is a valid method in the sea ice management (Yue, 2000). But, only the motion of big floe can be obtained because the big floe can be distinguished from the small ones in the radar images, and little information about ice motion is obtained by tracing method. It is hard to calculate the sea ice motion if there is no big floe in the field of radar imaging. With the help of cross-correlation technique of PIV system (Adrian,

[1] State Key Laboratory of Coastal and Offshore Engineering, Dalian University of Technology, Dalian 116023, China, e-mails: hqsun@dlut.edu.cn, ymshen@dlut.edu.cn and qiudh@dlut.edu.cn

1991, Westerweel, 1997), this problem can be solved easily and more information can be extracted from the radar ice images.

PIV is well-known as a non-intrusive, full field optical measuring technique based on cross-correlation to obtain velocity information about fluid motion and has been applied to a diverse range of flows including water dynamics, aerodynamics, air-conditioning systems, acoustics, blood circulation and boundary layer turbulence. With the development of computer science and image technology, great progress of PIV has been made in recent years. PIV has been adapted for use in hydraulic-model studies of ice-movement problems (Ettema et al, 1997), and its application to measurement of sea ice from radar ice images will be specified in detail in this paper.

By applying cross-correlation in PIV to radar ice images, two dimensional distribution of sea ice drift can be obtained automatically and efficiently, which will be helpful for sea ice monitoring and forecasting. The theory and corresponding implementation of cross-correlation will be presented briefly in the paper, and the correction method by low pass filtering is also specified. The velocity maps and motion coefficients of sea ice obtained from the radar images grabbed in Liaodong Gulf are provided in the paper, and the comparison is also conducted with the traditional tracing method to show the validity of PIV methods.

2. ALGORITHMS IN PIV

The fluid motion of interest in PIV is made visible by adding small tracer particles. The flow velocity field can be ascertained accurately from the displacements of tracer particles at two instances of time. In this paper, the floe ices in radar images can be taken as the tracer particle and can be processed by cross-correlation.

2.1. Cross-correlation

In general, two images of tracer particles within a fluid are taken in a short time, Δt. It is not possible to track an individual particle, and a statistical analysis is required. If the first image at t_1 is assumed as $p(x, y) = I(x, y)$ to represent the pixel value, the second one at t_2JS$t_1 + \Delta t$, $q(x, y)$, should be $I(x + \Delta x, y + \Delta y)$ with the displacement of $(\Delta x, \Delta y)$ because Δt is very short. The cross-correlation function of $p(x, y)$ and $q(x, y)$, $r_{pq}(\tau_x, \tau_y)$ is defined as

$$r_{pq}(\tau_x, \tau_y) = \int_{-\infty}^{+\infty}\int_{-\infty}^{+\infty} p(x, y)q(x + \tau_x, y + \tau_y)dxdy =$$

$$= \int_{-\infty}^{+\infty}\int_{-\infty}^{+\infty} I(x, y)I(x + \Delta x + \tau_x, y + \Delta y + \tau_y)dxdy. \quad (1)$$

Meanwhile, the auto-correlation function of $I(x, y)$ is defined as

$$r_{pq}(\tau_x, \tau_y) = \int_{-\infty}^{+\infty}\int_{-\infty}^{+\infty} I(x, y)I(x + \tau_x, y + \tau_y)dxdy. \quad (2)$$

Then, $r_{pq}(\tau_x, \tau_y) = r(\tau_x + \Delta x, \tau_y + \Delta y)$.

It is known that the auto-correlation function is even and its maximum value is found at the original point. So, the maximum value of cross-correlation function can be found at $(-\Delta x,-\Delta y)$, that is $r_{pq}(\tau_x,\tau_y) \le r_{pq}(-\Delta x,-\Delta y)$.

The displacement during Δt can be obtained from the position of the maximum of cross-correlation function. Scaling this displacement with the magnification of the camera system and dividing by Δt, the actual velocity for the fluid can be obtained.

Evaluating the cross-correlation in the direct way sounds very complicated. By using the fast Fourier transform, it is significantly efficient.

The cross-correlation property of Fourier transform states that a cross-correlation in temporal domain is equivalent to a multiplication in frequency domain, mathematically,

$$R_F(u,v) = P_F^*(u,v) \cdot Q_F(u,v), \tag{3}$$

where $R_F(u,v)$, $P_F(u,v)$ and $Q_F(u,v)$ are the Fourier transforms of $r_{pq}(\tau_x,\tau_y)$, $p(x,y)$ and $q(x,y)$ respectively, and $P_F^*(u,v)$ denotes the complex conjugate of $P_F(u,v)$.

With the help of the above property and fast Fourier transform, the cross-correlation can be calculated quickly, and a new method based on the Hartley transform has been developed to get more efficiency (Sun, 2002).

In actual, each image is divided into a grid of small sections known as interrogation areas. The corresponding interrogation areas within each image are then cross-correlated, and the displacement between two areas is obtained. This process is repeated at each grid point within the images, resulting a map of velocity vectors to describe the flow.

2.2. Smoothness in Frequency Domain

The noise is produced by the wind and the waves on the sea surface in the process of radar imaging, and its influence can not be neglected. It is also important to find an effective method to smooth and correct the invalid vectors caused by noise or inhomogeneous distribution of tracer particles in the fluid or floe ices in the sea. An effective method is developed in the frequency domain through the reasonable construction of two components of velocity vector.

A velocity vector in (x,y) can be expressed as $\vec{V}(x,y) = (u(x,y), v(x,y))$ with two components, and a complex function can be constructed as

$$w(x,y) = u(x,y) + iv(x,y). \tag{4}$$

The Fourier transform of the validated function $\tilde{w}(x,y) = \tilde{u}(x,y) + i\tilde{v}(x,y)$ can be expressed as

$$\tilde{W}(\omega_x,\omega_y) = \begin{cases} W(\omega_x,\omega_y), \omega_x{}^2 + \omega_y{}^2 \le B^2 \\ 0, else \end{cases}, \tag{5}$$

where $W(\omega_x, \omega_y)$ is the Fourier transform of $w(x, y)$, B is the bandwidth of the filter. Since the tidal current is dominant for the sea ice motion, the motion of sea ice is directional in the measurement area. By selecting the value of B properly, most of invalid vectors in the velocity map can be validated or removed via the above algorithm. In the next section, the value of B is equal to the quarter of the maximum value of the frequency.

3. MEASUREMENT OF SEA ICE DRIFT

Table 1 Information of sea radar images and related values

Sequence	Image name	Imaging time	Tracing method	PIV method
1	R0000920	2002-01-09, 06:40:52	7cm/s, 206º	6.1cm/s,197º
	R0000922	2002-01-09, 06:59:04		
2	R0001351	2002-01-21, 15:43:07	15cm/s, 176º	12.9cm/s,169º
	R0001353	2002-01-21, 16:00:57		
3	R0001976	2002-02-09, 17:00:02	45cm/s, 213º	39.6cm/s,220º
	R0001977	2002-02-09, 17:06:45		
4	R0002004	2002-02-10, 09:05:28	34cm/s, 209º	33.5cm/s,205º
	R0002005	2002-02-10, 09:11:14		

From December, 2001 to February, 2002, the researchers of China National Marine Environmental Monitoring Center established an observation station at the DPRW platform of JZ9-3 oil field in the Liaodong Gulf to observe the sea ice through marine radar FURUNO-1830 with X band, 3 cm of wavelength, 9410 ± 30 MHz of work frequency, 0.3 μs of impulse width, 1200 Hz of repeat frequency and 0.75 n mile of radius.

Many radar ice images were grabbed during three months. Some images were processed by the cross-correlation and the smoothness method, then the velocity vector maps were obtained. The detailed information of four pairs of radar ice images is in Table 1, and Figs 1, 2, 5 and 6 are the radar ice images listed from 1 to 4. Before cross-correlation, the color images should be converted to monochrome images, and the relationship between grey level value and three components of true color is expressed as follows.

$$Greylevel = \mathrm{Re}\, d \times 0.30 + Green \times 0.59 + Blue \times 0.11 \qquad (6)$$

Figs 3, 4, 7 and 8 are the vector maps obtained from the cross-correlation of two corresponding radar ice images, which have been smoothed by low pass filtering in frequency domain. The circle in the center of maps show the center of the radar image where the radar system is located.

By tracking a big floe in the border of radar ice images, its displacement was measured, and the result at the tracing point was obtained. Then, the comparison between PIV

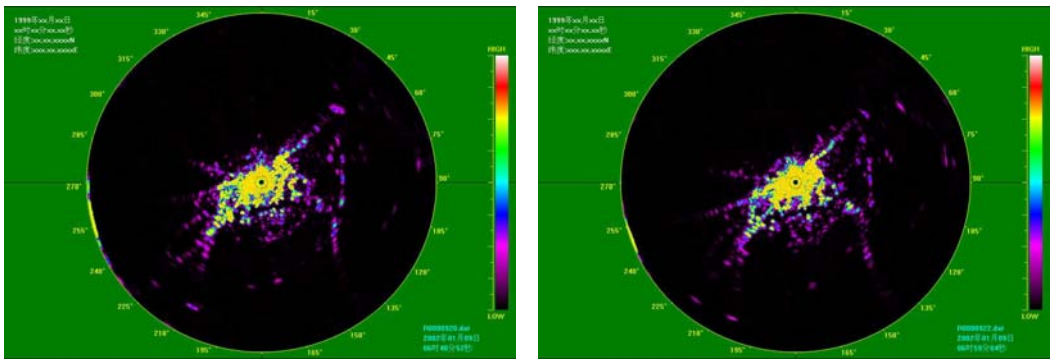

Fig.1. Radar ice images: R0000920 and R0000922

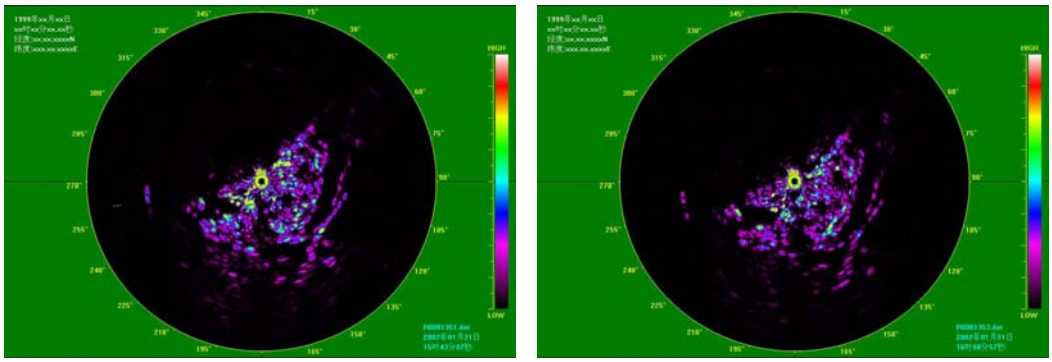

Fig.2. Radar ice images: R0001351 and R0001353

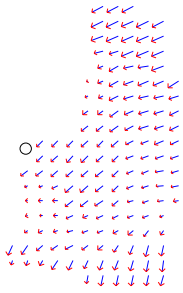

Fig.3. Velocity vector maps in Fig.1

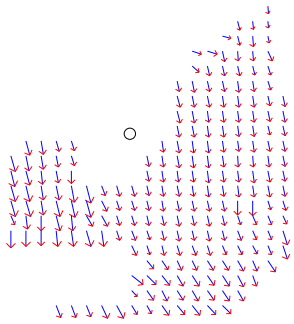

Fig.4. Velocity vector maps in Fig.2

method and the tracing method can be conducted. Through the displacements in the PIV vector maps and the imaging interval, the average velocity at the tracing point can be obtained. The velocity and moving direction in four pairs of images are listed in Table 1, which are calculated by two methods. The direction is calculated according to the convention of radar images. That is, the direction of zero angle is upwards and the angle increases along clockwise direction. From the values in Table 1,it is shown that the values at the tracing point by the PIV method coincide well with those by the tracing method.

Considering the flying-off and landing helicopter on the platform, the radar system was not installed at the highest place. Then, there is nothing at top right of radar ice images and velocity vector maps because the radar signal was sheltered by the building of the platform.

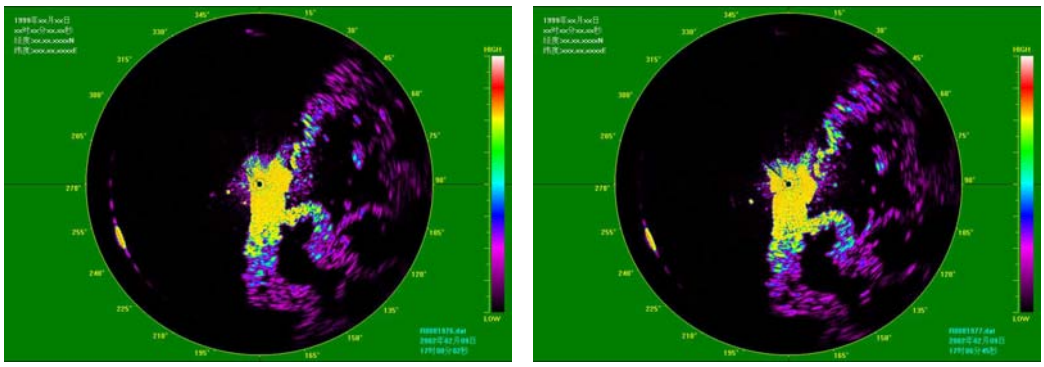

Fig.5. Radar ice images: R0001976 and R0001977

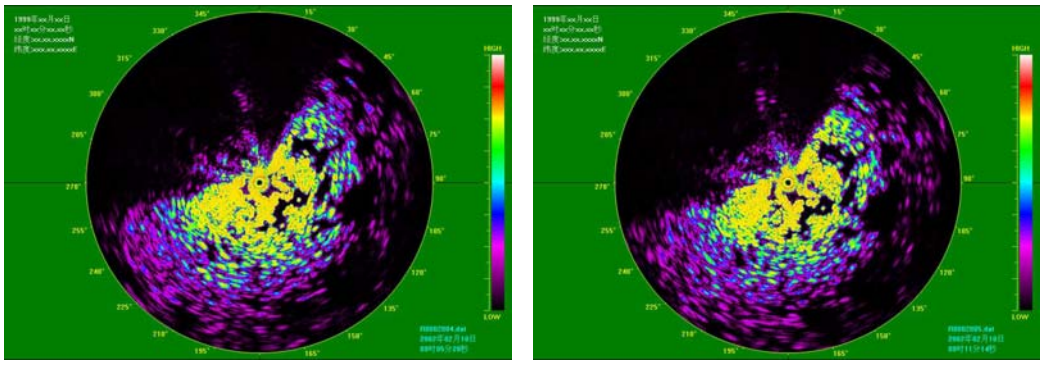

Fig.6. Radar ice images: R0002004 and R0002005

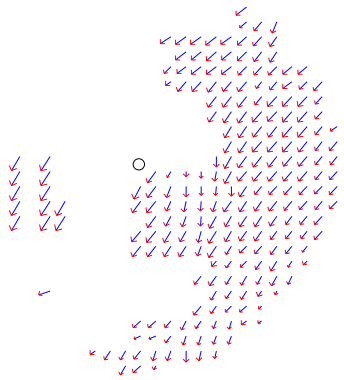

Fig.7. Velocity vector maps in Fig.5

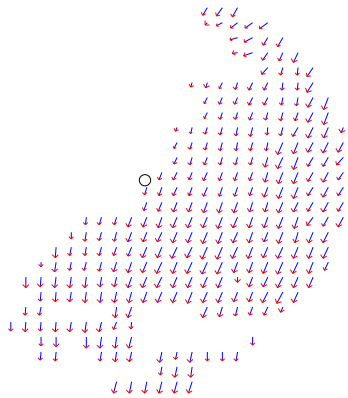

Fig.8. Velocity vector maps in Fig.6

4. CONCLUSIONS

PIV is a non-intrusive, full field optical measuring technique based on cross-correlation and has been applied to a diverse range of flows. By applying the cross-correlation technique in PIV to the radar ice images , full field measurement of sea ice drift around the platform can be obtained automatically and efficiently, then sea ice motion can be monitored and forecasted accurately, which is very helpful for the navigation of ships, the oil field exploration near the platform and the safety of the platform in winter. The velocity vector maps obtained from the cross-correlation of radar images grabbed in Liaodong Gulf are provided in the paper. Furthermore, To show the validity of the

application of PIV, the comparison between the PIV method and the tracing method is conducted, which the values of velocity by PIV method coincide well with those by the tracing method to track the big floe at the border of the radar images.

ACKNOWLEDGEMENTS

We thank Sun Y. W. very much for providing us the radar ice images and the values of velocity obtained by the tracing method.

This research is sponsored by the National Science Fund for Distinguished Young Scholars under Grant No.50125924 and by the National Natural Science Foundation of China under Grant Nos. 50379001 and 10332050.

REFERENCES

Adrian R. J., 1991, Particle-imaging techniques for experimental fluid mechanics,' *Ann. Rev. Fluid Mech*., Vol. 23, 261.

Ettema R., 1997, Fujita I., Muste M. and Kruger A., Particle-image velocimetry for whole-field measuremnt of ice velocities, *Cold Regions Science and Technology*, Vol. 26, 97.

Kwok R., 1990, Curlander J. C., McConnell R. and Pang S., An Sea ice motion tracking system at Alaska SAR facility, *IEEE J. Oceanic Engineering*, Vol. 15, No. 1, 44.

Kwok R., 1998, Schweiger A., Rothrock D. A., et al, Sea ice motion from satellite passive microwave imagery assessed with ERS SAR and buoy motion, *Journal of Geophysical Research*, Vol. 103, No. C4, 8191.

Meier W. N., 2001, Maslanik J. A., Improved sea ice parcel trajectories in the arctic via data assimilation, *Marine Pollution Bulletin*, Vol. 42, No. 6, 506.

Sun H. Q., 2002, Hartley Transform Applied to Particle Image Velocimetry, *Measurement Science and Technology*, Vol. 13, No. 12, 1996.

Sun Y. W., 1999, A radar monitoring system for surveying sea ice and wave, *Marine Forecasts*, Vol. 16, No. 3, 57.

Yue Q. J., 2000, Bi X.J., Ji S.Y., Zhang T., Recognition and tracing of sea ice by marine radar on a fixed oil/gas platform, *Journal of Dalian University of Technology*, Vol. 40, No. 4, 500.

Westerweel J., 1997, Fundamentals of digital particle image velocimetry, *Measurement Science and Technology*, Vol. 8, No. 12, 1379.

Zhang N. S. ,1996, A brief description of the real-time transmitting system for airborne remote sensing of disasterous sea ice, *Ocean Technology (China)*, Vol. 15, No. 2, 6.

17th International Symposium on Ice
Saint Petersburg, Russia, 21 - 25 June 2004
International Association of Hydraulic Engineering and Research

ON THE ANNUAL VARIATION OF CHARACTERISTICS OF SNOW AND ICE IN LAKE SAROMA

T. Kawamura[1], K. Shirasawa[2], M. Ishikawa[2], T. Takatsuka[2], T. Daibou[2] and M.Lepparanta[3]

ABSTRACT

Lake Saroma is a semi-enclosed embayment connected with two openings to the Sea of Okhotsk. River water inflow causes a gradual change in the salinity of the lake water body providing excellent conditions to study the role of salt in freezing processes. Sea ice studies have been conducted at five points on a line from a river mouth to one opening since 1997. One aim is to clarify the annual variation of the sea ice structure and the contribution of snow to the sea ice growth. The snow and sea-ice thickness data suggests the shore would cause spatial variations. The ice structure shows a significant annual variability, which strongly depends on the surface seawater condition. Different ice thickening processes were found from structural and oxygen isotopic observations.

INTRODUCTION

Lake Saroma is a semi-enclosed embayment connected with two openings to the Sea of Okhotsk. Most of the lake surface is covered with sea–ice during winter. Freshwater input, which is mainly supplied by two major rivers, causes a reduction of the salinity to less than 32 psu (Practical Salinity Unit = 1/1000) and a gradual decrease of water salinity toward the river mouths. This salinity decrease provides excellent conditions to study the role of salt in freezing processes.

Sea ice studies have been conducted in Lake Saroma since 1997 to investigate the following items: (1) The change of sea ice structure with the salinity of the parent water, and (2) The contribution of structural ice types. The contribution of snow to sea ice growth has attracted special interest in the Antarctica (e.g., Lange and others, 1990; Eicken and others, 1994; Jeffries and others, 1994, 1997) and it has also been included in the Finnish-Japanese co-operative project “Ice Climatology of the Okhotsk and Baltic Seas” (Kawamura et al., 2001, 2002; Granskog et al., 2004).

This report mainly gives an outline of the snow and sea ice properties in Lake Saroma, the ongoing observational programme, and first results.

[1] Institute of Low Temperature Science, Hokkaido University
[2] Sea Ice Research Laboratory, Institute of Low Temperature Science, Hokkaido University
[3] Division of Geophysics, University of Helsinki

OBSERVATIONS

We set up five observation sites on a line from the mouth of the Saromabetsu River, the largest river of Lake Saroma, to the opening in the eastern part of the lake (Figure 1). The water depth is about 2-3 meters at Site 1 and gradually increases to about 10 meter at Site 2, approaching to 12 meters to Site 5.

In this observation programme we have collected the following data at several times during the ice season: (1) Sampling of snow, sea ice and seawater, (2) In-situ measurement of the temperature of snow and sea ice of at several depths, and the density of snow, (3) In-situ measurement of temperature and salinity profiles in the water, (4) Structural analysis and density measurement of the sampled sea ice in a cold laboratory, and (5) Determination of the salinity and oxygen isotopic composition ($\delta^{18}O$ value) of the melted snow and sea ice samples together with seawater.

We used some of long-term meteorological data recorded at the cape of Kimuaneppu since 1989 (Fig. 1, K).

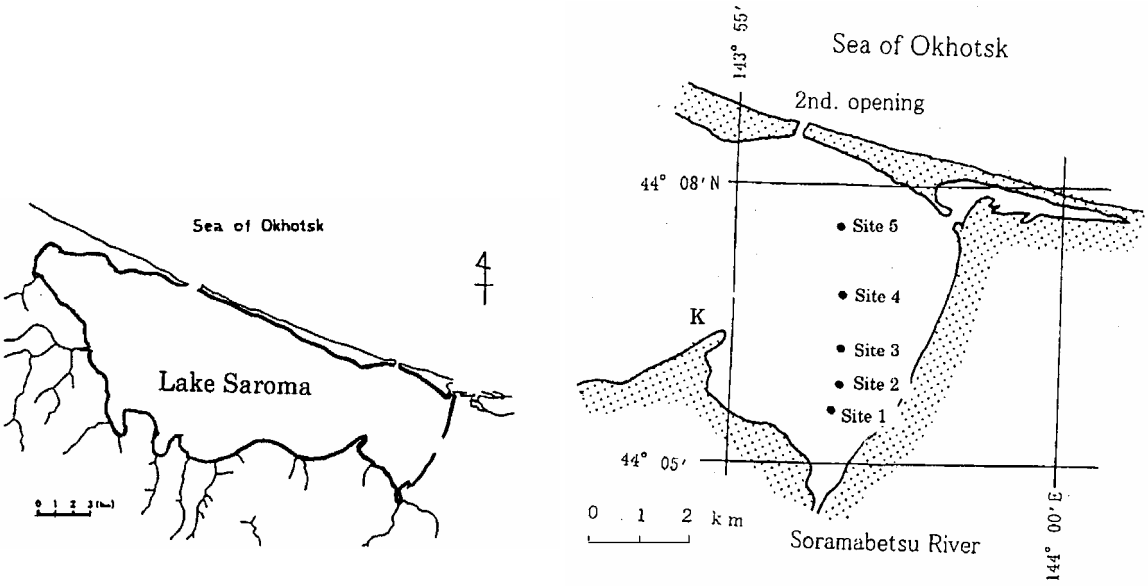

Fig. 1. Location of observation sites. K: Kimuaneppu meteorological observation site

RESULTS AND DISCUSSION

Figure 2 shows the water salinity both just under the ice bottom and at the depth of 5 m for the five observation sites. The salinity at the ice bottom increases steadily from approximately 5 psu at Site 1 to 25 psu at Site 5 with its large annual variability, showing a sharper front structure in some years. At 5 m depth, on the contrary, an almost constant salinity of about 30 psu was observed at Sites from 2 to 5, while near the lake bottom at Site 1 a large interannual variability from 20 to 30 psu was obtained. A similar spatial salinity variation was obtained at the last observation period as the first one as shown in the figure.

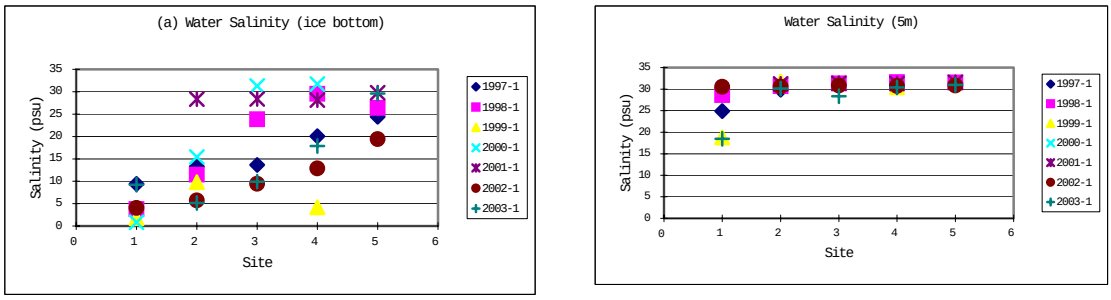

Fig. 2. Spatial variation of water salinity at (a) ice bottom and (b) 5 m depth

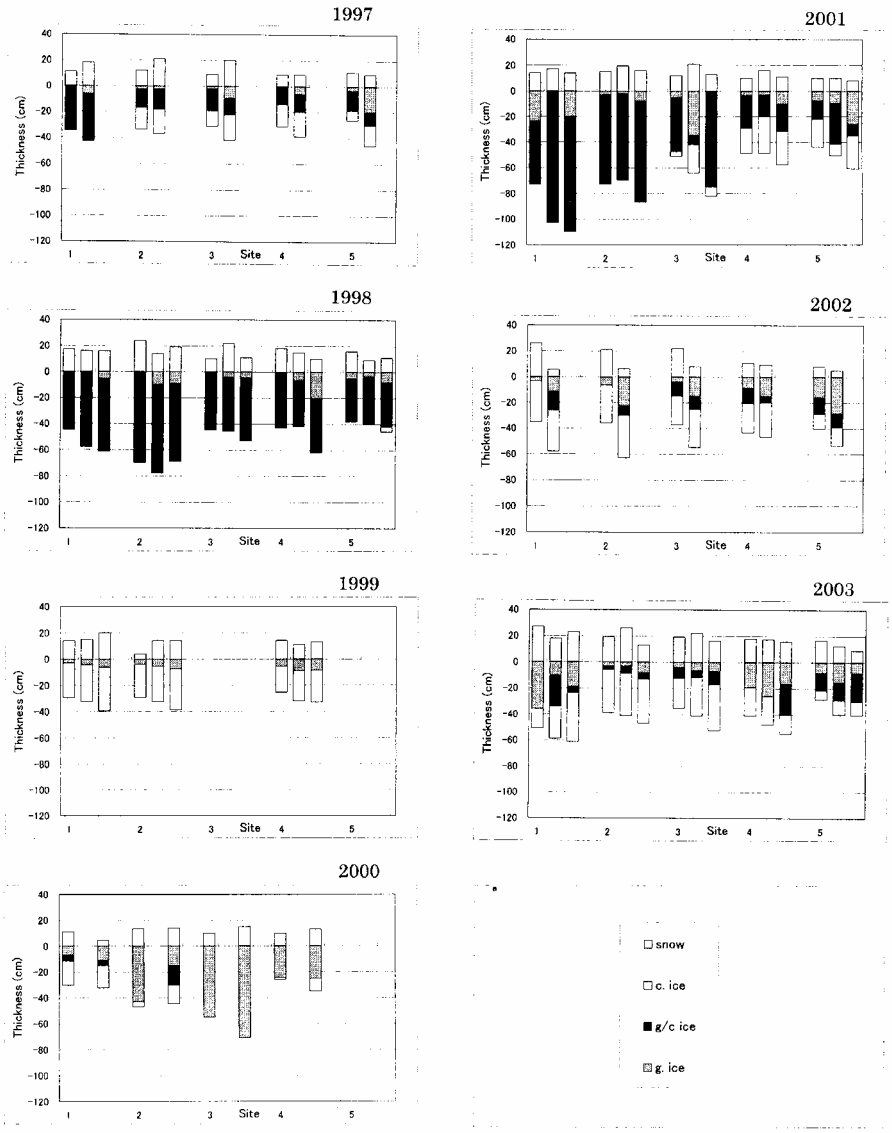

Fig. 3. Variation of snow and sea ice conditions from 1997 to 2003

Variations of snow depth and sea-ice thickness

Figure 3 shows temporal variations of snow depth and sea-ice thickness at Sites 1-5 from 1997 to 2003.

In general, the snow depth increases with the passage of time. Sites 1-3 in 1997 show a typical example of this trend. However, converse cases, where the snow depth decreases with time, were observed at Sites 1-3 in 2002 for example. Then the snow cover is transformed into a snow ice layer on the surface as will be discussed below.

The spatial variation of the snow depth shows a general decreasing trend from Site 1, the nearest site to the river mouth, to Site 5, the farthest one (Fig. 4a). This variation is likely caused by the shore; nearer to the shore more snow accumulates due to drift while farther from the shore the wind blows much of the snow away.

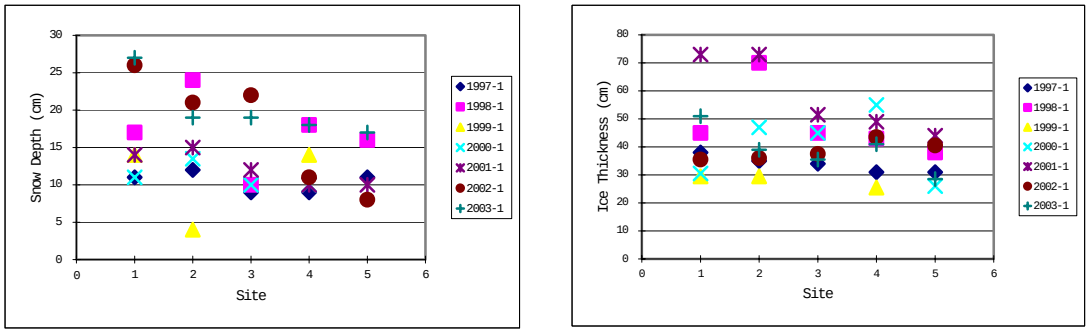

Fig. 4. Spatial variations of (a) snow depth and (b) ice thickness

Now we will consider the variation of sea-ice thickness. The sea ice grew steadily with time in our observation periods. Spatially the sea ice thickness decreased in general from Site 1 to Site 5 (Fig. 4b), similarly but not as remarkably as the snow depth. Therefore the sea ice thickness corresponds to the snow depth especially at the first observation date each year (see Fig. 3). The positive correlation between the snow and ice thicknesses could be due to the age of the ice or due to the production of snow ice.

In Figure 3, the contribution of different ice types is also found. The classification has been made according to Eicken and Lange (1989) and includes three types: granular, columnar and mixed granular/columnar (g/c) ice, an intermediate state resulting from oscillations between the granular and columnar ice growth modes. The figure shows a large annual variability in the ice type contributions. In 1997, 2002 and 2003, the ice was composed of granular ice, g/c ice and columnar ice in the upper, middle and lower layers, respectively, with some exceptions. In 1999 the ice sheet had a simple structure of upper granular ice and lower predominantly columnar ice. In the following year, granular ice was generally predominant; especially the whole thick ice sheet at Site 3 consisted of granular ice. However, no systematic spatial variation was found. In 1998 and 2001, g/c ice contributed significantly to the ice growth. This large contribution may be explained by differences in the conditions between these winters and the others. Eicken and Lange (1989) proposed the formation of the g/c ice type to be related to i) incorporation of frazil ice into the growing ice sheet, ii) enhanced growth rates due to changes in atmospheric conditions, and iii) changes in the hydrographic regime at the ice-water interface.

Table 1 shows the sums of the east component of the daily mean wind velocity (referred to as the sum of east wind component hereafter) for every ten days in the early winter. The sum of east wind component was obtained as follows: First the daily mean east component of the wind velocity was calculated from the wind speed and direction data at every 10 minutes, and then the positive components were integrated for every ten days. In 1998 and 2001, when g/c ice was predominant, the sum of east wind component was recognized to be large in the first ten days of January when the wind might cause a dynamic condition suitable to create the granular ice or g/c ice. The east component could transport and then accumulate the ice at the observation sites. Our observations of the g/c ice formation were made in the presence of dynamic conditions in the water column, which gives i) or iii) as possible explanation. Such dynamic sea ice growth process was also proposed by Granskog et al. (2003, 2004) to account for g/c ice formation in the Baltic Sea. A large sum of east wind component was also obtained at the same decade in 1999, but no predominant g/c ice was observed then. Therefore, the result suggests that other factors than the strong wind, such as hydrographical state, would effect the formation of g/c ice.

Table 1: Sums of the east component of the daily mean wind velocity for every ten days in the early winter

Year	Previous December			Present January		
	1st	2nd	3rd	1st	2nd	3rd
1997	19.5	24.7	39.8	26.7	22.0	42.5
1998	20.2	26.1	34.7	44.2	27.5	22.7
1999	32.3	33.6	44.8	54.4	29.2	32.3
2000	42.5	22.8	16.7	15.9	19.0	28.8
2001	43.8	34.3	46.7	40.6	26.5	16.1
2002	44.4	51.1	31.4	17.7	19.8	14.8

The sea ice grew steadily with time as described previously. Different thickening processes were realized as follows: (1) Upward growth by surface granular snow ice, typical examples are found at all sites in 2002; (2) Downward growth by columnar ice, e.g. at all the site in 1999 and Site 3 in 1997, 2002 and 2003; and (3) Downward growth by g/c ice or granular ice, e.g. at all the sites in 1998 and at Site 3 in 2000, respectively.

Sea ice properties

We will present an example for each structural profile together with the salinity and oxygen isotopic composition of sea ice to discuss the thickening processes and its possible origins.

Figure 5 shows the profiles of the first (a) and the second (b) observations at Site 5 in 2002. The change of the heights of the snow stake and snow thickness indicates about 150 mm upward ice growth. Judging from the low $\delta^{18}O$ values, the upper layer was originated from snow and seawater, i.e. snow ice. Thus these two methods agree very well. The decrease of the snow cover was estimated at about 30 mm during the period between the measurements. Therefore, newly accumulated snow was also transformed into snow ice.

During the same period, a significant decrease in snow thickness, about 200 mm, was observed at Sites 1-3 (Fig. 3). Upward growth by snow ice formation would be expected to have taken place, and actually the snow stake and snow-thickness measurements proved this. However, the upper ice layer at these sites has higher $\delta^{18}O$ values, rather close to those of the lower columnar ice layer or seawater as shown in Fig. 6. Although the higher $\delta^{18}O$ values suggest that the upper ice is made of seawater, it is difficult to

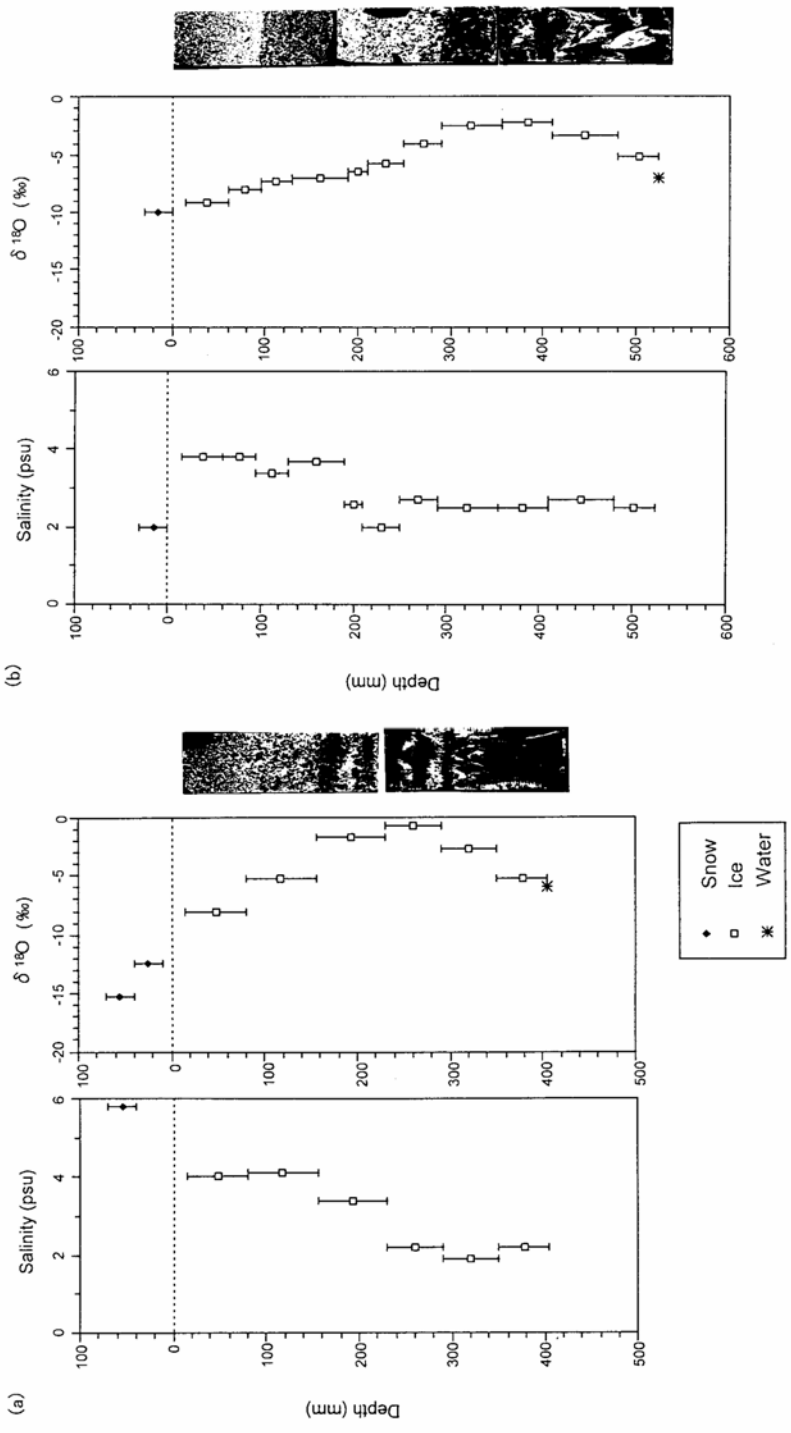

Fig. 5. Profiles of structure, salinity and isotopic composition of sea ice collected at Site 5 (a) in the 1st and (b) 2nd observation in 2002

imagine such pure sea ice growth upward on the existing ice surface. It is therefore possible that the water permeating into snow cover could have had a much higher $\delta^{18}O$ value, when the snow ice was formed. However, the true reason remains unsolved.

In the same year at Site 3, the lower columnar ice layer as well as the upper granular layer thickened significantly (Fig. 3). The $\delta^{18}O$ values of the columnar ice were slightly higher than those of the seawater (Fig. 6), indicating an increase by fractionation during freezing.

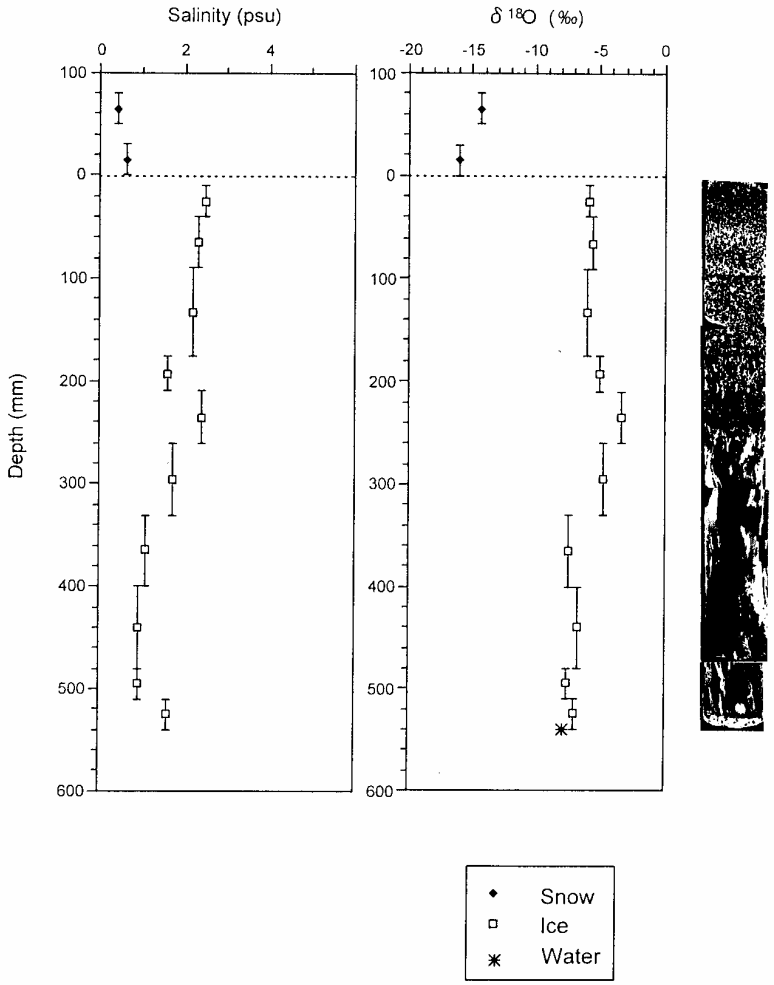

Fig. 6. Profiles of structure, salinity and isotopic composition of sea ice collected at Site 3 in the 2nd observation in 2002

Downward growth by g/c ice was found at all the sites in 1998 (Fig. 4). The profiles of one typical example at Site 3 are shown in Figure 7. The higher $\delta^{18}O$ values than those in the snow cover suggest that almost the whole ice layer was made of seawater, e.g. frazil ice with intermediate granular/columnar structure. The whole ice layer had higher $\delta^{18}O$ values; especially those of the middle layer are beyond the maximum fractionation of 3.0 ‰ (e.g., Craig and Hom, 1968), which probably reflects seawater values when the ice has been formed.

Since the salinity at the ice bottom increases steadily on the observation line (cf. Fig. 2), it is expected an effect of salt on ice structure formed; i.e. transition from fresh-water ice to sea ice. However, the all ice samples of this study have sea ice structure

characterized by columnar structure with jagged grain boundaries and sub-structure in the grains (Weeks and Ackley, 1982). Field observations (Palosuo, 1961; Kawamura et al., 2002) and a laboratory study (Weeks and Lofgren, 1967) showed the transition occurred at about 1 psu. In this study, even the closest site to the river mouth, the water salinity at the ice bottom was observed to be about 1 psu at least. A site with lower salinity was too shallow to obtain ice samples.

It should be noted that a mass of dendritic ice platelets was found attached loosely on the bottom of the sea ice at site 1 almost every year. These platelets, whose approximate size was 5-10 mm in width and 1-2 mm in thickness, had their crystallographic basal plane on the plate itself. It is likely that the existence of the platelets is related to the river water since they were observed only at the nearest site to the river mouth. It is worthwhile investigating its extent and formation process. Judging from the structure of the ice collected at Site 1, they were not included in the sea ice matrix. Thus the reason is also interesting.

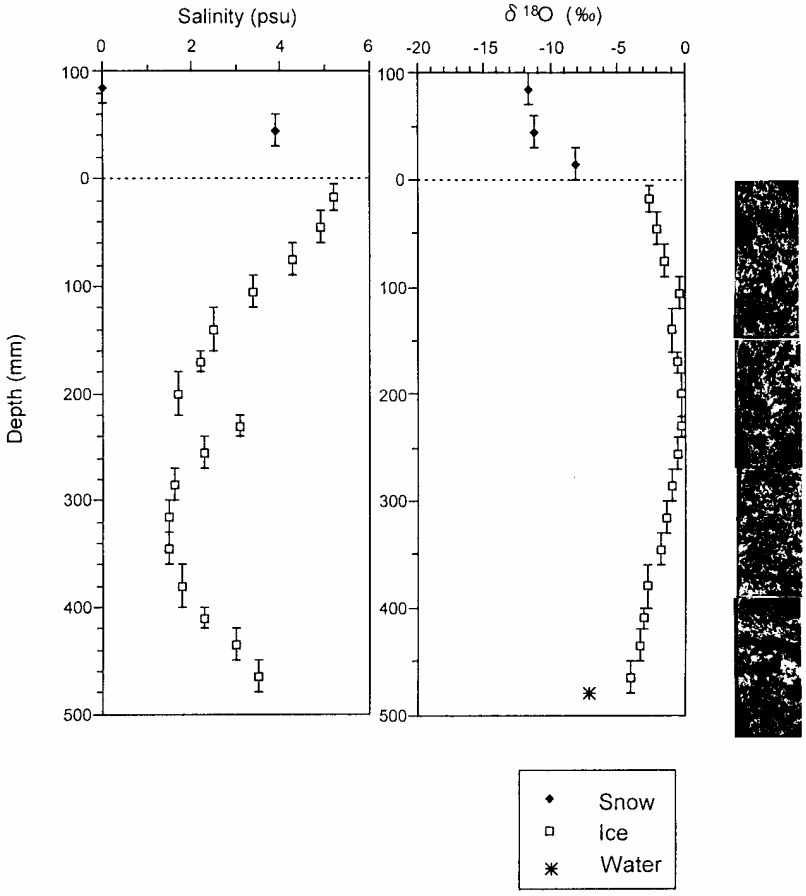

Fig. 7. Profiles of structure, salinity and isotopic composition of sea ice collected at Site 3 in the last observation in 1998

SUMMARY

Sea ice studies have been conducted in Lake Saroma since 1997 to clarify the annual variation of the sea ice structure and the contribution of snow to the sea ice growth. River water inflow causes a gradual change in the salinity of the lake water, and further influences the role of salt in freezing processes. However, we could not found such the

influence. The snow and sea-ice thickness data suggests the shore would cause spatial variations. A significant annual variability of the ice structure or the contribution of different ice types strongly depends on the surface seawater condition. Three different ice thickening processes were found from structural and isotopic observations; upward growth by surface granular snow ice, downward growth by columnar ice and downward growth by g/c ice or granular ice. A mass of dendritic ice platelets was found at the inshore site almost every year.

ACKNOWLEDGMENTS

We wish to thank the personnel of the Saroma Research Center of Aquaculture in Sakaeura for their kind offers to use their facilities. Part of this research was supported by the scientific research funds from the Japanese Ministry of Education, Culture, Sports, Science and Technology (Nos. 09680498 and 13490002; the supervisor is Dr. Kawamura, Hokkaido University, and No. 09308019; the supervisor is Prof. M. Takahashi, University of Tokyo). Matti Lepparanta was supported by the Institute of Low Temperature Science in 2003 for his research in Japan.

REFERENCES

Craig, H. and Hom, B. Relationship of D, ^{18}O and chlorinity in the formation of sea ice. *Trans. Am. Geophys. Union 49*▯ ▯ ▯ : 216-217 (1968)

Eicken, H. and Lange, M.A. Development and properties of sea ice in the coastal regime of the southern Weddell Sea. *J. Geopyhs. Res. 94*▯ *C6*▯ : 8193-8206 (1989).

Eicken, H., Lange, M.A., Hubberten, H.-W. and Wadhams, P. Characteristics and distribution patterns of snow and metric ice in the Weddell Sea and their contribution to the mass balance of sea ice. *Ann. Geophysicae 12(1)*: 80-93 (1994)

Granskog, M.A., Leppäranta, M., Kawamura, T., Ehn, J. and Shirasawa, K. Seasonal development of the properties and composition of landfast sea ice in the Gulf of Finland, the Baltic Sea. *J. Geophys. Res.*: (2004) in press.

Granskog, M.A., Martma, T. and Vaikmäe, R. Development, structure and composition of landfast sea ice in the northern Baltic Sea. *J. Glaciol. 49(164)*: 139-148 (2003)

Jeffries, M.O., Shaw, R.A., Morris, K., Veazey, A.L. and Krouse, H.R. Crystal structure, stable isotopes, and development of sea ice in the Ross, Amundsen, and Bellingshausen seas, Antarctica. *J. Geophys. Res. 99(C1)*: 985-995 (1994)

Jeffries, M.O., Worby, A.P., Morris, K. and Weeks, W.F. Seasonal variations in the properties and structural composition of sea ice and snow in the Bellingshausen and Amundsen seas, Antarctica. *J. Glaciol. 43(143)*: 138-151 (1997)

Kawamura, T., Shirasawa, K., Ishikawa, N., Lindfors, A., Rasmus, K., Granskog, M.A., Ehn, J., Leppäranta, M., Martma, T. and Vaikmäe, R. Time series observations of the structure and properties of brackish ice in the Gulf of Finland, the Baltic Sea. *Ann. Glaciol. 33*: 1-4 (2001)

Kawamura, T., Granskog, M.A., Ehn, J., Martma, T., Lindfors, A., Ishikawa, N., Shirasawa, K., Leppäranta, M. and Vaikmäe, R. Study on brackish ice in the Gulf of Finland. *Proc. 16th IAHR Symp. on Ice*, Dunedin, New Zealand (2002) 165-171.

Lange, M.A., Schlosser, P., Ackley, S.F., Wadhams, P. and Dieckmann, G.S. ^{18}O concentrations in sea ice of the Weddell Sea, Antarctica. *J. Glaciol. 36(124)*: 315-323 (1990)

Palosuo, E., The Gulf of Bothnia in winter. II. Freezing and ice forms. *Merentutkimuslait. julk./Havsforskningsinst. Skr. 209*. 42-64 (1963).

Weeks W.F. and Ackley, S.F. The growth, structure and properties of sea ice. *CRREL Monograph 82-1* (1982) 130 p.

Weeks, W.F. and Lofgren, G., The effect solution distribution coefficient during the freezing of NaCl solutions. In *Physics of Snow and Ice*, H.Oura ed. Inst. Low Temp. Sci., Sapporo 579-597 (1967).

17th International Symposium on Ice
Saint Petersburg, Russia, 21 - 25 June 2004
International Association of Hydraulic Engineering and Research

ANALYSIS METHODS OF ICE IMAGES DURING THE SECOND CHINESE NATIONAL ARCTIC RESEARCH EXPEDITION

Zhijun LI[1], Peng LU[2], Xilu DONG[3]

ABSTRACT

In the Second Chinese National Arctic Research Expedition (CHINARE) during July and August, 2003, the expedition area covered the latitude range of 72°N-80°N and the longitude range of 169°W- 150°E. A set of sea ice digital videos and photos along the investigation route was obtained by means of a digital video fixed on the side of *R/V Xuelong* and a digital camera fixed on the helicopter. This paper presents the methods of obtaining sea ice thickness and concentration from the digital images. And using these methods, the distribution of ice thickness and concentration along the route of CHINARE-2003 is obtained, which can provide the basic parameters for the state of sea ice characters along the investigation route and the farther research of the coupled atmosphere-sea ice-ocean model in the Arctic Region.

INTRODUCTION

The Arctic Ocean is one of the important cold sources on the earth, which affects global climate and ocean circulation seriously. Its interaction with the global climate system is represented by sea ice, which is the main character on the surface of the Arctic Ocean (Aagaard, et al., 1989). Firstly, sea ice plays a pivotal role in the heat and mass balance on the surface of the Arctic Ocean. Sea ice not only obstructs the heat exchange between atmosphere and ocean, but also reflects most solar radiation back to atmosphere because of its higher albedo (Greuell, et al., 2002). Secondly, seawater freezing, sea ice melting and movement affect the global water circulation. It is just the movement of sea ice, especially which inside the Arctic Ocean and transport outside, that provides a direct relation between sea ice and ocean (Lemke, et al., 1997).

To research the sea ice physical process and the coupled atmosphere-sea ice-ocean model, the basic parameters such as ice thickness and concentration are absolutely necessary. The direct method to obtaining these parameters is in situ measurement, but because of

[1] State Key Laboratory of Coastal and Offshore Engineering, Dalian University of Technology, 116024 Dalian, China. E-mail: lizhijun@dlut.edu.cn
[2] State Key Laboratory of Coastal and Offshore Engineering, Dalian University of Technology, 116024 Dalian, China. E-mail: xioshui@163.com
[3] School of Electronics and Information Engineering, Dalian University of Technology, 116024 Dalian, China. E-mail: dong_xl2000@163.com

the hostile climate in the polar regions which minimizes human activity, the amount of in situ validation data is limited (Richard, et al., 2002). As a result satellite observations have been employed to obtain areal coverage of the polar regions (Gennady, et al., 2002). Of particular interest are those satellite observations made in the microwave part of the electromagnetic spectrum due to the ability to obtain data independent of solar luminance and atmosphere conditions. The complex nature of the interaction of microwaves, and in particular microwaves from active systems, can make data analysis difficult.

With the development of digital photograph, ship-based video and aerial remote sensing are employed to record ice conditions in polar regions expeditions (Stern, et al., 1995). Comparing with the satellite data, these digital images have a higher resolution, and they record some ice characters in small scale which can not be obtained from satellite data in geophysical scale. Therefore, these digital images can provide supplemental information of ice characters in some cases and help to improve the precision of satellite data (Garcia, et al., 2002).

In the First Chinese National Arctic Research Expedition (CHINARE-1999), digital photography had been employed to sea ice observations (Zhao, et al., 2000). In the CHINARE-2003, shipboard videos and aerial photos were used for collecting sea ice states along the investigation route. These images had a high pixel resolution, and corresponding longitudes and latitudes were recorded synchronously. This paper is to discuss the methods of obtaining ice thickness and ice concentration from the images.

OBTAINING ICE THICKNESS

When a ship sails in the sea area infested by ice, the floating ice can be broken up and reversed under the shipboard, the cross section of the broken ice may come out of water, and the digital video fixed on the shipboard catches this status. Hence, the thickness of the broken ice can be obtained from the image (Worby, et al., 1996b). In CHINARE-2003, to collect ice thickness distribution along the investigation route, a digital video SONY 18E was fixed on the shipboard of *R/V Xuelong*, whose schema is shown in Fig.1. The recording area covered the latitude range of 74.11^{o}N-78.14^{o}N and the longitude range of 169.17^{o}W- 149.33^{o}W, all videos lasted 3052s. To get the absolute value of ice thickness, a fresh red ball was hung near the waterline of the ship as a reference substance, of course which was shot by the video recorder, and its diameter was known in advance. A sample of the image containing ice thickness information is shown in Fig.2. The idiographic method is as follows. Firstly, mark the thickness of the ice cross section and the diameter of the reference ball on the image, as which is shown in Fig.2, where *AB* is the ice thickness, *BC* is the thickness of the snow on the ice, and *DE* is the diameter of the reference ball. Secondly, record the coordinates of end points of the lines marked above, the points are *A*, *B*, *C*, *D* and *E* in Fig.2. The coordinates obtained from images are relative, the unit of which is pixel. Thirdly, calculate the distances of *AB*, *BC* and *DE* on the image using the distance formula of two points. Finally, the actual diameter of the ball is defined as *d*, according to the similarity criterion; the actual thickness of the ice is $AB \bullet d / DE$, likewise, the actual thickness of the snow on the ice is $BC \bullet d / DE$.

Because the digital video has a acquisition frequency of 16Hz, a same cross section of broken ice can be shot for many times. Therefore, in analysis process, thicknesses of the

same cross section in different space can be measured from these different images respectively; the average value of these thicknesses is treated as the actual thickness of this ice floe.

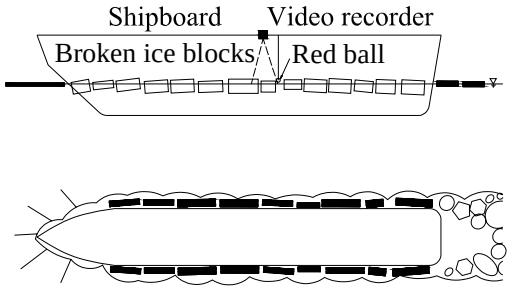

Fig.1. Digital video fixed on shipboard

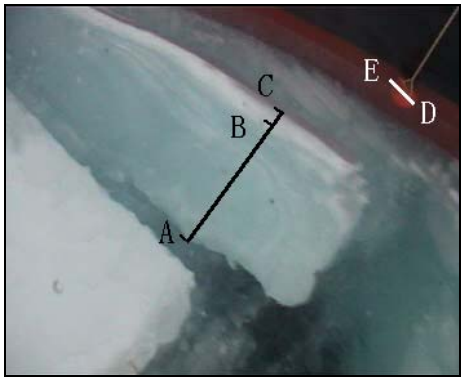

Fig.2. Image from shipboard video

When ship is sailing and in situ drilled measurements can not be performed, these ship-based videos can help record ice thickness information. They are supplemental data to the whole ice thickness distribution. Comparing to the traditionary observation by eyes, the ship-based video method avoids the randomicity of person estimate, the results of which are objective and quantitative. Moreover, because of the employment of digital technology, the precision of this method is much higher than traditionary observation by eyes.

OBTAINING ICE CONCENTRATION

In CHINARE-2003, a digital camera Canon G2 was fixed on the helicopter, the sea ice state below the helicopter was recorded while the helicopter was flying. The digital photos totaled to 4619, covered the latitude range of 75.02^{o}N-79.56^{o}N and the longitude range of 144.17^{o}W-169.59^{o}W, and had a high pixel resolution of 2272×1704, as a sample of which is shown in Fig.3.

The aerial photos contain the information of ice types, states of water leads, characters of broken ices around ice floes, distribution of ice ridges and melt ponds on sea ice, etc.
But ice concentration is the most important parameter in satellite sensing and numeric simulation (Thorsten, et al., 2003), so we obtain ice concentrations from these aerial photos firstly. Total ice concentration is an estimate of the total area covered by all types of ice, expressed in tenths, and entered as an integer between 0 and 10. In regions of very high ice concentration (95–99%) where only very small cracks are present, the recorded value should be 10 and the open water classification should be 1 (small cracks). Regions of complete ice cover (100%) will be distinguished by recording an open water classification of 0 (no openings) (Worby, 1999). Hence, if ice and water are distinguished from the photo, ice concentration can be worked out. Because the reflectance of ice and water is not the same in a photo, it is easy to distinguish them by eyes, but it is not the same in batch processing and achieving by computer. The key point is to ensure the separatrix of ice and water, i.e. the threshold value in photo segmentation. For an obvious photo (Fig.3), the peak value of ice and water can be seen clearly on its gray-level histogram (Fig.4), but which point should be selected to separate ice from water, it is difficult to define. At that time, an easy method is to select the minimum point in

gray-level histogram as the threshold point (Chen, et al., 2003). Unfortunately, this method has a big limitation under other conditions, sometimes the areas of ice and water are greatly different, there is only one peak value on the histogram; sometimes because of the sun's rays, ice is very similar to water on image, the histogram is very complanate, and there is no obvious peak point and valley point. Under these conditions, big errors will occur in segmentation.

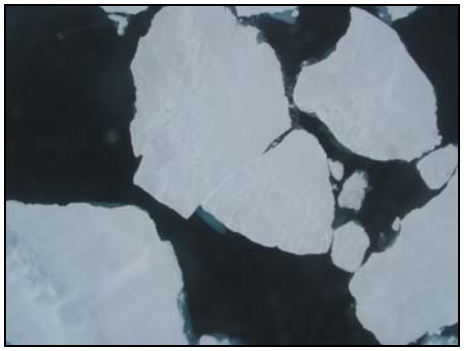

Fig.3. Aerial image

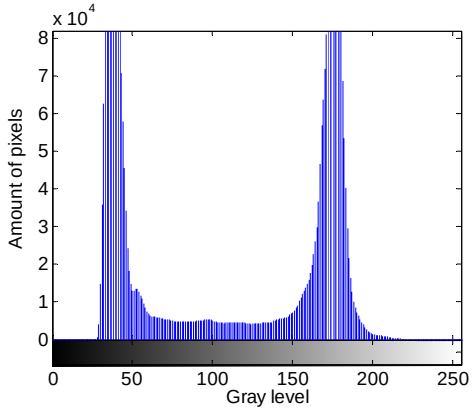

Fig.4. Gray-level histogram

After some compares, the *Ostu* method is ensured to be the threshold selection algorithm in image processing. The *Ostu* method selects the threshold value based on the difference of the image, which considers that a good segmentation method should maximize the difference between the object and the background, that is to say there will be the highest contrast between the object and the background after segmentation, so this method is also named as the maximum class variance method (Wu, et al., 2002).

Firstly the method assumes that a threshold value of t can divide the photo X with L gray levels into two classes: $C_0 \in [0,t]$, $C_1 \in [t+1, L-1]$, after unifying the histogram, the proportions of pixels at different gray level is given as:

$$p_i = \frac{n_i}{N} \qquad p_i \geq 0 \qquad \sum_{i=0}^{L-1} p_i = 1, \tag{1}$$

where N is the total amount of pixel in the photo X, n_i is the amount of pixel at i gray level. Then the probability and the average of C_0 and C_1 can be respectively written as:

$$w_0 = p_r(C_0) = \sum_{i=0}^{t} p_i = w(t); \qquad w_1 = p_r(C_1) = \sum_{i=t+1}^{L-1} p_i = 1 - w(t), \tag{2}$$

$$u_0 = \sum_{i=0}^{t} \frac{ip_i}{w_0} = \frac{u(t)}{w(t)}; \qquad u_1 = \sum_{i=t+1}^{L-1} \frac{ip_i}{w_1} = \frac{u_T - u(t)}{1 - w(t)}, \tag{3}$$

where $u_T = \sum_{i=0}^{L-1} ip_i$ is the average value of photo X.

The variance of these two classes is

$$\sigma_B^2 = w_0(u_0 - u_T)^2 + w_1(u_1 + u_T)^2 = w_0 w_1 (u_1 - u_0)^2. \tag{4}$$

The optimal threshold value t^* should maximize this variance, then

$$t^* = \arg \max_{0 \leq t \leq L-1} \sigma_B^2 \quad . \tag{5}$$

The *Ostu* method confirms the threshold value basing on the thought of maximizing the difference between the object and the background. It has been proved that the *Ostu* method has a high precision through tests; most aerial photos get satisfying segmentation results by means of this method. On the other hand, the calculation quantity is less than ordinary ones; batch processing of segmentation can be implemented by computer.

In the analysis process of aerial photos, threshold selection is the most important step. The next step is to divide the photo into a binary one by this threshold value, the black and white parts correspond to water and ice respectively. Lastly, the amount of black and white pixels on the binary photo can be given, the proportion of the white pixels is also worked out, that is the ice concentration, a binary photo after segmentation is shown in Fig.5. In analysis process it was found that the *Ostu* method was suitable for most aerial photos, but for the photos full of ice or water, big errors occurred because of the little contrast. So it is necessary to check the results, for the conditions above, ice concentration can be directly set as 0 or 10. In addition, for those photos containing sun glisten or fog, this method can estimate the bright parts or the fog into ice, which is obviously wrong. Fortunately, the amount of photos like that is 124, just 2.6% of all, which can be processed individually.

Fig.5 Binary photo

CONCLUSIONS

In CHINARE-2003, depending on the video recorder fixed on the shipboard, the ice condition along investigation route was automatically collected. After analyzing these images frame by frame using the similarity criterion discussing above, the ice thickness distribution along the route was obtained.

Aerial images were obtained by the camera fixed on the helicopter. The classical *Ostu* method in image segmentation was employed to process these images, which confirmed the separatrix based on the thought of maximizing the difference between the object and the background, and then the ice concentration was obtained.

The quantizing method of ice thickness and ice concentration discussing in this paper will do good to following sea ice image data process. The sea ice characteristic parameters obtained form these image data will also provide basic parameters for the analysis of ice distribution along investigation route and the farther research of coupled atmosphere-sea ice-ocean model.

ACKNOWLEDGEMENTS

The authors acknowledge support from NSFC under grant 40233032 and would like to thank Mr. Zhanhai Zhang, Mr. Zhi Chen, Mr. Shan Mei for their collections and contributions the videos and photos. Thanks also to the crew of *R/V Xuelong* and the Helicopter *Zhijiu*.

REFERENCES

Aagaard, K. and Carmack, E.C. The role of sea ice and other freshwater in the Arctic circulation. *Journal of Geophysical Research* 94: 14,485-14,498(1989).

Chen, D.L., Liu, J.N. and Yu, L.L. Comparison of image segmentation thresholding method. *Machine Building & Automation* 1: 77-80(2003). (In Chinese)

Garcia, E., Maksym, T., Simard, M., Dierking, W., Van, W.M., Nghiem, S.V. and Germain, K.St. A comparison of sea ice field observations in the Barents Sea marginal ice zone with satellite SAR data. *Geoscience and Remote Sensing Symposium, IGARSS '02. 2002 IEEE International* (2002)3035 -3037.

Gennady, I. B. and David, C. D. Seasonal comparisons of sea ice concentration estimates derived from SSM/I, OKEAN, and RADARSAT data. *Remote Sensing of Environment* 81: 67-81(2002).

Greuell, W., Reijmer, C.H. and Oerlemans, J. Narrowband-to-broadband albedo conversion for glacier ice and snow based on aircraft and near-surface measurements. *Remote Sensing of Environment* 82 :48-63(2002)

Lemke, P., Hibler, W., Flato, G., Harder, M. and Kreyscher, M. On the improvement of sea-ice models for climate simulations: the sea ice model intercomparsion project. *Annals of Glaciology* 25: 183-187(1997).

Richard, J.H., Nick, H. and Peter, W. A systematic method of obtaining ice concentration measurements from ship-based observations. *Cold Regions Science and Technology* 34: 97-102(2002).

Stern, H.L. and Rothrock, D.A. Open water production in Arctic sea ice: Satellite measurements and model parameterizations. *Journal of Geophysical Research* 100: 20,601-20,612(1995).

Thorsten, M., Donald, J.C., Mark, A.T. and Alvaro, I. Comparison of aerial video and Landsat 7 data over ponded sea ice. *Remote Sensing of Environment* 86: 458-469(2003).

Wu, W., Liu, J. and Li, X. Research on threshold selection for image segmentation. *Journal of XI'AN Institute of Technology* 22(4): 309-313(2002). (In Chinese)

Worby, A.P. Observing Antarctic sea ice: a practical guide for conducting sea ice observations from vessels operating in the Antarctic pack ice. *A CD-ROM produced for the Antarctic Sea Ice Processes and Climate (ASPeCt) Program of the Scientific Committee for Antarctic Research (SCAR) Global Change and the Antarctic (GLOCHANT) Program*, Hobart, Australia (1999).

Worby, A.P., Jeffries, M.O., Weeks, W.F., Morris, K. and Jaña, R. The thickness distribution of sea ice and snow cover during late winter in the Bellingshausen and Amundsen Seas, Antarctica. *Journal of Geophysical Research* 101: 28,441-28,455(1996b).

Zhao, J.P. and Ren, J.P. Study on the method to analyze parameters of Arctic sea ice from airborne digital imagery. *Journal of Remote Sensing* 4(4): 271-278(2000). (In Chinese)

17th International Symposium on Ice
Saint Petersburg, Russia, 21 - 25 June 2004
International Association of Hydraulic Engineering and Research

SCATTERING OF OBLIQUE ICE-COUPLED WAVES BY A PRESSURE RIDGE

Timothy D. Williams[1]

ABSTRACT

This paper seeks to investigate the amount of scattering by a pressure ridge. It builds on the work of Williams and Squire (2004), in which results were presented for various different types of ridges (e.g. triangular, rectangular, smooth) but for only a single thickness of ice. Here we study the scattering by a single type of ridge, and look at the effect that changing the thickness of the background ice cover has on the transmission spectrum, with an eye towards the goal of remote sensing of ice thickness. Some approximations that were found to be useful from a computational point of view are also presented.

INTRODUCTION

Until recently, most theoretical work on the passage of water waves through sea-ice has assumed ice is a homogeneous thin elastic plate. The assumption of elasticity has been well tested experimentally (e.g. Squire and Allan, 1980); however, the assumption that sea-ice is homogeneous is less accurate, as it is peppered with irregularities at both the microscale (brine pockets, algae), and at larger scales (cracks, open or refrozen leads, pressure ridges).

It is generally assumed that the waves are relatively long in comparison to imperfections on the microscale and that neglecting their effect will not be too detrimental. On the other hand larger scale imperfections cannot be ignored as readily, and recent calculations support their inclusion. Such calculations include scattering by a single abrupt change in ice properties (e.g. Chung and Fox, 2002), by either one or many cracks in an otherwise uniform single sheet of ice (e.g. Marchenko, 1997; Evans and Porter, 2003), and by one or many pressure ridges or leads (Marchenko, 1997; Williams and Squire, under review; Williams and Squire, 2004). Dixon and Squire (2001) solved the very similar problem of an embedded rectangular berg.

In the latter two papers by Williams and Squire (under review, 2004), the results of Squire and Dixon (2001) were extended to allow for incident waves arriving at an oblique angle, the water depth to be finite, and the thickness of the berg to vary arbitrarily. In effect, this means that the pressure ridges were taken to be an extension of

[1]Department of Mathematics and Statistics, University of Otago, Dunedin, New Zealand

the main ice sheet (i.e. they were still modelled by the thin plate equations), but with the ice thickness allowed to vary spatially over its width. This approach neglects the effect of the ridge keel, but does allow the solution to proceed in much the same way as for simpler problems such as the scattering by cracks; Marchenko's paper treats the ridge as a point irregularity which takes into account some of the torsional motion of the ridge, and the solution is also very similar to that of the crack.

By sampling from observed ridge height and spacing distributions, Williams and Squire (under review), were able to approximate the scattering by a field of a given number of ridges, and Williams and Squire (2004) extended these results to allow for the presence of extra features such as leads and cracks in the field. The next question to ask is, with sufficient information about the number and type of irregularities present in a given ice field, whether or not the transmission spectrum obtained from that ice field could be used to estimate its background thickness.

This paper makes a step towards answering this question by investigating the effect that changing the thickness of the main ice cover might have on the transmission spectrum obtained from a field of ridges of given dimensions. It also presents some approximations that can be used to speed up the various calculations.

MATHEMATICAL FORMULATION OF THE PROBLEM

Figure 1 illustrates the physical situation that will be modelled, including the coordinate system that will be used. A sinusoidal wave approaches a crack separating two sheets of ice at an angle from the *x*-axis, which is perpendicular to the direction of the ridge. The water beneath the ice is assumed to have constant density and to be of depth *H*. Assuming also that the flow is irrotational, it may be represented by a velocity potential Φ.

The ridge in the figure represents a considerable simplification of a "real" ridge – assuming that the depth of the keel is small compared to the wavelength of the incoming waves, we have approximated the ice-water interface by the $z = 0$ plane, and in addition, the sail, which is usually of a triangular shape, has been approximated by the rectangular ridge pictured. Williams and Squire (under review) showed that this last approximation was reasonably accurate if the average height was preserved.

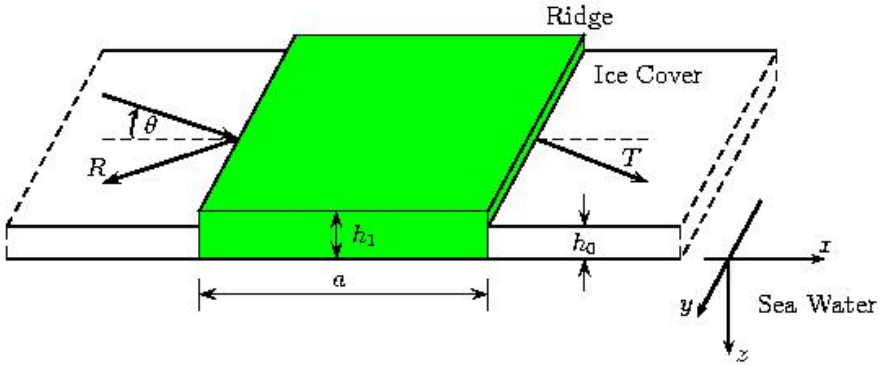

Fig. 1. The physical situation to be modelled: the scattering effect of the central ridge of ice as an obliquely incident plane wave approaches from the left. The incident wave is taken to have an amplitude of 1, and to be arriving at an angle θ to the x axis. The main ice cover, i.e. the ice to the left and right of the ridge, has a constant thickness of h_0, and the sea water has a finite depth of H. The coordinate axes are oriented as shown, but are displaced to the left so that the $x = 0$ line corresponds to the left hand edge of the ridge

Equations and Boundary Conditions

Φ must satisfy Laplace's equation throughout the fluid region, a sea-floor condition which states that there can be no flow through the sea-floor ($z = H$), and kinematic and dynamic equations at the sea/ice interface ($z = 0$) – the latter coming from the linearised Bernoulli condition. In addition, edge conditions (four at each "edge", $x = 0$ and $x = a$) must also be applied. The nondimensionalised forms of these equations are given below.

We first define the flexural rigidities of the ice cover and the ridge as $D_j = Eh_j^3/12(1-\nu^2)$ ($j = 0,1$), their mass per unit surface area as $m_j = \rho h_j$, and their characteristic lengths and times as $L_j = (D_j/\rho g)^{1/4}$ and $\tau_j = (L_j/g)^{1/2}$ respectively. E, ν, ρ' are respectively the Young's modulus, Poisson's ratio, and density of the ice, while ρ is the density of the water. Supposing then that the incident wave has radial frequency ω, we let the non-dimensional frequency and natural length that we will nondimensionalise with respect to (respectively) be

$$\overline{\omega} = \omega\tau_0, \quad L = L_0\,\overline{\omega}^{-2/5}.$$

Defining the following additional nondimensionalised quantities

$$(\bar{x},\bar{y},\bar{z}) = (x,y,z)/L, \quad \bar{a} = a/L, \quad \overline{H} = H/L, \quad \bar{t} = t/\tau_0,$$

$$\overline{D}_j = D_j/D_0 \quad \overline{m}_j = m_j/m_0, \quad \sigma(h_0) = m_0/\rho L_0,$$

and

$$\lambda = \overline{\omega}^{-8/5}, \quad \mu(h_0,\lambda) = \sigma\overline{\omega}^{2/5} = \sigma/\lambda^{1/4},$$

we assume Φ is harmonic in time and the y variable (as the geometry of the problem is invariant in that direction), and so can be written in the form

$$\Phi(x,y,z,t) = (L^2\omega/2\pi)\varphi(\bar{x},\bar{z})e^{i(\bar{l}\bar{y}-\overline{\omega}\bar{t})}. \tag{1}$$

If the incident wave arrives at an angle of θ away from normal incidence and has a nondimensional wave number of γ_0, $l = \gamma_0\sin\theta$ is the nondimensional wavenumber of the incident wave's component in the y direction.

Dropping the overbars for clarity, φ must now satisfy the conditions

$$(\nabla_{xz}^2 - l^2)\varphi(x,z) = 0, \tag{2a}$$

$$\mathsf{L}(x,\partial_x)\varphi_z(x,0) + \varphi(x,0) = 0, \tag{2b}$$

$$\varphi(0^+,z) - \varphi(0^-,z) = \varphi(0^+,z) - \varphi(0^-,z) = 0 \tag{2c}$$

$$\varphi_x(0^+,z) - \varphi_x(0^-,z) = \varphi_x(a^+,z) - \varphi_x(a^-,z) = 0, \tag{2d}$$

$$\varphi_z(x,H) = 0, \tag{2e}$$

where $\mathsf{L}(x,\partial_x)=D(x)(\partial_x-l^2)^2+\lambda-m(x)\mu$, $D(x)$ is the step function

$$D(x)=\begin{cases} D_0=1, & x<0,\ x>a, \\ D_1, & 0<x<a, \end{cases} \tag{3}$$

and $m(x)$ is defined analogously. One thing to note about the parametrisation is that $\sigma \propto h_0^{1/4}$ (a very slow variation) and so μ can be treated as being a function of λ only, which dominates the $\lambda - m\mu$ term for most periods. This fact will be used later in the Approximations section.

The edge conditions that must be applied at $\xi = 0$, and $\xi = a$ are:

$$\varphi_Z(\xi^+,0) = \varphi_Z(\xi^-,0), \tag{4a}$$

$$\varphi_{Zx}(\xi^+,0) = \varphi_{Zx}(\xi^-,0), \tag{4b}$$

$$\mathsf{M}(\xi^+,\partial_x)\varphi_Z(\xi^+,0) = \mathsf{M}(\xi^-,\partial_x)\varphi_Z(\xi^-,0), \tag{4c}$$

$$\mathsf{S}(\xi^+,\partial_x)\varphi_Z(\xi^+,0) = \mathsf{S}(\xi^-,\partial_x)\varphi_Z(\xi^-,0), \tag{4d}$$

where the operators M and S are given by

$\mathsf{M}(x,\partial_x) = D(x)(\partial_x^2-\nu l^2)$, $\mathsf{S}(x,\partial_x)=D(x)(\partial_x^2-(2-\nu)l^2)\partial_x$.

METHOD OF SOLUTION

The potential φ is put in terms of a Green's function that satisfies

$$(\partial_\xi^2+\partial_\zeta^2-l^2)G(x-\xi,z,\zeta) = \delta(x-\xi,z-\zeta), \tag{5a}$$

$$\mathsf{L}_0(\partial_\xi)G_\zeta(x-\xi,z,0) + G(x-\xi,z,0) = 0, \tag{5b}$$

$$G_\zeta(x-\xi,z,H) = 0, \tag{5c}$$

where $L_j(\partial_x) = D_j(\partial_x^2-l^2)^2+\lambda-m_j\mu$ (j=0,1). Such a Green's function was given by Evans and Porter (2003) as an inverse Fourier transform. As we will only be needing x and ξ derivatives of $g(x-\xi)=G_{z\zeta}(x-\xi,0,0)$ we will not present the full Green's function here, but only

$$g(x-\xi) = (1/2\pi)\int_0^a (1/f_0(\kappa))e^{-ikx}dk = i\sum_{n=-2}^{\infty} A_n e^{ik_n|x-\xi|}, \tag{6}$$

where the $k_n = \kappa_n^2 - l^2$ ($n = -2, -1, \ldots$) are defined as being either in the upper complex half-plane if they are complex, or positive real otherwise, the κ_n are the roots of the

dispersion relation $f_0(\kappa) = 1/\kappa - \Lambda$, $\Lambda = \kappa^4 + \lambda - \mu$, $A_n = \mathrm{Res}(1/f_0, k_n) = -\kappa_n^2/k_n C_n$, and $C_n = H(\Lambda^2(\kappa_n) - 1) + 5\kappa_n^4 + \lambda - \mu$. The roots κ_n are distributed as in Chung and Fox (2002) – there is one zero, κ_0, on the positive real axis, one in the first quadrant, κ_{-1}, another in the fourth quadrant, $\kappa_{-2} = -\kappa_{-1}^*$, and infinitely many zeros on the positive imaginary axis, κ_n, $n = 1,2,....$ Their negatives are also zeros as f_0 is an even function. When $l<0$, i.e. when $\theta < \pi/2$ (which is the case that we are interested in), the integral (6) has two real poles at $k = \pm k_0$. They are dealt with by rotating them infinitesimally in an anti-clockwise direction and taking the limit as they are rotated back onto the real line after the new transform has been inverted.

Integral Equation

First let us consider the type of behaviour that φ should exhibit as $x \to \pm\infty$. To the left of the ridge the potential ought to be asymptotically like that due to both an incoming and reflected wave, while to the right it should be that due to the transmitted wave only. This can be written explicitly as

$$\varphi \to \begin{cases} (e^{ik_0 x} + R \times e^{-ik_0 x}) \dfrac{\cosh \kappa_0 (z - H)}{\cosh \kappa_0 H}, & x \to \infty, \\ T \times e^{ik_o x} \dfrac{\cosh \kappa_0 (z - H)}{\cosh \kappa_0 H}, & x \to -\infty. \end{cases} \tag{7}$$

Assuming this behaviour then, we apply Green's theorem, as well as equations (2) and (5) to give us the following integral equation that was derived for $\varphi_z(x,0)$ in Williams and Squire (under review):

$$D(x)\varphi_z(x,0) = Ie^{ik_0 x} + \underset{\rho}{\psi}^T(x)\underset{\rho}{P}_0 + \underset{\rho}{\psi}^T(x-a)\underset{\rho}{P}_a + \int_0^a K(x-\xi)\varphi_z(\xi,0)d\xi, \tag{8}$$

where $I = -\kappa_0 \tanh \kappa_0 H$, $K(x-\xi) = (L_1(\xi,\partial_\xi) - L_0(\partial_\xi))g(x-\xi) - (1 - D(x))\delta(x-\xi)$. Applying (4c) and (4d), and defining $p_j(x) = D(x)\partial_x^j \varphi_z(x,0)$ $(j=0,1)$,

$$[\underset{\rho}{P}_\xi]_j = P_j(\xi) = p_j(\xi^+) - p_j(\xi^-) \quad (\xi = 0, a;\ j = 0,1),$$

while

$$[\underset{\rho}{\psi}]_0(x) = -(\partial_x^2 - (2-\nu)l^2)g'(x), \quad [\underset{\rho}{\psi}]_1(x) = -(\partial_x^2 - \nu l^2)g(x).$$

Equation (8) represents a Fredholm integral equation of the second kind in $\varphi_z(x,0)$ over the interval $(0,a)$ and we will solve it by numerical quadrature. Having done this, we obtain from (8) eigenfunction expansions for $\varphi_z(x,0)$ when $x<0$ and when $x>a$. These enable us to solve for the unknown constants $P_j(\xi)$ (ξ = 0,a; j = 0,1) by applying the remaining four edge conditions. This is done by substituting (4a) and (4b) into their definitions.

APPROXIMATIONS

There are two main approximations that we will use to speed up our results-gathering. The first, involves exploiting the slow variation of the parameter σ with thickness to calculate results for arbitrary thicknesses by referencing them back to a single ice

thickness, which we will take to be h_0=1m. One advantage of doing this is that we only need to find the roots of the dispersion relation once (as opposed to finding a set of roots corresponding to each background thickness and repeating this every period); another is that only one set of quadrature matrices need to be built up – corresponding to the minimum desired thickness (the largest value of a) – and from them the matrices needed when solving (8) for larger thicknesses (smaller values of a) can be obtained by discarding particular elements.

To do this we approximate σ by $\sigma_0 = \sigma(h_0^*)$ and $\mu(h0,\lambda)$ by $\mu_0(\lambda) = \mu(h_0^*,\lambda)$, noting also that λ is itself a function of $\tau h_0^{3/8}$. Thus for a given thickness $h_0=\alpha h_0^*$ and period τ, and for a given ridge of height h_r and width a and sea depth H, we can approximate R and T by calculating the scattering of a wave of period τ in ice of thickness h_0 by a ridge of height h_r/α, width $a/\alpha^{3/4}$, also scaling the sea depth to $H/\alpha^{3/4}$.

The second approximation involves calculating R and T by Chebyshev polynomial interpolation. This represents a significant decrease in computing time (90%) when only a single ridge is present, as only 15 or so coefficients need to be calculated exactly, and the remainder can be obtained by interpolating between them. Unfortunately, however, the effectiveness of the approach decreases as the number of ridges are increased – about 150 exact evaluations are required when 100 ridges are present.

RESULTS

In this section the following values for the required physical parameters are used: E = 5 GPa, ν = 0.3, ρ = 1025 kg m^{-3}, ρ' = 922.5 kg m^{-3} and g = 9.81 m s^{-2}. Also we use depth $H = 6L_0$ (about 90 m for ice thickness of 1 m), which is sufficiently large to satisfy the infinite depth approximation (Chung and Fox (2002) use a factor of $H/L_0 = 2\pi$). In addition only a single ridge will be used – a 1 m high triangular ridge of width 2 m, approximated by a rectangular ridge of the same width and height 0.5 m.

Figure 2 compares the scattering, by both one and 100 ridges, in ice of different thicknesses. In Figures 2(a) and (c), plots of $|R|$ against period are given for a series of ice thicknesses for one and 100 ridges. In both figures, there is more reflection in the thinner ice, as might be expected since each ridge is taller and wider in comparison to the thickness and characteristic length of the ice. And as also might be expected, there is quite a lot more reflection in the presence of 100 ridges than when there is only one. Both of these trends are also evident in Figures 2(b) and (d), which plot $|R|$ against ice thickness for a series of periods for one and 100 ridges. Again the more ridges the greater the reflection, and reflection decreases with ice thickness, although in the plots corresponding to the larger periods, $|R|$ rises to a maximum at about 1m before beginning its decline.

The results for 100 ridges are calculated using the serial approximation used by Williams and Squire (under review): in the presence of N identical ridges, $|T|\approx|T_0|^{2N}$ ($|R|^2=1-|T|^2$), where T_0 is the transmission coefficient for a single ridge – this showed good agreement with results calculated by averaging over all possible combinations of ridge separations, although the confidence limits were quite wide.

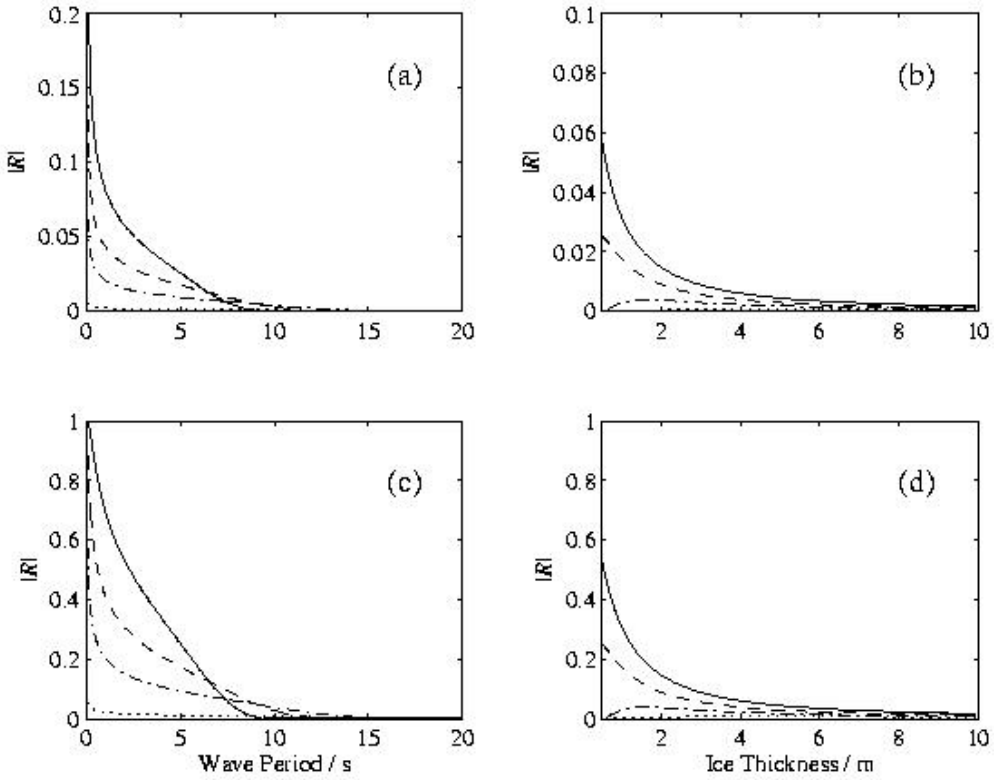

Fig. 2: (a) The behaviour of |R| in the presence of a single ridge with period, for ice thicknesses of .5 m (solid), 1m (dashed), 2 m (chained) and 10 m (dotted); (b) the behaviour of |R| in the presence of a single ridge with ice thickness, for wave periods of 2 s (solid), 5 s (dashed), 10 s (chained), and 15 s (dotted); (c) and (d) are the same as (a) and (b) (respectively), but |R| is calculated for when 100 ridges are present (using the serial approximation)

DISCUSSION AND CONCLUSIONS

As stated in the introduction, this paper was intended to investigate the potential of remote sensing of ice thickness by using water wave theory. This was first suggested by Shuchman et al (1994), although their intention was to model the marginal ice zone as a single thin plate and obtain an estimate of its average thickness, an idea rebutted by Squire (1995).

If we are to measure $|R|$ as a function of period, then take that function and estimate the ice thickness that produced it, the resolution between curves corresponding to different ice thicknesses needs to be quite large. This is especially true in light of the wide confidence limits for $|R|$ when ridge separations are taken into account. Taking into account that Figure 2 only considered identical ridges, and hypothesising that variable ridge heights would increase the curves' resolution further, it is thus promising that even without doing this their general behaviour seems to be fairly different. In addition real data would not be averaged over ridge separation, giving further opportunity to differentiate between different thicknesses, so further study could indeed be profitable.

ACKNOWLEDGEMENT

This work described was supported by a Marsden grant from the Royal Society of New

Zealand and by the Foundation for Research, Science and Technology.

REFERENCES

Chung, H., and Fox, C. Propagation of flexural-gravity waves at the interface between floating plates, *International Journal of Off-shore and Polar Engineering, International Society of Offshore and Polar Engineers* 12(3): 163–170 (2002).

Evans, D. V. and Porter, R., Wave scattering by narrow cracks in ice sheets floating on water of finite depth, *Journal of Fluid Mechanics* 484: 143–165 (2003).

Marchenko, A. V., Flexural gravity wave diffraction at linear irregularities in sheet ice, *Fluid Dynamics* 32: 548–560 (1997).

Schuchman, R. A., Rufenach, L. R. and Johannesen, O. M. Extraction of marginal ice zone thickness using gravity wave imagery. *Journal of Geophysical Research* (*C1*) 99: 901–918 (1994).

Squire, V. A. Geophysical and oceanographic information in the marginal ice zone from ocean wave measurements. *Journal of Geophysical Research* (*C1*) 89: 997–998 (1995).

Squire, V. A., and Allan, A. J. Propagation of flexural gravity waves in sea ice. In *Sea Ice Processes and Models, Proceedings of the Arctic Ice Dynamics Joint Experiment.* ed. R. S. Pritchard, University of Washington Press, Seattle, USA (2002) 327–338.

Squire, V. A. and Dixon, T. W. On modelling an iceberg embedded in shore-fast sea ice. *Journal of Engineering Mathematics* 40: 211–226 (2001).

Williams, T. D., and Squire, V. A. The scattering of flexural gravity waves by an ice field. In *Proceedings of the 12th International Offshore and Polar Engineering Conference, International Society of Offshore and Polar Engineers*, Cupertino, California, USA (2004, in press).

Williams, T. D., and Squire, V. A. Oblique scattering of plane flexural-gravity waves by heterogeneities in sea ice. *Philosophical Transactions of the Royal Society* (under review).

17th International Symposium on Ice
Saint Petersburg, Russia, 21 - 25 June 2004
International Association of Hydraulic Engineering and Research

THE METHODICAL RECOMMENDATIONS FOR THE PASSING OF ICE THROUGH THE CONSTRUCTING HYDRAULIC ENGINEERING STRUCTURES

I.N.Shatalina[1], A.M.Shvainshtein[1], M.G.Gladkov[1]

ABSTRACT

In the U.S.S.R. the first normative base standards for determination of ice-pass conditions through hydraulic constructions were created in 1970-s. From that time the passing of ice through the several large hydraulic structures was realized and many research works in this field were published. All of that, including an absence in early published normative base standards good enough coordination of ice-passing conditions and hydraulic working conditions of constructions, as an absence of information about ice-loads made a new situation for adoption more modern base standards.

In this recommendations install the field of using. The ice-passing conditions are connected with hydraulic working conditions of constructions. Shown recommendations for ice-passing conditions through constricted by the cofferdams waterway, non-finished dams and dam outlets. Shown specifics of the passing of ice through the canals, bypass spillways, diversion tunnels and pipes. Considerated the actions for ice-pass regulation through the hydraulic engineering structures.

This memorandum has just abstract form, because the real value of normative basic standards is very big. Importance of this work is connected with necessity for adoption of technical solutions in safety ice-passing process through the hydraulic structures depends from climate, construction specifics of hydraulic projects, steps of construction works and readiness of ice-passing frontage which is important for the Russian hydraulic engineering structures and mostly for located in the north part of the country. Today the most importance have the scientific prognosis which can be used for the ice and cream-ice passing through hydraulic structures or with it's delaying in upstream as for determination of thrust on parts of construction in ice-floating period.

Hydraulic conditions of ice transportation according with different schemes of the passing determinate by the next factors: water discharges in ice-floating period; value of the stream speeds and their directions; deep of the stream on approach and inside of constructions; design head on the top of spillway; difference of topline level of the pipe out-

[1] The B.E.Vedeneev All-Russian Research Institute of Hydraulic Engineering (VNIIG), Gzhatskaya str., 21, St.Petersburg, Russia.

lets and tunnels located under upstream level; conditions of free surface of the flow in-front of the hydraulic engineering structure (presence of immobile waves); arising of free surface vortex on approach of hydraulic construction.

The passing of ice through the hydraulic structures realize on the first steps of construction works or through construction which is working with not high difference between upstream and downstream. Ice-passing conditions connected with hydraulic working conditions for the different parts of construction waterway. Here shown the basic specifics of the passing of ice for the each discharge passing scheme (see table).

Partial delaying of ice in upstream before the next passing of ice through constructions with growing of environment temperature is promoting of ice-crushing on approach of constructions and inside of them.

Purpose of the ice-passing scheme must be realize with calculation of the next conditions: reserve of the ice in reservoir; character of flood hydrograph, intensity of water discharges growing; date of water emergence on ice and ice alienation out of shores, speed of ice moving along of upstream length; changing of air temperature for the period preceding of the ice floating; reserve of the cold inside of ice; changing of the ice solidity in flood period with presence or absence of snow on the ice surface; possibility of delaying of ice in upstream; quantity of the blocking ice in upstream; discharge of ice material; concentration of ice in the stream; readiness of construction frontage; width of ice droping frontage; hydraulic working regime of construction; evaluation character of the opening of downstream and cases of it's deliverance from the ice covering; maximum water and ice discharges in ice floating period.

During the passing of ice through constricted by the cofferdams waterways we solve the problems for determination of lowest significances for constriction of waterway, depth in constricted part and height of cofferdams for the maximum calculated ice floating, and also shown the ways for determination of ice loads on cofferdams. Shown the formulae for determination of lowest drop which is necessary for the crushing of ice on approach of constricted part and width of strip pieces of crushed ice.

$$\Delta Z_{min} = 0{,}03\sqrt{\frac{h_d R_f}{\rho_i g}}, \qquad l = 4{,}2\sqrt{\frac{h_d R_f}{\rho_i g}}.$$

For the passing of ice through a non-finished concrete dams shown the recommendations for determination of necessary width of the ice droping frontage and different spans of a non-finished dams, ratio of width of piers to width of spans in light, form of piers tops and possibility of their moving to the upstream side, lowest depth in spans of a non-finished dams during the passing of ice, loads on the different parts of a non-finished dam and on the mechanical equipment.

Also shown the recommendations for the following determination: width of the separate spans of a non-finished dams which is using for the passing of ice; total width of ice droping frontage; ratio of the piers thickness to the real width of the spans; forms of the piers; distances of the piers moving to the upstream side from the top line of construction; necessary depth of water in the spans of a non-finished dams.

Table

Schemes of water and ice discharges pass through constructions with their hydraulic specifics

Schemes of ice passing through hydraulic constructions	Specifics of hydraulic engineering structures	Hydraulic working specifics of constructions			Calculated hydraulic schemes of discharge passing	Ice-pass conditions
		нydraulic scheme of overflow	drowning conditions	character of entry fall		
Through constricted streamways	Part of streamway in sections of hydraulic engineering structure which is limited by the cofferdams for construction work in trench. Water and ice discharges are passing through the constricted channel	Weir without fall as a sort of broad-crested overflow	Free flow regime	Waterfall area with transformation of subcritical flow into supercritical flow with concentrated fall	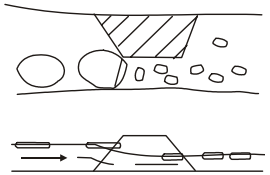	On concentrated drop the ice-fields with width more than wide of constricted part just breaking into small parts and going to downstream without any delay
			Submerged flow regime	Entrance drop in constriction is not high	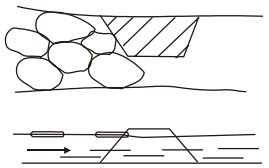	Passing of ice-fields with width more than wide of constricted part without additional actions is possible in case if blocks of ice will be destroyed after collision with cofferdam and shores
Through non-finished concrete dams	In limited by the cofferdams streamway install the special hydraulic structure for passing diversion discharges of water and ice. This special construction shaped like lower part of dam with piers on the top for installation of gates. It's two kinds of tops: with low drop and high drop	One of the form of overflow (including weir without fall) or nappe-crested weir			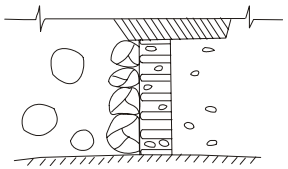	
		1. Low non-finished dam works like broad-crested fall	Free flow regime	Waterfall area with concentrated drop on entrance	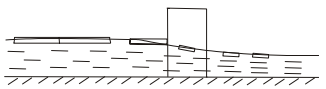	On concentrated fall the ice-fields are crushing and passing to downstream with big enough width of crest spans

Schemes of ice passing through hydraulic constructions	Specifics of hydraulic engineering structures	Hydraulic working specifics of constructions			Calculated hydraulic schemes of discharge passing	Ice-pass conditions
		нydraulic scheme of overflow	drowning conditions	character of entry fall		
			Sub-merged flow re-gime	Fall in constricted part is not high	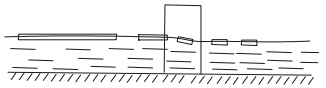	Passing of ice blocks is possible if kinetic energy of ice blocks is enough for their crushing after collision with piers
		2. High non-finished dam works like nappe-crested weir	Free flow	Concentrated fall on en-trance	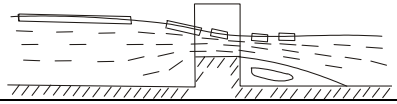	In waterfall area the ice fields are crushing and passing to downstream with big enough width of spans
		3. Non-finished dam with piers located in up-stream of hydrau-lic engineering structure	Free flow	All fall is concentrated in-side of constructions	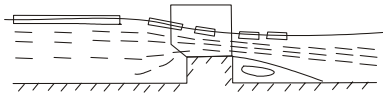	Passing of ice blocks is possible just after their crushing with piers
Through diversion canals and wasteways	Bypass canals which constructed on shore line in flood plain area or in one of the part of dam					
	1. No any regulation constructions on the waterway	Weir without sill	Free flow	Concentrated drop on short distance	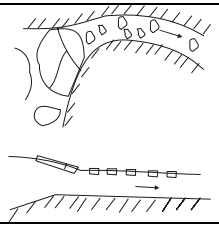	On concentrated drop the ice fields just breaking and going to downstream with their own sizes less than wide of entrance section

			Sub-merged flow	Entrance drop in constricted part is not high	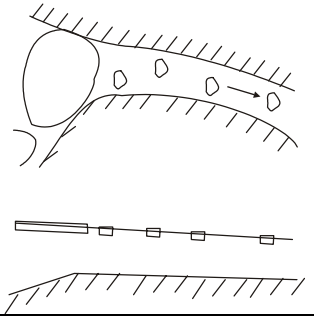	Passing of ice fields without additional actions is very difficult
	2. With special regulation construction on the waterway	Broad-crested overflow or nappe-crested weir	Free flow	The hydraulic working conditions just the same like with work without regulation construction but the width of breaking ice fields for the passing to downstream must be less than wide of regulation construction spans		
			Sub-merged flow	Low drop on entrance	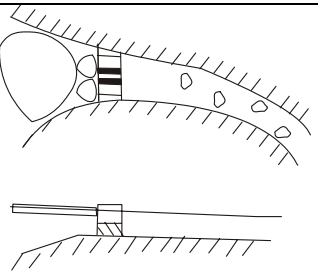	Passing of ice fields without additional actions is very difficult. Passing of ice blocks with less size than wide of carting section is analogous to work of a non-finished dams
Through the dam outlets	In constricted by coffer-dams waterway of constructed concrete dam with dam outlets on the fixed height for the passing of water	Working conditions of dam outlets with free inlet section is analogous to work of the non-finished dam				

Schemes of ice passing through hydraulic constructions	Specifics of hydraulic engineering structures	Hydraulic working specifics of constructions			Calculated hydraulic schemes of discharge passing	Ice-pass conditions
		hydraulic scheme of overflow	drowning conditions	character of entry fall		
		1. Bottom outlet works like weir without drop (non-finished dam with low drop)	Free flow	Waterfall area with concentrated drop on entrance	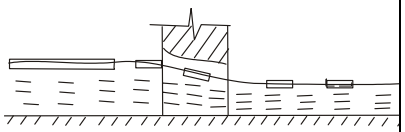	Analogous to work of a non-finished dams
			Submerged flow regime	Drop with constriction is not high	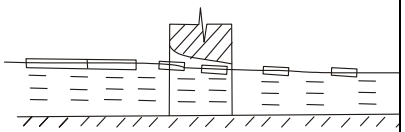	Analogous to work of a non-finished dam
		2. Dam outlet works as a non-finished dam with high drop	Free flow regime	Concentrated drop on entrance	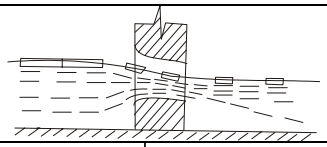	Analogous to work of a non-finished dam
		3. Dam outlet with piers located in upstream of hydraulic engineering structure	Free flow regime	Drop on entrance is concentrated inside of hydraulic engineering structure	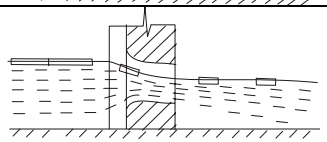	Analogous to work of a non-finished dam
Through dam outlets		With submerged inlet section we have the next working forms of dam outlets:				

		1. Flow from the hole		Drop in front of hydraulic engineering structure is almost absent	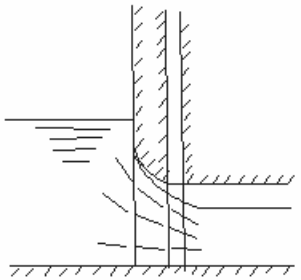	Crushing of ice blocks is realizing after collision with piers, under influence of free surface vortex and pressure of ice weight from the upstream. In this case the passing ice is very crushed and weak. Presence of free surface vortex in front of entrance for the best effect is very important
		2. Flowing through outlet with head regime of flow		Concentrated fall in front of hydraulic engineering structure is absent.	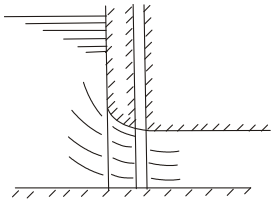	Same as shown before
Through the crest of temporary or permanent hydraulic engineering structures	Passing of water and ice with overflow through the crest of ground or concrete cofferdams, constructing dams and weir dams	Flow through the different type of weir: with free flow through the crest or with partial opened gates on the crest	Free flow or submerged flow or flow through the free hole	Sizes of drop is depending from submerged conditions		Conditions of the passing of ice is identical as in case with constructing dams or same as for passing of ice through the holes on entrance of dam outlet

Formulae for determination of width of the ice droping frontage various in depends from conditions of the ice covering on approach of a non-finished dams: the total ice covering or crushed into small pieces or the ice was condensed by the stream. Width of ice droping frontage and spans of a non-finished dams determinate depends from the form of free surface on approach of a non-finished dams. Shown dependings for determination of the falling down of free surface of water on approach of non-finished dam. Shown formulae for determination of the length of ice fields which is breaking on free surface before a non-finished dam. Shown the ways for determination of ice loads pushing on the vertical parts and piers of a non-finished dams, including the piers with the slope ice breaking face.

During consideration of working conditions of dam outlets in ice conditions determinate the width of ice droping frontage, total deep of spans under upstream level, distances of the piers moving to the upstream side, critical speeds of stream under the ice diving conditions. Depends from the real conditions the ice droping road of dam outlets can be used for the passing of ice into downstream and also for delaying of the ice. Significance of limited depth of the dam outlets seiling when ice diving process completely stoped determinate according by the next correlation:

$$H_k \geq \xi\sqrt{a}\,.$$

Where: a – height of dam outlet on approach; $\xi = (4 - 5)\ \mathrm{M}^{0.5}$ – empirical coefficient which is determinate by construction of the entrance part of dam outlet.

Shown recommendations for determination of influence on quantity H_k of formed free surface vortex in entrance of dam outlets.

In case of immobility of the ice fields infront of dam outlets shown the formula for the critical speed of water, when the ice diving process is started.

Calculation of possibility of the passing of ice through the dam outlets recommended to realize according with the basic methods for determination of limited pressure on the entrance part in cases of free flow and submerged flow in outlet section. Install the ice-loads on the dam with outlets and on the different parts of the dam.

In recommendations shown the basic specifics of the passing of ice through the bypass channels and spillways. Shown recommendations for installation of the shortest wide of entrance part of the canal. Shown formulae for determination of influence of the anchor ice dam on the walls of canal or on the different parts of canal.

Determinated , that conditions of the passing of ice through the diversion channels and pipes just identical to working conditions of channels, non-finished dams or dam outlets and depends from their working regime and from construction forms of the entrance part. During the passing of ice through the outlet dams in exploitation period possible the following schemes of the passing of ice:

- through the spans covering by gates. During droping of ice the gates picked up on all height or fall down in case of valve type of the gates. Ice fields are crushing on the droping curve infront of spans and later after blowing with piers;
- same like the last scheme but the ice fields coming to the separate piers without crushing on the droping curve. The passing of ice through the spans realize after

crushing in cooperation with piers and under influence of the moving down value of ice;

- through the coastal spans with the crest which is planed on the calculated level and through the central gate of outlet dam with the crest shaped on lower levels in case of large discharges after the lifting of the gates.

Shown instructions for determinations of width of outlet frontage and it's different spans and for determination of the lowest head on the crest of weir which is necessary for the passing of ice without delay. In case of the passing of ice with partial opened gates on the top of outlet dam shown the methodic for determination of the critical significance of the opening, when the ice diving process under the gate must be stopped.

Shown the actions for regulations of the passing of ice which must be used for delaying of the starting date of the ice floating infront of constructions, reduction of thickness and solidity of ice, decreasing of the sizes of ice blocks, for the passing of ice without forming of arches and blocking accumulations.

17th International Symposium on Ice
Saint Petersburg, Russia, 21 - 25 June 2004
International Association of Hydraulic Engineering and Research

DYNAMICS OF ICE JAM RELEASE SURGES

By Lianwu Liu[1] and Hung Tao Shen[2]

ABSTRACT
This paper investigates the dynamics of ice jam release surges. Numerical simulations were carried out using a two-dimensional ice dynamic model to examine the attenuation effect of ice on the surge propagation and the ice jam release processes. The simulated results are compared with the results of simplified simulations, in which the ice resistance effects were neglected. It is shown that at the instant of ice jam release, the peak discharge of the mixture of water and ice may be close to that simulated by neglecting the ice resistance. However, the ice resistance has significant effects on the stage and discharge hydrographs. The ice resistance can lower the peak discharge significantly at downstream locations.

INTRODUCTION
Sudden release or failure of ice jams in rivers accompanied by the release of channel storage often generates surges of water with high water velocity and rapid increase in stage. Modeling ice jam release and associated surges has been of significant interest because of the important impacts of this phenomenon on operations of water resources projects and flood forecasting. Henderson and Gerard (1981) used the classical dam break analysis to study the characteristics of the surge produced by the sudden release of an ice jam, neglecting the ice effect after release. Beltaos and Krishnappan (1982) carried out a one-dimensional analysis of the mechanics of surges due to ice jam release. By assuming that the concentration in the ice run remains constant, and neglecting the bank resistance to ice motion and internal ice resistance, the problem was simplified to a one-dimensional, unsteady, water-only flow by assuming the ice mass behaves like water. Beltaos and Krishnappan (1982) found that it was difficult to match the shape of the observed stage hydrograph with the simplified formulation. Blackburn and Hicks (2003) re-examined the feasibility of this approach by comparing the model results with the field data from the Saint John River upstream of Grand Falls, N.B. They concluded that accurate channel geometry is a key factor in modeling ice jam release surge events, and the ice jam mass can be treated as water. However, they were not able to match the observed stage and discharge hydrographs in their simulations. Jasek (2003) presented

[1,2]Research Scientist and Professor, Department of Civil and Environmental Engineering, Clarkson University, Potsdam, NY, 13699-5710, USA. Email: htshen@clarkson.edu

an excellent analysis on ice jam release processes based on field observations, and pointed out the differences of opinions on the importance of effects of ice.

In this paper, a two-dimensional coupled flow and ice dynamic model DynaRICE (Shen et al. 2000) is used to study the ice resistance effects, including both the internal ice resistance and boundary friction resistance, on ice jam release surges in river channels. The hydrodynamic component of the model has been refined using a streamline upwind finite element method (Liu and Shen 2003, Brooks and Hughes 1982, Hicks and Steffler 1992, and Berger and Stockstill 1995), which is capable of simulating high velocity and transitional flows. To avoid confusing the actual ice effects with the inaccuracy in field data an idealized channel, with a similar slope and length to the Saint John River, is used to study the ice effects. Simulation results with ice dynamics are compared with simplified simulations, in which the ice resistance effects are neglected, to clarify the ice effects on the surge. This comparison explains the discrepancies between the numerical results and observed data in Blackburn & Hicks (2003). Additional simulations were carried out to examine the jam release upstream of a run-of-river power dam.

RELEASE OF ICE JAM IN A LONG CHANNEL

In this case, ice jam release in a rectangular channel of 100 km long and 600 m wide is studied. Bed slope of the first 30 km of the channel is 0.0004, and the rest 70 km downstream is 0.0001. A constant Manning's coefficient of 0.03 is used for the river bed. A constant water discharge of 2000 m^3/s is used at the upstream boundary. At downstream boundary, a normal flow depth condition is used to represent uncontrolled downstream boundary. The water surface elevation changes automatically with water discharge at the downstream boundary. The initial steady state width-averaged longitudinal profiles of ice jam and water surface are shown in Figure 1.

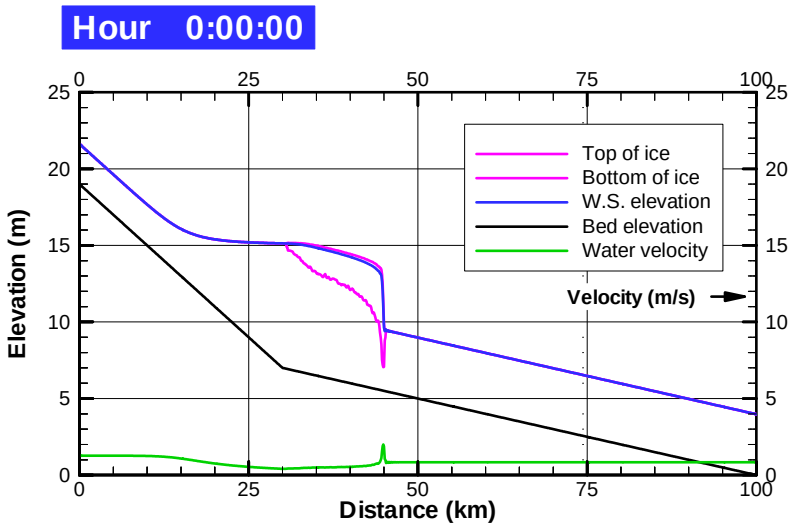

Fig. 1. Simulated ice jam profile and initial condition for jam release

The ice jam release simulation lasted for 24 hours following the initiation of the jam release. The water surface and ice jam profiles 4, 10, 20, and 60 minutes after the jam

release are shown in Figure 2. The water velocities along the river are also shown. The maximum velocity is about 3 m/s for the initial 15 minutes, comparing to 2 m/s under the jam toe before releasing. After that, the surge starts to attenuate and velocity becomes smaller. It is noticed that the velocity under the moving toe is higher than the water velocity of the open water reach ahead of the ice run.

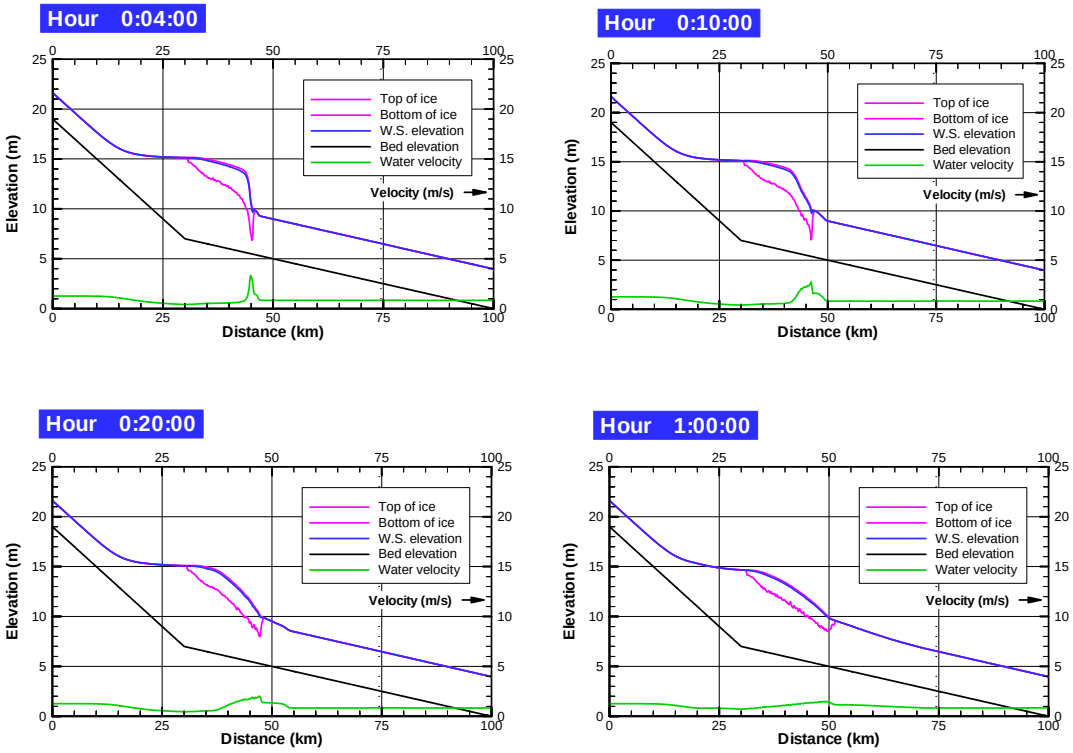

Fig. 2. Longitudinal profiles after the jam released

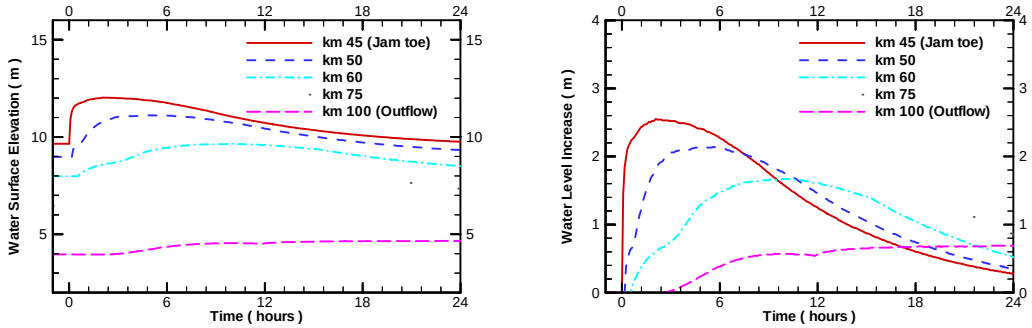

Fig. 3. a) Stage hydrographs at different locations along the channel, and
b) the increase in stage from the ice free condition

Stage hydrographs, and the profiles of water level increase over a steady state ice-free open channel flow with a constant discharge of 2000 m^3/s, at different locations downstream of the jam toe are plotted in Figure 3. Figure 4 shows the water and combined water and ice discharge at selected downstream locations. Figure 5 shows

simulated water discharge, ice discharge and water level at 30 km downstream of the jam toe. It shows that ice movement lagged the surge front by about 5 hrs, as expected.

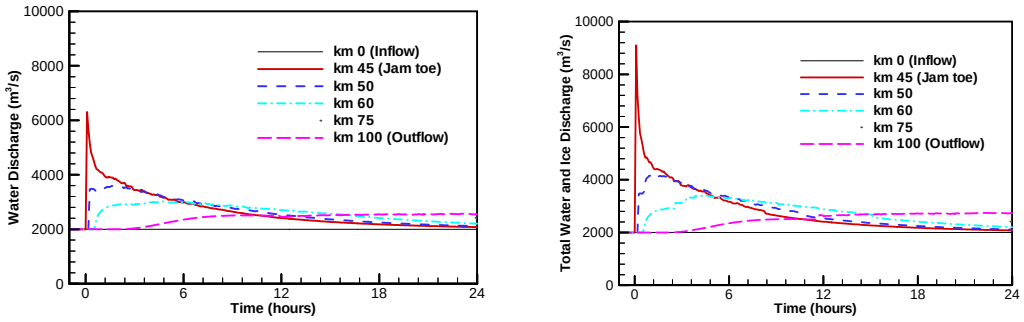

Fig. 4. a) Water discharge hydrographs; and b) combined water and ice discharge hydrographs, at different locations downstream of the jam toe

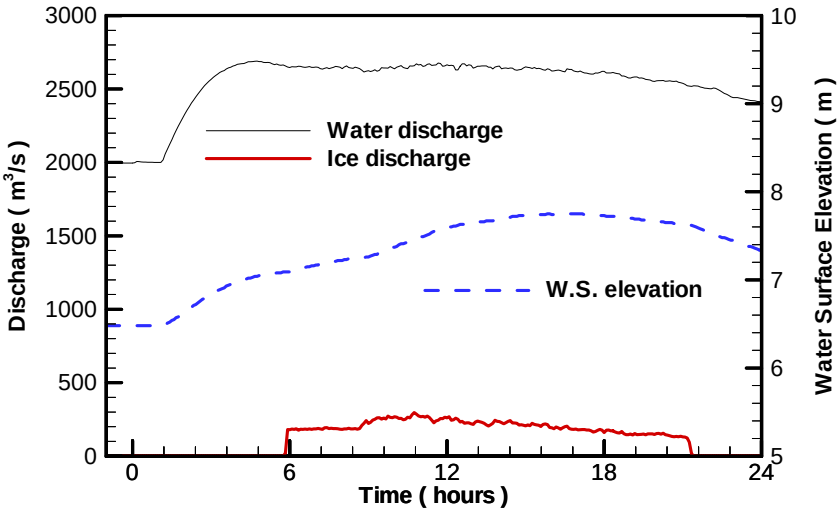

Fig. 5. Simulated water discharge and water level at 75 km

Simulation results with ice resistance neglected

A simulation was carried out for the above case using the same initial and boundary conditions, but neglecting the ice resistance effects by treating the ice mass as water. The simulated stage and discharge hydrographs are shown in Figure 6.

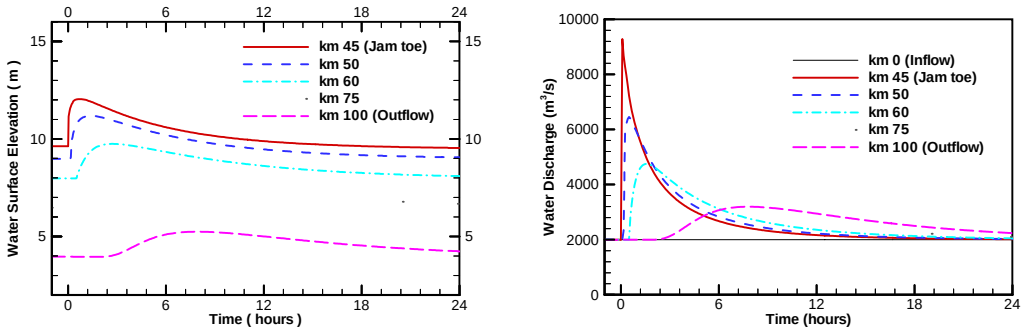

Fig. 6. Stage and discharge hydrographs at downstream location along the channel

Effect of ice resistance

The results from the above simulations showed that the ice resistance has significant effects on both stage and discharge hydrographs during an ice jam release. Figure 7 compares the stage hydrograph, as well as the hydrographs of the combined water and ice discharge, at km 50 for simulations with or without ice resistance. This figure showed that the peak stage values are about the same for both cases, but the stage hydrographs are significantly different. The surge with ice resistance recedes much slower than the case without ice resistance. The discharge hydrographs showed the ice resistance can lower the peak discharge significantly. The results also explained the discrepancies between the simulated results and observed data shown in Figure 3 of Blackburn and Hicks (2003), which neglected the ice resistance effects.

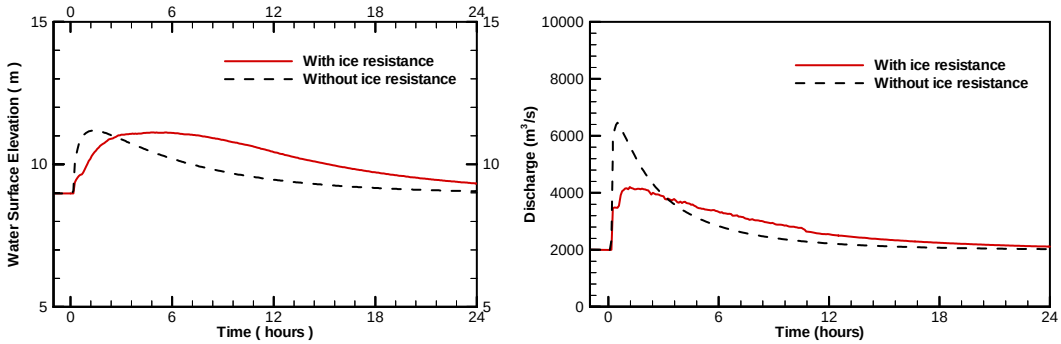

Fig. 7. Effects of ice resistance on stage and discharge hydrographs at 50 km

ICE JAM RELEASE IN A SHORT CHANNEL

In this case, ice jam release in a rectangular channel of 28 km long and 600 m wide is studied. Bed slope of the channel is 0.00012. A constant Manning's coefficient of 0.018 is used for the river bed. The maximum Manning's coefficient of the underside of the ice jam is 0.05. A constant water discharge of 3,600 m^3/s is used as the upstream and downstream boundary conditions. This simulation is used to demonstrate the jam release phenomenon in a reach between run-of-river power stations. The initial steady state longitudinal profiles of ice jam and water surface are shown in Figure 8.

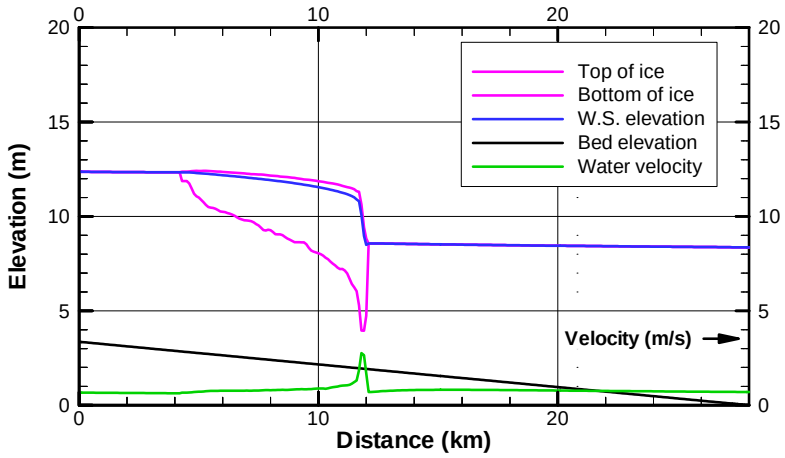

Fig. 8. Simulated ice jam profile and initial condition for jam release

The ice jam release simulation lasted for 10 hours. The water surface and ice jam profiles at 10 min., 35 min., 3 hrs, and 10 hrs after the jam release are shown in Figure 9. The water velocities along the river are also shown. The surge is reflected at the downstream boundary and moves back to upstream as shown in the plot at 35 minutes. The water level increased about 1.0 m at downstream locations due to the surge. This reflected surge is damped when it meets the ice rubble.

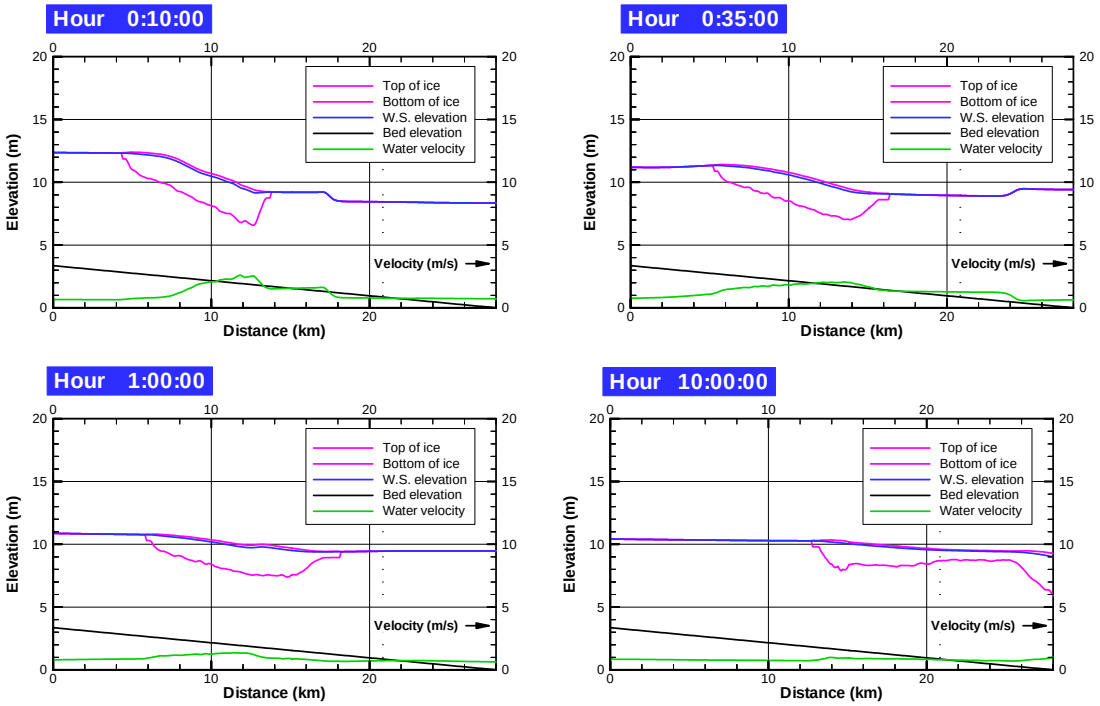

Fig. 9. Longitudinal profiles after the jam released

Simulation results with ice resistance neglected

A similar simulation is carried out for the above case using the same initial and boundary conditions, but neglecting the ice resistance effects by treating the ice mass as water. The simulated stage and discharge hydrographs are shown in Figures 10a) and 11a). To compare with the case with full ice dynamics, corresponding stage and discharge hydrographs with ice dynamics are shown in Figures 10 b) and 11b). These figures demonstrated the ice resistance and damping effects on the released surge.

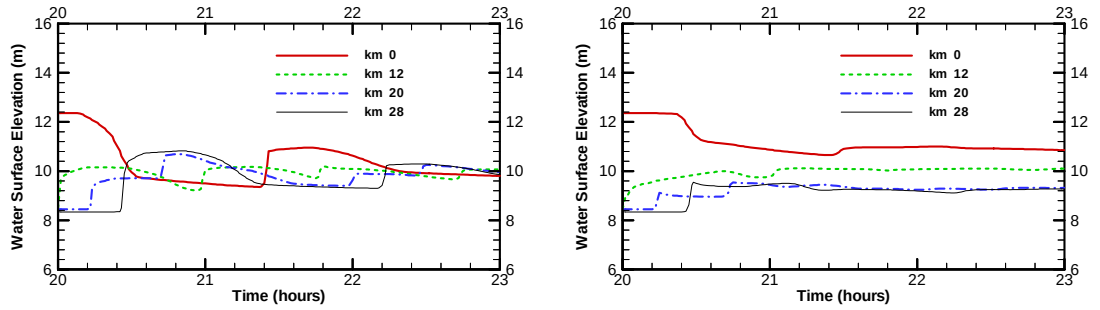

Fig. 10. Stage hydrographs at different locations along the channel:
a) without ice resistance effect; b) with ice dynamics

In the case with the ice resistance neglected, the stage hydrographs in Fig. 10 showed that the surge reflected by the downstream boundary several times before it is dissipated. On the other hand, in the case with ice dynamics, ice damped the surge very fast. Similar effects on discharge hydrographs can be observed from Figure 11.

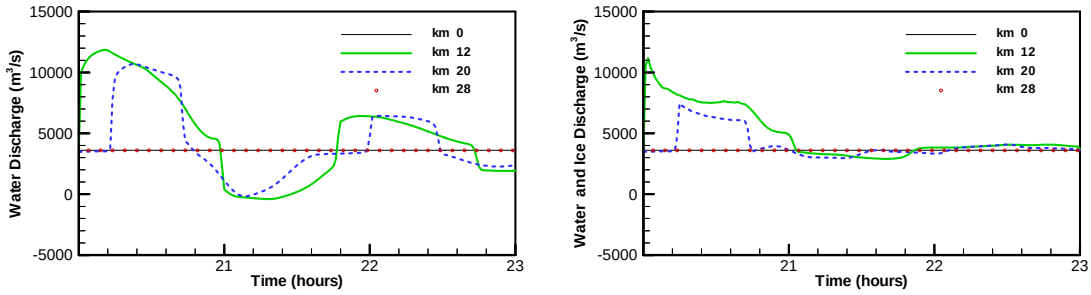

Fig. 11. Discharge hydrographs at downstream locations along the channel: a) without ice resistance effect; b) with ice dynamics

CONCLUSIONS

Surges produced by ice jam releases in idealized channels are simulated using a fully coupled flow and ice dynamic numerical model. The results showed that the resistance of ice jam slows down the release processes. The hydrographs at downstream locations are different from that of the simplified approach with ice resistance neglected. The real peak discharges at downstream locations can be much smaller than that calculated from the hydraulic-only approach.

Before the present study, most of the investigators used simplified hydraulic approach to study ice jam release. This study shows that ice dynamic effects cannot be neglected in the process of ice jam release and related surge propagation.

REFERENCES

Beltaos, S. and Krishnappan, B.G. Surges from ice jam release: A case study, *Canadian Jour.* Civil Eng., 9. 276-284, (1982).

Berger, R.C. and Stockstill, R.L. Finite-element model for high-velocity channels. *Journal of Hydraulic Engineering*, 121(10), ASCE, 710-716 (1995).

Blackburn, J. and Hicks, F.. Suitability of dynamic modeling for flood forecasting during ice jam release surge events, *Journal of Cold Regions Engineering*, Vol. 17, No. 1, (2003).

Brooks, A.N. and Hughes, T.J.R. Streamline upwind Petrov Galerkin Formulations for Convection Dominated Flows with Particular Emphasis on the Incompressible Navier-Stokes Equations. *Computer Methods in Applied Mechanics and Engineering*, 32, 199-259 (1982).

Henderson, F.M. and Gerard, R. Flood waves caused by ice jam formation and failure, *Proceedings, IAHR Symposium on Ice*, Quebec, (1981).

Hicks, F.E. and Steffler, P.M. Characteristic dissipative Galerkin scheme for open channel flow, *Journal of Hydraulic Engrg*, ASCE, 118(2), 337-352 (1992).

Jasek, M. Ice jam release surges, ice runs, and breaking fronts: field measurements, physical descriptions, and research needs. *Canadian Jour. of Civil Engineering*, 30, 113-127 (2003).

Liu, L. and Shen, H.T. A Two-dimensional Characteristic Upwind Finite Element Method for Transitional Open Channel Flow. *Report 03-04, Department of Civil and Environmental Engineering*, Clarkson University, Potsdam, NY (2003).

Shen, H.T., Su, J., and Liu, L. SPH Simulation of River Ice Dynamics, *Journal of Computational Physics*, 165(2), 752-770 (2000).

17th International Symposium on Ice
Saint Petersburg, Russia, 21 - 25 June 2004
International Association of Hydraulic Engineering and Research

ANCHOR ICE AND WATER EXCHANGE IN THE HYPORHEIC ZONE

E.W. Kempema[1] and S.K. Konrad[1]

ABSTRACT
Anchor ice formation can affect the local stage of rivers on a diel basis. Changing stage over distances of a few meters changes the head distribution in sub-stream sediments which in turn affects the exchange of water and heat between the river and the adjacent aquifer (the hyporheic zone). A vertical array of thermistors was placed in the bed of the Laramie River, Wyoming, to study this exchange. This array, which extended to 0.32 m below the sediment/water interface, was situated in of an area where anchor ice commonly forms. On nights when anchor ice formed, stage at the thermistor site decreased. Associated with stage decreases were temperature increases of up to 1.97^{o} C in the streambed sediment. The temperature rises were caused by advection of relatively warm aquifer water upward due to changing local hydraulic gradients associated with anchor ice formation. Changes in hyporheic flow paths associated with anchor ice formation may affect the final distribution of anchor ice on the streambed.

INTRODUCTION
The flow of stream water into and out of near-stream sediment over relatively short distances is known as hyporheic flow (Kasahara and Wondzell, 2003; White *et al.*, 1987; Malcolm *et al.*, 2002). The region where this exchange flow occurs, which can be either beneath or to the side of the stream channel (Harvey and Bencala, 1993; Brunke and Gonser, 1997), is the hyporheic zone. Water movement in the hyporheic zone can be characterized by Darcy's Law:

$$q = -K_h \frac{dh}{dl} \quad , \tag{1}$$

q is the specific discharge (m s^{-1}), K_h hydraulic conductivity, and dh/dl is the local head gradient. In a combined field and modeling study Harvey and Bencala (1993) found that stream-hyporheic zone water exchange is controlled by streambed and stream water slope variations. At small scales, stream water tends to infiltrate into the bed upstream of bed forms and large woody debris piles, at the tails of pools, at the heads of riffles and at the tail of steps in step/pool sequences. Hyporheic water tends to enter the

[1] University of Wyoming, Department of Geology and Geophysics, Dept 3006, 1000 University Ave, Laramie, WY 82071. corresponding email: kempema@uwyo.edu

stream at the downstream end of bed forms and woody debris piles, at the heads of pools, and at the tails of riffles (White *et al.*, 1987; Harvey and Bencala, 1993; Baxter and Haurer, 2000). Water exchange at larger scales is influenced by channel sinuosity, the flow of water through point bars, and flow to secondary channels (Kasahara and Wondzell, 2003). Hyporheic flow paths can vary from centimeters to kilometers in length (Brunke and Gonser, 1997), the time to transit these flow paths can vary from hours to months.

Although individual, local-scale hyporheic exchange flow events may be small, the sum of the exchange flows can be very important. Stream water/hyporheic water exchange can affect physiochemical gradients and nutrient concentrations (Brunke and Gonser, 1997) and faunal distributions (Baxter and Haurer, 2000; Malcolm *et al.*, 2002). Researchers have used several different methods for studying hyporheic exchange flow in the field, including chemical tracers (Harvey and Bencala, 1993), mapping the local hydraulic gradient (Harvey and Bencala, 1993; Baxter and Haurer, 2000; Kasahara and Wondzell, 2003; Wondzell and Swanson, 1999), and using heat as a tracer (White *et al.*, 1987; Alexander and Caissie, 2003; Silliman and Booth, 1993; Silliman *et al.*, 1995; Malcolm *et al.*, 2002; Constantz and Stonestrom, 2003).

Constantz and Stonestrom (2003) note that heat is especially well suited for delineating small-scale hyporheic flow paths. Naturally occurring temperature changes in the near stream environment are often large and rapid, providing an easily identified and measured thermal signal. They point out that temperature patterns can immediately indicate the general nature of the flow regime. Reaches of the channel in which sediment-temperature fluctuations are highly damped relative to in-stream temperatures indicate high rates of hyporheic discharge to the stream (*i.e.*, groundwater discharge to a gaining stream reach). Streambed temperatures that closely follow stream-water temperatures indicate high rates of stream water loss into bed sediments (*i.e.*, ground water recharge from a losing reach). The rates, locations, and timing of stream-water gains and losses can be quantified by deploying an array of temperature sensors in the stream and adjacent sediments.

Anchor ice is spongy masses of ice that form on the bottom of water bodies. Tsang (1982) outlines conditions leading to anchor ice formation and anchor ice characteristics. Anchor ice forms in turbulent, supercooled water, and can grow to cover large areas of a riverbed. Tsang points out that the bond between anchor ice and a riverbed is dependent on the heat balance of the water. When the water column is supercooled, anchor ice sticks tenaciously to the bed. When the water is slightly warmed, anchor ice can be easily dislodged from the bed, or will spontaneously release from the bed. Tsang (1982) notes that anchor ice is most commonly observed on boulder and gravel bottoms, and is almost never observed on fine-grained bottoms. One reason given for this is that fine-grained bottoms are under the influence of terrestrial heat flow in the laminar boundary sublayer rather than in the supercooled main flow. This implies that heat flow from the bed affects anchor ice adhesion.

In this paper, we look at time series data of river water and bed temperature during periods of anchor ice formation in a small river. Previous studies of bed temperatures during anchor ice formation include work in the Niagara River reported by Tsang

(1982), where temperatures 20 cm below the river bottom were ~0.4^{o}C when river water was supercooled. Baxter and Hauer (2000) note that hyporheic flow may have a moderating effect on river water temperatures in the Lion River, Montana. Ice cover was reduced in gaining reaches of the river but the effect was reduced downstream of the area where warm water flowed into the stream. The input of warm hyporheic water may have inhibited anchor ice formation.

METHODS

The study was carried out on the Laramie River, a meandering, riffle and pool stream that flows through a large, semi-arid intermountain valley in southeastern Wyoming, USA. Between October and March, the river is about 10 m wide, 20 to 75 cm deep, and has current speeds of 15 to 60 cm s^{-1}. Discharge during this period is <1.2 m^3 s^{-1}. A solid ice cover forms on the Laramie River in late November or early December. Anchor ice forms approximately 10 to 20 times during the transition from open water to a solid ice cover. The anchor ice forms on cold, clear nights and is released from the bed when the water warms in the morning. During the most extreme events, anchor ice will grow all the way to the water's surface in riffles, and form anchor ice dams with vertical faces up to 20 cm high.

For this study we collected stream stage data and temperature data of stream water and the alluvium under the stream. Stage was measured with a vented pressure transducer that was mounted 5 cm above the streambed. Temperatures were measured with thermistors that were accurate within ±0.04 ^{o}C, with a resolution of 0.005 ^{o}C. Thermistors were attached to a 1-cm-diameter wooden dowel that was driven into the streambed. Thermistors were mounted in the water column 0.11 m above the bed, and at -0.01, -0.17 and -0.32 m below the sediment water interface. The thermistors and pressure transducer were positioned about 2 m from the right stream bank in the right channel of Laramie River where the river bifurcates around a 75 m long by 25 m wide island. The instruments were placed at the tail of a riffle. This riffle extends 25 m upstream to the head of the island. The stream bottom in the riffle is composed of sandy gravel. This location was chosen because it is an area where anchor ice commonly forms.

The data used in this study were collected over an eight day period in November 2001 when anchor ice formed on the bed of the river. Morning trips were made to the river during this time to determine the extent of anchor ice formation. Time series data were collected at 15 minute intervals, and were later analyzed. Data analysis consists of a qualitative analysis of the records and the use of 1D, finite difference approximations of the advection/diffusion equation to determine the water velocity and heat fluxes during the study period. Vertical water velocity at -0.17 m is determined by:

$$\frac{\partial T}{\partial t} = \kappa \frac{\partial^2 T}{\partial z^2} - v \frac{\partial T}{\partial z}, \tag{2}$$

T is temperature, t is time, z is (vertical) distance, and v is velocity. These calculated velocities are then used to calculate the total heat flux, Q, with:

$$Q = Q_c + Q_a = -K \frac{\partial T}{\partial z} + \rho_f C_{\rho f} T v, \tag{3}$$

Q_c is the conductive heat flux, Q_a is the advective heat flux associated with water movement through the bed, K is a combined thermal conductivity for bed water and

sediment, set to 1.4 W m^{-1} $^oC^{-1}$, ρ_f is the water density, and $C_{\rho f}$ is the specific heat of water.

RESULTS

Anchor ice formation in the Laramie River is characterized by a diel cycle. As air temperatures decrease in the fall, anchor ice forms at night and is released during the following morning. Over the course of one to four weeks, as daily air temperatures decrease, a surface ice cover grows from the river's edge and thickens until it covers the entire river surface. At this point, anchor ice formation ceases. Anchor ice was first observed at the study site on day 323 (19 November 2001, Figure 1). On this day, the entire riffle upstream of the thermistors was covered by a layer of anchor ice at 0830. By 1130 all of the ice in the river had melted. On the mornings of days 324 and 325, the amount of anchor ice formation was even greater. On these two mornings, anchor ice filled the entire water column, forming anchor ice dams 1 to 3 m upstream of the thermistors. The water level upstream of the dams was raised by 10 to 15 cm, which flooded the riffle upstream of the dam, resulting in formation of a surface ice cover over the riffle. At the same time, the anchor ice dams increased stream flow to the left channel around the island, which decreased stage at the thermistors. On both of these days, the anchor ice dams and surface ice covers were gone by 1100. On days 326 and 327 a warm front moved through the region, and the water column did not cool to the freezing point. Anchor ice was again observed on days 328 and 329, when nighttime air temperatures dropped below the freezing point. However, anchor ice volumes were smaller than before because the open-water surface area of the stream decreased as border ice grew in the study reach. On day 330, air temperature dropped and 12 cm of snow fell at the study site. These conditions led to formation of a solid surface ice cover that lasted until the following February.

Figures 1 A and B show the stage and temperature data for the period when anchor ice formed in the Laramie River study reach. On nights preceding mornings when anchor ice was observed (the mornings of days 323, 324, 325, 328, and 329) the temperatures at all depths decreased to a minimum around 2400. At that time, the water column temperature was near 0^oC, and we assume that anchor ice started growing in the riffle. On these nights, river water stayed near the freezing point until mid-morning. In contrast, soon after the river water reached its minimum temperature, temperatures in the sub-stream sediment began to rise (Figure 1B). The largest bed temperature rise is seen on the early morning of day 324, when temperatures at -0.01 m reached 1.97^0C while the water column stayed near the freezing point. During periods when the water column warmed there was no divergence between the water column and -0.01 m temperatures. On nights when anchor ice formed, there were small drops in river stage at the thermistor site (~0.06 m on days 324 and 325, Figure 1A).

The 1D modeling of water velocity at 0.17 m depth (Figure 1C) shows that there were upward spikes in the vertical water velocity associated with the temperature increases seen in the sediment when anchor ice formed on the riverbed. These upward spikes, which range from ~3 to 6 X 10^{-6} m s^{-1} (1-2 cm $hour^{-1}$), occur when anchor ice first starts forming on the riverbed. This increased flux of water through the sediment drives an increased advective heat flux (Figure 1D).

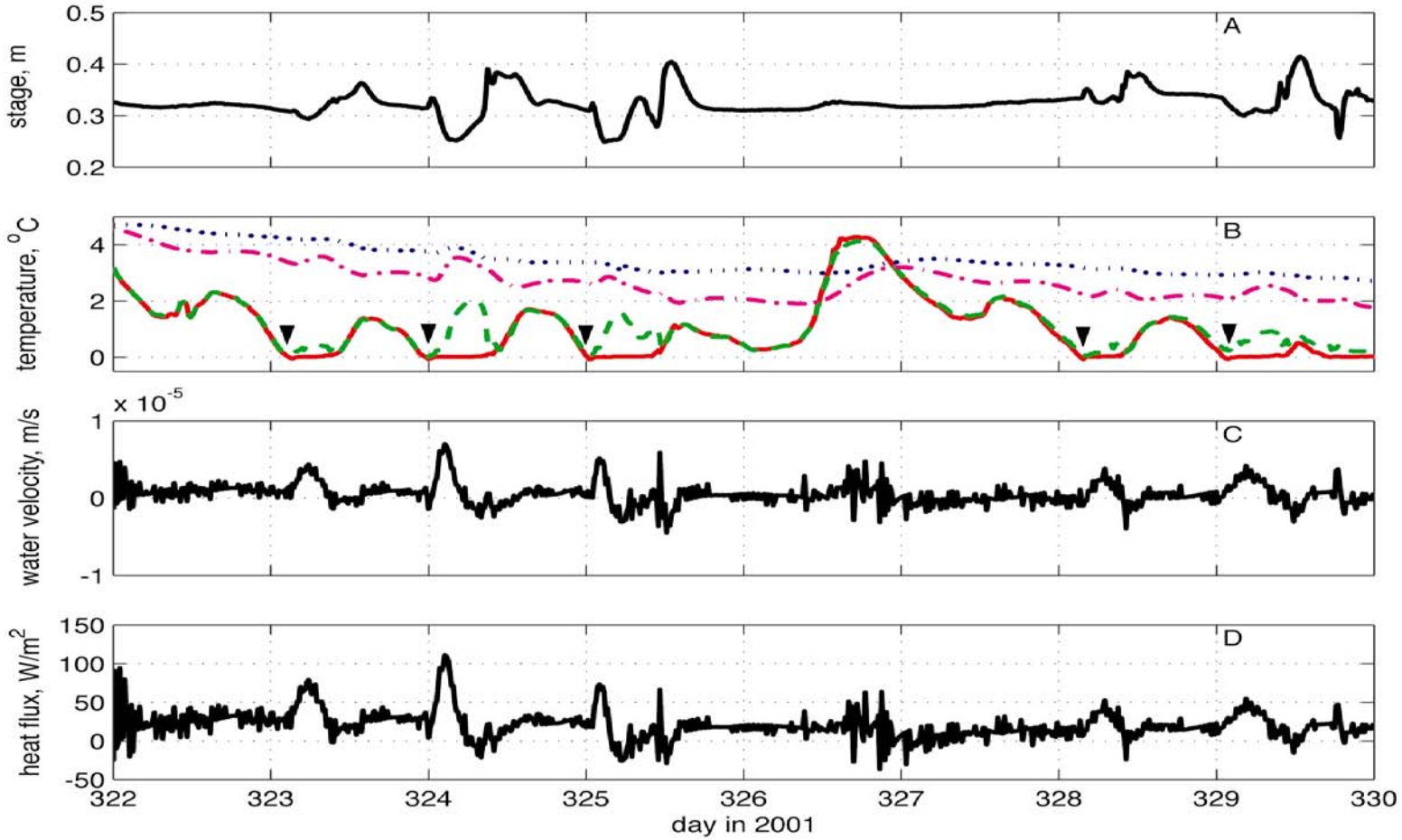

Figure 1. (A) River stage at thermistor site. (B) Temperatures at study site; solid: water column, dashed: 0.01 m below streambed (-0.01 m), dash-dot: -0.17 m; dotted: -0.32 m. Vertical arrows mark beginning of anchor ice formation events. (C) Modeled vertical water velocity. (D) Modeled heat flux.

DISCUSSION

The most surprising outcome of our observations is that temperature in the shallow sediment beneath the streambed increased during nights when anchor ice formed (Figure 1B). Qualitatively, the fact that streambed temperatures do not follow the water column temperature in a damped fashion when anchor ice is present suggests that hyporheic water is flowing out of the bed at that time (Constantz and Stonestrom, 2003). This qualitative assessment is confirmed by our modeling of water velocity at -0.17 m: on all five days when anchor ice formed there is an upward velocity spike of 3 to 6 X 10^{-6} m s^{-1} in fluid flow at 0.17 m depth in the bed (Figure 1C). Changes in vertical water velocity in the bed are driven by changes in head, so we solve Darcy's Law (equation 1) for *dh*, using the maximum velocity seen during the early morning hours of day 324 (6 X 10^{-6} m s^{-1}). To solve this equation, we use methods outlined by Fetter (1994) to estimate the hydraulic conductivity of streambed sediment based on the grain size (K_h = 0.001 m s^{-1}). We assume *dl* is 0.17 m. With these values a $dh \cong 0.001$ m is required to drive the observed upward flow. This analysis is based on the assumption that the change is head is instantaneous (*i.e.* dh/dl = 0.001 m/0.17 m). The observed 0.06 m stage change occurred over about a three-hour period (Figure 1A), but the gradient is large enough to account for our modeled upward flow. The drop in river stage means that the hydraulic gradient is reduced upward, so flow is out of the sediment into the streambed.

Although a 1D vertical model gives reasonable values for the vertical water velocity, the actual hyporheic flow was probably much more complex. In addition to the head drop at the thermistor site, on at least two nights (days 324 and 325), the formation of an anchor ice dam 1 to 3 m upstream of the thermistors raised the stream stage by 0.1 to 0.15 m. This change in head should have driven stream water into the bed upstream of the anchor ice dam, and may have contributed to the flux of water and heat out of the bed at the thermistor site. The thermistor site, at the tail of the pool, was at a site where hyporheic out flow often exits the streambed (Baxter and Haurer, 2000). Similarly, the area upstream of the anchor ice dam, nearer to the head of the riffle, is commonly identified as a site where river water flows into the bed. We speculate, therefore, that the formation of anchor ice on the bed did not initiate hyporheic flow, instead it may have enhanced flow along an already existing hyporheic flow path. The rapid change in streambed temperature associated with anchor ice formation (Figure 1B) illustrates how sensitive hyporheic flow is to small changes in the local head distribution. Anchor ice changes the stage in the stream by a few centimeters over distances of a few meters, which changes the head distribution in sub-stream sediments and the hyporheic flow characteristics. All of these changes occur on a diel cycle as anchor ice forms during cold nights and is released from the bed on the following mornings.

Hyporheic flow paths may also influence the distribution of anchor ice on the streambed. Stream reaches where supercooled water flows from the stream into the bed will cool rapidly, promoting anchor ice formation. In areas where relatively warm hyporheic water is discharging from the bed anchor ice growth is inhibited. This study shows that anchor ice formation and associated stage changes affect hyporheic flow on a daily cycle. This suggests that there may be some type of feedback mechanism between the anchor ice and hyporheic flow. The initial anchor ice that forms on the bed changes local stage, which changes the local hyporheic flow characteristics. The

changes in hyporheic flow may affect the final distribution of anchor ice on the streambed. Because of the limited instrumentation used in this study, we were unable to map changes in hyporheic flow over large areas. However, our observations suggest that hyporheic flow may be an important process in determining the distribution of anchor ice on a streambed, and should be considered when mapping anchor ice distributions.

REFERENCES

Alexander, M.D., and Caissie, D. Variability and comparison of hyporheic water temperatures and seepage fluxes in a small Atlantic salmon stream, *Ground Water 41(1)*: 72-82 (2003).

Baxter, C.V., and Haurer, F.R. Geomorphology, hyporheic exchange, and selection of spawning habitat by bull trout (Salvelinus confluentus), *Canadian Journal of Fisheries and Aquatic Science 57*: 1470-1481 (2000).

Brunke, M., and Gonser, T. The ecological significance of exchange processes between rivers and groundwater, *Freshwater Biology 37*: 1-33 (1997).

Constantz, J., and Stonestrom, D.A. Heat as a tracer of water movement near streams. In *Heat as a Tool for Studying the Movement of Groundwater Near Streams*, D.A. Stonestrom, and J. Constantz ed., *U.S. Geological Survey*, Reston, VA, (2003) 1-6.

Fetter, C.W. Applied Hydrogeology. *Prentice-Hall*, Upper Saddle River, NJ, (1994) 691 p.Harvey, J.W., and Bencala, K.E. The effect of streambed topography on surface-subsurface water exchange in mountain catchments, *Water Resources Research 29(1)*: 89-98 (1993).

Kasahara, T., and Wondzell, S.M. Geomorphic controls on hyporheic exchange floe in mountain streams, *Water Resources Research 39(1)*: 1005, doi:10.1029/2002WR001386 (2003).

Malcolm, I.A., Soulsby, C., and Young, A.F. Thermal regime in the hyporheic zone of two contrasting salmonid spawning streams: ecological and hydrological implications, *Fisheries Management and Ecology 9*: 1-10 (2002).

Silliman, S.E., and Booth, D.F. Analysis of time-series measurements of sediment temperature for identification of gaining vs. losing portions of Juday Creek, Indiana, *Journal of Hydrology 146*: 131-148 (1993).

Silliman, S.E., Ramirez, J., and McCabe, R.L. Quantifying downflow through creek sediments using temperature time series: one-dimensional solution incorporating measured surface temperature, *Journal of Hydrology 167*: 99-119 (1995).

Tsang, G. Frazil and Anchor Ice: a Mongraph. *Natural Resources Council Subcommittee on Hydraulics of Ice Covered Rivers*, Ottowa, Ontario, Canada, (1982) 90 p.

White, D.S., Elzinga, C.H. and Hendricks, S.P., Temperature patterns within the hyporheic zone of a northern Michigan river, *Journal of the North American Benthological Society 6(2)*: 85-91 (1987).

Wondzell, S.M., and Swanson, F.J. Floods, channel change, and the hyporheic zone, *Water Resources Research 35(2)*: 555-567 (1999).

17th International Symposium on Ice
Saint Petersburg, Russia, 21 - 25 June 2004
International Association of Hydraulic Engineering and Research

AN EXPERIMENTAL STUDY ON SNOW-AND SUPERIMPOSED-ICE FORMATION ON SEA ICE

T. Kawamura[1], O. Matsubaya[2], A. Sato[3] and Y. Kamata[3]

ABSTRACT

Contribution of snow cover to sea ice growth has recently become of major interest. The contribution is due to two specific types of sea ice growth process, i.e., snow-ice and superimposed-ice growth. An experimental study was conducted in a cold laboratory to clarify physical and isotopic processes controlling their formation. The sea ice growth progress was observed through windows of a tank, and temperature variations were recorded. Structure of the collected sea ice samples was analyzed, and ice properties, i.e. salinity and isotopic compositions, were measured. The results revealed different ice properties between the snow- and superimposed- ice as well as between granular and columnar ice. The relationship of hydrogen and oxygen isotopic compositions could determine the origin of water forming snow- and superimposed-ice and specify the mixing processes.

INTRODUCTION

From recent studies conducted in Antarctic Oceans, contribution of snow cover to sea ice growth has become of major interest (e.g., Lange et al., 1990; Lange and Eicken, 1991; Jeffries et al., 1994). The snow cover involved in two specific types of sea ice growth process, i.e., snow-ice and superimposed-ice growth. Snow ice is built from a mixture of surface snow and infiltrating seawater (e.g., Lange et al., 1990). Superimposed ice is formed by the refreezing of fresh melt water that percolates through surface snow cover onto ice. This type of sea ice growth was found on pack ice (Jeffries et al., 1994) and on landfast sea ice (Kawamura et al., 1997).

These upward growth processes can be very effective mechanisms for thickening, because the freezing interface is close to the cooling source. Hence, understanding these

[1] Institute of Low Temperature Science, Hokkaido University, Sapporo, Japan
[2] Faculty of Engineering and Resource Science, Akita University, Akita, Japan
[3] The Shinjo Branch, Nagaoka Institute of Snow and Ice Studies, National Research Institute for Earth Science and Disaster Prevention, Shinjo, Japan

growth processes is quite interesting and need to be investigated. In this study, therefore, both ice types were experimentally formed in a seawater tank placed in a cold laboratory. The paper discusses the physical and isotopic processes involved in the ice growth, using growth observation, ice structural analysis, and temperature, salinity and isotopic measurements. The experiment was repeated four times, including two preliminary runs. Since the results were similar among runs, the paper will focus on one of them, though some results of the other runs are discussed on the isotopic measurement.

EXPERIMENT

Equipment

Experiments were conducted in the Cryospheric Environment Simulator (CES, Fig.1, A), a highly equipped cold laboratory, located at the Shinjo Branch, Nagaoka Institute of Snow and Ice Studies, National Research Institute for Earth Science and Disaster Prevention (NIED). The CES is equipped with a snowfall machine (area: 3m x 5m) making a large amount of snow (intensity: 0-5 mm/h water equipment) with crystal shapes (0.025 mm spheres) similar to those of natural snow. It also includes a solar simulator (area: 3m x 5m) providing radiation similar to natural solar radiation with variable fluxes in the 0 - 1000 W/m^2 range.

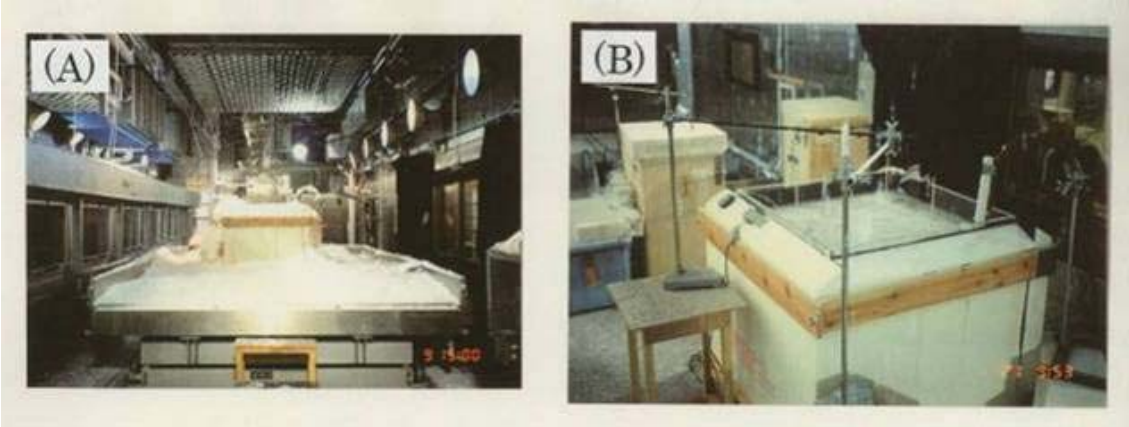

Fig. 1. Photographs of (A) the experimental facilities in the cold room and (B) the experimental tank

A rectangular transparent acrylic water tank, whose inner sizes are 800 x 800 mm and 600 mm in height, was set on a table in the cold laboratory (Fig. 1, B). Figure 2 shows a schematic drawing of the tank with some accessories. Its sidewalls and bottom were covered with insulation boards with 100 and 200 mm in thickness, respectively, to prevent ice growth from them. Belt-shaped heaters of 50 mm width were set around the sidewalls at the level of water surface to prevent growing sea ice from sticking to the walls. Seawater with a salinity of 32 psu was poured into the tank up to a height of 500 mm. Temperature was recorded every five minutes near a corner of the tank using total of 19 thermocouples at levels between 200 mm above and 200 mm below the initial water surface (Fig. 2).

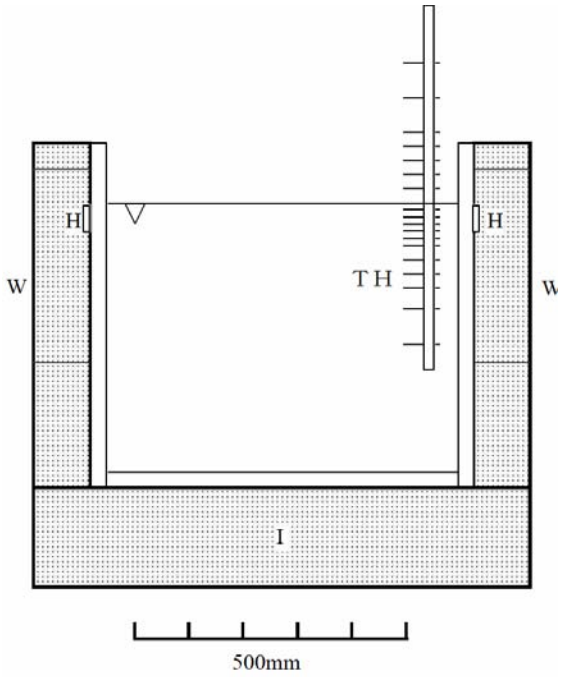

Fig. 2. A schematic drawing of a vertical section of the experimental tank with accessories. T: transparent acrylic water tank, I: insulation walls, TH: thermocouples, H: belt-shaped heater, W: observation windows. The 19 thermocouples are set at 10, 20, 30, 40, 50, 60, 80, 100, 120, 150 and 200 mm above the initial water surface, at 20, 40, 60, 80, 100, 150 and 200 mm under the surface, and just on the surface. The topside of the inversed triangle denotes the water level

Experimental procedures

Firstly sea ice grew to about 90 mm thick for 45 hours. Snowfall was then allowed for six hours till 200 mm of snow had accumulated on a reference plate beside the tank. The sea ice surface was depressed by its weight of the overlying accumulated snow. After "aging" for two days, some snow was piled onto the snow surface to simulate a newly accumulated snow cover (termed "second snow accumulation") of about 60 mm thick. Immediately after the snow accumulation, artificial light was shone on the snow surface for eight hours to melt the snow cover. Intensity of the radiation was selected at 750 W/m^2. On the next day, about 19 hours after the radiation, sea ice samples were collected with a small core sampler. The room temperature was kept constant at -20°, while varied to -10 or -15° for two short durations (cf. Fig. 3, a), considering a better growth progress. Occasionally we observed the features of sea ice growth through the viewing windows of the sidewall.

Measurements of ice properties

Structure of collected sea ice samples was observed through the vertical thick and thin sections. The samples were cut to small pieces at 10 to 20 mm intervals according to stratigraphic variability. The cut pieces were then melted and the chlorinity were determined by the titration method (TOA Electronics, SAT-210, accuracy of 0.1 psu) in Hokkaido University. The chlorinity was converted to salinity by a formula (e.g., Bennett, 1976). Their isotopic composition in hydrogen and oxygen (D/H and $^{18}O/^{16}O$) were determined with a mass spectrometer (Finnigan MAT 250) at Akita University, using standard techniques.

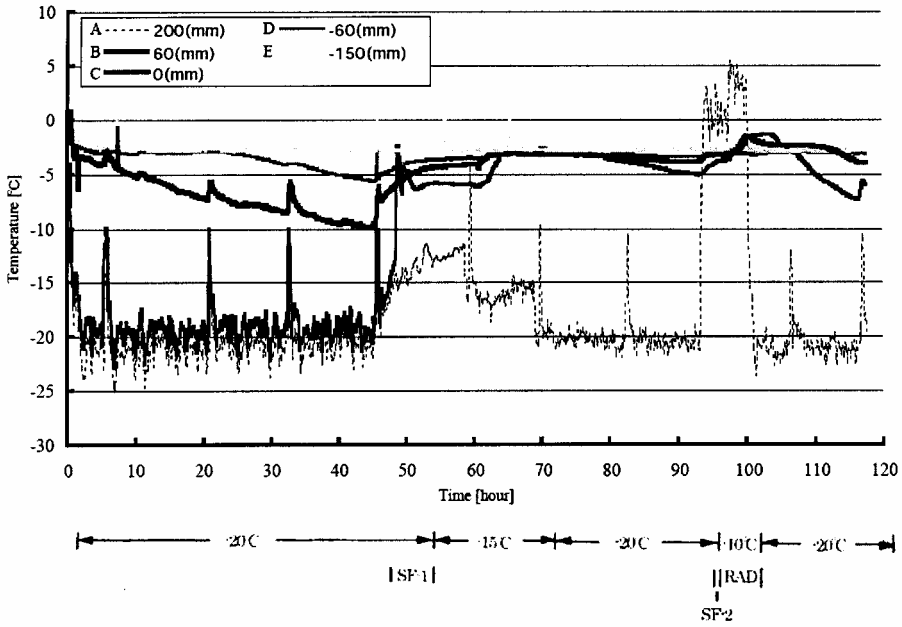

Fig.3. Temperature variations at the selected five points. The room temperature (a) and events (b) are shown at the bottom of the each figure. “SF-1” and “SF-2” mean the first and second snow fall, respectively. “RAD” denotes radiation

RESULTS

Temperature variations

Figure 3 shows temperature variations at five selected thermistor points during a 5-day experiment. The air temperature at 200 mm above the original water surface, shown by Line A, fluctuated around the set room temperature of – 20° except for the duration of snowfall and radiation. Several pulse-like increases were caused by heat from lamps for albedo measurements, which were also observed in the sea ice layer (cf. Lines A-C). Seawater temperature (e.g. Line E) was almost constant during the experiment.

Temperature at 60 mm above the surface (Line B) fluctuated around the room temperature until the snowfall and then increased quite steeply because the sensor was buried under the warm snow cover. Thereafter, it kept a constant value of about – 6° for about 10 hours. It increased steeply again at the elapsed time of 62 hours, when seawater infiltrated up around the sensor as observed through the windows. However, later on, the temperature decreased gradually, probably because a snow and seawater mixture had frozen. Due to the radiation, it increased again above the freezing temperature of seawater, implying this point was probably melted. After that, it decreased once again. The temperature just on the original water surface, denoted as 0 mm (Line C), started to decrease immediately after sea ice growth and continued to decrease gradually till the snowfall. Subsequently, it increased and then kept a constant level. Thereafter, it increased again, indicating seawater infiltration. Further, the

temperature kept a value constant at the freezing temperature for a while and then decreased again. Then the temperature behavior appears similar to the one recorded at Line B, suggesting melting and subsequent refreezing. The temperature at 60 mm under the water surface (Line D) kept a constant level, which might be the freezing temperature, till the elapsed time of 20 hours. Then it decreased gradually after the sensor was enclosed by sea ice. After the snowfall, it increased gradually and thereafter kept the freezing point of the seawater again.

Growth progress

The growth progress observed through the windows was illustrated schematically in Fig. 4. Initially, the water surface was covered with a continuous ice skim up to 10 mm thick. Thereafter, sea ice continued to accrete as congelation ice growth onto the bottom of the existing ice sheet, which observed commonly in calm sea surface conditions (Weeks and Ackley, 1982). After about 43 hours (Step A), columnar ice grew up to about 90 mm.

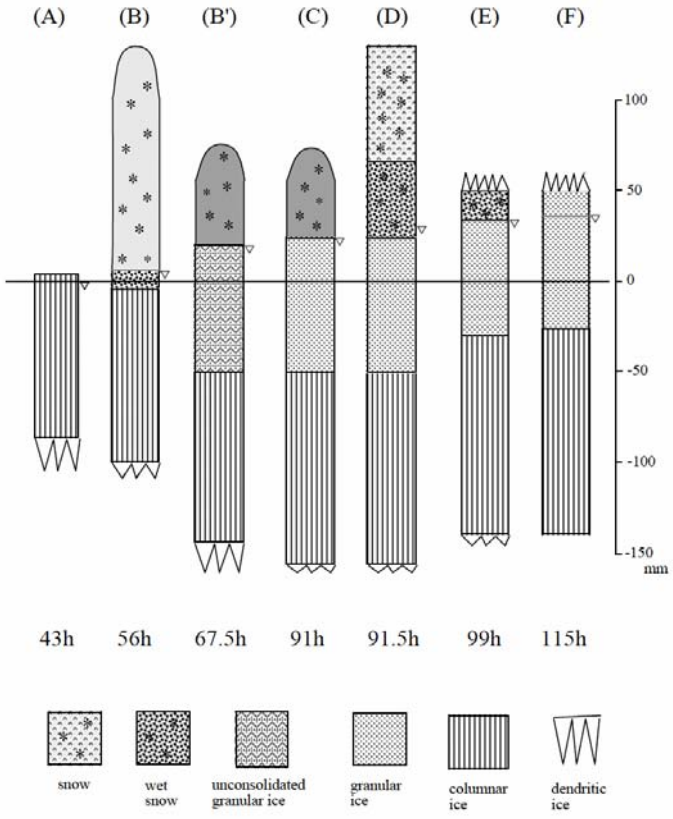

Fig. 4. Schematic drawings of sea ice growth progress observed through windows of the tank. The topsides of the inversed triangles denote the water level. The initial sea level is illustrated as the reference level. The elapsed time is shown at the bottom of the figures. The each figures are correspond to the following events: (A): before snowfall, (B): after snowfall, (C): before the second snowfall, (D): after the second snowfall or before radiation, (E): after radiation, and (F): before sampling. Ice types shown in the legend can be recognized not from the direct observation but from ice structural analysis described in section 3.3

During the snowfall and subsequent snow accumulation, the sea ice together with the overlying snow cover was depressed due to the increasing load of the snow cover. Exceptionally, in this case, because the “floe” stuck to the side-wall, only a 10-mm wet snow layer existed at the end of snowfall event (Step B). On removing of the causes of sticking, six hours after ceasing the snowfall, the floe sunk and, consequently, the part of snow cover located under the water level became soaked with seawater (Step B’). Wet snow patches were seen on the surface.

During the “aging” period preceding the second snow accumulation event, the seawater-soaked snow layer was frozen to create granular ice, i.e. snow ice (Step C). Step D shows the ice and snow conditions just after the second accumulation. After the artificial radiation, not only the whole snow cover but also the top layer of the granular ice was melted, forming a surface slush layer (Step E). After the radiation ceased, the slush layer gradually consolidated turning into superimposed ice (Step F).

Physical Properties

A thin section photograph (Fig. 5, D) shows the existence of a clear horizontal structural boundary between № 106 and № 107. A faint boundary was further found in the granular ice layer between № 102 and № 103, where size and density of bubbles were discontinuously changed. This could be recognized as the boundary between snow- and superimposed- ice. The salinity increased steadily in the granular ice layer from near 0 psu at the top surface to about 10 psu at the interface with columnar ice (Fig. 5, A). In the columnar ice layer, it shows a c-shaped profile except for a decrease at the bottom.

Isotopic compositions

Seawater used in the experiment has δD of -3 ‰, and $\delta^{18}O$ of -0.4 ‰. At the end of the experiments, the seawater shifted to -9 ‰ in δD and -1.1 ‰ in$\delta^{18}O$. The snow has δD of -42 ‰ and $\delta^{18}O$ of -7.3 ‰

The δD and $\delta^{18}O$ values increased regularly in the granular ice, and then in the columnar ice kept constant values of 9 to 10 ‰ in δD and 1.1 to 1.2 ‰ in $\delta^{18}O$, which are higher by about 12 ‰ in δD and 1.5 ‰ in $\delta^{18}O$ than those of the seawater (Fig. 5, B and C) due to fractionation during freezing (e.g., O’Neil, 1968). The values of the granular ice are intermediate of those of the snow and the seawater, suggesting mixing of these two components.

DISCUSSION

Snow ice

Snow ice is created through soaking snow cover with seawater and subsequent freezing of snow-seawater mixture. Therefore, two criteria, a “negative freeboard”, i.e. the height of the ice/snow interface lies below the seawater level, and permeable ice, which occurs above a critical temperature of – 8° (Crocker and Wadhams, 1989), are necessary for snow ice formation. In the present experiment, since temperature met the condition (cf. Fig. 3, Line C, D), seawater infiltration into snow layer could clearly take place. Therefore, the lower layer of the granular ice must be snow ice.

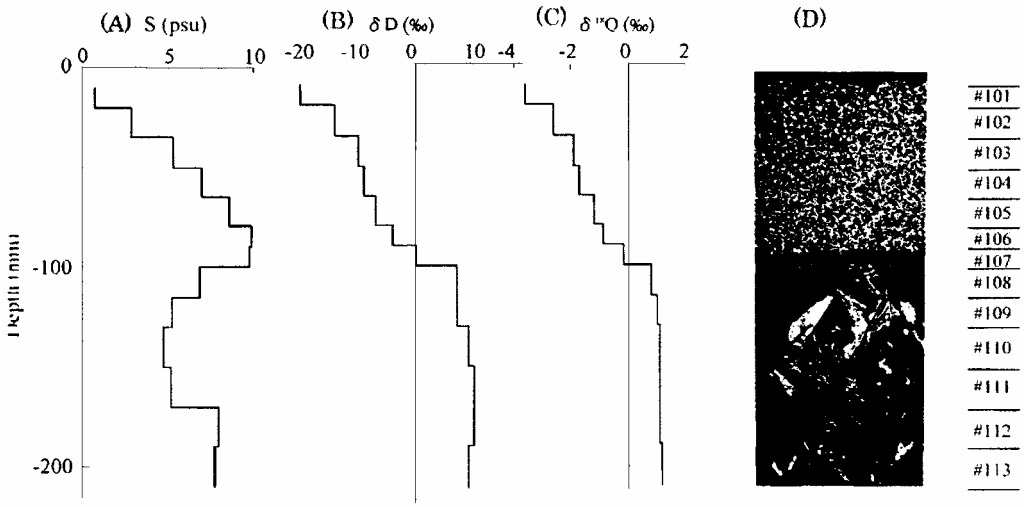

Fig. 5. Profiles of salinity (A), hydrogen and oxygen isotopic compositions (B and C, respectively), and photographic structure (D). The numbers in the rightmost column mean the sample numbers. The numbers in the leftmost column mean the sample numbers

The relationship of δD and $\delta^{18}O$ of ice (Fig. 6) can be used to determine the origin of water forming the ice and specify mixing processes between water of various origins. The relationship for the snow ice samples (№ 103 to №106) accords well with a mixing process between the snow and the columnar ice. Snow and columnar ice can then be considered as the end members of the snow ice in this case. In the case of another run, however, snow ice (№ 204 and № 205, Fig. 7) lies on a mixing line between snow and seawater as the end members. It is notable the difference of the end member that mixes with snow to form snow ice, i.e. columnar ice or seawater. It may be due to some difference in the processes of replacing of residual seawater with newly infiltrating seawater.

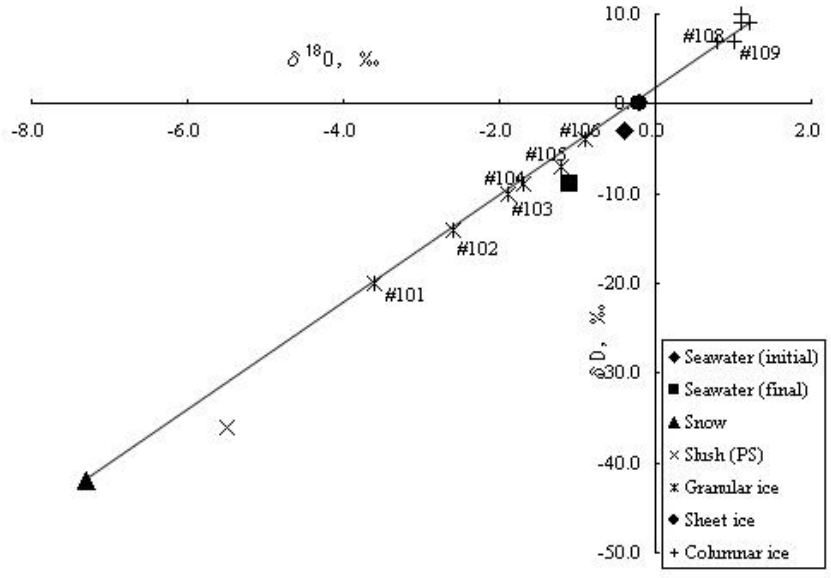

Fig. 6. Relation of oxygen and hydrogen isotopic compositions of the samples

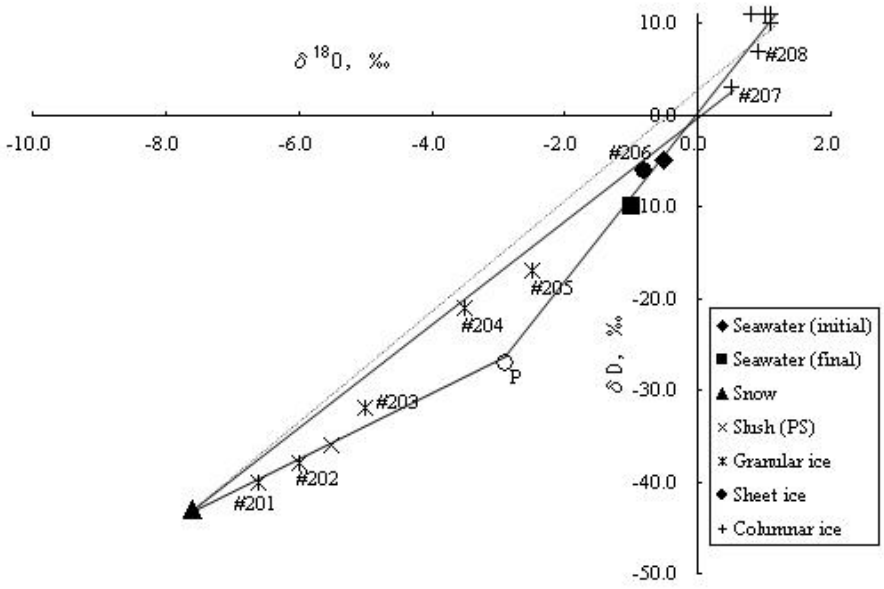

Fig. 7. Relation of oxygen and hydrogen isotopic compositions of another case

The proportion of snow in the snow ice is estimated to be 24 – 36 %. Snow fraction in snow ice collected in the southern Okhotsk Sea was estimated at 5 to 16 % (Toyota, private communication). The values obtained in the Antarctic sea ice range from 10 to 40 % (Lange et al., 1990; Jeffries et al., 1994, 1997). Our estimated range for the snow fraction therefore compares reasonably well with the field observations.

A thin surface patchy slush layer (PS), collected after the first snow accumulation (Step B' in Fig. 4), showed a high salinity of 45.5 psu, while the snow ice salinity ranges between 5 and 10 psu (Fig. 5), suggesting brine rejection during the snow ice formation. Takizawa (1985) found that wet snow soaked with seawater shows initial salinity as high as 30 psu, but abruptly decreasing to 20 psu. By freezing the wet snow to snow ice, the salinity further decreased gradually to approach 8 psu. Lytle and Ackley (1996) obtained a similar result; bulk salinity of a slush layer decreased from 17 psu to 6 psu, after the layer had frozen. The decreasing of the salinity during the freezing process demonstrates that high saline seawater or brine flows out from a consolidating wet snow or slush layer.

Superimposed ice

A faint boundary of the ice structure was observed in the granular ice at the depth of 35 mm. In the upper layer of the granular ice, i.e. superimposed ice, percolation of snow melt water into snow cover would be related. Isotopic compositions of such ice are expected to be similar to those of the snow, because snow melting could progress in thoroughly melting of individual ice grain without change in isotopic compositions. However, values of δD and $\delta^{18}O$ of the uppermost two pieces (№ 101, № 102) are quite different from those of the snow in our case (Fig. 6). The relationship of δD and $\delta^{18}O$ accords with the mixing line of the snow and the columnar ice or the snow ice. This

relationship is reasonably explained, if the uppermost part of the snow ice as well as snow cover melted during the radiation (Step E, in Fig. 4), consequently a mixture of the melt waters was made, and further the mixture was refrozen together with the unmelted snow cover. Actually the uppermost piece (№103) of snow ice has slightly lower isotopic compositions and salinity than the lower part. Further, the piece (№ 102) just above the snow ice has higher isotopic compositions than the upper piece (№ 101) and includes a considerable amount of salt (2.89 psu). These results strongly suggest mixing of the snow and the snow ice. The proportion of snow in the pieces (№ 101 and № 102) is 57 and 44 , respectively, being much smaller than the value expected for a simple mixture of snow and snow melt water. This is due to admixing of melt water from snow ice, where two third consist of seawater. On the contrary, in the case of another run shown in Figure 7, upper three pieces (№ 201 – № 203) show a quite different relation of the mixing line. The high saline slush layer (PS) has isotopic compositions similar to the piece №203. Further, a high saline residue (154 psu), shown by point P, after extreme progress of freezing in an additional experiment shows a relationship very close to the cross point of two extension lines of connecting between the initial and final seawater and of the three pieces. Therefore the superimposed ice of this case is explained as mixing of the snow and high saline residue of seawater.

The salinity of the superimposed ice is lower than that of snow ice. Furthermore, the salinity of the both ice types is much lower than that of the surface slush layer (PS). The result might be brought through the following process: high saline brine in the slush probably permeated the second accumulated snow cover, and after the radiation, the brine would be dispersed into both the upper layer of the snow ice and the lower layer of the snow cover soaked with snow melt water. The result shows brine is rejected from the mixed layer, like the snow ice formation, during the refreezing of its layer to create superimposed ice. The difference in the isotopic properties of superimposed ice mentioned above may be due to some differences in this brine rejection process.

SUMMARY

An experimental study was conducted to form both snow- and superimposed- ice on sea ice in a seawater tank located in a cold laboratory. Structural analysis reveals boundaries among columnar ice, snow- and superimposed- ice, where ice properties changed discontinuously. Growth observation through windows and temperature measurement show the growth progress of snow- and superimposed- ice. The isotopic compositions of snow ice lead an interesting result on its mixing member. It may be caused by some differences in the processes of upward infiltration of seawater and removal of residual seawater from snow ice layer. The salinity and isotopic data of the superimposed ice show that the ice is formed as an effect of melting of both the snow cover and the uppermost part of snow ice. A high saline surface slush layer may play an important role to the process.

The combined analysis of physical and isotopic properties could simulate basic growth processes of both the snow- and superimposed- ice formation. However, it does not provide complete answer to all precise processes during the formation. These unresolved topics need to be investigated further in the laboratory and field. A period of

the experiment seems to be shorter than that of the natural events. Longer experiments need to be conducted.

ACKNOWLEDGEMENTS

This joint study between the Institute of Low Temperature Science, Hokkaido University and National Research Institute for Earth Science and Disaster Prevention (NIED) was conducted in Cryospheric Environment Laboratory (CES) of the Shinjo Branch, Nagaoka Institute of Snow and Ice Studies, NIED. We are also grateful to Mr. Takeda for operating the equipment and supporting the experiment. This work was partly supported by Grants-in-Aid (09680498 and 13490002) for Scientific Research from the Ministry of Education, Culture, Sports, Science and Technology.

REFERENCES

Bennett, A.S., Conversion of in situ measurements of conductivity to salinity, *Deep-Sea Res., 23*, 157-165, 1976.

Crocker, G.B., and P. Wadhams, Modeling Antarctic fast-ice growth, *J. Glaciol., 35*(119), 3-8, 1989.

Jeffries, M.O., R.A. Shaw, K. Morris, A.L. Veazey, and H.R. Krouse, Crystal structure, stable isotopes ($\delta^{18}O$), and development of sea ice in the Ross, Amndsen and Bellingshausen seas, Antarctica, *J. Geophy. Res., 99*(C1), 985-995, 1994.

Jeffries, M.O., A.P. Worby, K. Morris, and W.F. weeks, Seasonal variability in the properties and structural composition of sea ice and snow cover in the Bellingshausen and Amndsen Seas, Antarctica, *J. Glaciol. 43*(143), 138-151, 1997.

Kawamura, T., K.I. Ohshima, T. Takizawa, and S. Ushio, Physical, structure, and isotopic characteristics and growth processes of fast sea ice in Lützow-Holm Bay, Antarctica, *J. Geophy. Res., 102*(C2), 3345-3355, 1997.

Lange, M.A., and H. Eicken, Textural characteristics of sea ice and the major mechanisms of sea ice growth in the Weddell Sea, *Ann. Glaciol., 15*, 210-215, 1991.

Lange, M.A., P. Schlosser, S.F. Ackley, P. Wadhams, and G.S. Dieckmann, ^{18}O concentrations in sea ice of the Weddell Sea, Antarctica, *J. Glaciol., 36*(124), 315-323, 1990.

Lytle, V.I., and S.F. Ackley, Heat flux through sea ice in the western Weddell Sea: Convective and conductive transfer processes, *J. Geophys. Res., 101*(C4), 8853-8868, 1996.

O'Neil, J.R., Hydrogen and oxygen fractionation between ice and water, *J. Phys. Chem., 68*, 3683-3684, 1968.

Takizawa, T., Salination of on sea ice and formation of snow ice, *Ann. Glaciol., 6*, 309-310, 1985.

Weeks, W.F., and S.F. Ackley, The growth, structure, and properties of sea ice, *CRREL Monograph, 82-1*, 130 p, 1982.

17th International Symposium on Ice
Saint Petersburg, Russia, 21 - 25 June 2004
International Association of Hydraulic Engineering and Research

SUMMER ICE CONCENTRATION COMPARISON OF IN SITU AND SATELLITE DATA IN THE ROSS SEA, ANTARCTICA

By Margaret A. Knuth[1], and Stephen F. Ackley[1]

ABSTRACT

In situ sea ice data taken from a Dec 1999-Feb 2000 cruise aboard the RVIB *Nathaniel B. Palmer* is compared with Special Sensor Microwave/Imager (SSM/I) satellite data from the same period. The in situ data comes from analysis of helicopter video covering over 18,000 km (track line) of the Ross Sea and from shipboard observations taken throughout the cruise. The ship measurements showed a complex of thick (3m) multiyear large floes with 1m thick snow and first year floes of thinner ice (<1.5m) with less, but still substantial snow covers (0.2-0.4m). Sea ice concentrations from both the Bootstrap and NASA Team Algorithms are used here for comparison. Previous work has suggested possible errors in estimating concentration, especially in summer, from microwave satellite data. Our objectives include attempted validation, with quantifiable errors, of these two widely used techniques to convert passive microwave data to ice concentrations in summer, using the helicopter video data base as the comparison data. We found that only 50% of the variance in video summer ice concentration is explainable by the passive microwave satellite data. Further, the passive microwave has the troubling nonstationary characteristic of overpredicting concentration at low concentrations and underpredicting ice concentration at higher video concentrations.

INTRODUCTION

Since the launch of the Nimbus-5 electrically scanning microwave radiometer (ESMR) in 1972, passive microwave satellite remote sensing has been used to provide scientists with sea ice coverage data. Particularly in the case of the polar regions, where obtaining in situ data is a difficult process, satellite data sets have given scientists an opportunity to obtain a significantly large spatial and temporal record of events. The data acquisition was taken over in 1987 by the Special Sensor Microwave/Imager (SSM/I) and since then has extended this data set. Of particular importance in Antarctica is its substantial seasonal change in total sea ice cover. Being able to track and predict the

[1] Civil and Environmental Engineering Department, Clarkson University, Potsdam NY 13699, USA

changes in sea ice concentration in Antarctica is important information for many processes. The heat exchange between the ocean and atmosphere is determined by the total coverage of ice in the polar regions and is of great importance for accurate climate models and regional weather prediction. Maps of ice coverage are also important for studies of the regional flora and fauna and for ship navigation.

The satellite data, derived by two well-known algorithms, used for comparison in this work is archived at the National Snow and Ice Data Center (NSIDC). The two algorithms, NASA Team (Cavalieri et al., 1990) and Bootstrap (Comiso, 1990), were both developed at NASA's Goddard Space Flight Center. While both of these algorithms use brightness temperatures, they use different channels and techniques to produce the total sea ice concentration. Much work has been done to validate both of these algorithms and results have shown that they both have difficulty recognizing newly forming, or thin, sea ice. Steffen and Schweiger (1991) showed further that the NASA team algorithm had a larger error in the summer, under melting conditions, and Comiso et al. (1997) have also noted that there are large differences in the two algorithms themselves. In some areas of Antarctica, the Bootstrap algorithm has shown ice concentrations higher than the NASA team by as much as 25% and in other regions lower by up to 30%. For these reasons it is appropriate to compare the satellite data with digital video data retrieved from helicopter flights from the RVIB *Nathaniel B. Palmer* from Dec 1999-Feb 2000, the austral summer. The *Palmer's* work took place in the eastern Ross Sea. This area consistently retains a large expanse (1-2 million km^2) of the residual Antarctic sea ice in the summer, when total sea-ice coverage around Antarctica declines to nearly 20% of its annual maximum (Gloerson et al., 1992). This research cruise represented the US component of the international Antarctic Pack Ice Seals (APIS) program and allowed for an extensive look at the sea ice structure of the region. In this work, not only are the ice concentrations compared, but also the relationship between error and variations in particular parameters including ice type, snow cover, floe size, and flooding.

DATA

Satellite data -The gridded sea ice concentrations for this work are from the Defense Meteorological Satellite Program's (DMSP) SSM/I. The large difference in emissivity between calm water and sea ice is what makes the measurement of sea ice using passive microwave data possible. Averaged data, gridded with a resolution of 25x25 km, is acquired from satellite passes throughout the course of a day. The SSM/I is a seven channel, four-frequency system that measures surface brightness temperatures. The NASA Team algorithm uses the vertically polarized 19.4 and 37.0 GHz channels and the horizontally polarized 19.4 GHz channel. It has the ability to differentiate between two radiometrically different types of sea ice and open water. The Bootstrap Algorithm uses only the vertically polarized 19.4 and 37.0 GHz channels and is only able to make a distinction between ice and open water. As previously noted, it has been documented that both algorithms have trouble recognizing areas of new ice and summer melting conditions over sea ice.

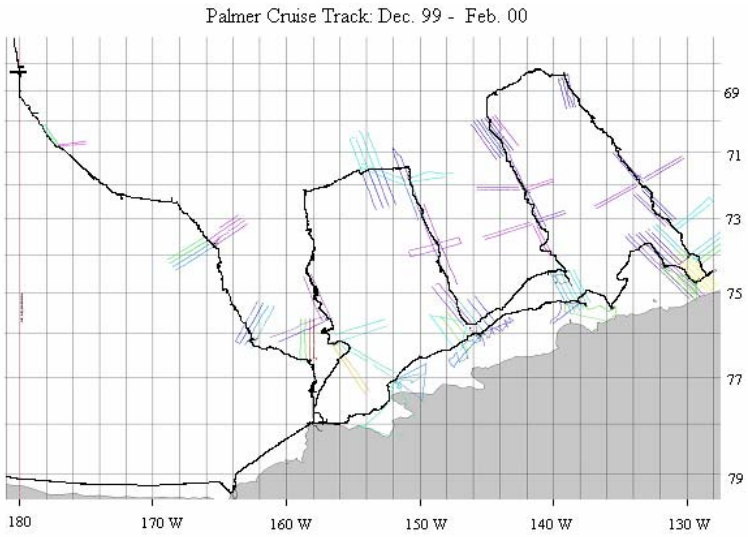

Fig. 1. Ship track (black) and helicopter survey transects (gray) in the Ross Sea. The southwestern end point of the cruise is McMurdo Station

Helicopter video data -From Dec 28 1999 to Feb 7 2000, helicopter flights were continuously taken off of the RVIB *Palmer* (Fig. 1). A digital video camera mounted under the helicopter recorded the landscape below. Although the main purpose of the helicopter flights was for seal reconnaissance, dependable evaluation of the videos for sea ice is possible because of the consistent flight altitude (~100m) and speed (~85 knots). Over 18,000 km (track line) was covered and analyzed for ice concentration and type, floe size, and ridging.

Because this extensive coverage resulted in approximately 200, 60 minutes videos, each video was examined and data was transcribed for one minute (~1.416nm) at 6 nm intervals for ice concentration, floe size, ice type, and surface ridging area. This comparison is different from those done in the past. Previous work compared single pictures, pixel by pixel with, among others, Landsat and advanced very high resolution radiometer (AVHRR) images for ice concentration only. This study takes advantage of a large data set and compares it to several days worth of algorithm results spaced through 5 weeks (28 Dec 99 to 6 Feb 00) of the summer period.

ANALYSIS

Because of the formats of the satellite and video data there is a large difference in the areas measured. Each one minute video reading is recorded as an average that covers approximately 0.5x2.6 km, but is compared to a 25x25 km average from the satellite data i.e less than 1% of the area of a satellite pixel. Ice concentration is recorded on a scale of 0-10 with 10 equaling 100% coverage. Plotting these values results in an extremely nonlinear relationship (Fig. 2). To better estimate sea ice coverage, we introduced some averaging into the analysis of the video data. Throughout the cruise the helicopter data was separated into a range of events (flights) that ranged from 1–12 observations per flight event. These events provided an easy way to break up the data

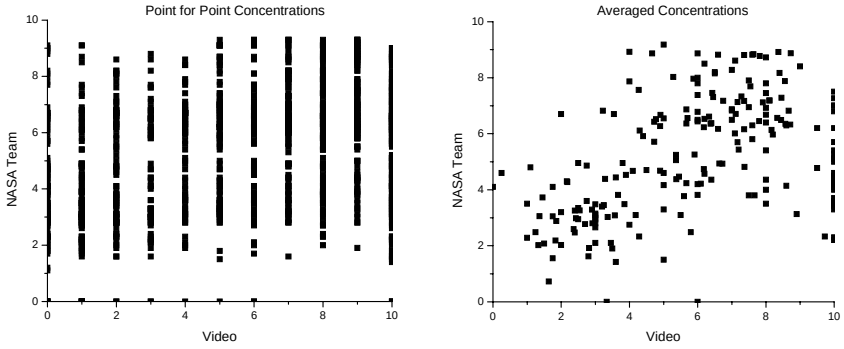

Fig. 2. Sea ice concentrations of the Video vs. NASA team algorithm. The Bootstrap algorithm, though not shown here, had similar results

for averaging. (The data discussed here represents that over drifting pack ice. Fast ice values were separated out and are discussed below.) Since the data was averaged over a various number of observations it is important to see if this causes a significant difference in the results. As shown in Figure 3, the data was separated into 1-3, 4-6, 7-9, and 10-12 observations per event. The linear fits for 4-6, 7-9, and 10-12 all have similar R values and all cross the y-axis at a concentration of approximately 2. The data represented by 1-3 observations per event is much more scattered. Looking more closely at the characteristics of these data points, i.e. ice type, floe size, and topography, no real similarities that might justify the variance other than undersampling was noted. This was also true for comparisons using the Bootstrap algorithm where the average R value for 4-6, 7-9, and 10-12 observations per event was 0.735 but for 1-3 observations it was 0.427. Given the issues in comparing data with only 1-3 observations per event these values will be removed from the data set for the ensuing analysis as well as the fast ice observations (video ice concentrations of 10). Even though the area compared for the higher number of observations is still a small fraction of a satellite pixel, the similarity in R values for numbers > 3 tops out at explaining only 50% of the variance (R=0.735) with no improvement for the higher number of observations. We infer that physical causes are therefore likely for the unexplained variance between satellite and video derived concentrations.

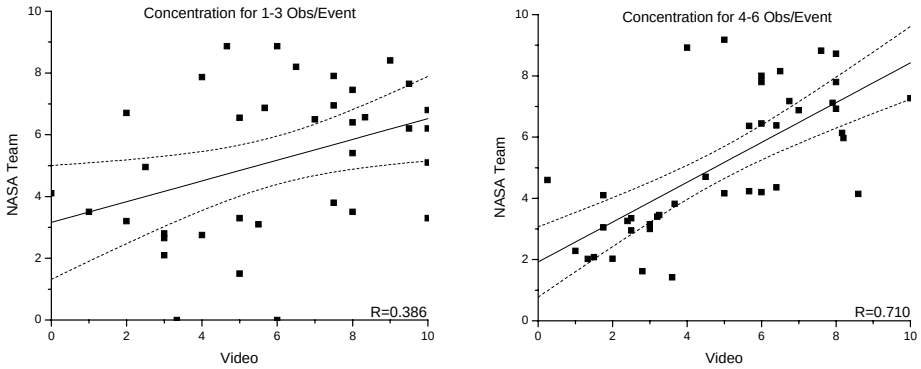

Fig. 3. Sea ice concentrations of the Video vs. NASA team algorithm. The solid line represents a linear fit of the data and the dashed lines represent 95% confidence levels

The most obvious discrepancy in the comparison of the video data versus the two algorithms is the absence of accurate satellite measurements in areas of known fast ice. As expected, the mean concentration of the fast ice video observations is very high at 9.480 while the NASA Team and Bootstrap algorithms had less than half this value, 4.408 and 4.640 respectively. However, there are several factors that can contribute to inaccurate satellite measurements near the coast. First, is the land mask being used for the algorithms. Some pixels could be designated ocean when in fact they are actually land and vice versa. Also, land ice has a lower brightness temperature than sea ice and with concentrations close to 100% and thick snow cover (>1m), as was reported from the ship data, the satellite is likely to underestimate the actual concentration of the sea ice area itself. This comparison suggests a strong effect of the snow cover on microwave brightness temperature in this region but a role for land mask (coastline) errors cannot be ruled out.

Sea ice conditions at the time of the cruise were very complex and generalized into five zones: Northern Marginal Ice Zone (NMIZ), Interior Pack Ice Zone (IPIZ), Ice Covered Shelf Zone (ICSZ), and the Coastal Polynya Zone (CPZ) as well as the Fast Ice Zone described separately. These zones can be estimated by latitude bands where 67-70°S represents the NMIZ, 71/72°S the IPIZ, 73/74°S the ICSZ, and 75/76°S the CPZ. Cruise observations described the two southern zones (CPZ and ICSZ) as dominated by thick and substantially ridged multi-year ice while the NMIZ and IPIZ were mostly less than a year old, with less ridging and snow cover than floes in the southern zones (Ackley et al., 2003). To examine the satellite algorithms' ability to predict, the ice concentration plots of satellite values minus the video mean (of a 5% bin) were made (Fig. 4). For the plot of 67-70° the linear fit of the data crosses from positive to negative at a concentration of 3.5. Therefore, we can say that in this area the NASA Team algorithm is under predicting in areas with a video-derived ice concentration greater than 3.5 and overpredicting for lower concentrations of < 3.5. In the 71/72° and 73/74° (IPIZ) zones, the linear fit of the data is very similar. In both cases, the fit of the data crosses from positive to negative near 6 i.e. overpredicting for video ice concentration <6 and underpredicting for video ice concentration >6. For the 75/76° zone the cut off between the two regions is back down to a concentration of 3. Though there are less events to analyze in this region, since the CPZ was documented as having older, thick snow covered floes it is possible that the condition of the surface is the effect distorting its microwave signature. Again, the Bootstrap algorithm is similar in that it crosses the x-axis at about 7 for the IPIZ and ICSZ and just slightly greater than 2 for the CPZ. However, for the NMIZ, the linear fit of the data never crosses the axis and thus under predicts the ice concentration, if only slightly, 100% of the time.

Several points are located well outside what would be considered an acceptable amount of error. These outliers, defined in this case to be points with a difference in concentration of >±2, can be found in all of the four zones. This produced 31 outlier events for the NASA Team algorithm and 29 for the Bootstrap algorithm, close to 20% of the total number of events in both cases. This can also be broken down into latitudes and we find that of the total number of outliers in the NASA algorithm, 13% are from

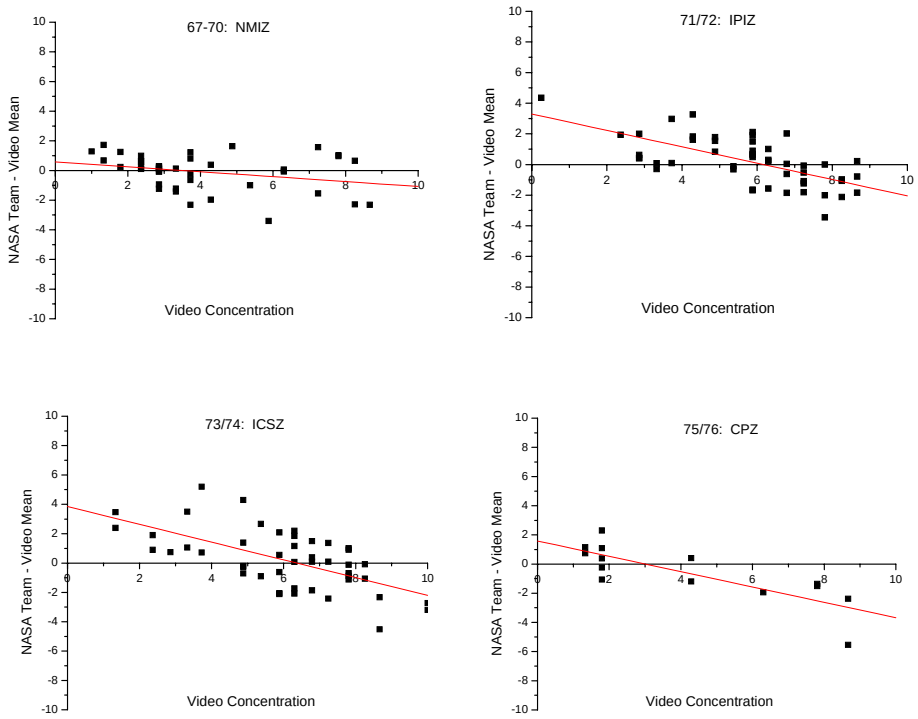

Fig. 4. Sea ice concentrations of the Video vs. NASA team – Video Mean. The solid line represents a linear fit of the data

NMIZ, 29% from IPIZ, 45% from ICSZ, and 13% from the CPZ. Similarly, the Bootstrap is 17%, 38%, 38%, and 7% respectively. In both algorithms data from the IPIZ and the ICSZ represent close to 80% of the points defined as outliers. Each events characteristic ice type, floe size, topography, and snow cover was also compared. 68% of the NASA Team and 79% of the Bootstrap outlier events were thick first year or multiyear floes with substantial snow cover. Of the NASA Team outliers, 73% of the events where the satellite underestimated the video, there were thin secondary and/or tertiary ice types also recorded in the region. Neither of these data sets exhibited a particular pattern related to the floe size or topography. Although the video data cannot be analyzed for surface flooding beneath the snow cover, ship observations and surface data collected concurrently showed extensive evidence for seawater flooding at the snow-ice interface (Ackley et al 2003), suggesting that surface flooding may be the the issue for underpredicting at higher concentrations.

CONCLUSIONS

In situ sea ice data taken from a Dec 1999-Feb 2000 cruise aboard the RVIB *Nathaniel B. Palmer* and its ship-based helicopters was compared with satellite data from the same period created using the NASA Team and Bootstrap algorithms. Cruise observations illustrated the complex nature of the Ross Sea in the summer months and comparison with satellite data demonstrates the algorithms capabilities in calculating sea ice concentration. Both algorithms tend to generally underestimate concentrations in the NMIZ and also close to shore in the CPZ. The NMIZ is often a zone of warmer ice in

summer and the algorithms' inability to make accurate predictions here may be related to surface flooding and/or the presence of wet snow. A serious underestimate was also apparent in the fast ice cases with cause somewhat indistinguishable between the presence of thick snow and land mask (coastline) errors in the microwave imagery. In between, in the IPIZ and ICSZ, the prediction was to over and then under estimate almost equally as the concentration increases. This region also had the highest incidence of events with a high percentage of error. It is also clear that both algorithms have difficulty dealing with multiyear floes with thick snow cover. More investigations should be done into the source of this problem. Currently, the Aqua Advanced Microwave Scanning Radiometer (AMSR-E) is being tested and used for passive microwave satellite remote sensing and with it comes enhancements to both of the algorithms studied here. These changes should be carefully studied over a variety of validation sites for different seasons. However, for historical data and comparing between the old and new instruments, it is important to know how accurate the sea ice concentrations from the SSM/I really are. The crossover from underpredicting to overpredicting concentrations and the variability of that crossover point, apparently dependent on ice type, lends little confidence in using microwave imagery in looking, for example at the interannual variations in summer concentration in this region. Based on this study, we conclude that the constraints on microwave imagery for predicting summer ice concentrations are probably so great as to restrict the SSMI microwave imagery to ice extent mapping (the presence or absence of ice only) for the summer sea ice in the eastern Ross Sea.

ACKNOWLEDGEMENTS

This research was funded by the National Science Foundation under grants OPP-9908694 and OPP-9814968. Thanks also to Hayley Shen for help in video analysis and paper review.

REFERENCES

Ackley, S., J. Bengtson, P. Boveng, M. Castellini, K. Daly, S. Jacobs, G. Kooyman, J. Laake, L. Quetin, R. Ross, D. Siniff, B. Stewart, I. Stirling, J. Torres, and P. Yochem. A top-down multidisciplinary study of the structure and function of the pack-ice ecosystem in the eastern Ross Sea, Antarctica. *Polar Record* 39 (210): 219-230 (2003).

Cavalieri, D., P. Gloerson, and J. Zwally. 1990, updated 2003. *DMSP SSM/I daily polar gridded sea ice concentrations.* Edited by J. Maslanik and J. Stroeve. Boulder, CO: National Snow and Ice Data Center. Digital media.

Comiso, J. 1990, updated 2003. *DMSP SSM/I daily polar gridded sea ice concentrations.* Edited by J. Maslanik and J. Stroeve. Boulder, CO: National Snow and Ice Data Center. Digital media.

Comiso, J., D. Cavalieri, C. Parkinson, and P. Gloersen. Passive Microwave Algorithms for Sea Ice Concentration: A Comparison of Two Techniques. *Remote Sens. Environ.* 60: 357-384 (1997).

Gloerson, P., W. Campbell, D. Cavialieri, J. Comiso, C. Parkinson, and H. Zwally. Arctic and Antarctic sea ice 1978-87: satellite passive-microwave observations and analysis. Washington, DC: National Aeronautics and Space Administration (NASA SP-511) (1992).

Steffen, K. and A. Schweiger. NASA team algorithm for sea ice concentration retrieval from defense meteorological satellite program special sensor microwave imager: Comparison with landsat satellite imagery. *J. of Geophys. Res.* 96(C12): 21,971-21,987 (1991).

17th International Symposium on Ice
Saint Petersburg, Russia, 21 - 25 June 2004
International Association of Hydraulic Engineering and Research

STUDY ON THE CHARACTERISTICS OF ICE FORMED IN REGION OF HEAVY SNOWS

K. Takahashi[1], N. Usami[1], T. Shibata[1], N. Otsuka[2], T. Terashima[3] and H. Saeki[4]

ABSTRACT

The authors have studied on the possibility of using the Ishikari River in Hokkaido Island as a commercial inland waterway. Hokkaido lies in a cold region, and the Ishikari River is freeze-up in winter. Therefore, any winter river navigation would require icebreaking. Towards that end, this study surveys the ice thickness along a proposed Ishikari waterway navigational channel. It also shows laboratory test data about the flexural strength of snow ice and columnar ice.

INTRODUCTION

Unlike rivers in Europe and the U.S., Japanese rivers tend to have steep gradients and experience large variations in seasonal flow. These topographical disadvantages are why most Japanese rivers are not currently used for inland waterway transport. Compared to other rivers in Japan, the Ishikari River in Hokkaido offers an unusually gentle gradient throughout its middle and lower reaches, giving it potential as a navigable waterway for inland transport. In recent years, rivers have been gaining renewed attention as a way to reduce inland transportation costs; address global environmental issues such as CO_2 emissions through a modal shift. Consequently, transportation options involving inland waterways are being looked at once again. The Ishikari River is situated in a cold, snowy region and it is freeze-up during the winter season. For vessels to navigate in winter months, icebreaking operation will be required by icebreakers or other such vessels to keep an open-water route. Therefore, the ship's power required for an icebreaker or icebreaking barge to navigate through level river ice must be estimated. Ice thickness and flexural strength are two important factors that must be determined to estimate this force. The purpose of this study is identify how much of the assumed

[1] Cold Region Port and Harbor Engineering Research Center, Japan
[2] North Japan Port Consultants Co., Ltd., Japan
[3] Kumashiro System Frontier Co., Ltd., Japan
[4] Hokkaido University, Japan

Ishikari River channel route is subject to ice coverage, how that ice grows, and what strength the ice has. To do this, field observations of the ice coverage and ice thickness were taken. In addition, flexural strength data was gathered both in situ and in the laboratory.

INVESTIGATION OF ICE COVERAGE

Ice coverage along the proposed navigation route was surveyed a total of seven times between late December 2002 and late March 2003. Data was obtained from the Ishikari River, Barato River, Shibi Canal, and Ishikari Drainage Channel (Fig.1). Fig.2 shows the ice coverage in simple graphical terms.

From its estuary, the Ishikari River remained free of ice for approximately three kilometers upstream, except during early January. Further upstream, the river also stayed ice-free throughout the survey period where free-flowing tributaries joined and where a riverside paper mill discharged into the river. However, almost all other parts of the river were freeze-up from late December to late February. The ice cover was almost completely melted away by early March. Both the Barato River and Ishikari Drainage Channel were completely freeze-up from late December to mid-March. By late March, the Barato River was entirely and the Ishikari Drainage Channel was almost free of ice. The Shibi Canal remained free of ice throughout, likely due to its quick current.

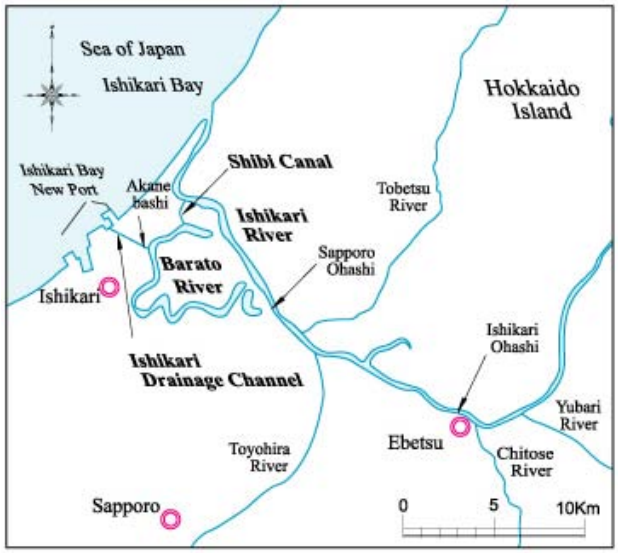

Fig.1. Ice Coverage Survey Area

INVESTIGATION OF ICE THICKNESS

Ice growth process in snowy regions

In the absence of snowfall, heat conduction theory holds sway, dictating that ice thickness increases, after freezing begins, in proportion to the square root of the cumulative freezing degree days, as shown by Stefan and others. Where there is snowfall, ice growth follows the following process (Fig.3).

a. Columnar ice cover of some initial thickness forms as the water surface cools.
b. Snow cover is formed on the columnar ice cover. Its weight pushes down the ice cover into the water and water infiltrates the snow cover, creating slush.
c. As it cools, the snow slush on the ice cover starts to solidify at the water surface and snow ice layer is formed. The snow ice then grows downward. Through this process, the overall ice cover thickness increases.
d. The ice cover sinks again with the next snowfall and another layer of snow slush forms. If there is another snowfall before the previous snow slush solidifies completely, the ice cover will have a cross section that contains snow slush layer inside.

There can also be cases where a snowfall occurs before any columnar ice cover forms (a), in which case snow ice is formed from the start. In these cases as well, overall ice thickness increases through repetitions of (c) and (d) every time a snowfall occurs. This dynamic process means that the internal structure of ice covers formed in snowy regions are typically very complex. Meteorological conditions (e.g. amount of snowfall at any one time, interval between snowfalls, ambient air temperature) can also have an extremely large influence on the ice growth process.

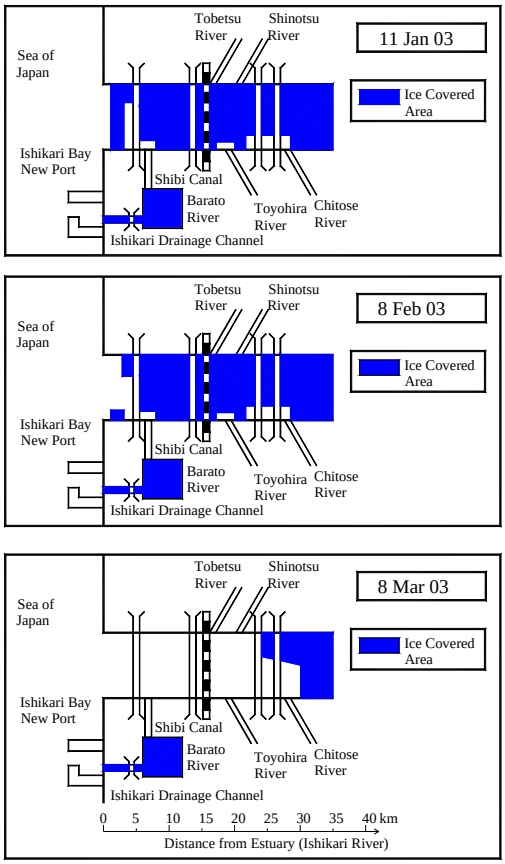

Fig.2. Ice Coverage

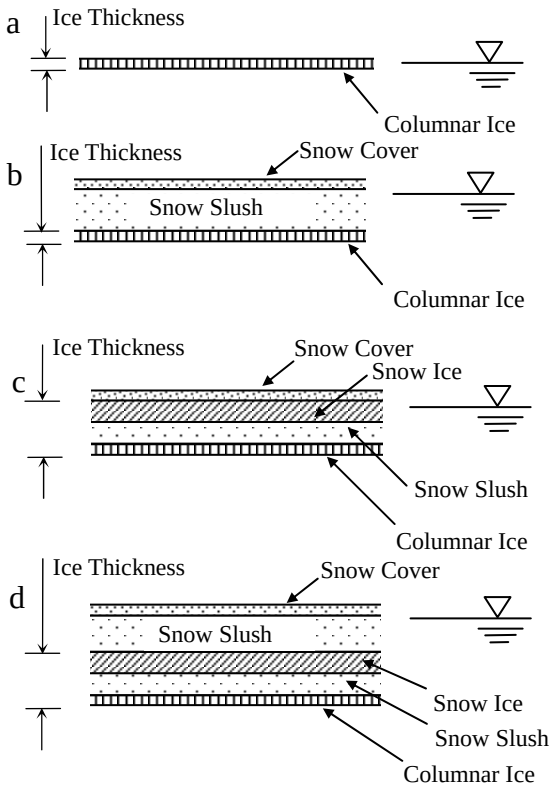

Fig.3. Ice growth Process in Snowy Regions

Findings

Ice thickness was measured at Ishikari River and Ishikari Drainage Channel. Ice cover formed in the Ishikari River consisted of snow ice with snow slush layer. Ice cover formed in the Ishikari Drainage Channel contained roughly three primary layers of snow ice and snow slush, and primary snow ice layers consisted of many thin snow ice layers (Fig.4). Columnar ice cover formed only under some bridges span across the drainage. Measured ice thicknesses at both areas are shown in Fig.5 – 7. The Ishikari River is impacted by the confluence of tributaries, warm water discharges, and other elements of the surrounding environment. This accounts for the observed fluctuations in ice thickness and explains why the river ice decayed earlier than the drainage channel

ice. Unlike the Ishikari River, there is almost no current at the Ishikari Drainage Channel. This is because its lower reaches are usually closed off by a water gate and it is not joined by other water sources. Thus this ice growth is similar to lake ice.

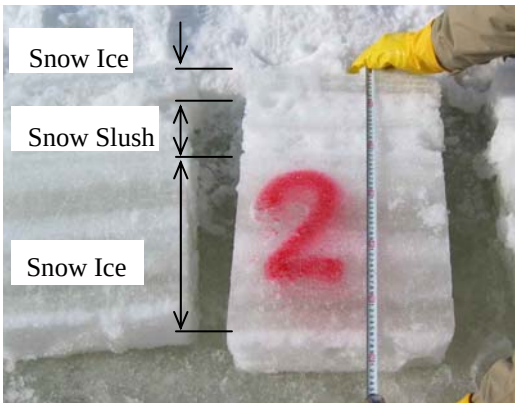

Fig. 4. Cross-Sectional Structure of Ice Cover (Snow Ice)

Fig.8 shows the theoretical ice thickness, calculated using Stefan's formula, and the measured ice thickness for the Ishikari Drainage Channel. Where snow ice, the measured data exceeded the theoretical figures, demonstrating that the cumulative freezing degree-days formula developed by Stefan cannot be used to directly estimate ice thickness in snowy regions.

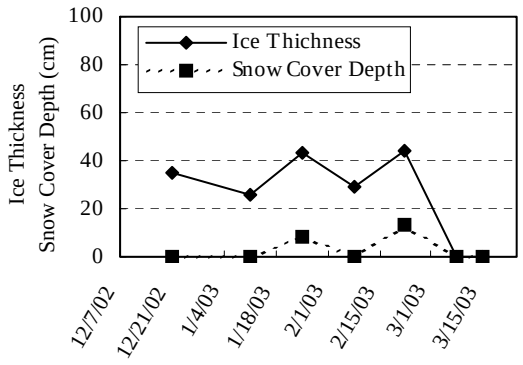

Fig. 5. Ice Thickness on Ishikari River (Snow Ice)

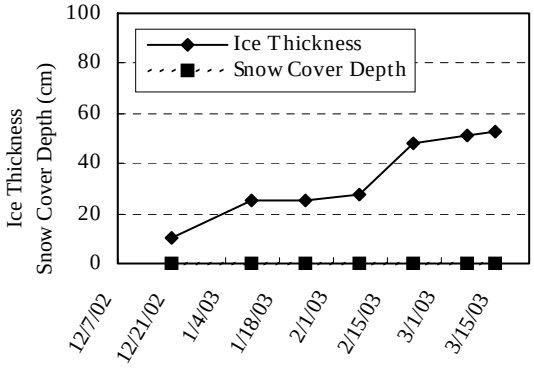

Fig. 6. Ice Thickness on Ishikari Drainage Channel (Snow Ice)

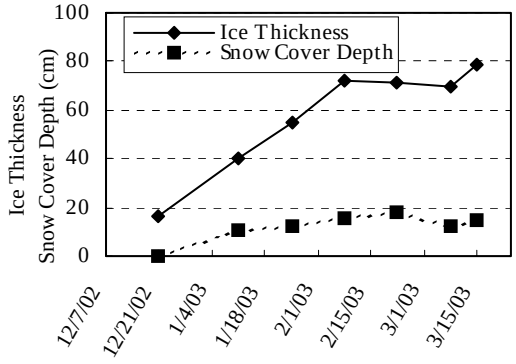

Fig.7. Ice Thickness on Ishikari Channel (Columnar Ice)

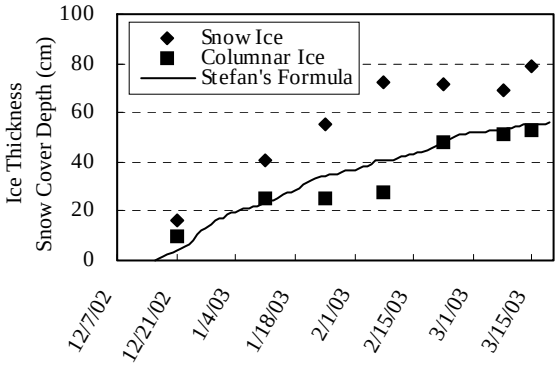

Fig.8. Comparison of Theoretical and Actual Ice Thickness

The actual thickness data also contradicts findings by Sakuraba that suggest ice growth is retarded when it is subject to snowfall due to the insulating properties of the snow cover.

FIELD TEST OF FLEXURAL STRENGTH

Test conditions

To better understand the flexural strength of the ice that forms along the proposed navigation channel, an in-situ bending test was carried out at the Ishikari Drainage Channel on February 15-16, 2003. To reflect local meteorological and ice conditions, a cantilever test method was adopted. The test piece was loaded vertically to downward with a hydraulic jack at its tip to induce initial failure from the surface layer. Forces were measured during loading with a load cell and vertical displacement was measured with a dial gauge.

Two test sites were selected, one on the left side of the channel (Site 1) and one on the right (Site 2). Approximately 10 test pieces were cut from the ice cover at each site. At both sites, ice thickness (h) was measured at two points and the average values (Site 1: 62 cm, Site 2: 55 cm) were used to represent the thickness of all test pieces for their respective sites. The test pieces were cut approximately 37 cm in width (b) and 230 cm in length (L). Parameters of the test pieces size are $0.5<b/h<1.0$ and $3<L/h<5$. They are included the area of neutral influence on flexural strength that found by Maeda et al. The air temperature ranged from -1.0 to -3.2°C and the ice temperature was -0.5°C.

Test results

The test pieces were loaded in time series until failure. Two patterns were observed: in one case a series of small force increases precede a maximum peak force (Fig. 9), and in the second case there is a staircase progression of small peak forces (Fig. 10). Taking into account the layered composition of the ice cover, the first pattern indicates that the lower layer of the three-layer cross section was solidified. The second pattern can be expected where the lower layer contained layer of non-solid material (snow slush).

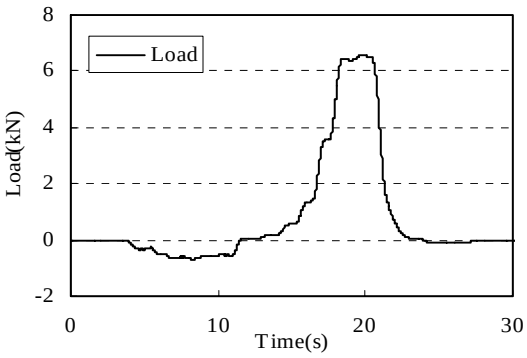

Fig. 9. Time Series of Ice Load (Case 1)

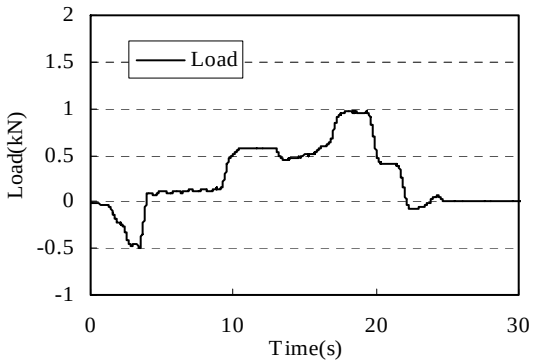

Fig. 10. Time Series of Ice Load (Case 2)

Fig. 11 shows that the flexural strength was nearly uniform among the test pieces of Site 2. At Site 1, however, there was nearly an order of difference among the test pieces. A logical explanation of this would be that the lower layer of some test pieces had frozen solid, whereas others had not. Thus, Site 1 results indicate that internal structure of ice cover is not a uniform distribution within a small area. When estimating the ship's power that will be required of an icebreaker or icebreaking barge, the solidified state should be assumed.

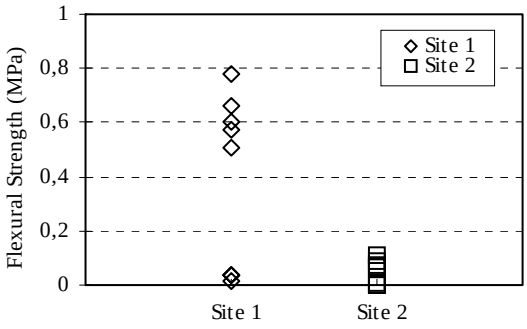

Fig. 11. Flexural Strength of Snow Ice (Field Test)

LABOLATRY TEST OF FLEXURAL STRENGTH

Test conditions

As mentioned previously, the local ice cover consisted of roughly three layers. To understand the strength characteristics of each layer, additional test pieces were cut and 3-point bending tests were carried out on each layer at the laboratory. Laboratory test was also carried out on columnar ice test pieces cut from under the bridge.

The cross section of these snow ice contained solid layers on top and bottom. However, the middle layer was in a snow slush state and it was impossible to form it into a testable specimen. Consequently, only the top and bottom layers were tested. As the bottom layer was quite thick, it was sliced horizontally into two thinner layers that were tested separately. The columnar ice sample was also sliced into two thinner layers. To ensure that the test sample dimensions would not influence the results, specimens were cut to the following dimensions:

Snow ice: 40 cm (L) x 8-17 cm (h) x 10-15 cm (b), -2°C ice temperature
Columnar ice: 80 cm (L) x 20-22 cm (h) x 18-20 cm (b), -2°C to -5°C ice temperature

Test results

Fig. 12 and 13 show the flexural strength and elastic modulus of the snow ice. The top layer of the snow ice exhibited greater strength than the bottom layer. With the top layer, it ranged 0.3-0.6 MPa. And the upper and lower sections of the bottom layer, it ranged about 0.1-0.3 MPa and 0.1-0.5 MPa, respectively.

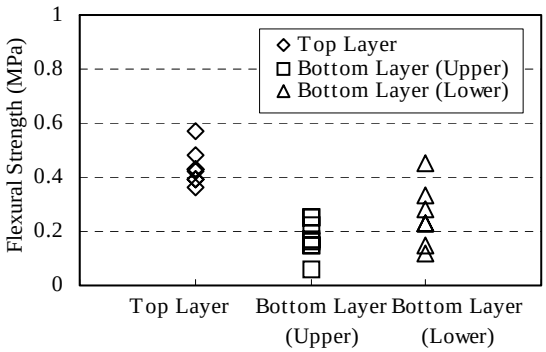

Fig.12. Flexural Strength of Snow Ice (Laboratory Test)

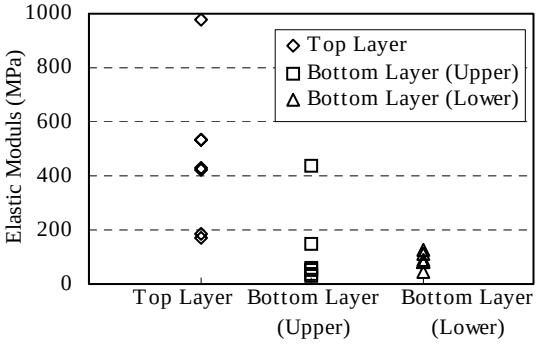

Fig.13. Elastic Modulus of Snow Ice (Laboratory Test)

The ratio of elastic modulus to flexural strength (E/σ_f) was about 400-1,200 in the top layer, 200-600 in the each part of the bottom layer. Fig. 14 and 15 show the flexural strength and elastic modulus for the columnar ice. There was some dispersion overall in flexural strength among the test pieces, with data ranging from 0.3 to 1.2 MPa. E/σ_f was roughly between 500 and 3,000.

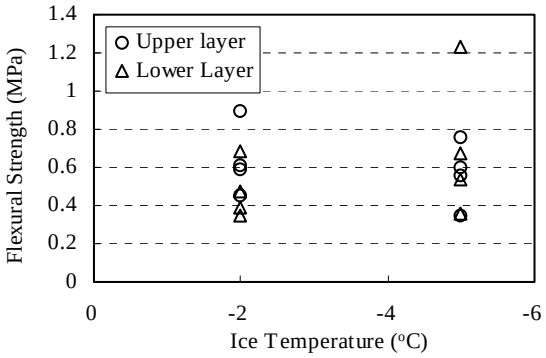

Fig.14. Flexural Strength of Columnar Ice (Laboratory Test)

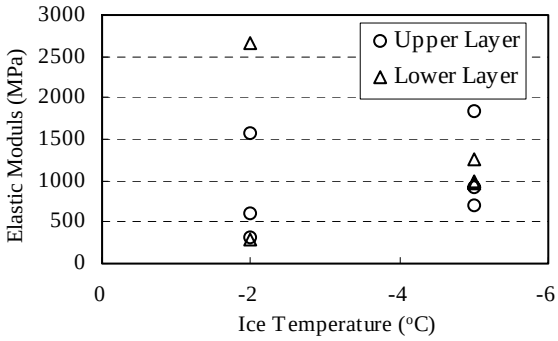

Fig.15. Elastic Modulus of Columnar Ice (Laboratory Test)

ICEBREAKING IN THE NAVIGATION CHANNEL

For an icebreaker or icebreaking barge to navigate the waterway's level ice, it will have to produce sufficient ship's power to exceed resistance (R). One of the formulas is shown below:

$$R = C_b \cdot \sigma_f \cdot B \cdot h + C_s \cdot \rho \cdot g \cdot B \cdot h^2 + C_i \cdot \rho \cdot B \cdot h \cdot V^2 + C_f \cdot \rho \cdot g^{1/2} \cdot B \cdot h \cdot V^{3/2}. \quad (1)$$

Where $C_b, C_s, C_i,$ and C_f are coefficients, σ_f is flexural strength, h is ice thickness, B is the width of the ice cover being broken, V is vessel speed, ρ is the liquid density, and g is gravitational acceleration.

In the event that the proposed navigation channels start to be used for inland transport, however, icebreaking would take place regularly, thus eliminating the need to break ice at its maximum thickness. And for the flexural strength, as a safety factor it should be assumed that the internal structure is solid snow ice. The possibility that resistance could increase due to a dramatic accumulation of snow on the ice cover and internal snow slush for icebreaking should also be recognized.

The navigation channel proposed in this paper can be divided into two areas: one area subject to current and other area that is virtually free of current. Where current exists, broken ice produced from icebreaking operations would naturally flow downstream. So there is no need for ice removal after icebreaking. Possible exceptions would be the curved parts of the lower reaches, areas where the river narrows, and areas where there is a sudden change in riverbed gradient. All these areas present potential for the broken ice to remain and to form ice jams. In the sections free of current, the broken ice would remain and refreeze, and that the ice thickness would increase with repeated breaking and refreezing. Therefore, methods of ice removal after icebreaking operation will have to be required.

CONCLUSIONS

1. The Ishikari River is freeze-up almost entirely in the winter. The ice thickness increased to about 40cm, and due to the large influence of snow, formed entirely of layered snow ice and snow slush. Columnar ice was not observed.
2. Snow ice also formed in both the Ishikari Drainage Channel and Barato River. The maximum ice thickness in the Ishikari Drainage Channel was about 80 cm. Under bridges, columnar ice was formed and this ice thickness reached to approximately 50 cm. There was almost no freezing observed on the Shibi Canal.
3. In-situ bending tests indicated large differences in the flexural strength of Ishikari Drainage Channel snow ice. This means that the local ice cover consists of a jumble of different cross sectional structures, some with non-solidified layers and others that are completely solidified. From a safety point of view, a completely solidified state should be assumed when estimating the ship's power that will be required of icebreakers or icebreaking barges.
4. Laboratory bending tests were also carried out both snow ice and columnar ice. The flexural strength of the snow ice was lower than that of the columnar ice. This indicates that the the ship's power required of vessels navigating parts of the route subject to snow ice can be lower than that required where columnar ice forms. The flexural strength data should also allow the ship's power required of an icebreaker or icebreaking barge to be estimated.

REFERENCES

K. Takahashi, N. Usami, T. Shibata, T. Terashima, N. Otsuka, H. Saeki. Study on the possibility of inland waterway transport in the Ishikari River, *Marine Technology* V, pp. 235-61, (2003)

A. Sakuraba, R. Izumi, H. Saeki: Effect of accumulated snow on ice thickness, A *Collection of Papers by Japan Society of Civil Engineers*, Hokkaido Chapter, pp. 309-12, (1984)

G. D. Ashton, Editer: River and Lake Ice Engineering, *Water Resources Publications*, (1986)

T. Maeda, M. Sasamoto, S. Sasaki, H. Ishida, K. Hirayama: Parametric expressions for compressive strength and bearing strength of ice, *Proc. of '89 Cold Region Technical Conference*, Vol.5, pp. 364-69, (1989)

17th International Symposium on Ice
Saint Petersburg, Russia, 21 - 25 June 2004
International Association of Hydraulic Engineering and Research

EXPERIMENTAL STUDY ON FRAZIL ICE CONTROL SYSTEMS FOR WATER INTAKES

N. Usami[1], T. Ueda[2], K. Takahashi[3], Y. Hayama[1] and H. Saeki[4]

ABSTRACT

In cold regions, such as Japan's Hokkaido Island, rivers and lakes often freeze up in the winter season. Consequently, frazil ice accretions often clog riverside water intakes. To counter this problem, Kubit (2000) suggested that ice-skimming booms be used to block the flow of frazil ice into such intakes. The purpose of this study was to increase the efficiency of this approach. Four types of Frazil Ice Control Systems (FICS) were tested to compare their effectiveness. Bent-type and variant-type FICS both performed well in comparison with a straight type. However, the most effective system for controlling frazil ice was a variant-bent type, which had characteristics of both the bent-type and variant-type configurations.

INTRODUCTION

Intakes constructed along rivers in cold, snowy regions can become clogged in winter when frazil ice forms and they accrete at the intakes. This is a topical issue in northern Japan's Hokkaido. Nagayama Intake, constructed on the Ishikari River in Asahikawa, was recently clogged when extremely cold air temperatures and heavy snowfall generated frazil ice and snow jams that flowed from the river into the intake. Kubit (2000) proposed countering frazil ice inflows by installing ice-skimming booms on the upstream side of target intakes. Using Kubit's work as a reference, the authors devised a system that was expected to demonstrate greater effectiveness. The basic concept is similar to that suggested by Kubit. The authors propose installing a Frazil Ice Control System (FICS) on the upstream side of the intake to control frazil ice inflow. The FICS is designed to be installed adjacent to the intake and to control the inflow of frazil ice by blocking it and then using its upstream edge to direct the ice downstream. The ultimate goal is to prevent frazil ice floating in the downstream current from entering the intake.

[1]Hokuden General Engineering Design and Consulting Company Inc., Japan
[2] Fujitsu FIP Corporation, Japan
[3] Cold Region Port and Harbor Engineering Research Center, Japan
[4] Hokkaido University, Japan

This study clarifies the mechanisms that cause frazil ice to flow into FICS-equipped intakes. It also reports on hydraulics model test conducted on FICS models of different shapes conceptualized by the authors to identify the optimum FICS configuration.

EXPERIMENTAL METHOD AND DOWNSTREAM FLOW OF FLAZIL ICE

Experimental method

Hydraulic model test was carried out to gain a better understanding of the mechanisms that cause frazil ice flowing down a river's mainstream to enter an intake. The experiments were performed in a circular water tank equipped with a pump that was 10.6 m long, 2.0 m wide, and 0.6 m deep. A partition offset 1.0 m from the sidewall divided the channel lengthwise. An intake was placed approximately 6.0 m downstream from channel's upper limit, causing the watercourse to diverge (Fig.1). This resulted in a main channel width (B) of 1.0 m and a divergent channel width (Bi) of 0.53 m. The intake width (Bd) could be set for either 0.25 m or 0.5 m. Weirs (W, Wi, Wd) were installed at the downstream end of the main channel and the divergent channel, and behind the intake. The flow rates of the main channel (Q) and divergent channel (Qd) were regulated by adjusting the heights of the weirs. Test was carried out at main channel flow rates (Q) of 18.8, 38.9, and 71.1 (*l*/sec). Polypropylene particles with a specific gravity of 0.95 and a diameter of 3.0 mm were used to model the frazil ice. During the experiment, a fixed amount of the model frazil ice was fed into the upstream end of the channel and observations were made of its flow into the intake. The model frazil ice that entered the divergent channel was collected and an intake frazil ice inflow ratio (I)—amount of frazil ice flowing into the divergent channel/amount of frazil ice fed into the main channel—was calculated.

The experiment was first carried out without installing a FICS (Fig.2). This showed that the inflow ratio of frazil ice (I) is largely dependent upon the flow rate ratio (Qr), which is the ratio of the main channel flow rate (Q) to the divergent channel flow rate (Qd).

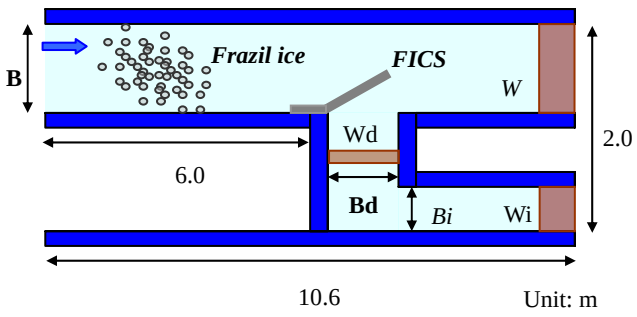

Fig.1. Circular Water Tank

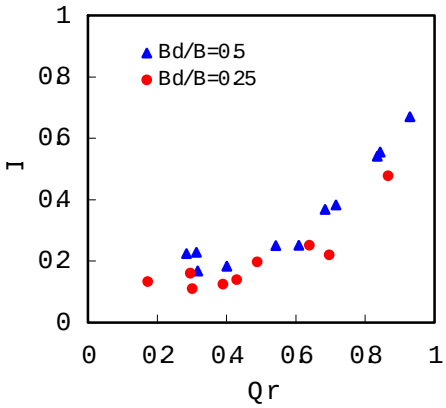

Fig.2. Relationship between Qr and I

Shape and installation of the FICS models

Fig.3 and 4 show the FICS models and test parameters. In the experiments, FICS shapes and dimensions were varied and tested under different Qr. The model frazil ice was distributed evenly across the channel in the upper end and allowed to flow downstream. Observations were made of frazil ice accretion upstream of the FICS, tip vortices, and if frazil ice passed beneath the FICS. The inflow ratio (I) was calculated for each test case. Through repeated testing, the effectiveness of each of the four FICS types in controlling frazil ice was identified, and the optimum shape was evaluated. Froude numbers for the experiments ranged 0.1 to 0.2.

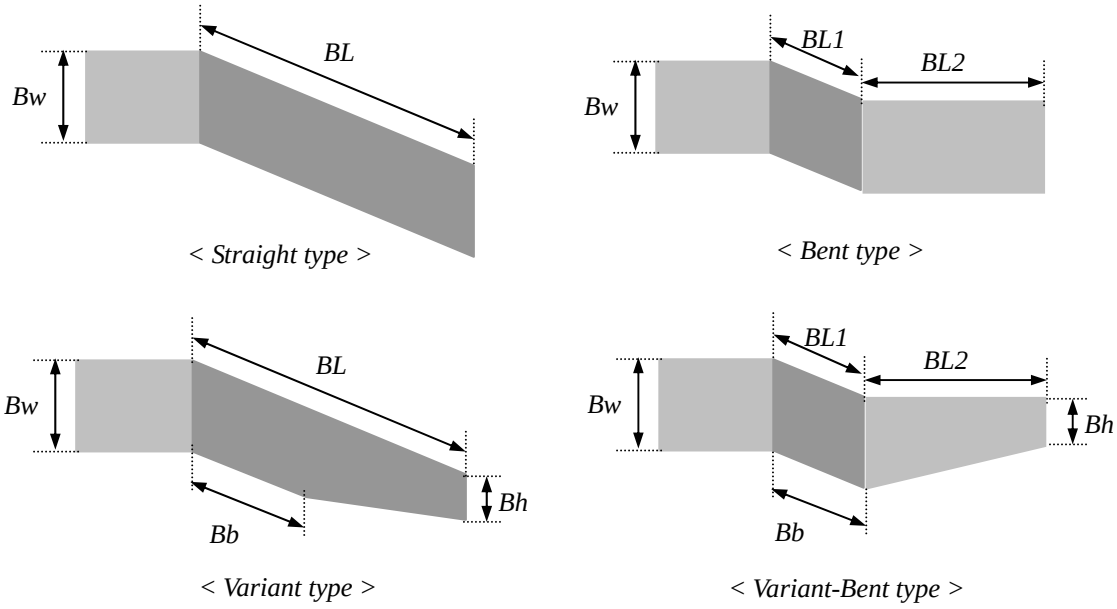

Fig.3. FICS Model Configurations

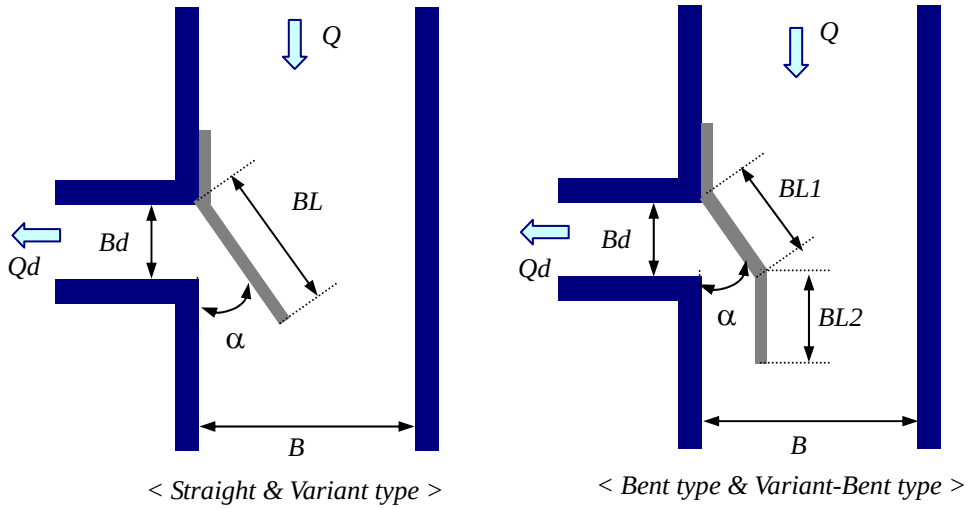

Fig.4. Experimental Parameters

Flow mechanism of frazil ice

Fig.5 shows the mechanisms by which frazil ice flows downstream and into an intake when a FICS is installed. The intake flow net (S) has a large impact on the downstream flow of frazil ice and its entry into an intake. In general, the majority of frazil ice inside the flow net is flow into the intake. Installing a FICS affects frazil ice both inside and outside the flow net as ice from both regions collides with the FICS. After colliding with the FICS, ice passes under the FICS to enter the divergent channel or travel downstream along the FICS in a controlled manner. The controlled frazil ice that flows downstream along the FICS follows one of two paths when it reaches the tip: it either continues to flow downstream or it is engulfed by tip vortices and pushed back to the intake.

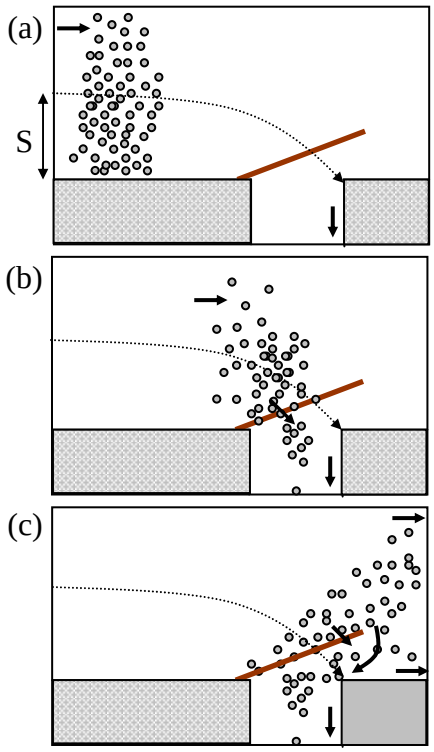

Fig.5. Downstream Flow mechanisms of Frazil Ice

EFFECTIVENESS OF STRAIGHT-TYPE FICS

Influence of the installation angle

Experiments were carried out with a straight-type FICS, where the FICS length (BL) to intake width (Bd) ratio (BL/Bd) was 2.8 and the FICS draft depth (D) to main channel water depth (h) ratio (D/h) was 0.3-0.4. Installation angles (α) of 0°, 30°, and 45° were tested. Frazil ice inflow ratios were measured for each angle to evaluate the influence of the FICS installation angle (α) on frazil ice control.

Fig.6 shows the relationship between the frazil ice inflow ratio (I) and flow rate ratio (Qr) at each angle setting. Regardless of α, I tended to increase as Qr increased. At α=0°, the tendency of frazil ice to accrete on the upstream side of the FICS increased as the flow rate ratio increased. The amount of ice passing beneath the FICS also increased. At α=30°, the inflow of frazil ice was almost completely controlled until Qr reached approximately 0.35, after which I began to increase. At high flow rate ratios, frazil ice was found to accrete in much the same way as it did at α = 0°. At α = 45°, the area of the FICS disrupting the current flow increased and flow velocities increased at the FICS tip. As a result, tip vortices became more

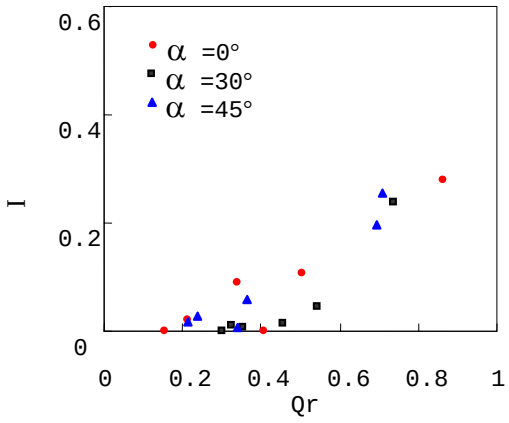

Fig.6. Influence of α

conspicuous and the currents beneath the FICS became stronger, creating a complicated flow pattern in the lower reaches. Consequently, frazil ice entered the intake even when the flow rate ratio was low. These results indicate that the most effective installation is to have the FICS angle out from the intake at 30°.

Influence of draft depth

To investigate how the FICS draft depth affects its control of frazil ice, experiments were carried out in which the draft depth (D) to main channel water depth (h) ratio (D/h) was varied between 0.19 and 0.55. For these experiments BL/Bd=2.8 and α=30°. At D/h ratios of 0.51 and 0.55, tip vortices were observed. Frazil ice was caught up in these vortices and subsequently flowed into the intake. At shallow draft depths (D/h=0.12 and 0.18), some of the controlled frazil ice sliding downstream along the FICS was observed to pass beneath the FICS and flow into the intake. Fig.7 shows the relationship between I and D/h. When D/h<0.35, I tends to increase as D/h approaches 0. When D/h>0.5, I increased, though only slightly, as D/h increased. These results indicate that the optimum draft depth for preventing frazil ice from passing under the FICS while also minimizing the effects of tip vortices should be in the range of 0.35<D/h<0.45.

Influence of length

The next series of experiments compared the frazil ice control effectiveness of FICS with differing lengths (BL). Tests were carried out for FICS length (BL) to intake width (Bd) ratios (BL/Bd) of 1.4, 2.1, and 2.8. The D/h was 0.35-0.45 and α was constant at 30°. Observations confirmed that increasing quantities of frazil ice would flow into the intake as BL/Bd was decreased. It was also confirmed that as the flow rate ratio becomes larger, turbulence at the FICS tip traps frazil ice and causes it to flow into the intake, regardless of BL/Bd. Fig.8 shows the effectiveness of various BL/Bd ratios in controlling frazil ice inflows. This figure shows that greater control comes with increasing BL/Bd. However, the FICS length (BL) must also take into account the anticipated intake capacity.

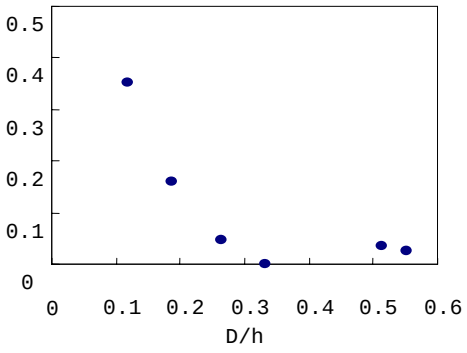

Fig.7. Relationship between D/h and I

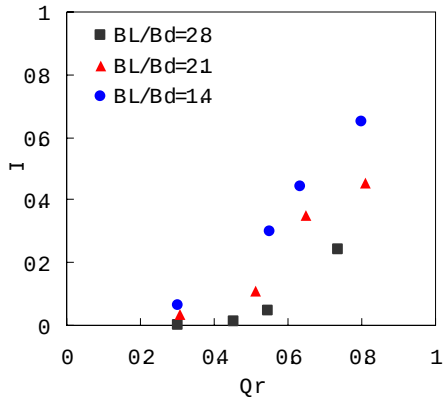

Fig.8. Influence of BL/Bd

EFFECTIVENESS OF MODIFIED FICS

Frazil ice control with bent-type FICS

Data from the experiments described previously show that a straight-type FICS can control the flow of frazil ice into an intake, especially when Qr<0.5. On a typical river in Hokkaido, however, the flow rate ratio (Qr) inevitably increases during winter when river flow rates decrease, and it can be assumed this would decrease FICS effectiveness. This necessitates improvements to the FICS model. Observations made while testing straight-type FICS configurations suggested that frazil ice control effectiveness could be increased by minimizing tip vortex trapping and reducing the frazil ice accretions that lead to ice passing beneath the FICS. To address these two goals independently, two different FICS configurations (bent type and variant type) were tested and evaluated.

The concept behind the bent-type FICS was to control the inflow of frazil ice with the BL1 segment and then to restrain tip vortices by aligning a BL2 segment parallel with the current, all of which should allow the frazil ice to flow smoothly downstream. The following data relates to experiments on bent-type FICS configurations.

The effect of different BL1 to BL2 ratios on the inflow of frazil ice was investigated. BL1/BL2 values of 0.5, 1.0, and 2.0 were tested. α was constant at 30°, BL/Bd = 2.8, and D/h = 0.35 – 0.45. Observations showed that at Qr < 0.6, tip vortices were restrained and the downstream flow of frazil ice was smooth. At higher flow rate ratios (Qr > 0.7), however, frazil ice accretions occurred on the upstream side of the FICS. In addition, frazil ice was sucked around the FICS tip and into the intake. At BL1/BL2 of 0.5, frazil ice passed beneath the BL2 segment and entered the intake. This is because the angled segment of the FICS terminated within the intake's width and strong currents flowing into the intake formed underneath the BL2 segment. At BL1/BL2 = 2.0, frazil ice exhibited a downstream flow very similar to that seen with the straight-type FICS because of the long length of the BL1 segment.

Fig.9 shows how varying BL1/BL2 affects frazil ice control. In all cases where Qr<0.6, the FICS models prevented the vast majority of frazil ice from entering the intake. However, at Qr>0.6, the inflow ratio tended to increase. Based on observations and the data presented in Figure 8, BL1/BL2 = 1.0 appears to give the most suitable proportions.

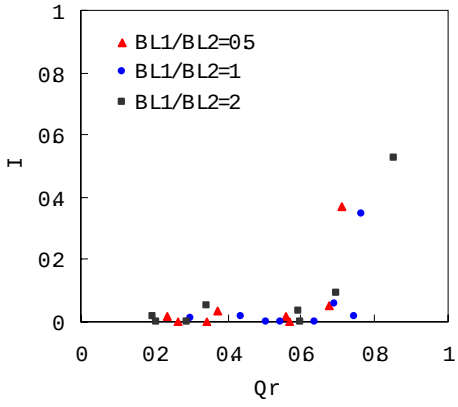

Fig.9. Influence of BL1/BL2

Frazil ice control with variant-type FICS

The concept behind the variant-type FICS is to completely prevent the passage of frazil ice beneath the FICS by increasing the overall draft depth ratio (D/h) while restraining tip vortices by tapering the draft depth of the FICS at its tip. Three variant-type FICS models were prepared, one each for Bb/BL = 0.71, 0.50, and 0.25. For all three, D/h was about 0.5, α was 30°, and BL/Bd was 2.8.

For the Bb/BL=0.71 model, tip vortices were observed under most test conditions. This was attributed to the extended length of Bb, which impeded the smooth inflow of water to the intake. At Bb/BL = 0.50 and 0.25, tip vortices were observed when the flow rate (Q) reached 38.8 *l*/sec. However, these tip vortices were unlike other observed vortices in that they developed and separated at a regular time step. As their occurrence was noted regardless of Qr, it can be assumed that they developed solely due to the elevated flow velocity. Also interesting was an observed lack of frazil ice accretion, even under high flow rate ratios. This was because the unique model shape reduced the area most responsible for impeding flow, thus preventing areas of stagnation from developing upstream side of the FICS.

Fig.10 shows the frazil ice control effectiveness of the variant-type FICS. At Bb/BL = = 0.71, frazil ice was flow into the intake by tip vortices, which occurred under all combinations of test parameters, when Qr exceeded 0.2. However, the inflow did not produce I values of significance. At Bb/BL = 0.50 and 0.25, the inflow of frazil ice was almost totally controlled until Qr approached 0.5, and even at higher flow rate ratios I was reasonably insignificant. Tip vortices were observed in some cases, but they were a separating type and their impact was believed to be minimal as they engulfed frazil ice only intermittently and thus directed only minimal amounts into the intake. Low I values in all cases, despite some influence by vortices, were also due to a complete absence of frazil ice passing beneath the FICSs.

Based on these findings, the variant-type FICS produces conspicuous tip vortices when Bb/BL exceeds 0.5. When Bb/BL is less than 0.5, separation vortices occur as flow velocity increases. The occurrence of vortex turbulence can be restrained by adjusting Bh and decreasing D/h, although this can also allow frazil ice to pass beneath the FICS. A D/h of 0.5 completely controls the passage of frazil ice beneath the FICS. Since experiments with straight-type FICS showed almost no vortex influence when 0.35 < D/h < 0.5, the authors believe that the controlling effects of the variant-type FICS could be further improved by keeping the D/h ratio within this range.

Frazil ice control with variant-bent-type FICS

Based on the previous experimental results, an additional experiment was carried out in which the Bb/BL = 0.50 variant-type FICS was modified with an additional bend. This produced a variant-bent-type FICS with a BL1/BL2 of 1.0 that possessed characteristics of both the variant and bent-type FICS. No clear occurrence of tip vortices was observed in all test cases, and the inflow of frazil ice was completely controlled, even at high flow rate ratios (Fig.11). Thus the variant-bent-type FICS demonstrated the greatest effectiveness seen during this series of experiments.

The results show that, regardless of configuration, all manner of bent-type FICS is free of the influence of tip vortices. It was also shown that it is possible to control frazil ice engulfing at the tip at high flow rate ratios by modifying the basic bent-type shape to taper the draft depth at its tip.

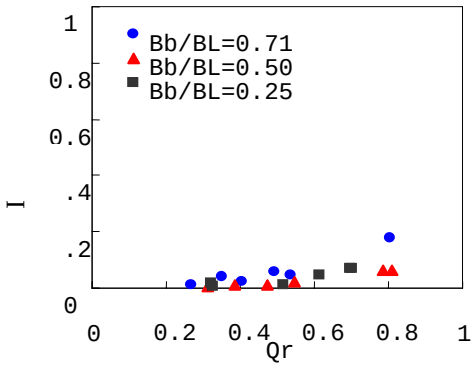

Fig.10. Influence of Bb/BL

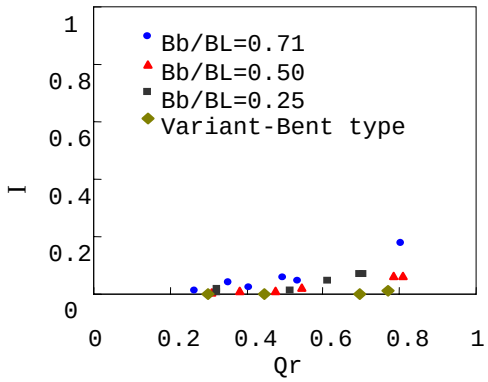

Fig.11. Frazil Ice Control of Variant-Bent Type FICS

CONCLUSIONS

Hydraulic model test was carried out on four types of FICS and evaluate their ability to control the flow of frazil ice into an intake. The results are shown that bent-type FICS can restrain the occurrence of tip vortices and other engulfing turbulence than straight types, and that variant-type FICS can prevent frazil ice accretions even when flow rate ratios are high. Both types demonstrated better overall frazil ice control than straight-type models at high flow rate ratios. Furthermore, a variant-bent-type FICS, which combined the characteristics of both the variant-type and bent-type FICS configurations, exhibited the greatest frazil ice control of all the models tested. The results suggest that almost any required quantity of water intake can be maintained without frazil ice interference, even during winter when flow rates are low.

REFERENCES

O. Kubit, R. Ettema: Ice-Skimming Booms for River Diversions, *15th International Symposium on Ice*, pp. 243-249, 2000.

T. Ueda, S. Yokoyama, K. Takahashi, and H. Saeki: Study on a Frazil Ice Control System at Riverside Diversions, *Proc. of 2002 Cold Region Technology Conference*, pp117-123, 2002.

17th International Symposium on Ice
Saint Petersburg, Russia, 21 - 25 June 2004
International Association of Hydraulic Engineering and Research

A LABORATORY STUDY OF FRAZIL ICE SIZE DISTRIBUTIONS

S. Clark[1] and J.C. Doering[1]

ABSTRACT

The formation of active frazil ice is a phenomenon experienced by many northern rivers that can present several problems. In particular, the blockage of trash racks at hydroelectric generating stations can significantly restrict power production causing significant economic loss. This type of situation will continue to occur until a better predictive model or management strategy is developed.

Despite the magnitude of the negative effects of frazil ice formation, it is still relatively poorly understood. High quality field and laboratory studies of frazil are quite rare, yet these studies are necessary to achieve a fundamental understanding of the processes involved. This improved understanding should help mitigate the aforementioned problems and aid in the management and operation of hydraulic structures.

Frazil ice size distributions from a series of experiments have been obtained and analyzed. The evolution of these distributions is shown for four experiments with various air temperatures. In addition, the temperature data for the experiments has been given, and several diameter to thickness ratios have been measured. These results are intended to enhance the work performed by Daly and Colbeck (1986), and should be beneficial for numerical models used to simulate frazil ice formation.

INTRODUCTION

Despite the numerous experimental observations of frazil ice many questions remain. In particular, there remains some uncertainty as to how frazil ice size distributions will change under various thermal and hydraulic conditions. Buckina (1967) measured size distributions of ice formed in a crystallization tray with turbulence generated using an agitator. The water was supercooled using cooled alcohol, and seeding material was introduced to initiate frazil ice nucleation. Images were captured either at a given time interval or when an appreciable number of crystals were observed. Although an equation for the distribution was developed, it can be observed that the distributions have the

[1] University of Manitoba, Canada

general shape of a lognormal curve. Daly and Colbeck (1986) used a crystal imaging system to measure frazil ice distributions at several locations along their 36.6 m long flume. Various speeds and bottom roughnesses were used to study their effects on the distributions. The water was cooled by heat loss to the -12°C air, and seeding particles were used to initiate frazil nucleation. Daly and Colbeck concluded that a lognormal distribution fit their data quite well.

The results of four experiments conducted in the counter-rotating flume at the Hydraulics Research & Testing Facility (HRTF) are presented herein. By varying the cooling rate and keeping the remainder of the hydraulic and thermal conditions constant, an attempt has been made to determine the effect that the cooling rate has on frazil particle size distributions.

LABORATORY FACILITIES & EQUIPMENT

Problems associated with typical flumes used for frazil ice experiments include the requirement of a large coldroom and pumps to recirculate the water. The counter-rotating flume located in the HRTF circumvents this problem by studying the frazil behaviour in an annular volume of water over a certain period of time. The channel width of the rectangular annulus is 0.20 m, and the centerline diameter is 1.2 m. Water velocity is generated by independently varying the wall and bed speeds. The level of turbulence can be further controlled by placing bed plates on the bottom using various sizes of gravel. The air temperature in ducts under the bottom plates and lining the inner and outer walls can be controlled to within 0.15°C. The entire flume is located in a cold room that maintains air temperature within 0.1°C. Water temperature is measured at a rate of 2 Hz using a Hart Scientific - Black Stack thermistor with an uncertainty less than 0.001 °C and a resolution of 0.0001°C. Images were acquired with two Hitachi KP-F100A high resolution ccd cameras mounted in the flume walls and two Data Translation DT-3162 frame grabber boards. One 50 mm and one 25 mm lens were used. Images were back-lit with one 400 W and one 250 W metal halide bulbs producing approximately 60,000 lumens combined. The light was passed through a polarizer before entering the water and then through another polarizer turned 90° to the first attached to the camera lens. This caused the normally transparent frazil particles to look white (or some shade of grey), while the background appeared black. Shutter speeds of 1/4000 s and 1/2000 s were used to ensure that the particles didn't become blurred because of the apparent particle velocity. The images used in this paper were taken with the 25 mm lens and provided a resolution of 1 pixel = 0.055 mm.

DIGITAL IMAGE PROCESSING

During an experiment, images are typically acquired on a duty cycle where 30 images will be captured at a rate of 2 frames per second followed by a 45 second pause. Up to 3000 images can be acquired per camera during an experiment. With sometimes more than 100 particles per image, one quickly appreciates the necessity for a computer algorithm to analyze this enormous amount of data. For the following experiments an improved version of the digital image processing system presented by Morris and Doering (2002) has been used. The new algorithm was developed using Matlab, and begins by subtracting a reference image (one taken prior to ice particles being present) from the image to be analysed. The background of this subtracted image should contain only zeros, while the ice particles should be white (255). In practice a wide range of intensities

are found. The pixels within this subtracted image that have an intensity greater than a certain threshold – called threshold 1 – will be converted to a 1 in a new binary image, while those less than threshold 1 will be converted to zeros in the binary image. The pixels just beyond the perimeter of the detected particles in the binary image are then compared to the corresponding pixels in the subtracted image. If these pixels then have an intensity greater than some lower threshold – called threshold 2 - , they will also be converted to ones in the binary image. This process will be looped until the binary image does not change from the previous iteration. This iterative procedure allows one to be sure that a detected particle is actually ice by using a high threshold value. Very light particles won't be detected. It also allows the actual size of these known particles to be detected using a more sensitive threshold, ensuring that part of a particle isn't 'cut-off' by using only one high threshold.

A Matlab function is then used to calculate the area and centroid of each of the particles. An ellipse with second moments equal to that of the particle is fit to each of the particles and the major axis, minor axis, and orientation of the fitted ellipse is given. Since the predominant frazil particle shape is that of a circular disk, this method of fitting an ellipse works quite well. The circular particles are generally at some angle to the camera causing them to appear elliptical. The major axis of this ellipse still remains the disk diameter. Further analysis can determine the particle's actual perimeter, as well as the area and perimeter of the fitted ellipse. By comparing the actual particle area to the area of the fitted ellipse, and doing likewise with the perimeters, each particle can be labeled as being elliptical or not Despite the fact that an elliptical particle can overlap with another particle and be labeled as non-elliptical, this labeling algorithm works quite well.

To demonstrate the capabilities of the imaging system, several interesting frazil ice images are shown. Figure 1a shows a large star-shaped particle with a very intricate texture, while figure 1b shows two large circular disks whose edges have become scalloped. Figure 2a shows a large disk-shaped particle whose edges have become scalloped.

Results

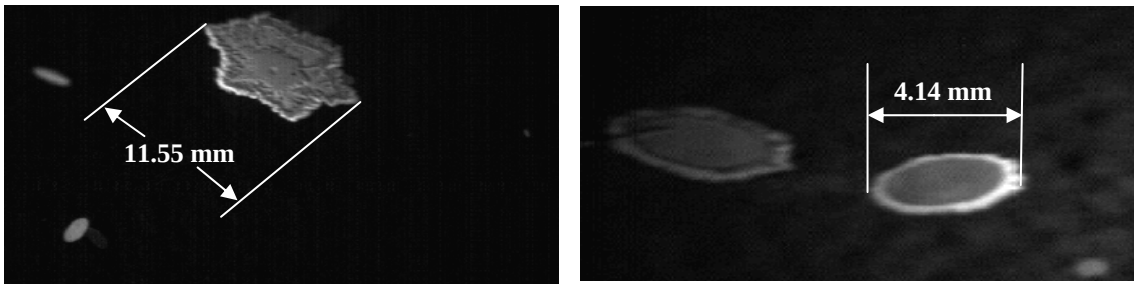

Fig. 1. a) Star-shaped particle. b) Large disk-shaped particle with scalloped edges

As previously mentioned, four experiments with different air temperatures were conducted while keeping the remaining variables the same. Experiments 1 through 4 had air temperatures of -7.5, -10, -15, and -20° respectively. The water depth was 0.15 m, wall and bed speeds were 0.505 and 0.603 m/s, respectively, wall and bed duct temperatures were 2.75 °C and 1.75°, respectively, and the bottom bed plates had a uniform

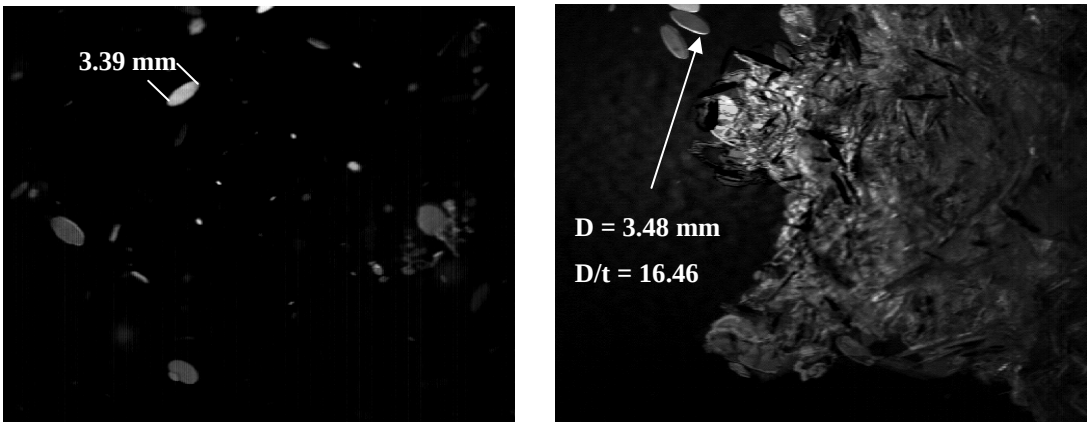

Fig. 2. a) Typical frazil ice image. b) Frazil floc, as well as a few frazil discs.

layer of 3 mm gravel. There was no seeding of the water; frazil nucleation occurred through either mass transport or from small particles of ice sheared from the thin layer of border ice that formed on the flume walls.

Temperature Data

The temperature curves from the four experiments have been superimposed so that they cross the zero axis at the 10 minute point shown in figure 3. Although a few 'spikes' of noise have been removed, the data is otherwise in its raw form. As expected, it can be seen that the cooling rate is a function of air temperature. Interestingly, the maximum degree of supercooling (T_{min}) does not appear to be a function of air temperature. Note that the experiment with the lowest air temperature does not have the greatest degree of supercooling. Although the full temperature data history is not shown, by allowing the experiments to proceed for at least half an hour after the water temperature stabilizes a good measurement of the residual temperature (T_r) can be obtained. It seems that this residual temperature is also not a function of temperature. The time it takes for the water temperature to pass below 0°C, reach $T_{min,}$ and then reach T_r will be called the time to reach residual temperature (t_{Tr}). This time can be quite long since the curve asymptotically approaches T_r. Again, this variable is a function of time. Table 1 summarizes the data obtained from these temperature measurements.

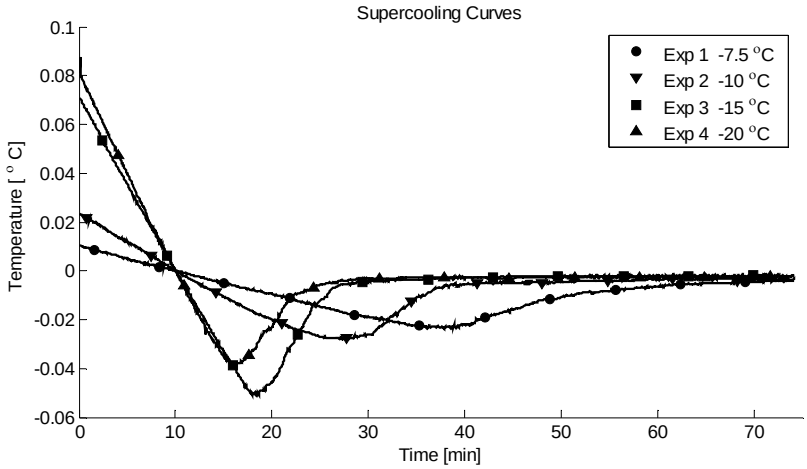

Fig. 3. Temperature data obtained from the 4 experiments

Table 1. Summarized results from the above temperature data

Experiment	Air Temp. [°C]	Bed/Wall Speed [m/s]	Water Depth [m]	Cooling Rate [°C/hr]	t_{Tr} [min]	T_{min} [°C]	T_r [°C]
Exp 1	-7.5	60.3/51.5	0.15	-0.0625	78.06	-0.0237	-0.0028
Exp 2	-10	60.3/51.5	0.15	-0.1421	50.78	-0.0279	-0.0031
Exp 3	-15	60.3/51.5	0.15	-0.437	37.9	-0.0508	-0.0019
Exp 4	-20	60.3/51.5	0.15	-0.499	26.6	-0.0384	-0.0024

Diameter to Thickness Ratio

For each of the experiments it was possible to find approximately 20 particles that were of a large enough size and positioned in such a way as to allow the measurement of both diameter and thickness. These particles do not all appear at the same point in time of the experiment. The average diameter of these particles was 3.48 mm, with an average thickness of 0.22 mm. It can be noted that the diameter of these particles could be measured with greater confidence than the thickness since 0.22 mm is only approximately 4 pixels, while 3.48 mm is just over 63 pixels. That notwithstanding, it is quite interesting that from these four separate experiments the diameter to thickness ratios are all so close. Table 2 summarizes these measurements and shows that the average D/t ratios were between 15.04 and 16.33.

Table 2. Summarized results of diameter to thickness measurements

Experiment	Mean Diameter [mm]	Mean Thickness [mm]	Mean D/t Ratio
Exp 1	3.43	0.23	15.04
Exp 2	3.5	0.22	16.01
Exp 3	3.5	0.22	16.33
Exp 4	3.47	0.22	15.92

Particle Size Distributions

Once the images were analyzed it was possible to find the elliptical particles using the method described. For each image cycle (1 cycle = 30 images) the number of particles with major axis diameters fitting into bins of 0.055 mm width were counted. The average and standard deviations were calculated and a log normal distribution was fit based on these statistics. Figure 4 shows several plots of the resulting histograms and fitted distributions for different times during experiment 3. For cycles prior to the water temperature reaching T_{min} there were not many particles present in the water. This causes a fluctuation in mean particle size and standard deviation. The lower end of the size distributions are quite sparse, which is emphasized by using a log x-axis. From Daly and Colbeck (1986) it is known that frazil particles can be smaller than the 0.055 mm resolution of the camera used here. It can therefore be concluded that there are certainly smaller particles not being taken into account with these distributions.

Figure 5 shows how the measured mean particle diameter changes with time. Although the initial means fluctuate significantly due to the lack of data, there does seem to be an increasing trend. All four experiments show this behaviour, and all four seem to reach a plateau after some period of time. It is interesting to note that each of the four experiments seems to plateau at a diameter in the range of 1.2 and 1.4 mm. The equations are given to provide a sense of the degree of slope, and are not considered to be reliable. The break point has been manually selected, although it seems to approximately correspond to

the point of maximum supercooling. It can be noted that for the first 3 experiments, increasing the cooling rate seems to increase the rate of mean particle size growth. Just as the difference in cooling rates between experiments 3 and 4 is not large, their growth rates are also quite similar. To give more confidence to this data a much larger series of identical experiments would have to be conducted to provide additional data.

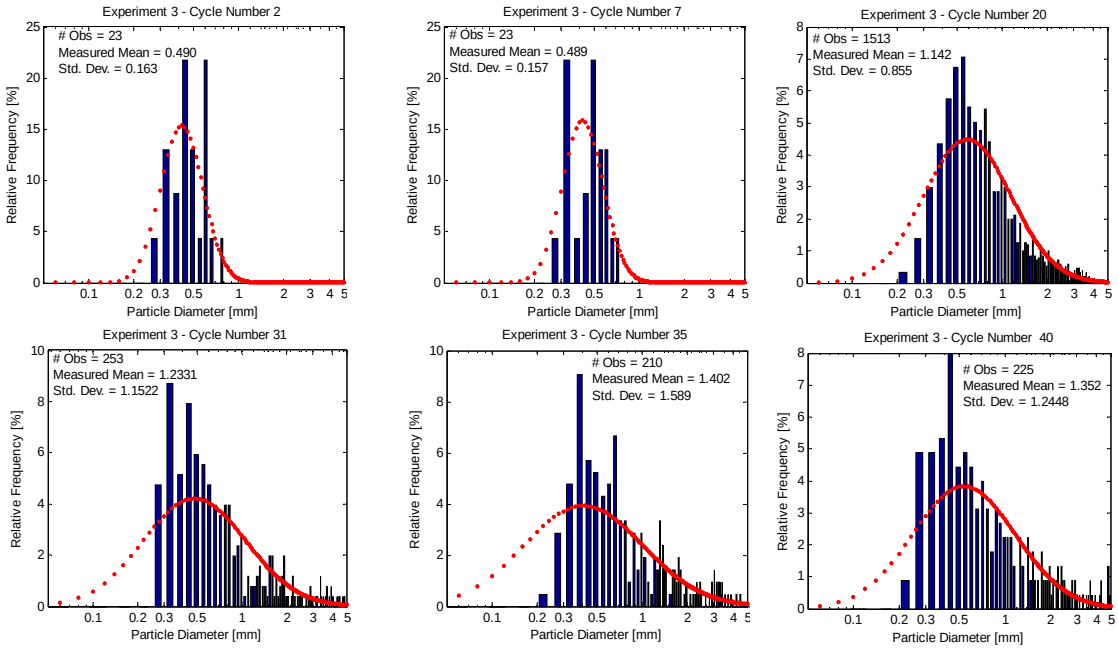

Fig. 4. Measured particle size distributions and lognormal fit

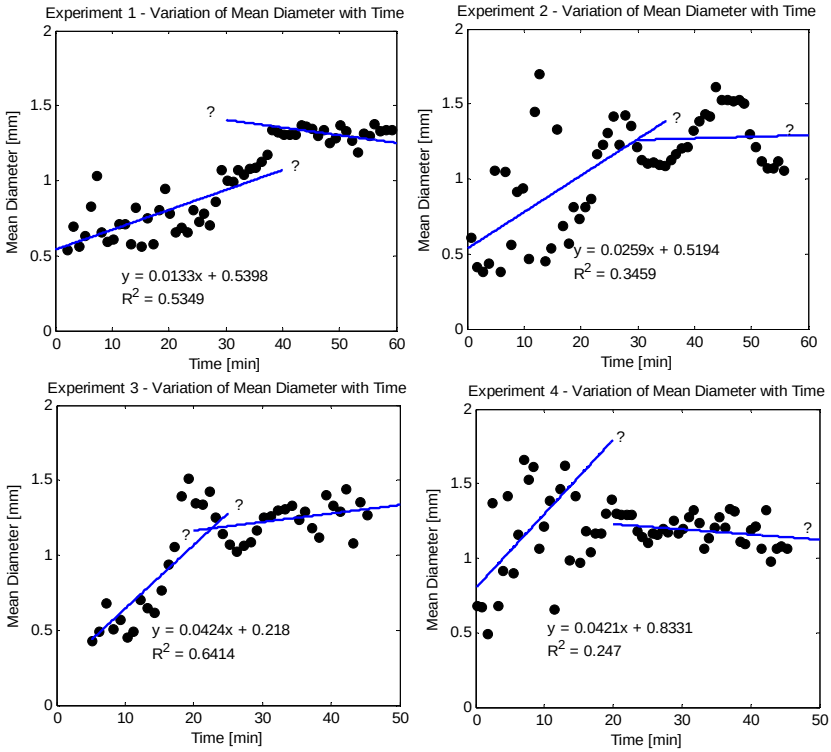

Fig. 5. Temporal variation of mean particle diameters for each of the experiments

CONCLUSION

From the results of these experiments several conclusions can be made regarding water temperature behaviour, particle diameter to thickness ratios, as well as particle size distributions. The cooling rate and the time to reach residual supercooling seem to be functions of air temperature, while the maximum degree of supercooling and the residual supercooling temperature do not. Diameter to thickness ratios for large circular disk particles in the counter-rotating flume seem to have a D/t ratio of around 15.8, which differs from many published values of 8 – 10. Despite not having the resolution to see very small frazil particles, a lognormal distribution fits the measured data quite well beyond the peak, and reasonably well at the peak itself. It is suggested that the mean particle diameter seems to increase until some time around the point of maximum supercooling at which point the mean diameter seems to remain approximately constant in the range of 1.2 – 1.4 mm. The rate of increase seems to increase with decreasing air temperature. There is not enough confidence in the data to determine whether this final value is a function of air temperature or not.

ACKNOWLEDGEMENTS

The authors wish to thank Manitoba Hydro's R&D committee and NSERC for funding this research. The guidance provided by Manitoba Hydro's line advocates B. Shumilak and K. Sydor was also appreciated. Further thanks are extended to S. Ye, S.Wang., and R. Hartle.

REFERENCES

Bukina, L.A. Size Distribution o fFrazil Ice Crystals in Turbulent Flows. *Atmospheric and Oceanic Physics* 3(1):58-68 (1967)

Daly,S.F. and Colbeck, S.C. Frazil ice measurements in CRREL's flume facility. In *Proceedings of the IAHR Ice* Symposium *International Association for Hydraulic Engineering and Research*, Iowa City, Iowa, USA (1986) 427-438

Doering, J.C. and Morris, M.P. A digital image processing system to characterize frazil ice. *Canadian Journal of Civil Engineering* 30(1):1-10,. (2003).

17th International Symposium on Ice
Saint Petersburg, Russia, 21 - 25 June 2004
International Association of Hydraulic Engineering and Research

OBSERVATIONS OF ICE FLOW ON THE RIVER VYCHEGDA

Aleksey A. Kosarev [1]

ABSTRACT

The special transition VL 100 kV Zaovrazhie-Solvychegodsk is situated 2 km downstream the river Vychegda from the town Solvychegodsk between the Solvychegodsky and the upper Sheshurovsky rapids. Recently intensive erosion of the left bank near the transition support №34 has been found out. The change of the river natural hydrological mode owing to the simulated rectification of the riverbed executed in 1987-1988 caused this erosion. To work out the guidelines on the avoidance of the bank erosion it is necessary to have the data about the hydrological and ice mode of the Vychegda in the transition region including parametric observations of the spring ice run in 2003.

RESEARCH PROBLEMS

The parametric investigations of ice mode of the Vychegda in the transition region and in the upstream region of the pontoon bridge in Koryazhma were executed. The research problem included

- ✓ ice-measuring survey upstream the extension of warm sinks of the Koryazhsky PPC;
- ✓ route examination of the river bed from the extension of warm sinks up to the lead of the transition support;
- ✓ determination of floe size, floe speed and the density of the ice run for all the period of its evolution.

RESULTS OF INVESTIGATIONS

The researches of the ice mode were executed from the 21st of April till the 3rd of May 2003.

A polynya that had its beginning in the region of warm sinks of the Koryazhsky PPC (pulp and paper centre) was watched in the transition region. The polynya length was about 17-18 km downstream.

It is the ice situated upstream the polynya that can exert influence on the riverbank in the transition region at the period of the spring ice run.

[1] The B.E. Vedeneev All-Russian Research Institute of Hydraulic Engineering (VNIIG), Gzhatskaya str., 21, St.Petersburg, Russia

The ice run in the region of the special transition started on the 29th of April. The sectoring of the hydrometric leads and the topographic survey of the left bank of the Vychegda in the support region had been executed up to this moment.

Before the beginning of the ice run (the 18th of April) the employees of the electrical system of the Solvychegodsky region had executed the ice-measuring survey upstream the extension of warm sinks of the Koryazhsky PPC. The results of this measurement are shown in fig. 1.

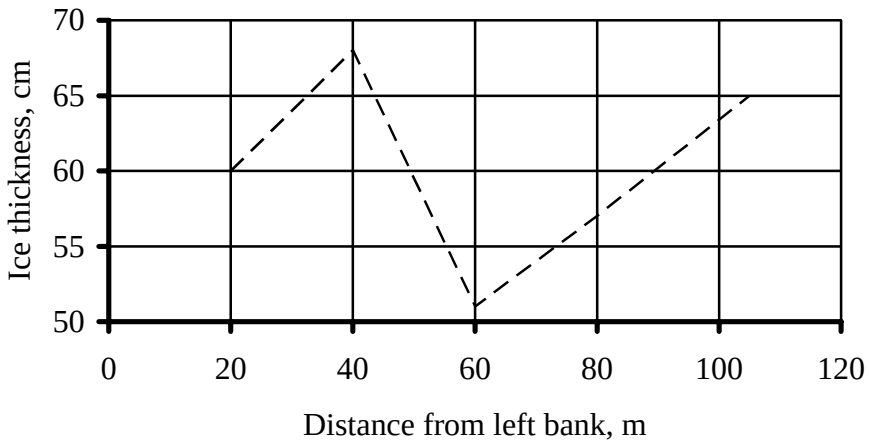

Fig. 1. Ice thickness upstream the extension of warm sinks of the Koryazhsky PPC (the results of the ice-measuring survey of the electrical system of the Solvychegodsky region on the 18th of April)

As it can be seen from the figure, before the river break-up the maximum ice thickness in the observation lead. 40 m apart from the left bank was 68 sm while the average ice thickness was 59 sm.

The power effect of ice on the bank essentially depends on ice structure.

Ice structure in the beginning of the ice run (the 21st of April) was learned directly in the lead of the transition support on the polynya edge where ice thickness was 15-16 sm and less than in the region of the pontoon bridge. The data on ice thickness of ice layers with different structures are shown in a fig. 2 and in tab. 1.

Table 1. Structure of ice cover in the beginning of ice run

Layer thickness, (from the upper ice surface), cm	Structure
2,4	snow ice
4,2	granular ice
9,0	fibrous ice

As it was marked above, the ice run in the lead of the support arrangement of the special transition began on the 29th of April. It was characterized by density of about 8 points. Ice floes were unhummocked and level. Floe length did not exceed 5 m on the first day of the ice run (fig. 3). The scheduled floe size increased up to 20x30 m on the subsequent days. 10 % of ice floes had length about 150 m.

Fig. 2. Layer structure of ice cover in the support №34 region of the special transition. (the 21st of April)

Fig. 3. 500-meter ice run upstream the special transition (the 29th of April)

Floe speed was measured on the 30th of April; to execute it two leads were made perpendicularly the river flow 150 m apart from each other. Two alidades and a stop watch were used to measure the parameters of the ice run (the scheduled floe size and floe speed) – table 2.

The following characteristics of a trial-and-error ice speed series were obtained basing on statistical processing of observation series:

average ice speed was 1,94 m/s;
average quadratic deviation was 0,367 m/s;
coefficient of velocity variation was 0,189;
duration of the spring ice run in April of 2003 was 5 days from the 29th of April till the 3rd of May.

Table 2. Time to pass the distance between measuring leads; ice speed

Measurement	Time, s	Floe speed, m/sec
1	99	1.52
2	82	1.83
3	73	2.05
4	105	1.43
5	113	1.33
6	80	1.88
7	102	1.47
8	90	1.67
9	71	2.11
10	69	2.17

CONCLUSION

There were executed parametric investigations of ice mode of the river Vychegda in the transition region. These investigations included topographic and ice measuring survey and observations of ice thickness, floe speed and floe length. The observations showed that

- ✓ the length of the polynya downstream the extension of warm sinks of the Koryazhsky PPC was 17 km;
- ✓ maximum ice thickness was 68 sm upper warm sinks;
- ✓ average speed of an ice floe at the period of ice run was 1,94 m/s;
- ✓ the density of ice run was 8 points;
- ✓ maximum length of an ice floe was 150 m, while average length of an ice floe was 30 – 40 m.

17th International Symposium on Ice
Saint Petersburg, Russia, 21 - 25 June 2004
International Association of Hydraulic Engineering and Research

FREE SURFACE DRAWDOWN AT ENTRANCES TO WASTEWAYS

A. M. Shvainshtein[1]

ABSTRACT

The breaking pattern of ice blocks is greatly dependent on drawdown of water levels at entrance to free-flow wasteways. Generalization of the data on the water level drawdown makes it possible to evaluate the surface level differential along the length of the ice blocks. The mean dimensionless outline of the free surface depends on the relationship between the water head at the weir crest *H* and the design head. For a 2-D idealization, the water level drawdown at the upstream face of unfinished dam would be (0.085±0.1) *H*. Comparing to the upstream level, the relative free surface drawdown would depend on the distance from the upstream face *x* and from *H*. For a weir with wide sill and piers the mean drawdown at the approach to the weir would also be determined by a relative length of the weir sill. Given is an approximate assessment of the level drawdown at the entrance under significant submergence of the weir. Presented are computation charts for determination of free surface drawdown along the bank and the upstream portion of a cofferdam.

INTRODUCTION

Breaking of ice blocks at entrances to free-fall wasteways is a function of the drawdown differential at those zones. In a number of publications the position of the free surface near the entrance into the structures is either assigned arbitrarily due to insufficient knowledge of the question (Panfilov, 1965), or is not considered at all (Manuel, 1977; Gotlib et al.,1990). Processing of previous experimental results is useful for giving some recommendations for approximate assessment of the position of the free surface curve at the entrance zone. The ice breaking probability may be defined as a comparison between the water level drawdown over the length of an ice block and a minimal drawdown at which this breakage may occur (Manuel, 1977; Gotlib et al., 1990). The relationship for the determination of minimal drawdown includes the thickness and strength of the ice blocks varying over a wide range. Three types of ice passage structures are considered: nonaerated weirs, concrete dams under construction, river obstruction by cofferdams.

[1] The B.E. Vedeneev All-Russian Research Institute of Hydraulic Engineering (VNIIG), Gzhatskaya str., 21, St.Petersburg, Russia.

Free surface drawdown above upstream face of nonaerated weirs

The shape of the free surface at the overflow face of such weirs is assessed by measurement of the lower surface of a jet of flat-plated weir. The coordinates of the overflow face are determined by slightly moving its profile onto the shape of the lower surface of a jet of flat-plated weir. Let us compare the coordinates of the upstream surface of the jets at those weirs. Curve 1 (Figure 1), reduced to the unit head, determines a relative water level drawdown to the upstream face of flat-plated weir (x=0 is coincident with the line of the upstream face of the weir). The x-axis is directed upstream and the coordinate axis z is counted from the upstream level vertically downward. The acting head of nonaerated weir amounts to 0.831 of the flat-plated weir. The same Figure presents curve 2 determining the drawdown of the levels upstream of the nonaerated weir. The same Figure presents the data of experiments determining the free surface drawdown at the nonaerated weir WES (Chow, 1959) in a 2-D idealization. The solid lines 3 – 5 refer to the surface drawdown in front of such weir for crest heads equal to 1.33; 1 and 0.5 of the design head H_{des}.

Curve 4 for $H=H_{des}$ is located lower than curve 2 due to some advancement of the weir profile into the shape of the lower surface of a jet of the flat-plated weir. The operation of WES-shaped weir would result in a relative lowering of the free surface for $H>H_{des}$ and relative raising of the free surface for $H<H_{des}$, as compared to a case of $H=H_{des}$.

For weirs with piers on the crest along the span axis, the maximum value of the free surface drawdown curve is diminished by (0.035-0.050) H compared to a 2D problem (Figure 1). At the lateral surface of the piers this diminution is even more substantial. The comparison between the drawdown near the piers and along the span axes is indicative of a complex spatial relief of the water free surface for a case of piers at the weir crest. The head at the weir crest during ice passage will be less than the design head. For preliminary estimates of the free surface drawdown in front of such weirs one may use curves 5 in Figure 1.

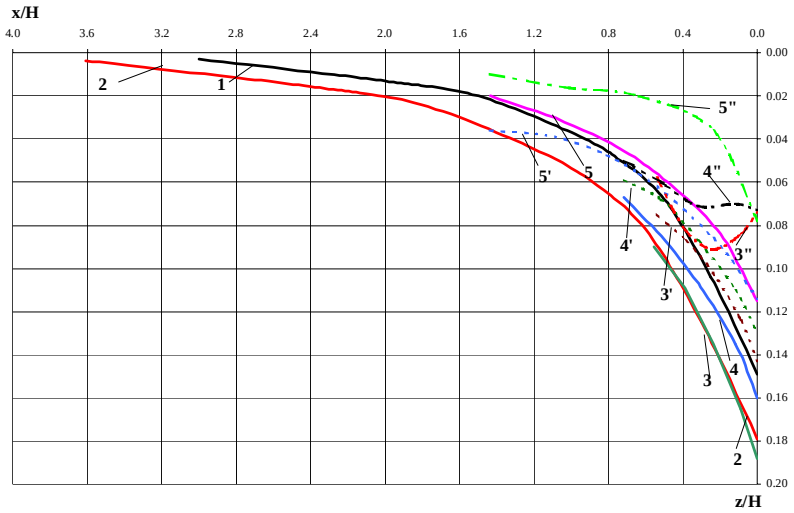

Fig. 1. The z/H – x/H relationships for thin-plate and nonaerated weirs:
1 – thin-plate weir for p/H>2.5; 2 – nonaerated weir whose profile corresponds to the lower surface of the flow on thin-plated weir for p/H>3.0; 3 – 5 – WES-shaped weir for H/H_{des} equal 1.33, 1.0 and 0.5 for p/H>6.0; 3'–5' and 3" –5" – same as in the previous case but respectively along the axis of span and along the piers with semicircular shape of the upstream tip, for $b_s/b = 0.84$ (b_s and b–effective and axial width of span)

Assessment of water free surface drawdown in front of concrete dams under construction

By the hydraulic conditions, non-finished concrete dams are broad-crested weirs. Directly above the upstream face of such a weir the motion has an unevenly varying mode. Detailed data on the water depth measurements above the upstream face of broad-crested weir can be found only in (Berezinsky, 1950). Before analyzing this data, it should be noted that:

1. The above studies were made in a wide range of parameters : the head on the sill was 5.5 – 18 cm; there were various relationships between the height p and the width C of the weir sill; the studies were made for rectangular and rounded inlet edge for a 2-D problem in the presence of piers and for free and submerged flows.

2. The maximum lowering of depth above the upstream face line does not exceed 0.1 H and amounts to no more than 1.5 –1.8 cm. Even when making careful measurements, the error in the determination of the free surface drawdown is quite considerable.

3. When forming the computation relationships it is assumed that the drawdown of the free surface curve in front of the weir is proportional to the crest head. This value is not much dependent on other parameters. This fact as well as a considerable measurement error is responsible for a wide scatter of the test points on the diagrams below; the relationship discussed herein are rough estimates only.

The analysis of the experimental data indicates that in the framework of 2-D problem the maximum free surface drawdown z_b at the upstream face of non-submerged broad-crested weir (C/H=2.5 – 9.0) is (0.075 – 0.095) H. No regularities have been found in a mode of variation of z_b as a function of C/H, p/H or the shape of the inlet edge. In a context of 2-D problem for a broad-crested non-submerged weir, the free surface drawdown may be approximated by (Figure 2):

$$z/z_b=\exp(-\alpha x/H), \qquad (1)$$

in which the proportionality coefficient α for a rectangular broad-crested weir is 1.8 and for a weir with rounded inlet edge – 1.3.

When the flow passes over the piers on the crest of a non-submerged broad-crested weir, the difference of the water depths over the width of the upstream face of the weir along the flow axis and at the lateral surface of the piers amounts to 0.5 – 1.2 of a mean free surface drawdown at this site. Under such inlet conditions, z_b is understood as a mean free surface over the flow width at the upstream face of the weir. The additional lateral drawdown of the water level at the inlet into non-finished dam promotes a more intensive breakage of the ice blocks. The data for a non-submerged weir with wide sill and piers on the crest (Berezinsky) are indicative of the fact that, comparing to a case of 2-D problem, the free surface drawdown near the upstream face z_b will be increased with the increase of C/H, and is dependent on the shape of the inlet edge of the pier (Figure 3). For the same values of C/H, the average values of z_b/H prove higher for a non-rounded than for a rounded edge. As found by the tests, the shape of the inlet cap of the pier does not produce any important effect on z_b/H. The values of z_b are determined from the expressions differing in the value of a free term (Figure 3) :

$$z_b/H=0.005C/H+A\ . \qquad (2)$$

a)

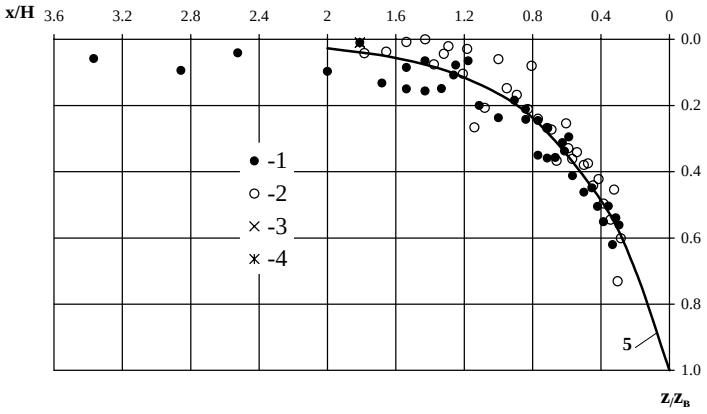

b)

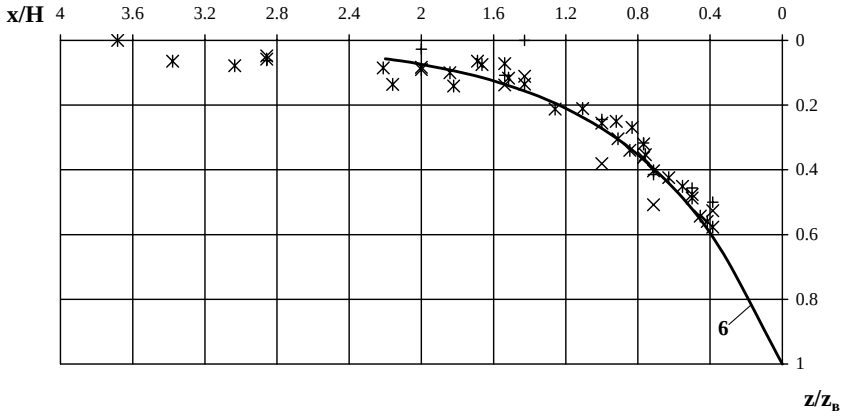

Fig. 2. Charge of relative differential z/z_b as a function of relative distance from the upstream face x/H for a rectangular nondrowned weir (a) and rectangular nondrowned weir with rounded inlet edge (b): 1-2-without rounding of inlet sill and C/p equal to 1.25 and 4.67; 3-4-with rounded inlet sill varying from 0.2÷0.46 with C/p equal to 2.4 and 4.67 respectively;5-z/z_b=exp(-1.8x/H); 6- z/z_b=exp(-1.3x/H)

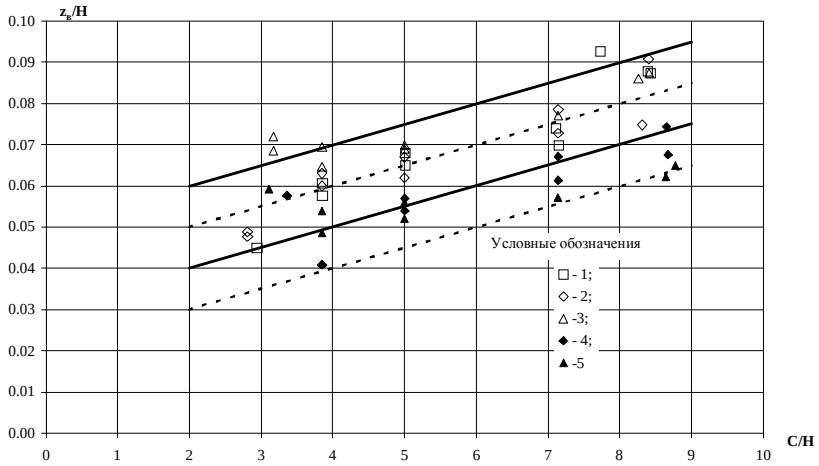

Fig. 3. Mean values of relative level drawdown at the upstream face of rectangular undrowned weir with piers present at the crest (b_s/b=0.84) and (p/H=0.6÷1.82):
1-3- for non-rounded inlet wedge of weir and, respectively, for rectangular, semicircular and curvilinear-sharpened outline of upstream head of piers; 4-5-for circular inlet wedge of weir (r/p≈2.34) and semicircular and curvilinear-sharpened outline of upstream head of piers

The values of A for the upper and lower boundaries of cross-sectionally rectangular weir are equal to 0.05 and 0.03, and for weirs with rounded inlet edge 0.04 and 0.02 respectively.

For a case of a free-flow weir with wide sill of piers on the crest, the mean drawdown of the free surface compared to the upstream level may be determined according to empirical relationship (Figure 4):

$$z/z_b = \exp[-2.5(x/H - 0.25)]. \quad (3)$$

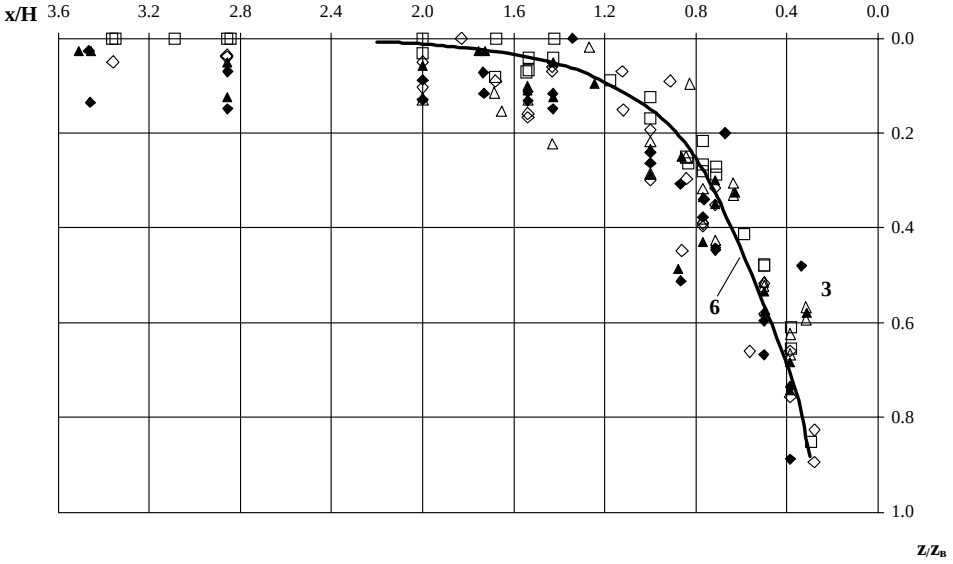

Fig. 4. Relationship between relative differential and x/H for rectangular undrowned weir with piers present at its crest (b_s/b=0.84) and (p/H=0.6÷1.82):
Notation 1-5-same as in Figure 3; 6-z/z_b=exp[-2.5(x/H-0.25]

A wide scatter of experimental points in Figure 4 results from severe errors in the determination of the mean values under the spatial flow conditions. In the upstream zone near the piers there does not appear any mean free surface lowering directly at the upstream face of the weir in the range $0 < x/H < 0.2 - 0.3$.

At $t < 0.8H$, the lowering of the free surface in front of a drowned weir is determined by the relationships for a free-flow weir. The lowering of the free surface in front of the presently analyzed weir for $t > 0.8H$ will be less than for a free-flow weir (Berezinsky, 1950). The value of this lowering is dependent on the maximum differential between the head and the minimal depth at the weir sill. This differential may be determined as

$$Z_0 = H + \frac{V_0^2}{2g} - t + Z_{rec} \quad (4)$$

where V_0 – the velocity at the approach to the weir, Z_{rec} – the differential of recovery.

For the analysis of experimental data for a drowned weir with wide sill it is possible to give only approximate values of the lowering of the free surface curve, proportional to the differential Z_0, due to great error of those measurements (see Table). In the above equations it is possible to substitute Z for Z_0, that is to determine the differential paying no attention to the approach velocity.

Table. Approximate values of free surface drawdown at approach to drowned weir with wide sill

Design features of weir	z_b/Z_0 ($x/H = 0$)	z/Z_0 for various x/H		
		0,5	1,0	2,0
Constant width rectangular weir	0,20-0,25	0,10	0,05	0
Constant width weir with rounded inlet edge	0,30-0,40	0,15	0,05	0
Rectangular weir with piers ($b_s/b = 0.84$)	0,15-0,20	0,10	0,03	0

The above empirical relationships for weirs with wide sill make it possible to determine the lowering of the free surface of a portion of the upstream zone at the upstream face of concrete dams under construction. For a 2-D problem, this estimate should give acceptable results in cases of wide span of unfinished part of the dam [$b>(3-4)H$] as well as in case of "narrow" spans [$b<(2-3)H$], separated by relatively thin piers ($b_s/b>0.8$). In case of thick piers ($b_s/b<0.5-0.7$) or the removal of the upstream head of the sill above the upstream face, the assessment values would become more approximate.

Lowering of free surface in front of cofferdams obstructing the river channel

For a drowned flow through a river channel obstructed by a cofferdam ($0 < Z_0/t < 0.25-0.3$), the lowering of the free surface curve at a section before the obstruction is determined on the basis of experimental studies (Rubinshtein, 1960) as a level differential between the upstream zone and the constricted section, and as a relationship of angle Θ between the upstream portion of the cofferdam and the dynamic axis of the flow (between the upstream and the longitudinal sections of the cofferdam with a trapezoidal outline in plan and the longitudinal portion of the cofferdam parallel to the bank of the flow).

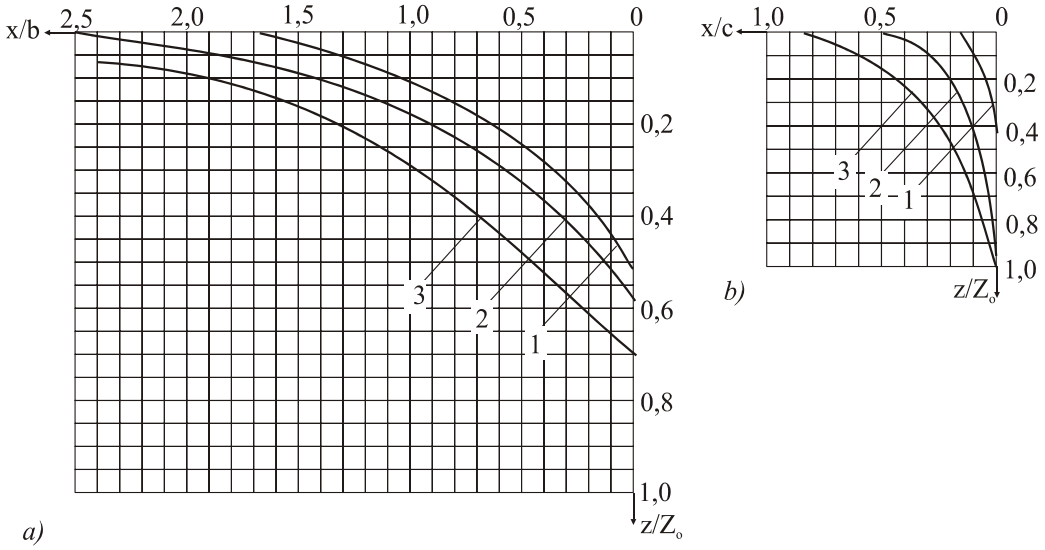

Fig. 5. Relative lowering of water free surface upstream of river obstruction by cofferdam:*a* – along the bank nearest to the channel; *b* – along upstream portion of cofferdam:

1– 3–for Θ equal to $\frac{\pi}{2}; \frac{2}{3}\pi; \frac{5}{6}\pi$

Figure 5 presents the plots for the determination of the lowering of the free surface at a portion of the upstream zone before the cofferdam. The lowering in the Figure is given as a fraction of the differential at the structure for various outlines of the cofferdam in plan. On the plots, x is a distance counted from the upstream angle of the cofferdam; b is a width of the obstructed portion of the river; c – a length of the upstream lateral portion of the cofferdam. When using these plots, the water level differential Z_0 may be found out by the relevant Guides, e.g. (Manual…,1974).

CONCLUSION

Based on the analysis and processing of a set of experimental data the relationships are obtained for determination of hydraulic operation conditions in front of the inlets into nonaerated weir dams, concrete dams under construction, channels obstructed by cofferdams. These relationships permit to assess the possibilities of ice breakage in the above circumstances. The obtained results may be summarized as follows:

1. The assessment of the free surface drawdown in front of nonaerated weirs (relative effective width $b/H > 3 \div 4$) may be made for a case of 2-D problem, using curve 5 from Figure 1. For a relative width $1 < b/H < 2$ and small relative thickness of piers ($b_s/b \leq 0.8$), such assessment is made using curves 5' and 5" of the same Figure.

2. The relative drawdown of the water free surface in front of wide spans of unfinished portion of dam ($b_s/H > 3 \div 4$) under free flow regime may be found on the basis of empirical relationship (1), in which the drawdown of the water free surface in the section of the upstream face of unfinished dam is assumed $z_b = 0.075H$. For narrow spans of unfinished portion of dam ($b_s/H > 2 \div 3$) and the same flow discharge regime, the drawdown of the water level in front of the unfinished portion of dam may be assessed using equations (2) and (3).

3. The approximate values of the water drawdown in front of the upstream face of the unfinished dam portion under drowned flow ($t > 0.8H$) may be found out from the data shown in the Table.

4. The assessment of the drawdown of the free surface curve at a channel portion located directly upstream of its obstruction by cofferdam should be made using the plots in Figure 5.

REFERENCES

Chow V.T. Open-channel hydraulics; *Mc Grow-Hill Book Company*. New York, Toronto, London, 1959, 680p.

Berezinsky A.P. Discharge capacity of broad-crested weir. *L. Stroiizdat*, 1950, 186 p.

Consideration of ice passage conditions during the design, construction and operation of hydraulic schemes: *Manual BCH 10-76/ Ministry of power industry, USSR (the B.E.Vedeneev VNIIG)*, L., 1977, 18p.

Panfiliov D.F. Breakage of ice fields under the effect of local changes in the water level. *Hydraulic Construction*, 1965, N12, p 21-25.

Gotlib Ya.L., Korzhavin K.N., Korenkov V.A., Sokolov I.N. Ice passage over hydraulic structures. M., *Energoatomizdat*, 1990, 182p.

Recommendations for hydraulic assessment of weirs. Part 1. Frontal weirs: *П18-74/VNIIG*, 1974, 58p.

Rubinshtein G.L. Evaluation of flow regime in the zone of cofferdam and its upstream blanket. L., *Energoizdat*, 1960, 52p.

17th International Symposium on Ice
Saint Petersburg, Russia, 21 - 25 June 2004
International Association of Hydraulic Engineering and Research

ASSESSMENT LOCATION AND PARAMETERS OF ICE JAM ON THE BASIS OF RIVER WATER LEVEL REGIMES STUDY

Sergey D. Vinnikov[1], Lubov' S. Banshchikova[2]

ABSTRACT

Definition of the ice jam formation time, its length along the river channel and value of the ice mass is an important point for the ice jam phenomena forecasting as well as for the decision of engineering hydrology tasks.

So, let's consider this problem on the example of well-known ice jam on the Lena river near Lensk [town] formed in May, 2001.

Ice breaking on the Lena and, particularly, near Lensk town is frequently accompanied by the ice jam formation. The jam extends on tens of kilometers, causing the water level elevation.

It results in the flood-lands flooding and numerous destructions in and near the river course.

The accurate forecast of river breaking-up and certain information on ice passing conditions during ice floating permits us to undertake some adequate measures to prevent the consequences of the ice jam in due time.

The problems of the Lena ice conditions, ice jams, and water level rise were deeply studied by K. Polyakova, Rudnev, V. Kilyaminov etc.

But, as the Lensk'2001 ice jam showed, the problem is rather far from the final solution.

In this work we make an attempt to show, how to define the point of the ice jam formation and how to locate the "head" of the jam.

This will allow us to destroy the jam's lock in no time.

Further, using the same water level measurements and the river bed hydromorfological adjectives of the considered frontage, we can find out the ice thickness for a length of the jam.

The problem may be solved more effectively, if the water level observations on standard and transient gauging stations will be sampled more frequently.

[1] Russian State Hydrometeorological Univercity (RSHU) Saint-Petersburg, Malookhtinsky ave. 98
[2] State Hydrologic Institution, scientific institution Saint-Petersburg, Vasil'evsky Island, 2nd line, 23. E-mail: banshchicova@hotmail.ru , vasilenko@hotmail.ru

Of course, the unified elevation fixing of the water gauges in absolute or conventional altitudinal system is necessary.

Basing on water level gaugings, let's construct a graph of water level posteriority $Z = (x, \tau)$.

The axes of the graph are directed as shown below (different from V. S. Antonov's work): the longitudinal axe x is a distance up the river and the vertical one is a time axis.

In the field of these coordinates the points with water levels should be marked according to gauge stations arrangement.

Then, the dipstick marks with equal meaning are connected with a line and, hence, we have several lines of equal water-level *z*.

Due to the behavior of these lines we can do a corresponding conclusion.

For example, if the ice-jam exists, the isolines near its "head" will start coming together.

As soon as the erosion of the ice jam begins, and especially if the bursting occurs, the isolines start to disperse and later they go in the same direction.

The graph $Z = (x)$, reflecting the water level surface in the river, will be a good support for the graph shown above.

These graphs, examined and formatted for the Lena near Lensk, allowed us to state the following:

In 2001 the catastrophic ice jam, consisting of two jams, was formed in the following conditions: at first it occurred downstream Nua village (probably near Glukhoi island) on 14/15 May.

Then, as this jam expanded up-stream, the second ice jam was formed near the Batamayski island.

According to the graph analysis, we can suppose that either natural factors or blasting operations caused the shearing of ice in the jam and its thickness increase, which, in its turn, affected an extreme water level rise near Lensk and down the river.

The rise of water-level in this time is conditioned by the ice-jam head compression.

As is followed from the above, if in the initial period the jam was affected with breaking load, evidently, the job will be done better than an out-of-date impact on the ice jam mass.

Using equal water-surface contours for 18/05/2001 we can determine the down gradient, and the flow width finds over cross direction profiles.

By the water discharge Q on the Solyanka village hydrologic section we'll find out the ice thickness in the ice jam, applying, for example, the hydraulic design methods.

According to the above, we'll use the following empiric formula:

$$Q = \left[\frac{I^{1/2}}{(1.6 B^{2/3} n_{np})} \right] F_{ж}^{5/3}, \qquad (1)$$

where I is a down gradient, B is stream width, n is an effective roughness factor, F is the river free area.

On certain values of Q, B, I, $n_{пр}$ using the formula (1) let's find the river free area below the ice jam and, then, the cross-section area of the ice-jam for the above-mentioned sections.

$$F_p = F_{общ} - F_{ж}, \tag{2}$$

where $F_{общ}$ is a cross-section area of the ice-jam $F_з$

The ice thickness in the jam on the considered plot is found by dividing the cross-section area $F_з$ on the river width B.

The result of the carried-out calculations on the stated plan was that the ice thickness in the head of the ice-jam to 18/05/2001 (2380-2400 km from the Lena's outfall) came to 12.0 meters.

Headed for Lensk, it reduced with some variation to 10 meters.

Here, we can't agree with the authors of [3], which analysis showed the ice-jam accumulation on the night of 16/17 May near Nua village.

The equal water-surface contours $Z = (x, \tau)\ Z = (x)$, examinated carefully, produce another conclusion, as said above.

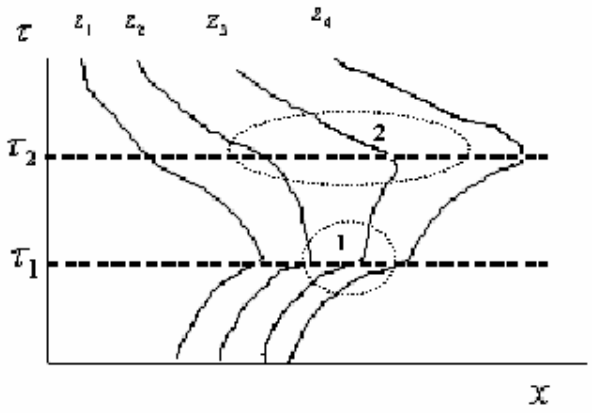

Fig 1. Diagram of water level change isolines in the ice-jam formation;
; where τ_1 is a jam formation point, τ_2 - is a jam destruction point,
1 – is the isolines convergence area , 2 – an area of the isolines dispersion.

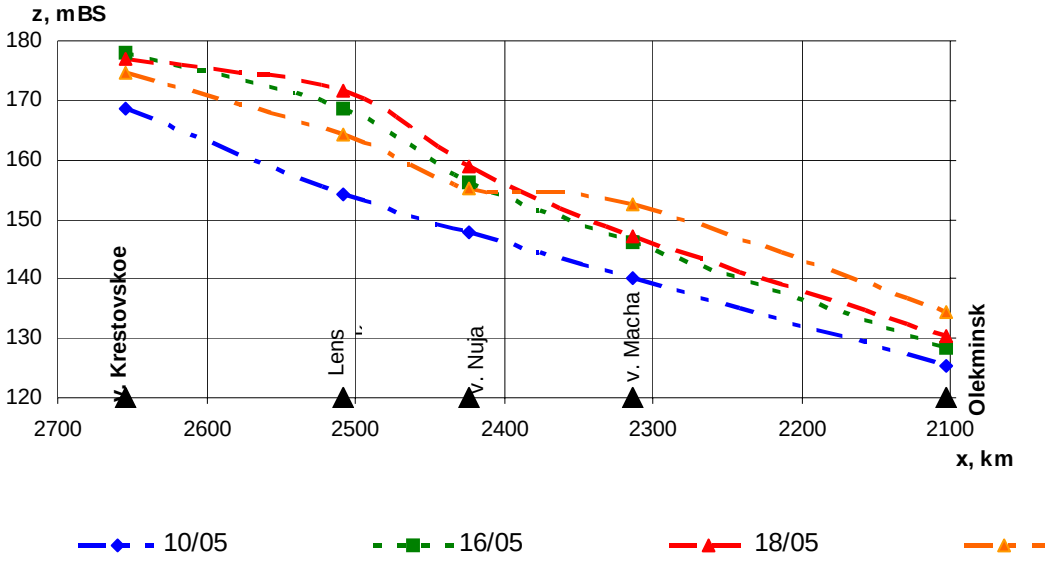

Fig.2. Water surface curves on considered plot during the ice-jam formation on different days (10/05, 16/05, 18/05, 20/05)

REFERENCES

Vinnikov S. D. On the generalized water level and discharge graphs plotting. Intercollegiate Collected articles issue "Hydrological study questions and conservation of natural waters". LPI publishing house, 1986, pub 94, p. 93-97

Vinnikov S. D. , Proscuryakov B.V. Hydrophisics. L., Hydrometeoizdat, 1988, p. 160-190.

Kilyaminov V.V., Tazatinov V.M., Shepelov V.V. Ice jams – the ice monsters of Yakutia rivers. Journal of science and technique in Yakutia, № 1. 2001. p 36 -40

17th International Symposium on Ice
Saint Petersburg, Russia, 21 - 25 June 2004
International Association of Hydraulic Engineering and Research

THE DETERMINATION OF THE EQUIVALENT ICE THICKNESS USING PERFORMANCE DATA OF MT UIKKU AND ICE THICKNESS MAPS

Hänninen, Samuli[1]

ABSTRACT

MT Uikku is a powerful ship and well suited for ice navigation in the Baltic ice conditions. During the winter 2003 ice-induced loads were measured in the bow area of the ship. In addition to ice load measurements, propulsion parameters were recorded. The measured data gives an opportunity to study relationships between ship operations, ice conditions and ice-induced loads. In this paper, measured data is compared with ice thickness maps. The maps are generated using RADARSAT SAR images and ice thickness history. If correlation between ice thickness information and ship operation parameters can be found, these kind of maps could be used in route optimisation, to avoid heavy ice and to minimize travel time needed between two winter ports.

INTRODUCTION

During the winter 2003, three test voyages onboard MT Uikku were made between the Gulf of Finland and Bay of Bothnia. The purpose of these voyages was to conduct ice load measurements, to gather data of ice conditions and to collect data from ship performance in different ice conditions. During the winter 2002-03 the maximum ice cover extent in the Baltic Sea was approximately the same as the long-term average value (Fig. 1), but in many areas there were thick ridged and rafted ice. The ice season lasted approximately two weeks longer than usual. From that point of view, the winter navigation season 2002-03 in the Baltic Sea was difficult. Daily mean temperatures, cumulative freezing degree-days and ice thickness data from two weather stations are presented in Figure 1. The northernmost station, Hailuoto, is located in the Bay of Bothnia near Oulu. Rankki is located in the Gulf of Finland near Kotka. Maximum cumulative freezing degree-days (FDD) were about twice as much in the Bay of Bothnia than in the Gulf of Finland. The ice season started about one month earlier in the Bay of Bothnia than in the Northern Quark and in the Gulf of Finland. The maximum ice thickness was reached in early April. It was about 80 cm in the Bay of Bothnia and 60 cm in the Gulf of Finland.

[1] Helsinki University of Technology, Ship Laboratory, Finland

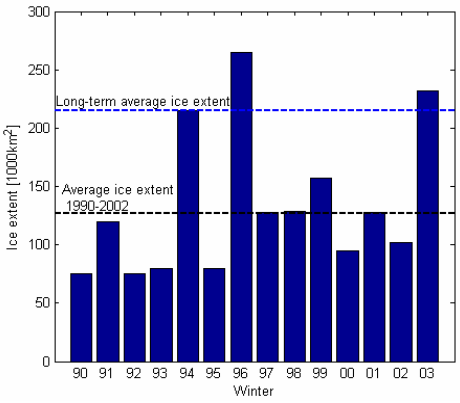

Fig. 1. Maximum ice cover extents during the winters 1990 – 2003 (FIMR), and daily mean temperatures, cumulative freezing degree days (FDD) and ice thickness data during the winter 2002 – 03 (FMI, 2003)

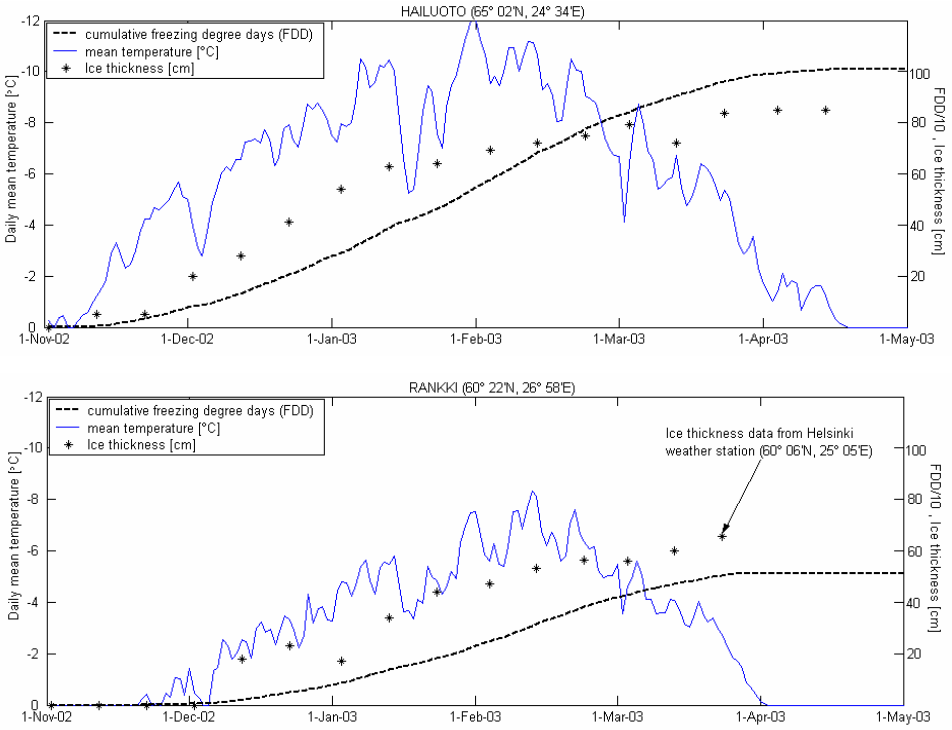

In this paper, ship speed, propulsion parameters and ice-induced loads will be compared with ice thickness maps (Karvonen et al. 2003). Ship speed is in principle determined by ice characteristics and propulsion parameters. This means that if the propulsion power is kept constant, the ice characteristics will determine the speed and its variation. The relations of the propulsion power, speed, ice conditions and ice load level are sketched in Figure 2.

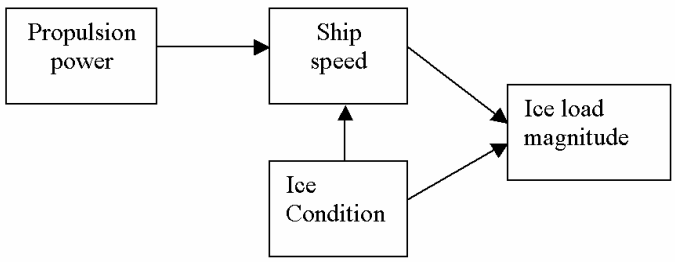

Fig. 2. Relation of operational parameters, ice conditions and ice load level

THE MEASURING SYSTEM

MT Uikku is a double hull ice breaking motor tanker with eight cargo tanks. The ship was built in 1977. The vessel was constructed to the highest Baltic ice class, I A Super. The ship's propulsion system has an Azipod unit and four diesel generators. In 1998, the hull was strengthened to allow her to sail more safely in the Arctic waters. After the strengthening the hull was stronger than what Baltic ice class I A Super demands. The main particulars of MT Uikku are presented in Table 1.

Table 1. The main particulars of MT Uikku

Length, overall	164.4 m	Deadweight	15750 ton
Breadth moulded	22.2 m	Propulsion power	11.4 MW
Draught	12 m	Speed	17 knots
Displacement	22600 ton	Block coefficient	0.72

During the winter 2003 MT Uikku navigated regularly between the ports in the Gulf of Finland and in the Bay of Bothnia. The ship has more power than average Baltic tanker, so she is able to navigate independently without icebreaker assistance most of the time. Normally the ship uses ½ or ¾ of the full propulsion power in ice, but sometimes in difficult ice conditions she has to use full power. The performance curves i.e. the speed the ships may attain in different level ice thicknesses with different power levels are presented in Figure 3. The level ice h-v –curves are calculated using Lindqvist (1989) formulations.

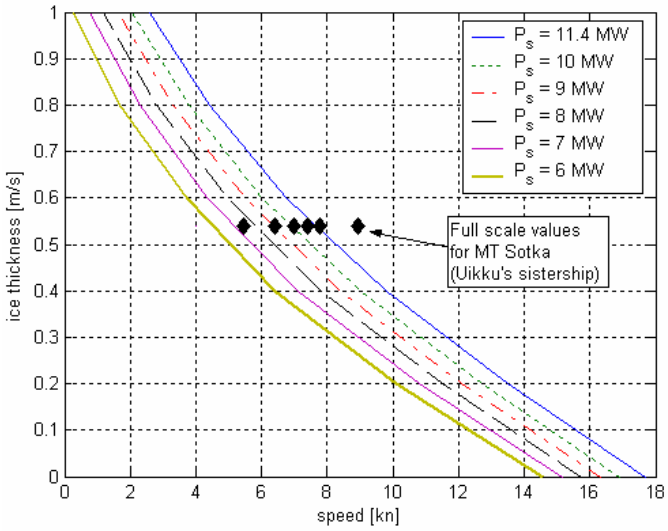

Fig. 3. MT Uikku performance in level ice with different propulsion powers compared with some full scale values

For purposes of the ARCDEV-voyage (Kotisalo and Kujala, 1998), MT Uikku was instrumented to measure ice loads from different parts of the hull. The bow ship instrumentation was repaired in 2000 (Lensu, 2002). During the winter 2003 this instrumentation was used. Measurements included loads on transverse frames in the bow and bow shoulder areas, stresses in the shell plating and frames in the bow and bow shoulder areas, power, torque, and propeller revolution. The measuring system was

designed for operative ice load monitoring purposes. The description of the measuring hardware and monitoring program has been reported in Lensu and Karttunen (2001) and Karttunen (2001). All channels (propulsion and ice load data) were sampled at 200 Hz. During the voyages, GPS measurements were also made. In addition to the ice load and ship performance measurements, ice conditions were visually observed.

THE VOYAGES AND THE RESULTS FROM THE MEASUREMENTS

Voyage I (Porvoo-Oulu-Porvoo)

Uikku left the port of Porvoo on 31-Jan-2003 in cargo condition. The average ice thickness was about 30 cm. There was some amount of ridged ice east of Helsinki. Air temperature was about –10°C and wind direction was from the south. The next stop was in Pori 1-Feb-2003. Outside Pori there was mainly newly frozen thin ice. From Pori the ship continued towards Oulu. The ship entered into an ice field on the same day at 63 degrees north. In the Bay of Bothnia, there was ridged and rafted ice north of Kokkola. The average ice thickness was approximately 40 cm. During the last part of the voyage near Oulu, the ship got stuck in ice. Then the ship had to use full propulsion power for some time in order to carry on. She managed independently to the port of Oulu in 2-Feb-2003. The ship continued from Oulu to Porvoo in ballast condition. The ship got stuck in an ice channel near Oulu and needed IB Urho to assist. The icebreaker assisted her for 4 hours. After that, ice conditions became much easier. The wind was blowing from south about 18 m/s and it was snowing. On 4-Feb-2003 at 22:00 in the Gulf of Finland ice conditions changed into more difficult again. The ship needed full propulsion power and IB Sisu to assist her. MT Uikku arrived to Porvoo on 5-Feb-2003. It can be noticed that in cargo conditions the ship managed without icebreaker assistance throughout, but in ballast condition she needed icebreaker assistance both in the Bay of Bothnia and in the Gulf of Finland. Speed as a function of time and distance travelled are presented in Figure 4. The distance travelled was about 550 nm in both cases, of which half was spent in ice.

The route of MT Uikku from Porvoo to Oulu is plotted on the ice thickness map in Figure 5. The speed of MT Uikku is also presented. In open water the speed was over 15 kn. In thin ice (below 20 cm) the ship's speed decreased to 14 kn.

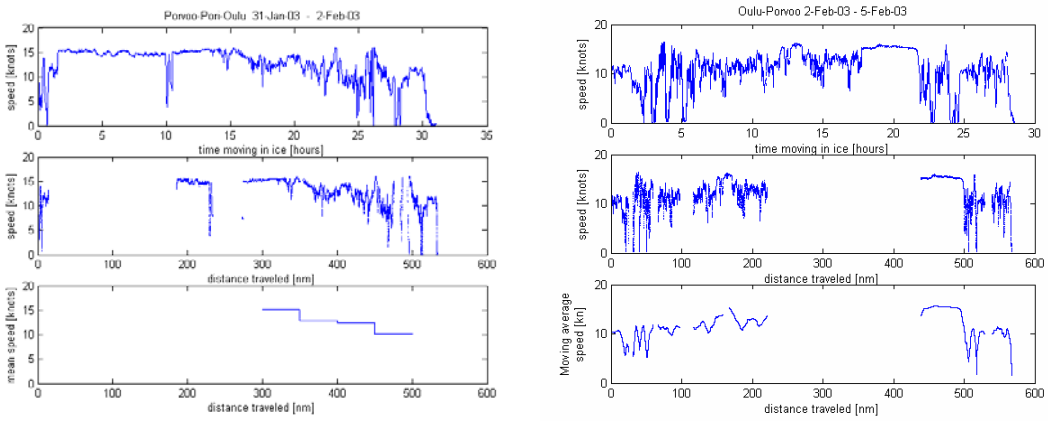

Fig. 4. The ship speed as a function of time and distance travelled and mean speed plotted as a distance travelled in cargo and ballast condition

Near the shore where the ice was thickest (over 40 cm) the speed was about 10 kn. It can be seen that speed decreased in locations where the ship entered to thicker or thinner ice. In this intermediate area the ice field was more ridged than usual. The variation of speed was greatest in areas of thick ice.

The route of MT Uikku from Oulu to Porvoo is presented in Figure 6. The ship was in ballast condition. It seems that the speed variation in thick ice is even larger in ballast than in cargo condition. In ballast condition, she needed icebreaker assistance near Oulu for 4 hours and twice near Helsinki. The ship got stuck in ice 5 times in cargo conditions and 6 times in ballast conditions.

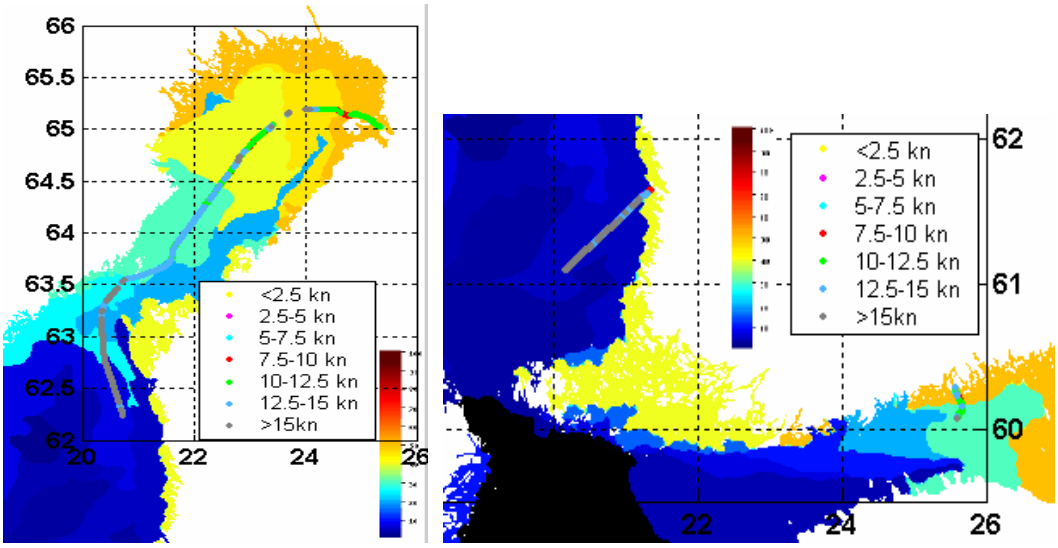

Fig. 5. Route of MT Uikku between 31-Jan-03 and 2-Feb-03 from Porvoo to Pori and Oulu plotted on ice thickness charts. The ice thickness scale is from 0 cm to 100 cm and it is shown with the colorbar

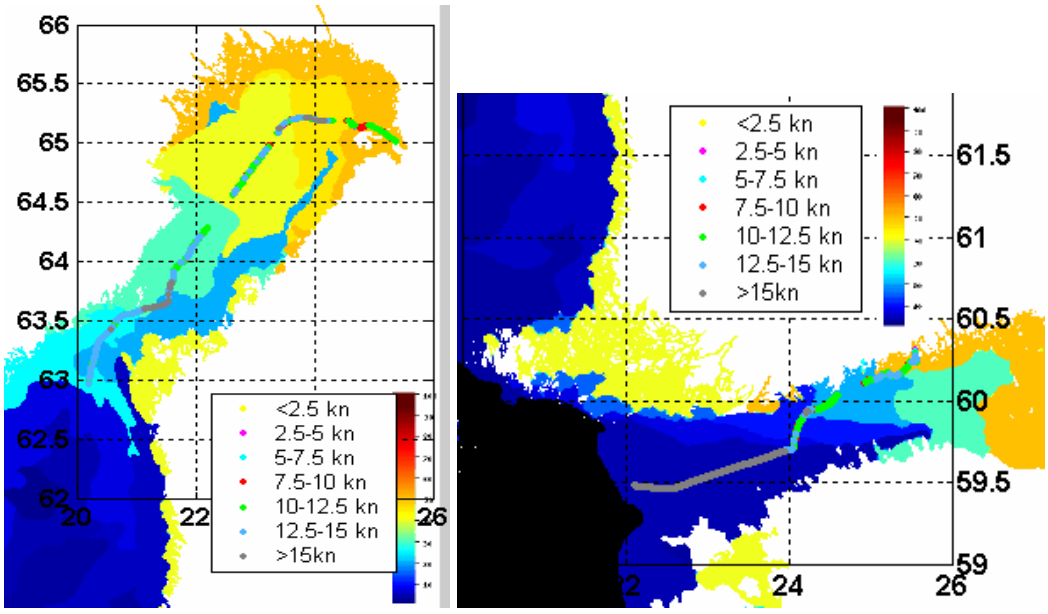

Fig. 6. Route of MT Uikku between 2-Feb-03 and 5-Feb-03 from Oulu to Porvoo plotted on ice thickness charts

The ship route and speed is plotted in the ice thickness chart of the northern part of the Bay of Bothnia in Figure 7. According to the ice thickness maps, the thickness varies between 40 cm and 60 cm. The speed varies from 5 to over 15 knots, being most of the time about 10 knots. Some portion of the GPS data is missing.

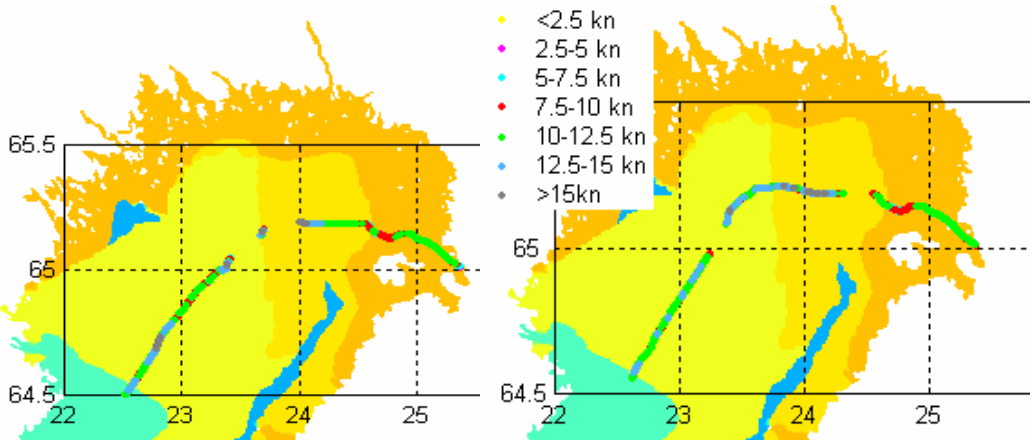

Fig. 7. Route of MT Uikku in the Bay of Bothnia in cargo (left) and in ballast (right) conditions

Speed histograms in cargo and ballast conditions are presented in Figure 8. The speed distribution has two peaks. One is near the open water speed, 16 knots, and the other is at the ice-going speed, which is typically 10 to 12 knots. Speed values near zero are mainly due to the ship being stuck in ice. In ballast condition the “ice peak” is higher and a bit more to the left than in cargo condition.

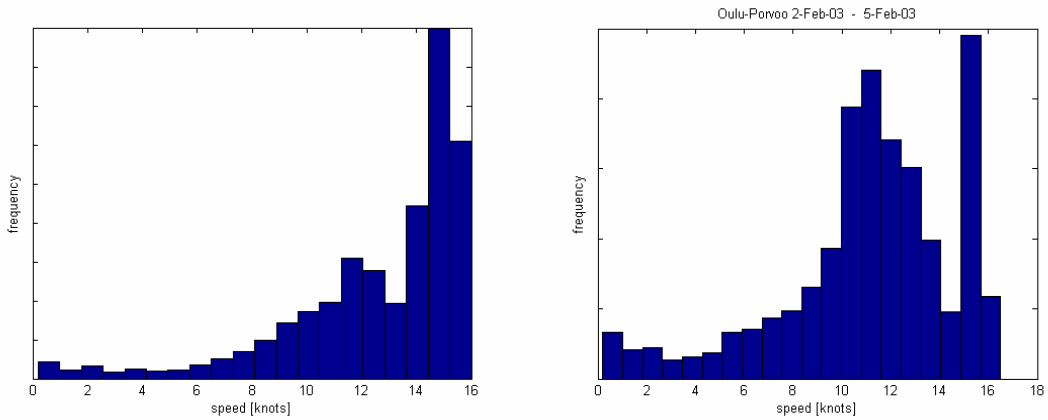

Fig. 8. Histograms of speed data in ice in cargo (left) and in ballast (right) conditions

Examples of propulsion power, torque, propeller revolution and ice loading histories are presented in Figure 9. In cargo condition the ship had to use full propulsion power, 10 MW, for 5 hours in the Bay of Bothnia. According to propeller revolution history (Fig. 9) it can be seen that MT Uikku got stuck in ice for 5 times during these 6 hours. The highest load peak in the bow frame, 900 kN/m, was observed on February 2nd at 01:10. The ship had just confronted an ice ridge that she could not get through on the first attempt. Then she backed and hit the ice ridge again with a speed of 11 kn. In that situation, the high ice load value was observed.

The ship had to use full power for 4 hours in ballast condition in the Bay of Bothnia. During that period the ship got stuck in ice 4 times. IB Urho assisted the ship all this time. The highest ice load value, 1700 kN/m, was observed quite near to Oulu in an ice channel. It might be due to contact with an ice edge at speed of 15 kn.

In the Gulf of Finland the ship had to use full power for 1.5 hours and the ship got stuck in ice twice. When she got first stuck, IB Sisu cut the ship free. The highest ice load value, 1100 kN/m, was observed when the ship was turning in easy-going floe ice.

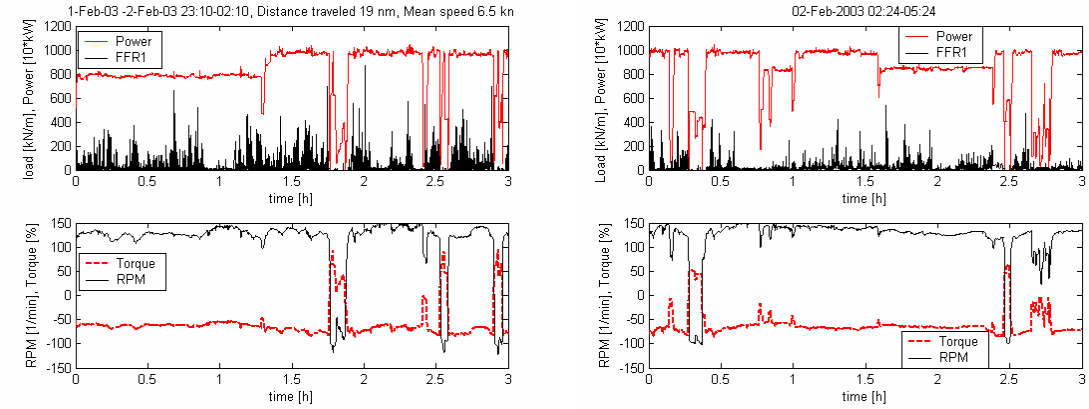

Fig. 9. Machinery data and ice induced loads during 1-2-Feb-2003 near Oulu

Voyage II (Pori-Kotka)

The voyage was done between 20-21-Feb-2003, from Pori to Kotka. The ship had a draught of 6 m in the fore ship and 7.35 m in the aft ship. Ice conditions were light from Pori to Helsinki. East of Helsinki to Kotka there was thick (50 cm) rafted ice. The air temperature was about +5°C during the day and -5°C during the night. The weather was very bright during the day, but during the night there was fog. Wind was from the NE at about 4 m/s. The route and the speed of MT Uikku from Pori to Kotka is plotted on the ice thickness map in Figure 10.

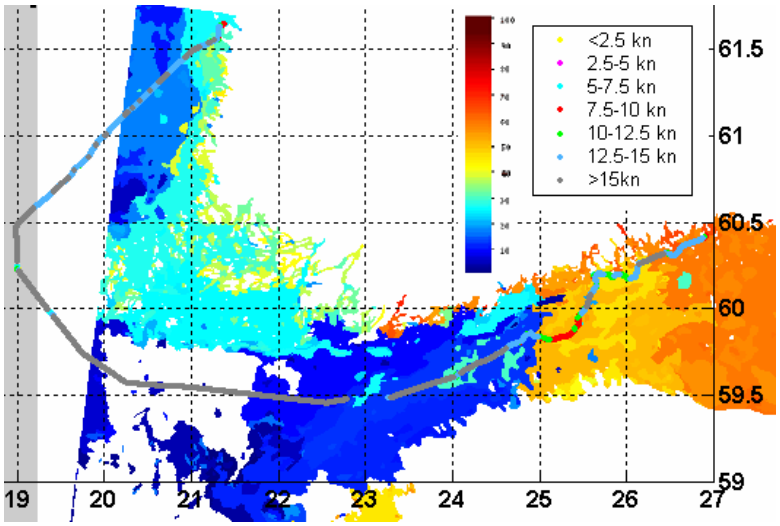

Fig. 10. Route of MT Uikku from Pori to Kotka 20-21-Feb-2003

Thicker ice (40 cm-60 cm) is found east of Helsinki. East of 25 degrees eastern longitude ship speed dropped to 7.5-10 kn. After that the ship found an old ice channel and the going was less difficult. The ship used full propulsion power only near Pori and in the Gulf of Finland for 0.5 hour. The ship got stuck in ice three times at one particular location, when she tried to break her way into an old ice channel.

Voyage III (Porvoo-Oulu-Kemi)

The voyage was done in mid April from Porvoo to Oulu and Kemi. The ship was in cargo condition. There was thick ice (over 50 cm) in the Gulf of Finland and in the Bay of Bothnia. The air temperature was about +5°C during the day and 0°C during the night. There was an easterly wind most of the time. The wind velocity was below 10 m/s. The ship had some difficulties due to difficult ice conditions in the Gulf of Finland and outside Oulu. From Oulu to Kemi the ship traveled in an old ice channel without any difficulties. The route and the speed of MT Uikku from Porvoo to Oulu and Kemi are plotted on the ice thickness map in Figure 11. In the Gulf of Finland the ship speed in ice was 12.5 kn-15 kn. In the Bay of Bothnia the ship used open water areas near Finnish coast. From Oulu to Kemi, MT Uikku moved in an old consolidated ice channel with a constant speed of 10 knots. Overall the speed varied more in areas where ice thickness changed. The total distance travelled was 700 nm, of which ice-going was about 400 nm. The voyage from Porvoo to Oulu took 48 hours and from Oulu to Kemi 5 hours.

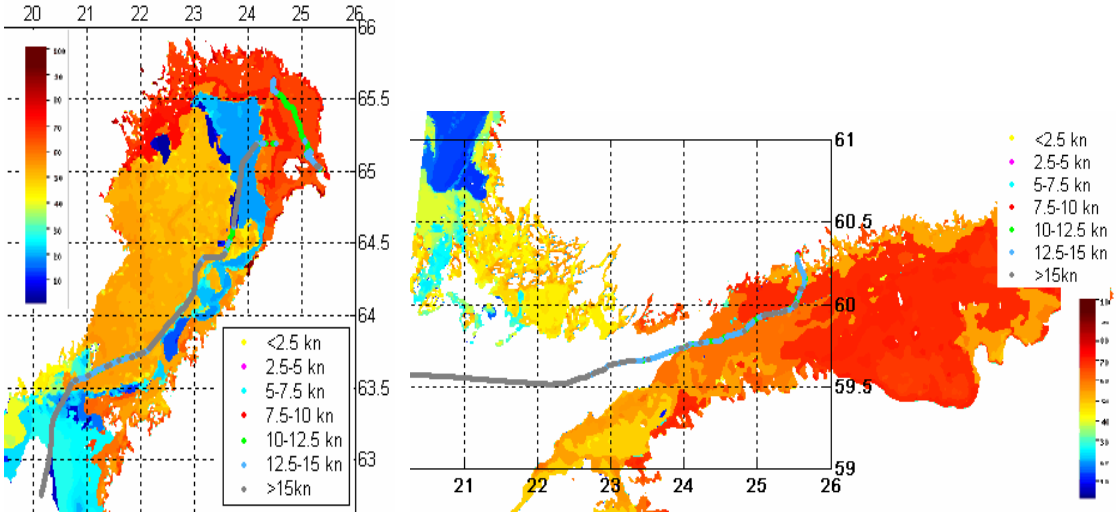

Fig. 11. Route of MT Uikku during 11-13-Apr-2003 in the Gulf of Finland and in the Bay of Bothnia plotted on the ice thickness maps

During this voyage the ship got once stuck in the Gulf of Finland. That was when she hit an ice ridge with moderately low propulsion power. In the Gulf of Finland the ship used 9 MW propulsion power for 0.5 hour. The largest ice load, 1000 kN/m, was observed in ridged ice field with propulsion power of 7 MW and speed of 13 kn. The ship used power of 9 MW for 1.5 hours and full power, 10 MW, for 2 hours in the Bay

of Bothnia. She got stuck in ice 5 times in one difficult location and she needed icebreaker assistance in order to carry on. The highest ice load, 1300 kN/m, was observed just before open water in rafted ice. The speed was 13 knots and the propulsion power was 9 MW. From Oulu to Kemi the ship traveled in old consolidated ice channel using 6 MW with a constant speed of 10 knots. One large ice load, 1200 kN/m, was observed, possible reason was contact with edge of the ice channel.

CONCLUSIONS

During the voyages ship ice-going speed was normally 12 knots and the open water speed was 16 knots. In ice-going situations the speed varied greatly and in heavy ice she had to use the full propulsion power of 10.5 MW. Normally she used power of 7 MW in ice. The ship route and speed was compared with ice thickness maps. The speed was kept at 12.5 kn-15 kn in thin ice (20 cm) and 9 kn-12.5 kn in thicker ice (40 – 60 cm). These values are above the level ice *h-v* -curves shown in Figure 3. The possible reasons are:

- In reality the ice conditions varied continuously and practically there were no level ice (as it seems based on the ice thickness maps).
- The real ice thickness may deviate from the ones shown in ice thickness maps.
- If the ship used ice channels or leads or if she had icebreaker assistance the speed was higher than it would have been in natural ice field.
- The ice concentration has a strong effect on a ship speed.

Thus, the ice thickness shown in the maps should be understood as equivalent ice thickness. If the transit speed and equivalent ice thickness are compared to the performance of MT Uikku in level ice (Fig. 3) it can be seen that the values are clearly above the *h-v* –curves. If the results are translated into equivalent transit speed in ice, the equivalent ice thickness is approximately $1.5^* h_{level\_ice}$. Ship speed varied a lot in the intermediate area between thicker and thinner ice. In those areas there was ridged and rafted ice. Usually the propulsion power was increased when the ship entered into a thicker ice field. During the voyages the ship got stuck in ice 20 times, mostly in rafted and ridged ice. Icebreaker assistance was needed 3 times, twice near Oulu in the Bay of Bothnia and once in the Gulf of Finland. During the voyages 2200 nm were travelled, of which about 1100 nm were ice navigation. For each of the voyages the plots of distance travelled in ice as a function of time are presented in Figure 12. Ice thickness maps can be of assistance in the planning of ships' routes. However, more information of varying ice conditions is needed (amount of ridged ice, ice leads etc.) for ice routing system.

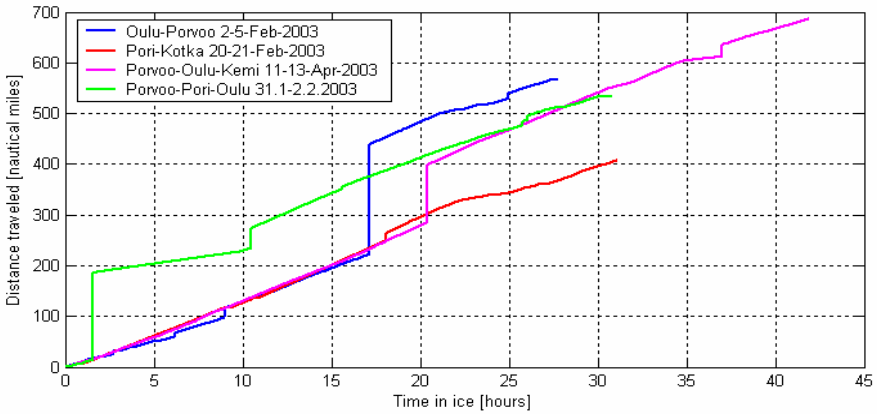

Fig. 12. The distances travelled as a function of time in ice

ACKNOWLEDGEMENTS

This work was funded by IRIS (Ice Ridging Information for Decision Making in Shipping Operations), the EESD-ESD-3 project EVK3-CT-2002-00083.

REFERENCES

Kotisalo, K. & Kujala, P. Analysis of Ice Load Measurements Onboard MT Uikku. *Helsinki University of Technology, Ship Laboratory*, Report D-50. (1999) 36 p.

Lensu, M. MT Uikku as an Ice Load Measurement Platform. *Helsinki University of Technology, Ship Laboratory*. Report M-267. Espoo. (2002) 70 p.

Lensu, M., Karttunen, J. Operative Ice Load Monitoring on Board MT Uikku in March 2001. *Helsinki University of Technology, Ship Laboratory*. Report M-264. Espoo. (2001) 47 p. + app. 10 p.

Lindqvist, G. A Straightforward Method for Calculation of Ice Resistance of Ships. *POAC'89, June 12-16,* 1989. Luleå, Sweden. (1989) pp. 722-735.

Karttunen, J. Ice Load Monitoring System for Ice Going Ship. *Helsinki University of Technology, Ship Laboratory*. Master's Thesis (in Finnish). (2001) 84 p.

Karvonen, J., Similä, M., Heiler, I. Ice Thickness Estimation Using SAR Data and Ice Thickness History. *IGARSS 2003*, 21-25 July 2003. (2003).

Vuorio, J. Ice Load Measuring Instrumentation of M/T Uikku (in Finnish). *VAL37-980525. Technical Research Centre of Finland.* (1998).

17th International Symposium on Ice
Saint Petersburg, Russia, 21 - 25 June 2004
International Association of Hydraulic Engineering and Research

ICE COVER THICKNESS DUE TO WAVE RAFTING

By Mingrui Dai[1], Hayley H. Shen[1], Mark A. Hopkins[2], and Stephen F. Ackley[1]

ABSTRACT
Vertical thin sections of cores taken from the ice cover in the Weddell Sea and the Okhotsk Sea show distinct layering structure. These observations suggest wave rafting may be important in defining the ice cover thickness in addition to the thermodynamic growth. Although wave rafting is intuitively apparent, a quantitative study of this phenomenon is absent. In this study we utilize both laboratory experiment and numerical simulations to determine the rafting thickness of a pancake ice field. We provide a theory that predicts the final rafted ice cover thickness. This thickness increases with the square of the wave amplitude and the floe diameter, but decreases with the cubic of the wavelength. We also conduct laboratory experiment with plastic model pancake ice, and numerical simulations using field scale wave conditions to study the rafting process. Both the laboratory and the computer simulation results compare favorably with the theory.

INTRODUCTION
The first stage in sea ice development is the formation of individual ice crystals in the surface layer of the ocean. These crystals, known as frazil ice, form in open water areas when the temperature of the water is below the freezing point. These crystals coagulate to form a layer known as grease ice. How the sea ice proceeds to develop depends on whether the surface is calm or disturbed. With calm conditions the frazil and grease ice may consolidate into continuous flexible sheets called nilas. Under rough conditions, with the influence of waves the frazil crystals consolidate into small circular discs called pancake ice. The pancakes have raised rims due to collisions with other pancakes. They also grow by accumulating ice crystals from the surrounding water. By bonding together the pancakes may rapidly increase to a few meters in diameter and up to 40 cm thick. As the penetrating waves gradually lose energy, the pancakes eventually freeze together to form a consolidated ice cover. The pancake ice process has been speculated as responsible for a significant portion of ice production in the Southern Ocean (Wadhams 1991, Meldrum et al, 2000).

[1] Department of Civil and Environmental Engineering, Clarkson University, Potsdam, NY 13699-5710
[2] Snow and Ice Division, USACRREL, Hanover, NH 03755

The thickness of a pancake ice cover is determined by both the initial formation process as describe above and by mechanical rafting due to the wave action. Direct field observation of the rafting process is difficult to make. The timing of cruises, to make appropriate wave and ice measurements to coincide with rapid ice cover growth and expansion (over hours to a day or two), is prohibitively challenging. Indirect observations made after the wave/ice interaction episode have revealed clear evidence of the rafting process. The ice core samples taken in the Weddell Sea (Ackley and Shen, 1996) and from the Sea of Okhotsk (Toyota 1998) show layering structures in the thin section, Fig. 1. The number of layers varied from two up to seven.

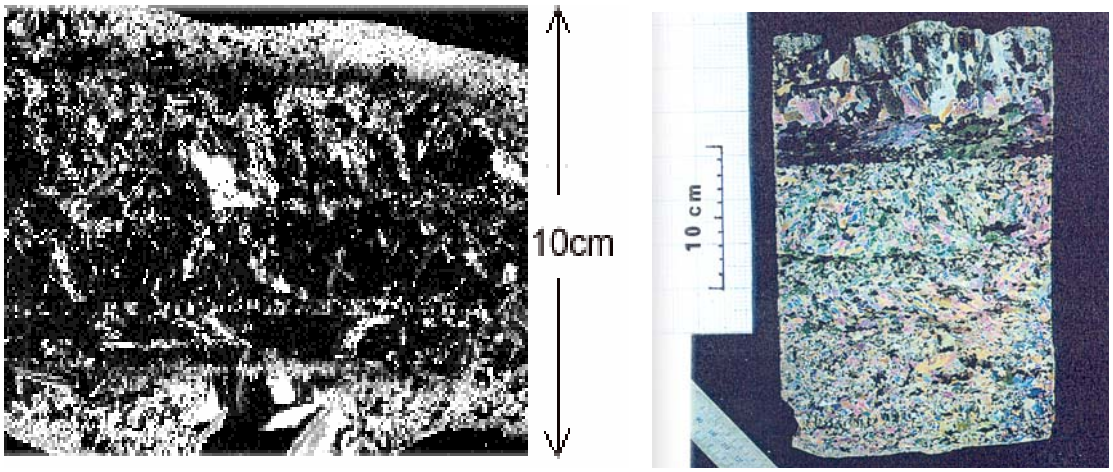

Fig. 1. Vertical thin sections of pancake ice covers. Left: From the Weddell Sea that consists of three layers of individual pancakes rafted together (Ackley and Shen, 1996).
Right: From the Sea of Okhotsk having five layers (Toyota 1998)

In the early formation season, to survive diurnal warming is critical to ice cover establishment. Several numerical studies have demonstrated amplified discrepancies between model and observed ice cover areas in the formation season (e.g. Hibler and Ackley, 1983, Geiger et al., 1997). These models showed less areal coverage than observed from satellite data. A plausible reason for this discrepancy is the redistribution of ice under wave rafting. So far, no air-ice-ocean models have included the wave effect. If waves can raft ice floes together to rapidly thicken the ice cover, this increased thickness can provide earlier ice establishment. A better understanding of the mechanical thickening due to rafting is therefore essential. This paper provides a theory with supporting laboratory and numerical simulation data for the rafting process.

A THEORY FOR RAFTING THICKNESS

We can idealize the situation of mechanical thickening of pancake ice field as shown in Fig. 2. Pancake ice floes are driven by waves toward the pack ice and pile up in front of it. The piled ice is frozen to become part of the pack ice. In studying the movement of pancake ice in a wave field from a numerical experiment, Hopkins and Shen (1999) found that the force due to ice pile up in front of a barrier approached an asymptote. This fact suggests the existence of an equilibrium thickness in front of a pack ice.

As shown in Fig. 2, wave travels in the direction from open water to the pack ice and drives the ice floes toward the pack ice. L is the length of our domain of interest, x_0 is

the position of ice edge, defined as the location where the equilibrium rafted ice meets the compacting pancakes. Since this transition is gradual, we nominally define this location as half way of the sloping profile joining the pack ice boundary and the compacting pancakes. At the open ocean boundary, there is only one layer of ice with a given areal concentration. Each ice floe under water is subject to water drag force, collision force between ice floes, buoyancy force and gravity force. These forces control the drift of pancakes. Pancake ice floes stops drifting in front of the pack ice. Thereafter, the ice areal concentration increases first. If there is no wave action, the stopped ice floes juxtapose with nearly 100% areal concentration and that is the final stage. However, if there is a wave, and if the wave amplitude is sufficient to jostling the floes out of their horizontal alignment, then rafting can occur. In this way, wave acts as the compacting agent that thickens the pancake ice cover.

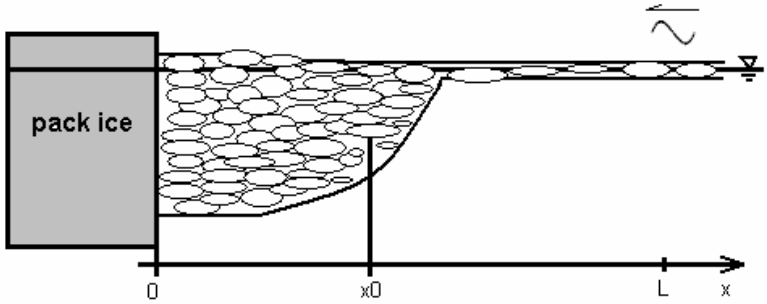

Fig. 2. Definition sketch of ice thickness distribution

Consider the floes as an assembly of granular materials. When compacting granular materials, the internal friction created by the inter-particle friction as well as the geometry of the packing resists compaction. When the stress state inside the granular assembly exceeds yield strength described by the Mohr-Coulomb criterion, the assembly fails. The failure criterion is described by

$$\sigma_x = [(1+\sin\phi)/(1-\sin\phi)]\sigma_z, \qquad (1)$$

where σ_x is the normal stress exerted by the wall, σ_z is the normal stress due to gravity, and ϕ is the internal friction angle which is a function of both the inter-particle friction and the packing geometry of the assembly (Lambe and Whitman, 1979).

In the case of pancake ice in a wave field, the active pushing comes from the wave. Because wave induces floe collisions, these collisions generate normal stresses against the granular assembly of floes. This normal stress compacts and thickens the floe assembly. On the other hand, the packing geometry and the surface friction between floes resist this compaction/thickening. An effective internal frictions angle for pancake ice piles exists. Given that a pile of floes acts the same as a soil pile, when the wave induced normal stress exceeds the Mohr-Coulomb criterion as described in Eq. (1), we must have pile thickening. At the time when the normal stress becomes lower than the strength of the pile, equilibrium thickness is reached. Fig. 3 shows a cross-section of the pancake pile.

The normal stress over the vertical cross-section in the pile up is generated totally by the collision of particles. Collision induced stresses in a granular medium has been

extensively studied in the past couple of decades (e.g. Ackerman and Shen 1982, Campbell 1990). We follow the conceptual development first introduced by Bagnold (1954). The collision force in a unit vertical area is proportional to the number of particles in this area, the collision frequency and momentum change of each particle. That is

$$\sigma_x = Nf\Delta M_x, \tag{2}$$

where σ_x is the *x*-direction normal stress, *N* is the number of ice floes in unit vertical area, ΔM_x is the momentum change of each particle due to the collision.

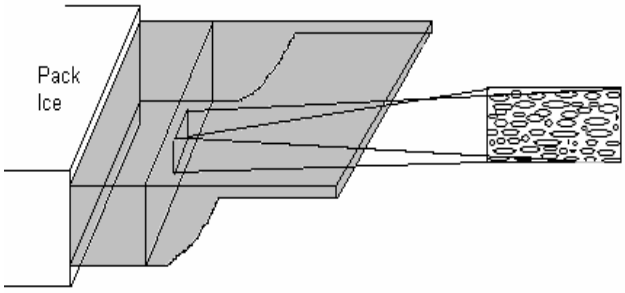

Fig. 3. A cross-section in the ice-water mix layer

The number of ice floes may be estimated as $N \propto C/Dd$, where *C* is the vertical concentration; *D* is the diameter of ice floe and *d* is the thickness of ice floe. The collision frequency *f* is estimated as the relative velocity between two floes divided by the distance between two floes. That is $f = \Delta V / \Delta x$ where *f* is collision frequency, ΔV the relative velocity between two ice floes and Δx the distance between two ice floes. The relative velocity ΔV is proportional to the gradient of the local water velocity, $\Delta V \propto \frac{\partial U}{\partial x}\Delta x$ where *U* is the velocity of water. Hence $f \propto \frac{\partial U}{\partial x} \propto \omega A e^{kz} k$ where ω is the angular frequency of wave, *A* amplitude of wave, *z* the vertical location and *k* wave number respectively.

The exchange of momentum at each collision between floes is modeled as $\Delta M_x = m\frac{\partial U}{\partial x}\Delta x \propto \rho_i D^3 d\omega A e^{kz} k$ where *m* is the mass of one ice floe, ρ_i is the density of ice. Here Δx is considered as the distance between the centers of two ice floes when collision happens. Because collisions can happen in a variety of pair configurations, this distance is not exactly but roughly in the order of *D*.

Substitute the expression of number of ice floe, collision frequency and momentum change into (2), we obtain the *x* direction normal stress as

$$\sigma_x \propto C\omega^2 A^2 k^2 \rho_i D^2 = K_c C\omega^2 A^2 e^{2kz} k^2 \rho_i D^2. \tag{3}$$

This stress compacts the pancake ice floes. When the pancake ice layer is thin, the normal stress in the *z*-direction is small, and the failure criterion described by the Mohr-Coulomb condition (1) indicates that thickening must occur.

As the ice cover rafts and thickens, the normal stress in the *z*-direction increases. Referring to Fig. 4, the normal stress in *z* direction in the layer above the water level at an arbitrary location is

$$\sigma_z = (1-n)\rho_i g(h_1 - z)\,, \tag{4}$$

where n is the porosity of ice, h_1 the thickness of the layer above the water, z the vertical coordinate with origin at calm water.

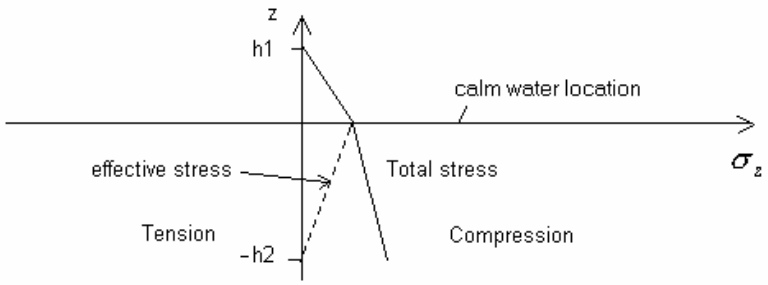

Fig. 4. The vertical stress distribution

The normal stress in the *z*-direction below the water at an arbitrary location is

$$\sigma_z = (1-n)\rho_i g(\rho_w / \rho_i - 1)(z + h_2)\,, \tag{5}$$

where ρ_w is the density of water and h_2 is the total thickness below the water.

Since the pancake ice layer is free floating, we may assume a neutrally buoyant condition. Thus h_1 and h_2 are related to the overall thickness *h* by

$$h_1 = (1 - \rho_i / \rho_w)h\,; \tag{6}$$

$$h_2 = (\rho_i / \rho_w)h\,. \tag{7}$$

The average vertical normal stress can be obtained by integrating (4) and (5) over the thickness of the ice water layer using (6) and (7),

$$\overline{\sigma}_z = \frac{1}{h}\int_{-h_2}^{h_1} \sigma_z dz = \frac{1}{h}\left(\int_0^{h_1} \sigma_z dz + \int_{-h_2}^{0} \sigma_{zx} dz\right) = Kh\,, \tag{8}$$

where $K = \frac{1}{2}(1-n)\rho_i g\left(1 - \frac{\rho_i}{\rho_w}\right)$ is a constant. As long as the rafting/thickening is underway the average normal stress in the *x*-direction is related to the *z*-direction through (1). Therefore the total normal force resisting thickening for a pancake ice cover of thickness *h* is

$$F_r = K_r h^2\,; \tag{9}$$

$$K_r = K\left(\frac{1+\sin\phi}{1-\sin\phi}\right) = \frac{1}{2}\left(\frac{1+\sin\phi}{1-\sin\phi}\right)(1-n)\rho_i g\left(1 - \frac{\rho_i}{\rho_w}\right). \tag{10}$$

As the thickening progresses, the resistance force increases and eventually when the resisting force equals to the compacting force given in (3), equilibrium thickness is reached.

Integrating (3) in the range of ice thickness, assuming wave is simple wave, gives

$$F = \frac{K_c C g A^2 k^2 \rho_i D^2}{2}(1 - e^{-2kz}). \tag{11}$$

Expanding e^{-2kz} and neglecting 2nd and higher order terms, we have

$$F = \frac{K_c C g A^2 k^2 \rho_i D^2}{2}(1 - (1 - 2kh)) = K_c C g A^2 k^3 \rho_i D^2 h. \tag{12}$$

Equating (3) with (12) we have

$$h = \frac{K_C}{K_r} C \omega^2 A^2 k^2 \rho_i D^2. \tag{13}$$

Because we consider rafting after the maximum areal concentration, hence C is 1. Eq. (13) provides a way to estimate the equilibrium pancake ice cover thickness under wave rafting. For generality, Eq. (13) can be non-dimensionalized. Assuming a monochromatic deep water wave, from the dispersion relation, Eq. (13) can be rewritten as

$$h = \frac{K_c}{K_r} g A^2 k^3 \rho_i D^2. \tag{14}$$

We define $S = Ak$ as dimensionless wave steepness, $D' = kD$ dimensionless ice floe diameter, $K_r' = \frac{1}{2}\left(\frac{1+\sin\phi}{1-\sin\phi}\right)(1-n)\left(1-\frac{\rho_i}{\rho_w}\right)$ dimensionless friction coefficient and $h' = hk$ dimensionless thickness. Eq. (14) can be expressed in terms of these dimensionless variables as follows,

$$h' = \frac{K_c S^2 D'^2}{K_r'}. \tag{15}$$

VERIFICATION

A series of experiments were carried out in a wave tank at Clarkson University Civil and Environmental Engineering Department, as shown in Fig. 5. In addition to the laboratory experiment a three dimensional discrete elements model (Hopkins and Tuhkuri, 1999; Hopkins and Shen, 1998) is used to carry out a series of numerical experiments. This model explicitly simulates the behavior of each ice floe. We tested both frictionless and friction floes in this numerical experiment.

Results of the comparison between the dimensionless theory and the experimental data, both physical and numerical, are given below. Take logarithm on both sides of Eq. (15) and we obtain Eq. (19).

$$\log(h') = \log(\frac{K_c}{K_r'}) + 2 * \log(S * D'). \tag{19}$$

Fig. 5 The Clarkson wave tank

We applied linear regression analysis on observed $\log(h')$ and $\log(S * D')$, and present the physical experiment results in Fig. 6, and numerical experiment results in Fig. 7.

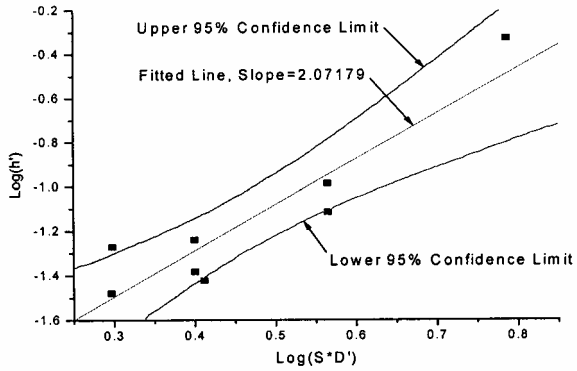

Fig. 6. Relationship between dimensionless ice thickness h' and the product of dimensionless wave steepness and floe diameter $S * D'$ for physical experiments

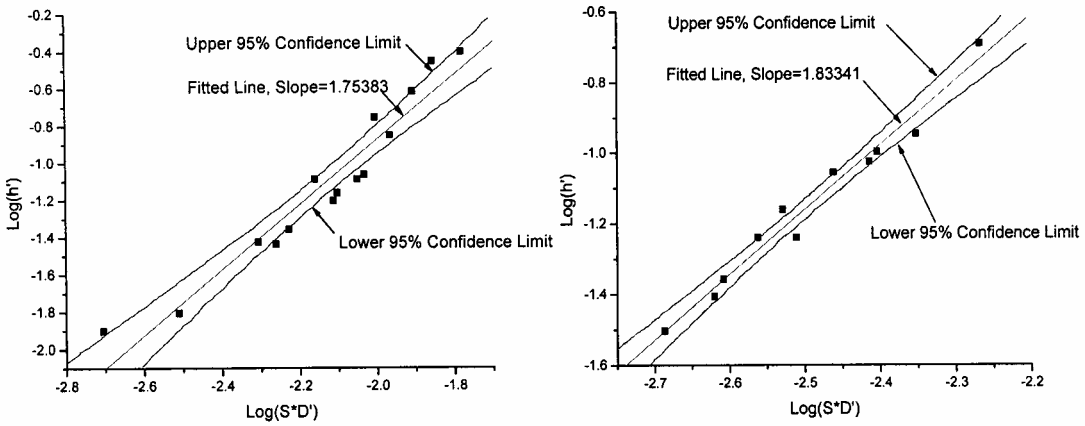

Fig. 7. Relationship between dimensionless ice thickness h' and the product of dimensionlessl wave steepness and floe diameter $S * D'$. The left is for frictionless floes and the right is from floes with a friction coefficient of 0.35

DISCUSSIONS AND CONCLUSIONS

All experiments, physical and numerical, show favorable comparison between the observed data and the theoretical prediction. This study shows that rafting can be quantitatively related to wave characteristics. Since ice thickness may affect early development of the ice cover, it is necessary to include this mechanism in future modeling effort. For an air-ice-ocean coupled modeling, ice edge dynamics may be modified in such a way that total ice volume is determined by existing frazil ice production model, but the thickness may be parameterized using the wave rafting results, and the areal coverage is calculated as the volume divided by the thickness. It would be very interesting to test this new ice edge model to see if the discrepancies mentioned in the introduction are removed.

ACKNOWLEDGEMENTS

This research was funded by the National Science Foundation under grants OPP-9814968.

REFERENCES

Ackermann, N. L. and H. H. Shen (1982) J. Eng. Mech., 108(EM1):95-113.

Ackley, S.F. and H. H. Shen, (1996) Pancake ice formation in a laboratory wave tank. Western Pacific Geophysics Meeting, Brisbane, Australia, Trans. Sup. AGU, 77(22):54.

Campbell, C.S. (1990). Rapid granular flows. *Ann. Rev. Fluid Mech*. 22:57-92.

Geiger, C.A., S.F. Ackley, and W.D. Hilber III (1997) Year-round pack ice in the Weddell Sea, Antarctica: response and sensitivity to atmospheric and oceanic forcing. Ann. Glacio. 25, 269-275.

Hibler, W.D. and S.F. Ackley (1983) Numerical Simulation of Weddell Sea pack ice, *J. of Geophys. Res.*, 33:2873-2887.

Hopkins, M. A. and H. H. Shen (1998). Simulation of pancake ice in a wave field, *Proc. 12th Eng. Mech. Conf/ASCE*, La Jolla, May 17-20

Hopkins, M. A., and J. Tuhkuri (1999) Compression of floating ice fields, *J. Geophysical Research*, 104, (C7), 15815-15825.

Lambe, T. W. and R. V. Whitman (1979) Soil Mechanics, SI Version, John Wiley & Sons, 97-116

Meldrum, D, Doble, M, Mercer, D, Peppe, O, Wadhams, P and Wilkinson, J, (2000) A Study of the Winter Antarctic Marginal Ice Zone using an Innovative Ice Drifter. In: *Proceedings of Oceanology International 2000*, Brighton, 73-85. Spearhead Exhibitions Ltd, Kingston upon Thames.

Toyota, T., A study on growth processes of sea ice in the southern region of the Okhotsk Sea, evaluated from heat budget and sea ice sample analysis, *Ph.D. Dissertation*, Hokkaido University, 1998.

Wadhams, P. (1991) Atmosphere-ice-ocean interactions in the Antarctic. In *Antarctica and Global Climatic Change* (ed. C Harris, B Stonehouse) Belhaven, London, 65-81.

17th International Symposium on Ice
Saint Petersburg, Russia, 21 - 25 June 2004
International Association of Hydraulic Engineering and Research

A LABORATORY STUDY OF WAVE ATTENUATION IN A PANCAKE ICE FIELD

By Ose Negbenebor[1], Hayley H. Shen[1], and Stephen F. Ackley[1]

ABSTRACT

The formation of pancake ice has been attributed to wave action. It is well known that ice cover can attenuate wave energy. This attenuation self-regulates the extent with which wave can maintain the pancake ice field. When wave amplitude drops below some critical value, pancakes will start to freeze together to form a continuous solid cover. This solid cover eventually becomes the final seasonal ice. In this paper we report a laboratory study conducted at USACRREL. Pancake ice was grown in a wave tank in a cold room. The evolution of the diameter and ice thickness, and the attenuation of the wave from open water through the ice cover are reported. The attenuation obeys an exponential decay. The decay coefficient is related to the wave and the ice conditions. The sharpest increase of the decay coefficient is correlated with the most rapid growth in pancake ice diameter.

INTRODUCTION

Attenuation of waves when they propagate through an ice field has been reported by seaman for centuries. Systematic field observations are scarce (e.g. Martin and Kauffman, 1981, Squire 1984, Wadhams et al. 1988). Due to the logistic challenges in measuring wave attenuation in the field, laboratory study provides an effective alternative. This approach was adopted by Newyear and Martin (1997). Due to the short length of the wave tank (~4m), they were only able to study the wave attenuation in a frazil/grease ice cover. Full formation of pancake ice was limited by the size of the wave tank. The present report describes a study using a much longer wave tank that allows for direct measurement of wave attenuation as it propagates into a pancake ice field.

1 Department of Civil and Environmental Engineering, Clarkson University, Potsdam, NY 13699-5710. Email: hhshen@clarkson.edu

From May 5th to May 9th, a series of experiments were performed at USACRREL, Hanover, NH, to investigate the pancake ice formation process for various wave field conditions. We will present the May 8th results as an example of the phenomena observed. The experiment was conducted in an indoor wave tank (36.6m long and 1.22m wide) made of glass and metal frames. The water depth was 51cm doped with 1% by weight urea as oppose to salt in order to prevent corrosion. Sixteen pressure transducers were installed to measure the wave conditions along the tank. Fig. 1 is the layout of the experiment. The pressure transducers were installed in groups of 4 with 20cm spacing between each transducer at four locations. The wave data were taken at 1min intervals at a rate of 10Hz for 1000 points. Above each group of pressure transducers, a digital surveillance camera was installed to monitor the ice cover growth.

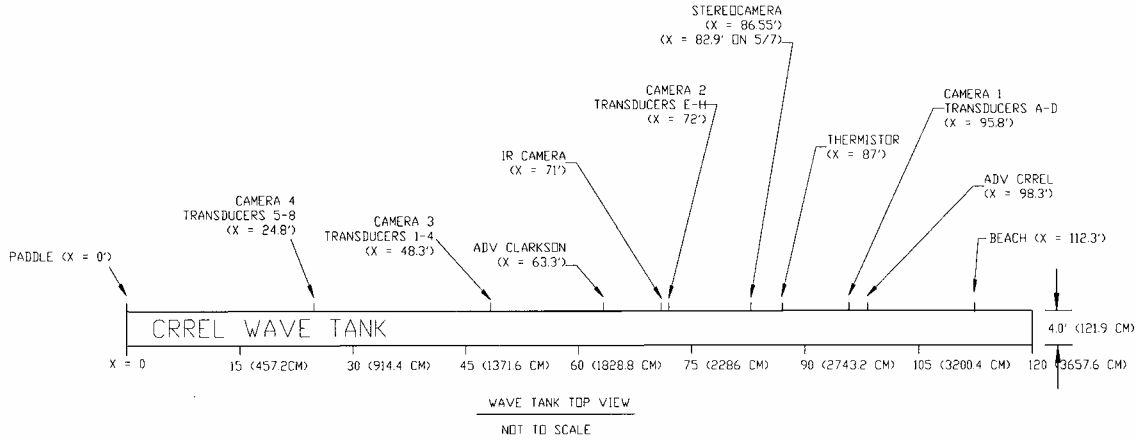

Fig. 1. Experimental Layout

EXPERIMENTAL DATA

All of the data reported here are from the May 8th experiment. Fig. 2 shows the air and water temperature near the paddle (label 1) and near the beach (label 2). The procedure for obtaining the wave characteristics from the pressure transducers is similar to that reported in Ackley et al. (2002) and detailed in Shen et al. (2003).

As shown in Fig. 2, near constant temperature (~-15^{o}C) was maintained after a couple of hours of cooling in the beginning of the day. The water temperature after the termination of the experiment was due to warm water injection into the tank for ice removal.

Throughout the day, ice observations were made to determine both pancake ice diameter and the ice cover thickness development. The following figures show the ice thickness evolution obtained at locations of Cameras 1 – 4. The diameter of the pancakes was obtained from putting a ruler over the ice cover. Three readings were obtained at each location. The average is reported here.

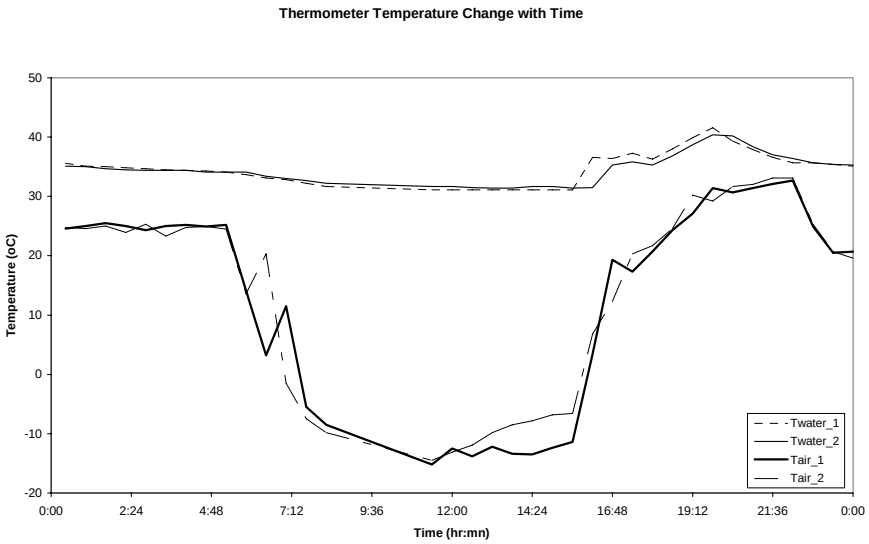

Fig. 2. The air and water temperature during the test

The ice cover thickness was measured by carefully lowering a wire scoop to the bottom of the ice cover and lifting the pancake as well as the slush ice under it. After draining the water away, the thickness was measured by a ruler. The pancake ice diameter evolution throughout the day is presented in Fig. 3. The ice thickness evolution is presented in Fig. 4.

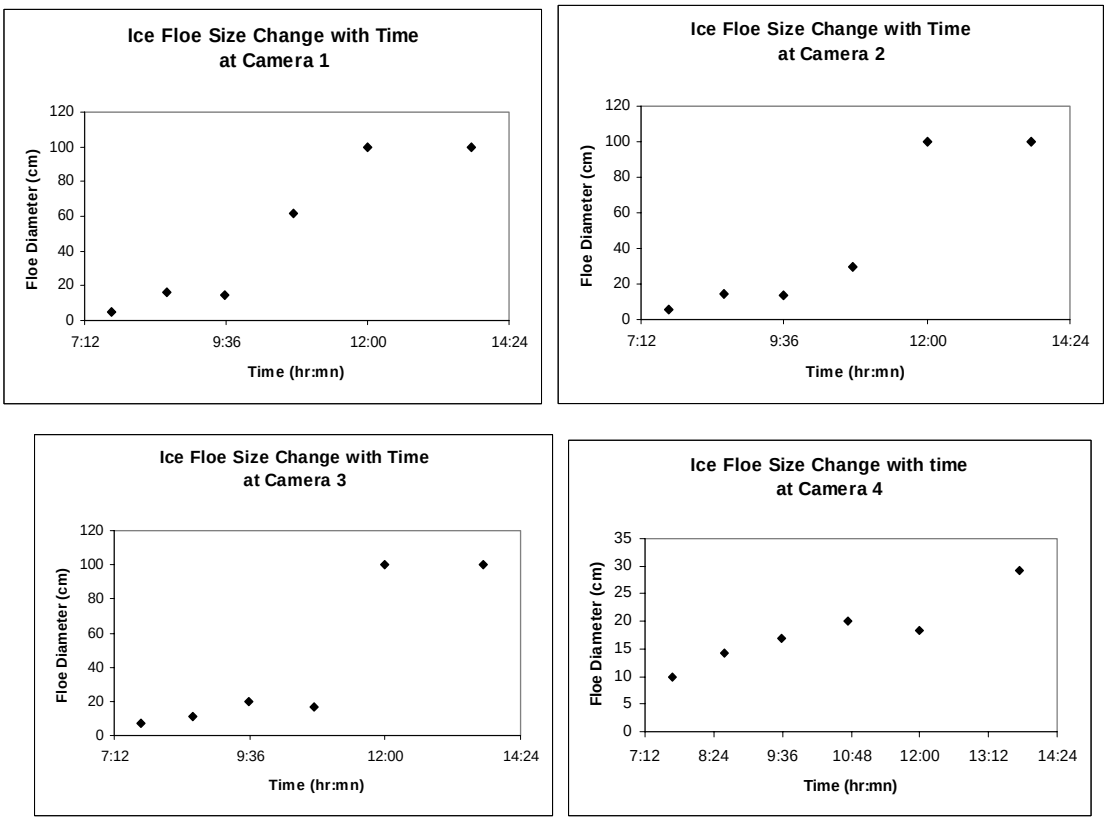

Fig. 3. Evolution of pancake diameter at the four locations. Camera 4 is closest to the wave paddle

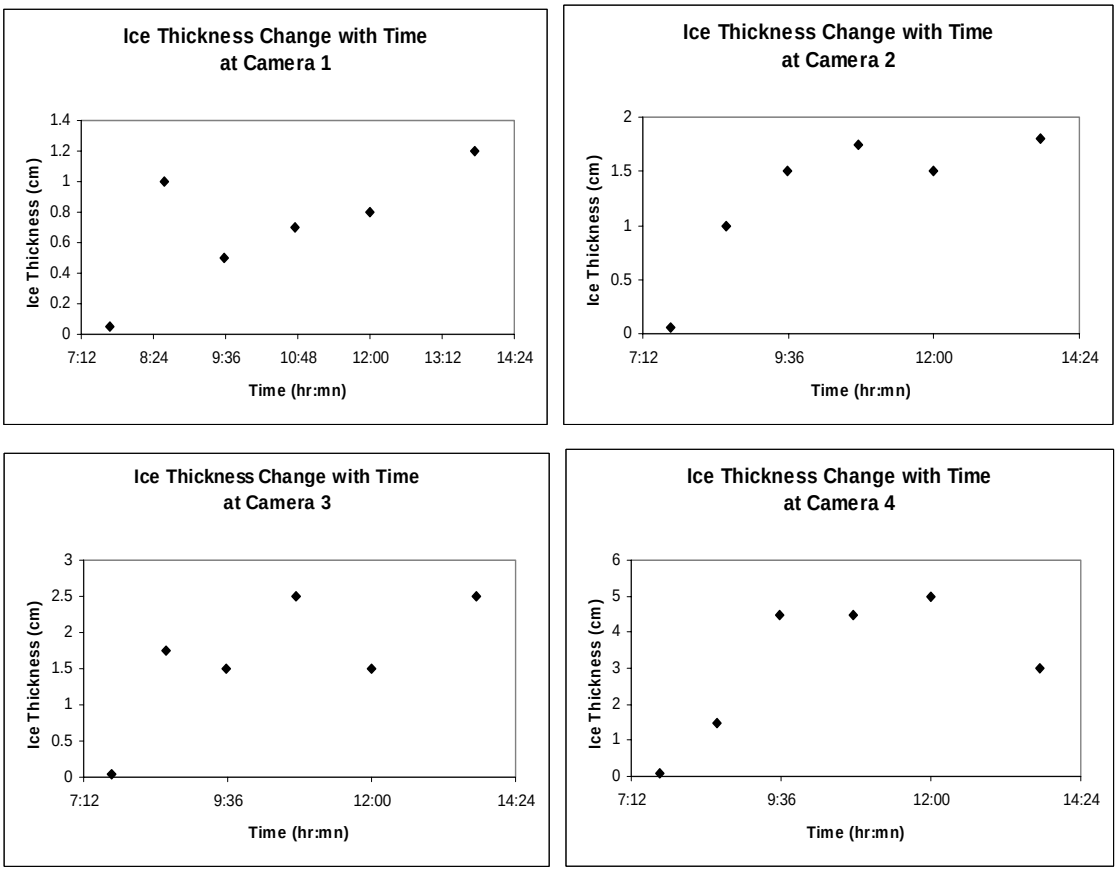

Fig. 4. Evolution of ice cover thickness at the four locations. Camera 4 is closest to the wave paddle

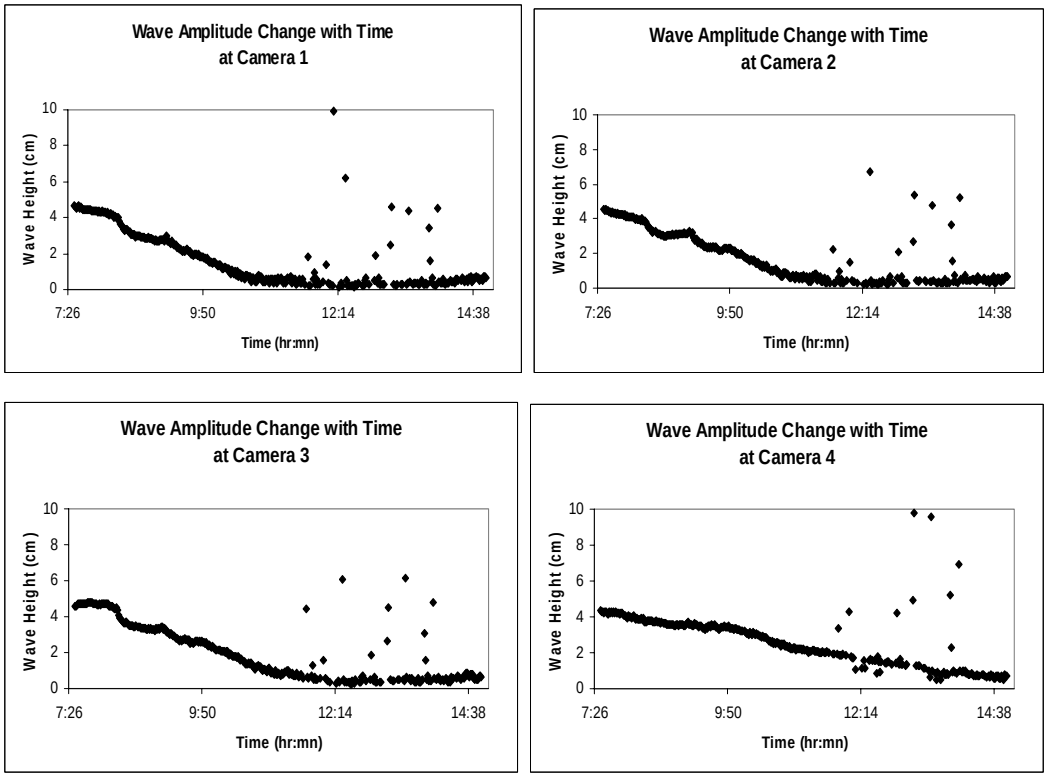

Fig. 5. Evolution of wave amplitude at the four locations. Camera 4 is closest to the wave paddle

The wave attenuates with respect to both time and space. In Fig. 5 we show the wave decay with respect to time at the four camera locations. The wave amplitude shows occasional spuriously high values. This is due to the electronic noise in the environment.

DISCUSSIONS

From Figs. 3 – 5, we observe several things as will be discussed below. Both the pancake diameter and ice cover thickness increase with time, as expected. The pancake diameter growth may be categorized into three periods: mild, rapid, plateau. In the mild growth period, the diameter increased slowly. It is followed by a rapid increase over a short time. This rapid growth then approaches a constant final value even the ice thickness may still increase. This phenomenon is observed at all locations except at camera 4 that is closest to the wave paddle. We believe at this location the pancake ice has not reaches its maturity. The ice cover thickness fluctuates at each location. But the general trend is an increase with time, except at camera 4. Where again, due to its proximity with the wave paddle, the integrity of the ice cover is more difficult to establish. Local rafting can redistribute the ice mass near the edge. The final drop of ice thickness as observed at camera 4 is not due to melting, but due to advection loss. The wave amplitude can also be categorized into three periods: relatively flat, declining, constant final floor. The rapid growth of pancake diameter closely corresponds to the time wave amplitude drops to the floor value. The time at which the wave amplitude reaches its final floor value depends on the location. The farther the location is from the paddle, the sooner this final value is reached. Concomitantly, the sooner the pancake reaches its final diameter.

To study the attenuation of the wave as it travels into the ice cover, we use the exponential decay model as suggested in Wadhams (1973): $A = A_0 e^{-\alpha(x-x_0)}$. To determine the attenuation coefficient α , the wave amplitude data at each location was plotted, using an exponential curve fit, the coefficient α may be obtained. This attenuation coefficient is a function of time as given in Fig. 6 together with the ice properties. The most interesting observation from this result is that the attenuation peaks at the time when the pancake ice diameter increases most rapidly. In addition, it is also seen that as the pancake diameter stabilizes and the ice thickness reaches its final value, the wave attenuation also stops increasing. The value of the attenuation for this wave (0.51Hz) is much higher than field values (~10^{-4} per meter). Comparing with the laboratory results of Newyear and Martin (1997), these attenuation coefficients are lower than theirs (~0.1 per meter). The field waves are in the order of 0.1Hz, much lower than the laboratory case. In the case of Newyear and Martin, their wave frequencies were around 1.5Hz with ice cover at least twice the value of the present study. Wave attenuation is strongly dependent on the wave frequency and ice cover thickness, with higher frequencies decaying more rapidly and enhanced by increasing ice thickness, as observed in this case.

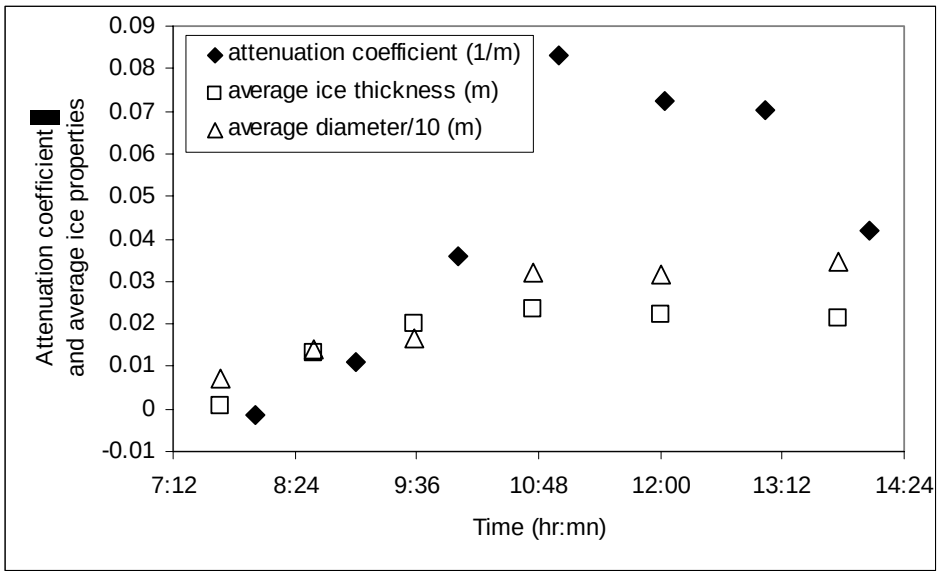

Fig. 6. The evolution of wave attenuation and ice cover properties. The pancake diameter is divided by 10 to fit into the same scale in the figure

CONCLUSIONS

This paper summarizes the data obtained in a laboratory study of wave and pancake ice interaction in the growth period. We investigate the entire initial period of ice cover growth from open water condition until mature pancakes are formed, where the diameter of pancake reaches a plateau value. The pancake diameter, ice thickness, and wave amplitude evolutions are monitored continuously. We find that the attenuation peaks when the pancake diameter grows most rapidly. The attenuation is much higher than the field values, due to the higher frequency wave used in the laboratory. Comparisons between the current findings with existing theory and data from other experiments are underway. The long term goal of such studies is to establish a data base for theoretical development. Wave attenuation is closely linked with ice edge establishment. At present there are only two types of theories exist for wave attenuation. One is based on viscous properties of the ice cover (Keller 1998) and the other on pancake ice collisions (Shen and Squire 1998). Experiments such as presented here and reported in previous studies will eventually lead to a quantitative theory for ice edge modeling.

ACKNOWLEDGEMENTS

This study is supported by a grant from the National Science Foundation Grant #OPP-9814968. We would like to thank the following CRREL staff for their generous assistance before, during, and after our experiment: Leonard Zabilansky was the coordinator, John Gagnon provided everyday technical assistance, Bruce Elder helped installing thermistors and the associated data acquisition, Keran Claffey processed all ice crystal samples.

REFERENCES

Ackley, S.F., H.H. Shen, M. Dai, and Y. Yuan (2002) Wave-Ice Interaction During Ice Growth: The Formation of Pancake Ice, *Proceedings of the 16th IAHR Ice Symposium*, Dunedin, New Zealand, Dec. 12-16, 2002, 158-164.

Keller, J.B. (1998) Gravity waves on ice-covered water, *J. Geophys*. Res. 103(C4):7663-7669.

Martin, S. and P. Kauffman (1981) A field and laboratory study of wave damping by grease ice, *J. Glaciol.*, 27:283-313.

Newyear, K., and S. Martin (1997) A comparison of theory and laboratory measurements of wave propagation and attenuation in grease ice, *J. Geophys. Res.* 102:25091-25099.

Shen, H.H. and Squire, V.A. (1998) Wave Damping in Compact Pancake Ice Fields Due to Interactions Between Pancakes, AGU Antarctic Research Series 74, Antarctic Sea Ice: Physical Processes, Interactions and Variability, (Ed. Dr. Martin O. Jeffries): 325-342.

Shen, H.H., S.F. Ackley, O. Negbenebor, K. Fellows (2003) Data from Pancake Ice Growth at CRREL May 5-9, 2003, *Dept. Civil and Environmental Engineering Report*. № 03-11.

Squire, V.A. (1984) A theoretical, laboratory, and field study of ice-coupled waves, *J. Geophys. Res*., 89(C5):8069-8079.

Wadhams, P. (1973) Attenuation of swell by sea ice, *J. Geophys. Res*., 78(18):3552-3563.

Wadhams, P., V.A. Squire, D.J. Goodman, A.M. Cowan and S.C. Moore (1988) The attenuation rates of ocean waves in the marginal ice zone, *J. Geophys. Res.*, 93(C6):6799-6818.

17th International Symposium on Ice
Saint Petersburg, Russia, 21 - 25 June 2004
International Association of Hydraulic Engineering and Research

WEAKENED ICE COVER ON RESERVOIRS, INFORMATION THROUGH THE INTERNET VIA NVE-ATLAS

Randi Pytte Asvall[1]

ABSTRACT
In Norway there are more than 900 water reservoirs for water power production, with all but a very few exceptions established by damming of natural lakes, which normally have an ice-cover in the winter season. Although the use of the ice cover for transport has changed somewhat, "safe" ice is still important for providing safe travelling routes for domestic and leisure traffic. The water power development has often influenced the ice conditions in a way so that the ice on new areas are no longer safe for travel. Such weakened areas are being digitalized and are now made available on internet in a map-system termed "NVE-Atlas".

INTRODUCTION
Ice on lakes and rivers is a part of nature in most parts of Norway. Historically ice covered lakes provided easy and safe travelling routes for goods and personal transport. When regulation of the water courses for power production was introduced, it was soon realized that the ice conditions were influenced. In many areas one could no longer depend on traditionally safe winter roads, nor ice for personal traffic. It is therefore required that the power companies mark areas with weakened ice and give sufficient warning to the public. In some cases subsidiary roads and new bridges have been required built.
Many power reservoirs are located close to inhabited areas, and thus the ice is important for the local environment. Both the local and more remote areas are being used for leisure and tourist traffic, mainly snow scooters skiers and fishermen.

ICE CONDITIONS ON LAKES
Due to the density changes of water versus temperature there is a thermal equilibrium in the lakes at a water temperature of 4 ^{o}C. The time required to reach the fall equilibrium and the development of ice cover vary with the weather conditions, hydrology and bathymetry of the lakes. In Norway most lakes have a seasonal ice cover. A few large and deep lakes in the lower elevations do not have a complete ice cover every year. The winter water-temperature varies between 1 and 3 ^{o}C in the deeper layers. The ice thickness and quality will vary depending on the winter weather.

[1] Norwegian Water and Energy Directorate, P.O. Box 5091 Maj, N-0301 Oslo, Norway

ICE CONDITIONS ON RESERVOIRS

The ice conditions will undergo some changes when the lake is transformed to a reservoir. By transforming a lake to a reservoir there are hydrological changes related to water level and depth, water area, through-flow, locations and water temperature of natural and man-made inlets and outlets .These changes will influence the ice conditions, and the reservoirs may be influenced by one or several of the points listed above.

Many reservoirs may experience minor changes in ice conditions over large areas in the main winter season, or even all winter season, while other reservoirs may have severe reductions in ice quality.

CHANGES IN WATER LEVEL

The changes in water level is set by the highest regulated water level (HRW) and lowest regulated water level (LRW) given in the permission for regulation. The reservoirs will generally have a high water level in fall. With a large increase in water level the cooling of the water mass will be delayed, and thus the time required establishing ice cover.

Normally water is withdrawn from the reservoir throughout the winter, and the reduction in water level will cause crevasses to develop along the shoreline. The shape and width of the crevasses depend on the slope and roughness of the regulated zone. On areas with a gentle slope and bottom the ice may fall to rest on the ground without any serious crevassing. On steep and rough ground the crevassed area may instead be almost impossible to traverse. Often the crevasses are covered with snow – or snow bridges, that might or might not be strong enough to pass - and thus represent a very dangerous area if the travellers are not aware of the problem. As the water level decreases shallow areas will appear as ice bumps covered with crevassed ice.

Along the shoreline there will generally be increased possibility for water seeping up on the ice through the crevasses. When there is variations (ups and downs) in water level the area covered with surface water on the ice will increase, and there may also be open water along the shoreline. Such variations in water level are mostly caused by the peaking of power plants in the system.

INCREASED FLOW THROUGH THE LAKE/RESERVOIR

In natural lakes there is increased water velocity through narrow sounds and other areas where there will be a mixing of warmer deepwater with water of 0^{o}C close to the ice cover. This delays the ice formation, and even on natural lakes there might be open areas or reduced ice thickness all winter. Increased flow will exaggerate this and make these areas larger. Deep reservoirs will be less influenced than more shallow reservoirs. As the water level decreases new sounds may appear where the ice is weakened. This depends on the bathymetry and the discharge through the reservoir.

NATURAL INLETS AND OUTLETS

In natural outlets and inlets there might be decreased or increased discharge. The inlet and outlet area with open water and weakened ice will be smaller with decreased discharge, and larger with increased discharge. Increased winter discharge is caused by regulation upstream. When tapped from deeper layers in the reservoir upstream the water may be “warm” ($0.2 – 3\ ^{o}$C), and thus create a larger open area.

TUNNELS

Tunnels are common water ways in a power production scheme in Norway. Outlets and intakes of tunnels may be compared to natural inlet- and outlet areas, with mixing and

up welling of warmer deepwater, specially if the tunnel discharges near the surface. A submerged tunnel will also cause some mixing of the water mass, but will have less influence on the ice conditions, at least at high water stage. As the water level drops the tunnel might no longer be sufficiently submerged to avoid a weakening of the ice. Tunnel inlets and outlets are especially dangerous areas as the locations of weakened ice can not be identified by terrain details.

IMPORTANCE OF RECOGNITION OF WEAKENED ICE ON RESERVOIRS

When the ice has a sufficient strength, ice cover on lakes represents safe and easy winter roads. Even though more and more traffic now is routed on land, there are still advantages in many areas to use the ice as winter-roads. The use of ice for leisure use has been more and more popular, both by local people and tourists.

In Norway the power plant industry is the main man made source for a weakening of ice cover in the water courses. As this was recognized already at the start of the power plant exploitation in our country, it was determined that ice investigations were performed along with the planning. Even more important, in this context, is that among the claims following the permission for power plant building is a claim to give sufficient warning in the field where the ice is weakened.

There are directions which are recently revised, given in collaboration by the national water and energy authority (NVE) the power company association (EBL), on how the marking and warning of weakened ice should be done. This is in short a combination of signing, fencing, roping-off selected areas, and general information.

INTERNET PRESENTATION OF ICE WEAKENED BY POWER PRODUCTION

In Norway there are ca 900 reservoirs and lakes where the ice is influenced by water power regulation. As it is required to indicate areas where the ice cover has been weakened by the power development, the majority of the power plant owners also have maps showing these areas available to the public.

In some regions there are several power plants with drainage areas and thus reservoirs fairly close to each other, and it is necessary to have information from several power plants to cover a limited geographical region. To make such information more accessible weakened ice will be included as a theme on “NVE-Atlas”.

NVE-Atlas is a geographical tool for showing various water themes on digital maps oninternet. Among the themes already included are reservoirs, tunnels, dams and power stations. These themes form the background for the theme on weakened ice on reservoirs that is now being prepared. This work is a joint venture of all the power plant owners and NVE. The local power plant producers are giving information on areas of weakened ice. The data are controlled and digitized and included as a theme in the “NVE-Atlas”.

Entrance to the program on the internet is a zoom able map of Norway. By identifying an area by the cursor this will be shown on the screen. In the basic introductory map lakes have a light blue colour and the reservoirs are darker blue. When reaching a certain scale dams, power plants and tunnels show up. Areas of weakened ice due to power production is indicated as a red marking .When the reservoirs are reviewed they will be marked with a very dark blue contour along the water level appearing on the map.

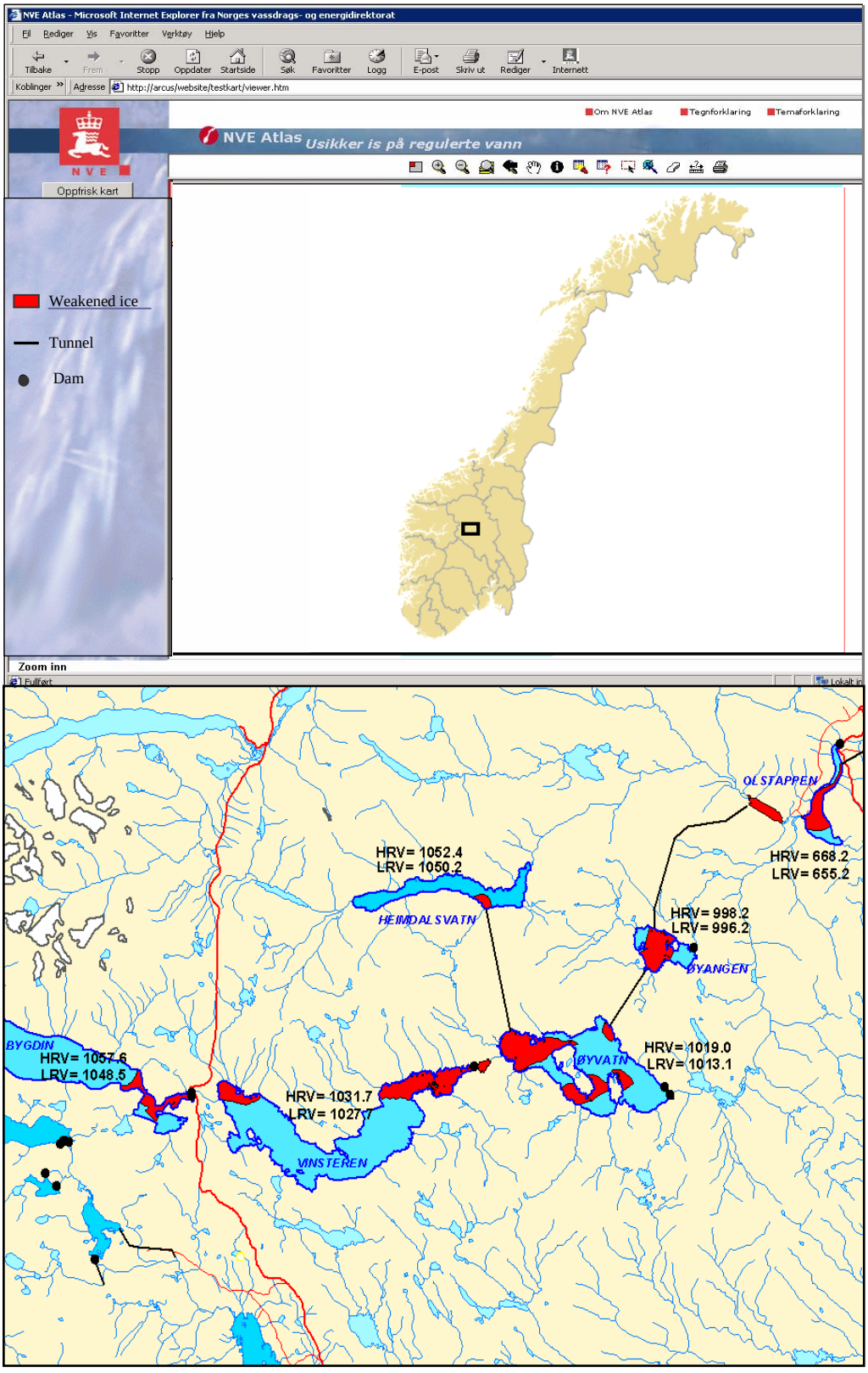

Fig 1. Example of ”weakened ice” in ”NVE Atlas”

This indicates the possibility of crevassed ice along the reservoir edge. Names of reservoirs and regulation limits are given on the map. Contour lines may be added. Lakes with no regulation that are influenced by water power exploitation are also included. We are still in the process of producing these maps, and an example is shown on fig 1. It will be accessible on internet www.nve.no.

It is very important to emphasize that these maps are presenting the areas where the ice is weakened by power plant regulations. The general ice conditions will vary from winter to winter and throughout the winter. Information of the actual ice conditions are given separately.

17th International Symposium on Ice
Saint Petersburg, Russia, 21 - 25 June 2004
International Association of Hydraulic Engineering and Research

MORHOLOGY OF RIVER AND LAKE ICE

Anatoliy Levashov[1] , Irina Levashova[1]

ABSTRACT
Analyze of long nature observes results for river and lake ice, as well as experimental research of reflex in water flows permits to decipher track "written" flow in ice, and to apprise influence of ice on carrying capacity of bed.

INTRODUCTION

Rivers of Russia and some other countries flow in winter conditions, so one of the most important problems for our national economy is our knowledge of water flows structure, ice waves parameters and other factors of ice cover. It is important for rational working in gas region, particularly, in Siberia. They began to study theoretic and experimental research of wave's roughness ice cover rather late from the 1980s.Theoretic manner of bottom surface ice cover studying based on J.Kennedy's conception of means condition acceptance of smallness of insurrections. At the same time wave insurrections of bottom surface ice cover in nature are not smallness and their contours differ from sinusoidal. Models of wave roughness on lower surface of ice cover in riverbeds, as Melkonian G. and Stepanov A. mark, have qualitative nature; these models contain coefficients, which quantity value must be determined from experiments. Systematic natural investigations of lower surface of ice are rather difficult and practically seldom realized. In this connection the knowledge stored by authors in period of carrying out winter practices with student-hydrologists RSHU (Levashov A.A. has been leading these practices for more than 25 years on the river Oredesh and reservoir Chikino, Leningradskaia oblast) is unique; these are systematic observations for ice cover in the same object, these are systematic sawing ice on all width of river, submarine shooting of ice and others. Authors analyzed, generalized priceless materials of nature, they give concrete calculation, recommendations for calculation of influence ice on riverbed and on process of river discharge in winter conditions.

STRUCTURE OF FLOW

We established there are ice dams in zones meeting of streams, islands, flows, bridges, in zones of different obstacles. Ice dams, detaining under and in front of them their

[1] Russian State Hydrometeorological University

loose ice (pack), slushfield and others sag climb up, bend of ice, which sharply change unevenness of flow and conveyance in this part of river. First by, considerably roughness of lower ice surface smoothes out in time on flowage parts of rivers with small depths, then wave ridge longitudinal and diametrical roughness of ice is created in this place (fig.1).

Fig.1.

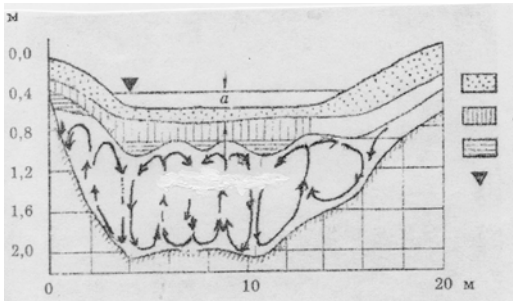

Fig.2. Cross-section of channel of river Oredech

Wave ice form on the lower ice surface with it is possible hypothesis about existence of longitudinal-spiral movement consisted of some jets (fig 2). It is demonstrated in wave from of crystalline lower ice surface in cross-section of ice from left to right riverbanks. Tracks of influence of longitudinal-spiral movement on bottom are noticeable in relief of bottom in section made sawing. They are independent gutters. There are these structures of ice and bottom by lower water stage in period winter dry-weather.

So tracks of flow interaction with lower ice surface and bottom taking into consideration their reflection from different surface and local masses of water, mean relative steady complicated organized structure of flows (Levashov and Levashova, 2003). It is necessary to know and take into account this structure by organizing measurements of river discharge, estimation of strength of river bed rendered flow, and it is important to understand the development of river-bed process in winter conditions.

Holes made in ice for measuring flow velocity reform quickly and complicated under influence of flow, whirlpool zones, arised in holes, it is necessary to know and take into account by measuring flow velocity in vertical (fig 3).

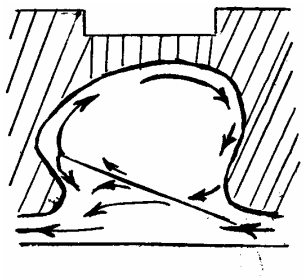

Fig.3. Vortical zone in hole and transit flow under ice

LAKE ICE AND RIVER ICE

Lake ice is on average 1.5 times thicker than river ice and it has important differences from river ice by its structure. There are clearly two layers in lake ice:1. upper – nasslood, flaky, 2.lower - crystalline, often also flaky (fig 4). It is possible to know quantity and number of precipitation on lake analising upper layers, and number of sharp warm or fall of temperature by lower, crystalline layers. It is possible to use these particular specifics to estimaten fall precipitation on lakes in regions without any observations.

River ice differs in crack structure, roughness of lower surface, flaky of upper nasslood layer and lower crystalline. There are often horizontal ice cavities often on river bends, there are not any of them on the lakes. Morphology of river bed and the dynamics of flow condition help to differ river ice from lake ice. Fig.5 shows that there are horizontal longitudinal openings in ice on bend of river, taking in consideration dynamics of flow conditions. There are cracks near banks, on meadstream in river ice and there are diametrical oblique cracks in zones bend of tortuous, turning river. Structure of river ice is also different in width from lake ice.

It is possible to use tracks of these differences to decipher freezing river speed along width and also for understanding of happened processes by these. It is necessary to take into account in measuring discharge in winter conditions.

INFLUENCE OF ICE APPEARANCES ON DISCHARGE CAPACITY

Authors devised morphology formula for coefficient C (Shezi) of carrying capacity of channel:

$$C = g^{1/2}\left(h_a / h_w\right)\left(h_a / B\right)^{(h_a / B)}(h_w / l_w)^{h_w / l_w}(\Delta h_i / \Delta l_i)^{\Delta h_i / \Delta l_i}.$$

There is ice member $(\Delta h_i/\Delta l_i)^{\Delta hi/\Delta li}$ in these formula. Ice member estimates influence of ice appearances (phenomenons) on discharge capacity. Where g = 9/81 m/c^2; h_a – average depth of section; h_w – depth of wave or bottom unevennesses, this is difference between average depths, being in separate distance equal 2 – 4 average depths; l_w – length of wave or distance between unvennesses defined on meadstream of channel.

Coefficients h/B, h_w/l_w , considerating influence of banks and steepness of waves accordingly, are with variable index of power. Where B is width of river channels, Δh_i, Δl_i – accordingly height and length unevennesses (waves) on lower ice surface in distance equal 2 – 3 average depths of section. Comparative calculations made by formula Chezi show quite similar results (≈ 4% difference).

ICE WAVES ON A SURFACE

There are ice microwaves on surface of freez-up with notsynchronous freezing water along width and length of flow (fig.6).

It happens with water stage change and splash of water on the edge of ice if air temperature is negative. Cellular forms are supposed to be formed on lower ice surface being influenced by vortical movement (fig. 7).

Fig.6. Ice wave on a surface

Fig.7. Cellular lower surface of ice

There are different vorticals in stream if local water masses reflax from different obstacles: on the edge of the ice, on waves and others. Cell have different sizes, forms because there are different obstacles, speed, depths.

There are large lensform, washness, hollowness on lower ice surface. RSHU Students took photo using submarine camera under ice on the river Oredesh (fig.8).

These ice lensforms were formed by reflexes of running flow on steep bank of island. There was wave ice surface with height and width wave of 0.1 and 1.5 m accordance on relatively rectilinear wide part of bed river Oredesh by B/h_a=18, where B – width, h_a – average depth.

Number of longitudinal waves in cross sections, including coastal, made 3 – 5. This phenomenon is simultaneously evidently fixed in February, 2003 by seismic-acoustic method (fig.9). The supervision is executed in small depths (up to 1,0 м), when the reflection of jets of a flow from bed reached the bottom surface of ice. Therefore on this surface was formed wavy relief (rice).

Ice can “write” different obstacles,unvennesses of bottom. So there is dented, chipped, uneven not wave lower ice surface on the photo (fig.10), reflexed of flow from uneven obstacle-tree (log) conditions.

Ice jams greatly influence on discharge capacity and channel deformation.

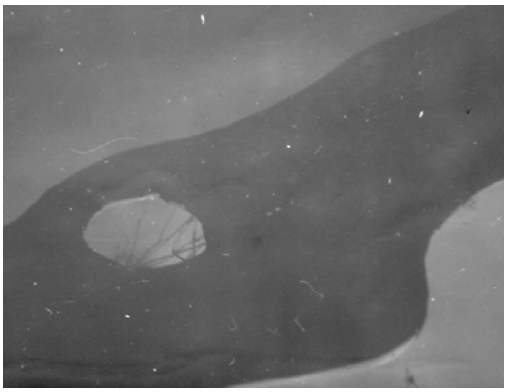

Fig.8. Lower ice surface

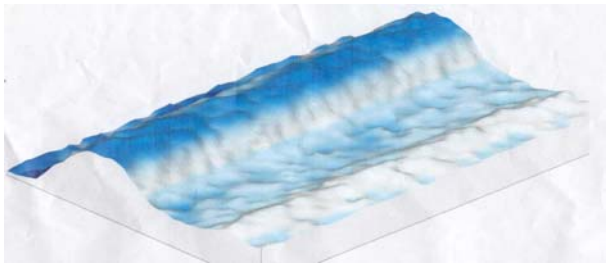

Fig.9. The lower ice surface received with help sesmic-acoustic method

So authors observed ice jam on the river Oredesh in February 2001. There was the same discharge: before and after jam, but with different water stages. Knowing measurement of water stage, fall of water stage with frazil and without you can measure hydraulic resistance. There was the same discharge – 4 m^3/s – with fall of water stage – 0,5 m with release of bed from frazil and taken of frazil out of first obstracted its bed.

There are often longitudinal wave ribbed lower ice surface with fall of water stage near banks (fig.11).

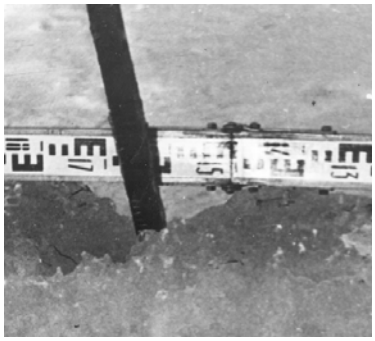

Fig.10. Dented ice surface

Fig.11.The wave ribbed lower ice surface

Ribbing is often parallel to the bank. Authors have made photo (fig.12) above that lower wave ice surface from above can be seen through upper surface of transparent ice after some days of freezing. Waves of lower ice surface have been founded by getting slush field under edge of the ice. There are wave forms of lower ice surface in some parts of rivers form polynias, where slush field falls under the edge of the ice.

Masses of water vegetation, carrying by flow, often freeze to lower ice surface in attenuation of speed zones near back-water. Authors have observed these layers (thickness10-15 cm) along half of bed width on some Oredesh anabanches (fig.13).

So lower ice surface forms on the river depend on severity of winter, height of snow on ice, form of river in plan, form bed (wave, smooth and other), variation of water stages in winter (flashes, falls and other) and have big variety in time and space.

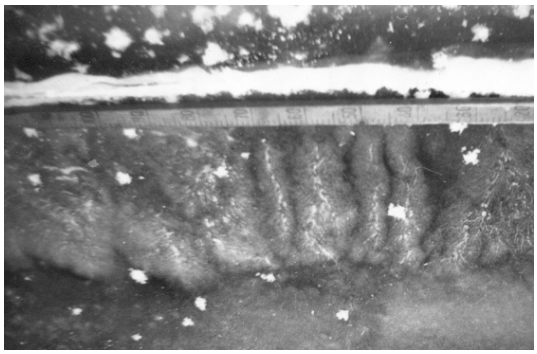

Fig.12. The microforms of ice from above, trough transparent ice

Fig.13. Layers of water vegetation

CONCLUSIONS

Knowledge of this variety helps us to understand the existence of different discret form in flow and interaction flow with ice and bed forms (waves and others), processes of reflection of flow from different surfaces, influence of ice to development of bed process in winter conditions. Besides, knowledge of morphology ice river can broaden our conceptions about hydraulic resistance and characteristics of flow in beds with freez-up.

REFERENCES

Levashov A.A., Levashova I.A. Field and experimental research methods of the river flows. *Hydrometeoizdat*. St.-Petersburg (2003) 192 p.

17th International Symposium on Ice
Saint Petersburg, Russia, 21 - 25 June 2004
International Association of Hydraulic Engineering and Research

SUB-DAILY FLAW POLYNYA DYNAMICS IN THE KARA SEA INFERRED FROM SPACEBORNE MICROWAVE RADIOMETRY

Stefan Kern[1]

ABSTRACT
Flaw polynyas develop frequently at the fast-ice border along the Russian coast. The dynamics of such flaw polynyas occurring in the Kara Sea has been investigated with the Polynya Signature Simulation Method (PSSM) by Markus and Burns (1995) for a 10-day period of the winter 2002/2003 using brightness temperatures acquired by the Special Sensor Microwave/Imager (SSM/I). Results obtained with SSM/I data of two Defense Meteorological Satellite Program (DMSP) spacecraft, i.e., f13 and f15, have been used in order to resolve the sub-daily polynya dynamics. Polynya area, size and shape as inferred with the PSSM from f13 data agree with those obtained using f15 data and with NOAA AVHRR infrared imagery. The observed polynya dynamics is in line with changes in prevailing air flow during the period.

INTRODUCTION
In polar regions open water and/or thin ice areas can develop within an otherwise ice-covered region if wind speed and direction permit that the sea ice is pushed away from the coast, an ice shelf, or the fast-ice border (Smith et al, 1990). Such areas are known as polynyas. If they develop as described above then they can be commonly referred to as latent heat polynyas wherein the latent heat of fusion released during the ice formation keeps the polynya open which obtains an equilibrium state for given wind speed, temperature, short- and longwave fluxes, vertical oceanic heat fluxes, and oceanic currents (Smith et al, 1990). Polynyas that develop along the fast-ice border are called flaw polynyas. They are common along the Russian coast and develop frequently during off-shore winds. According to Dmitrenko et al. (2001), these polynyas often cannot be regarded as a pure latent heat polynya due to a substantial sensible heat supply by rivers.

These polynyas act as ice factories and locations of substantial heat input into the atmosphere during winter, and as starting points for summer melt due to enhanced intake of solar radiation during spring. A long-term continuous monitoring of polynyas is required in order to estimate possible changes in the heat and moisture budget of the

[1] University of Hamburg, Centre for Marine and Climate Research, Institute of Oceanography, Bundesstrasse 53, D-20146 Hamburg, Germany

atmosphere on the one hand, and in the heat and salt budget of the ocean on the other hand. Any identified trend, e.g., in the polynya extent could point to a change in one or more of its steering environmental conditions. Moreover, a positive trend in the polynya extent might be of interest to authorities dealing with the protection of the Russian coast against enhanced erosion caused by a longer period during which the coast is affected by wind waves and swell. Finally, the dynamics of these polynyas is of interest when navigating along the North-East-Passage. Rapid temperature and/or wind changes may affect the polynya extent significantly within hours and could severely hamper shipping activities along this route of growing interest.

Spaceborne microwave radiometry is the only useful data source to monitor these polynyas independently of daylight and cloud cover. In this paper a method developed by Markus and Burns (1995) is used together with brightness temperatures acquired by the Special Sensor Microwave/Imager (SSM/I) aboard two spacecraft of the Defense Meteorological Satellite Program (DMSP) to derive time series of the polynya extent in the Kara Sea for a 10-day period in March 2003. The paper is organized as follows: the next two section describe briefly the data and the method. Results are given in the third section after which some discussion and conclusion finish the paper.

THE DATA

The spaceborne microwave radiometer SSM/I is equipped with channels operating at the frequencies of 19, 22, 37, and 85GHz. The SSM/I is mounted on the polar orbiting DMSP spacecraft. It is aft-looking, and scans the Earth conically at an incidence angle of 53.1°, yielding an about 1400km wide swath at the surface. The effective field-of-view, polarization, and sampling interval are given in table 1.

Table 1. SSM/I sensor characteristics

Frequency [GHz]	19.35	22.235	37.0	85.5
Polarization	h, v	v	h, v	h, v
Effective field-of-view [km x km]	69 x 43	50 x 40	37 x 29	15 x 13
Sampling interval [km]	25	25	25	12.5

Three DMSP spacecraft are in orbit: f13, f14, and f15, providing excellent spatial and temporal coverage – particularly of the polar regions. SSM/I data of two spacecraft were used and interpolated onto polarstereographic grids (true at 70°N) with a spatial resolution of 5km x 5km (85GHz) and 12.5km x 12.5km (19, 22, and 37GHz) using the Backus-Gilbert-Interpolation technique as given in Hunewinkel et al. (1998).

THE METHOD

Currently used sea ice concentration retrieval algorithms, e.g., the NASA-Team algorithm, and the COMISO Bootstrap algorithm (see for both algorithms Comiso et al., 1997) are merely based on 19 and 37GHz SSM/I data. Obtained sea ice concentration maps therefore have a spatial resolution of 25km x 25km. More recently developed algorithms which use 85GHz SSM/I data (e.g. Kaleschke et al., 2001) permit to obtain the sea ice concentration with a spatial resolution of 12.5km x 12.5km. These methods, however, suffer from the large weather influence at 85GHz, and have to be combined with an algorithm using low-frequency SSM/I data (see above). These algorithms are not suitable to monitor the extent of polynyas and/or to obtain the associated thin-ice area. The Polynya Signature Simulation Method (PSSM) which was developed by Markus and Burns (1995) combines the

finer spatial resolution of the 85GHz SSM/I channels with the lower weather influence of the 37GHz SSM/I channels to obtain high-resolution maps of the polynya extent and the associated open water/thin-ice area.

The steps of the PSSM are as follows (for a more detailed description see Markus and Burns (1995) and Hunewinkel et al. (1998)):

I. Generate maps of the polarization ratio *P* (vertically minus horizontally polarized brightness temperature divided by the sum of both) at 37GHz (*P(37)*, map I) and 85GHz (*P(85)*, map II); associated spatial resolutions: 12.5km x 12.5km and 5km x 5km, respectively.

II. Use map II to first generate a two-class image containing the surface types open water and ice, and to secondly subdivide the ice area into two classes: thick ice and thin ice, so that the result is a three-class image containing the surface types open water, thin ice, and thick ice. The thresholds of *P(85)* used for this classification are chosen such that the open water and thin-ice area are underestimated first.

III. Generate a so-called synthetic map of *P(37)* (map III) by assigning typical values of *P(37)* of the surface types to the three-class image.

IV. Convolute map III with the antenna pattern and the sampling distance of the 37GHz SSM/I channels to create a so-called simulated map of *P(37)* (map IV) which has the resolution of the 37GHz SSM/I channels.

V. Compare map I and map IV in terms of correlation and RMS error.

By iteratively changing the thresholds of *P(85)* used in step II) and going through steps III) to v) the correlation is maximized and the RMS error is minimized until convergence is achieved. The three-class image belonging to the pair of map I and IV which has the best correlation and the least RMS error provides the actual distribution of open water, thin and thick ice, i.e., polynya extent and thin-ice area. This method was already used, e.g., by Hunewinkel et al. (1998) in the Southern Ocean, and by Dokken et al. (2002) in the Arctic Ocean.

For the present paper the PSSM was applied to SSM/I data acquired aboard DMSP spacecraft f13, f14, and f15 in the Kara Sea from March 8 - 16. The SSM/I swath data obtained regularly via ftp from the Global Hydrology Resource Center were split into single-channel files and then gridded using the Backus-Gilbert interpolation technique. The gridded data were then investigated with the COMISO Bootstrap algorithm and the PSSM. For the COMISO Bootstrap algorithm tie points and weather filters as given by Comiso et al. (1997) were used. For the PSSM the following tie points for *P(37)* were used: open water: 0.18, and thin ice: 0.08. Values of *P(37)* for thick ice were calculated from areas where the ice concentration as calculated with the COMISO Bootstrap algorithm takes values between 90% and 100%. These values are between 0.024 and 0.035 for the investigated period.

RESULTS

Figure 1 shows a time series of maps of PSSM-derived areas of thick ice, thin ice, and open water as derived from SSM/I data of DMSP spacecraft f13 of March 8 to March 16, 2003, of the morning (around 4UTC) and the noon (around 11UTC) SSM/I overpass. The shown area covers the entire Kara Sea (size: 2000km x 1350km). The shown period can be divided into three regimes. The first regime lasted from the beginning of the time-series to the second half of March 10.

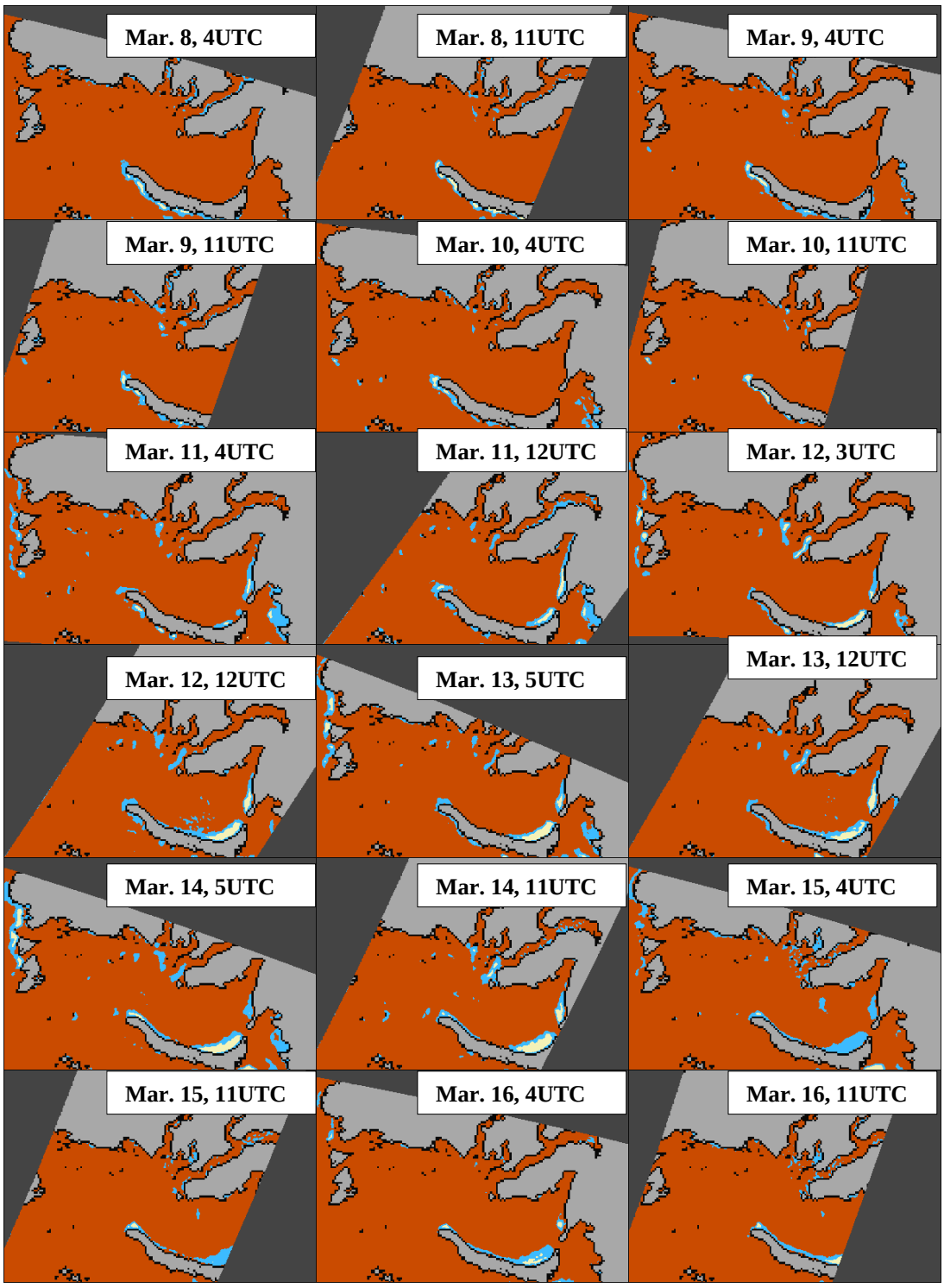

Fig. 1. Time-series of maps of PSSM-derived areas of thick ice (red/brown), thin ice (blue), and open water (pale yellow/white) of SSM/I data acquired by DMSP spacecraft f13 from March 8 to 16, 2003, in the Kara Sea. Grey denotes land, black missing data and coast lines. Nowaja Semlja and Sewernaja Semlja can be identified at the bottom (left edge) of each image. Size of the shown area is 2000 km x 1350 km. The box in the topmost left image marks the subarea used for figure 2

Several polynyas (note that unless specified otherwise, the term *polynya* is used for both the open water and the thin ice area of a polynya) developed along the western coast and at the northern tip of Nowaja Semlja. Some small polynyas developed in the estuaries of the rivers Ob and Jenissej. The second regime started March 10/11 and lasted until the morning of March 15. During this regime large polynyas developed along the eastern coast of Nowaja Semlja and Waigatsch. The polynyas in the esturaries of Ob and Jenissej increased in size and became oriented northwest-southeast. At the same time all polynyas along the western coast and at the northern tip of Nowaja Semlja vanished. Finally, during the third regime, the polynyas in the estuaries of Ob and Jenissej vanished and only the polynyas along the eastern coast of Nowaja Semlja remained open. A similar time-series was derived using SSM/I data of DMSP spacecraft f15. The correlation between synthetic and simulated maps of *P(37)* (see section THE METHOD) takes values between 0.879 and 0.941 (average: 0.911) for f13, and between 0.878 and 0.939 (average: 0.912) for f15.

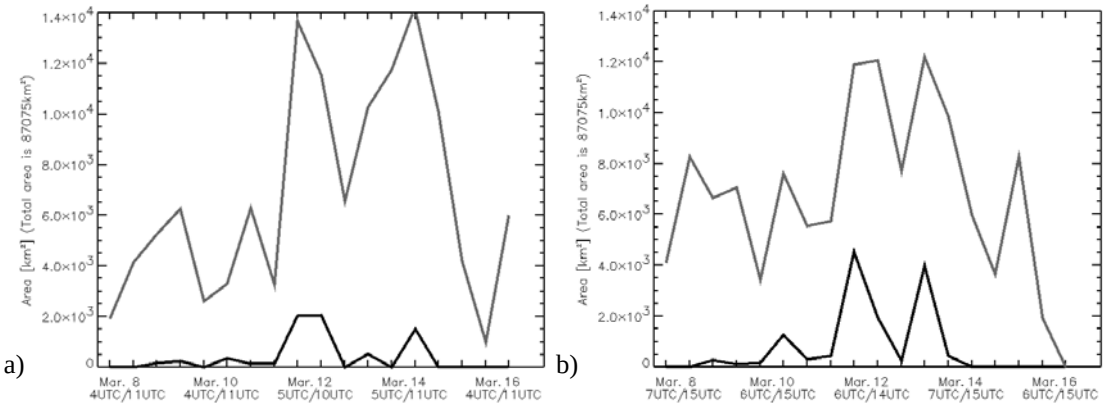

Fig. 2. Comparison of thin ice and open water area obtained with the PSSM from SSM/I data of DMSP spacecraft f13 (a)) and f15 (b)) for March 8 - 16, 2003, for 350km x 300km large subarea situated in the flaw-polynya area in estuaries of Ob and Jenissej (see box in topmost left image of figure 1)

Figure 2 shows time series of the areas covered by thin ice and open water as obtained with the PSSM from SSM/I data of DMSP spacecraft f13 and f15 for March 8 - 16, 2003, for a 350km x 300km large subarea situated in the estuary region. For f13 overpasses around 4UTC and 11UTC are used; corresponding overpass times for spacecraft f15 are 6UTC and 15UTC. Note the increase of the thin ice and open water area for the days of the second regime (see above). Significant open water areas are observed on March 12 and from March 13 to 14. Note also that the thin ice area may change within six to eight hours by as much as 6000km², e.g., during March 15, and within 18 hours by as much as 10000km², e.g., from March 11 to 12 (see a) for both).

Figure 3 shows the time series of the PSSM results obtained with SSM/I data from almost all DMSP spacecraft f13 and f15 overpasses (12 in total; actually the total number is 17, but some swath overlap and/or have the same overpass time) available for March 12, 2003. Many polynyas can be identified almost all of which have a considerable open water area: northeast of Sewernaja Semlja, in the flaw-polynya area of the estuaries of Ob and Jenissej and along the east coast of Nowaja Semlja.The prevailing strong southwesterly air flow keeped these polynyas open during the day.

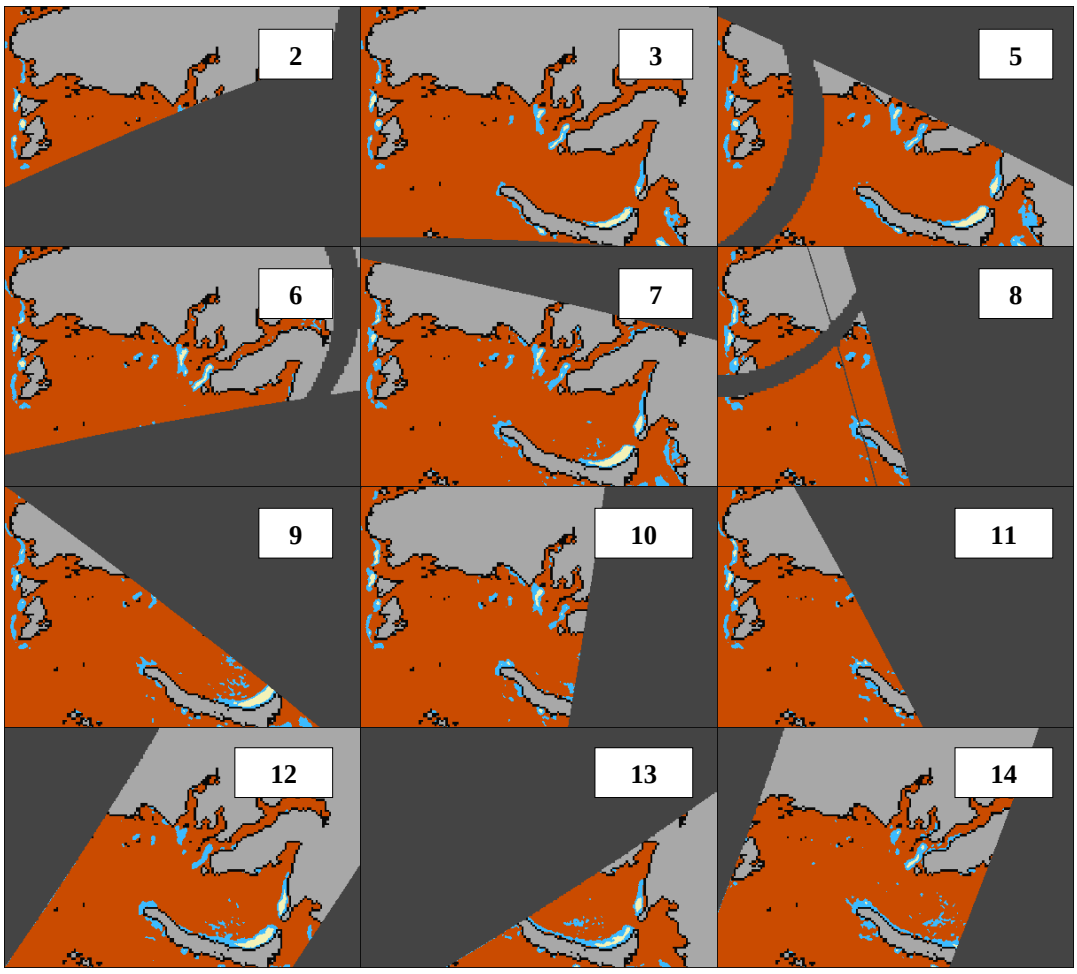

Fig. 3. Panel of PSSM results of all available overpasses of DMSP f13 and f15 on March 12, 2003 (see figure 1 for colors). The numbers denote the time of the overpass of f13 (2, 3, 5, 8, 10, 12, 13UTC), and f15 (6, 7, 9, 11, 14UTC)

Note the agreement in location, size, and shape of the polynyas between data obtained from different DMSP spacecraft, i.e. between images 5 and 6, 7 and 8, 8 and 9, 9 and 10, as well as 10 and 11. Despite the prevailing southwesterly air flow a considerably dynamics of the area of some polynyas can be identified: for instance the opening of the polynya at the northern tip of Nowaja Semlja between 5 and 10UTC, or the increase of polynya extent along the eastern coast of south Nowaja Semlja between 3 and 7UTC and then the decrease of its open water area between 9 and 13UTC.

DISCUSSION AND CONCLUSIONS

SSM/I data of DMSP spacecraft f13 and f15 have been investigated using the PSSM in order to estimate the areas of thin ice and open water of polynyas in the Kara Sea. A period of nine days (March 8 – 16, 2003) was selected during which the air flow changed substantially from first easterly to southeasterly directions to southwesterly directions and finally to northwesterly directions. This is shown in the surface pressure analysis charts given in figure 4. The opening and closing of polynyas that can be identified, e.g., in figure 1 is in line with the changes in wind direction associated with the pressure field shown in figure 4.

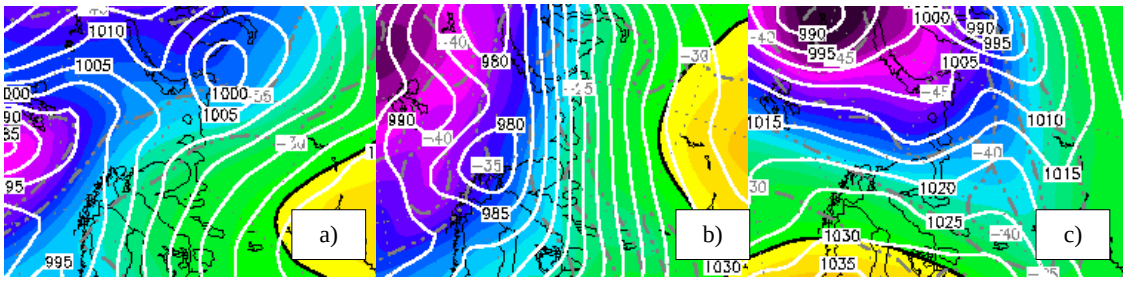

Fig. 4: Charts of the surface pressure (in hPa, white lines) and height of the 500hPa level (in gpdm, yellow – blue: high – low) on March 9 (a), March 11 (b), and March 16 (c). Taken from the 0UTC analysis of the global weather forecasting model of the American weather service as provided by http://www.wetterzentrale.de/topkarten/

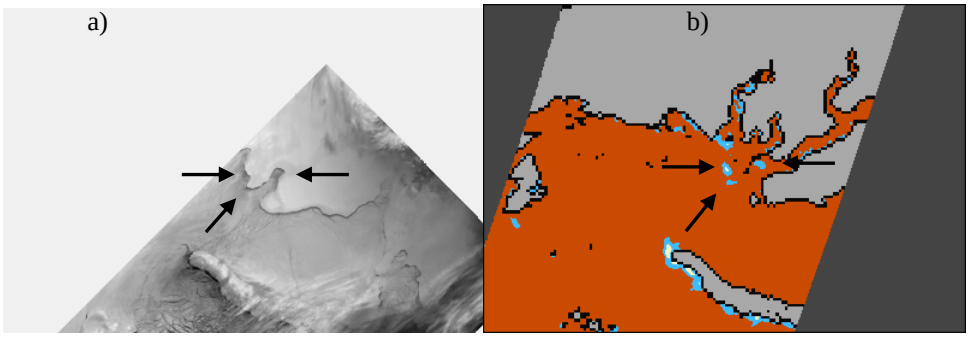

Fig. 5: Comparison of NOAA 17 infrared imagery (AVHRR channel 4, acquired March 9, 10:10UTC) (a) with results of the PSSM (b) of March 9, 11UTC. Colors in b) are the same as in figure 1

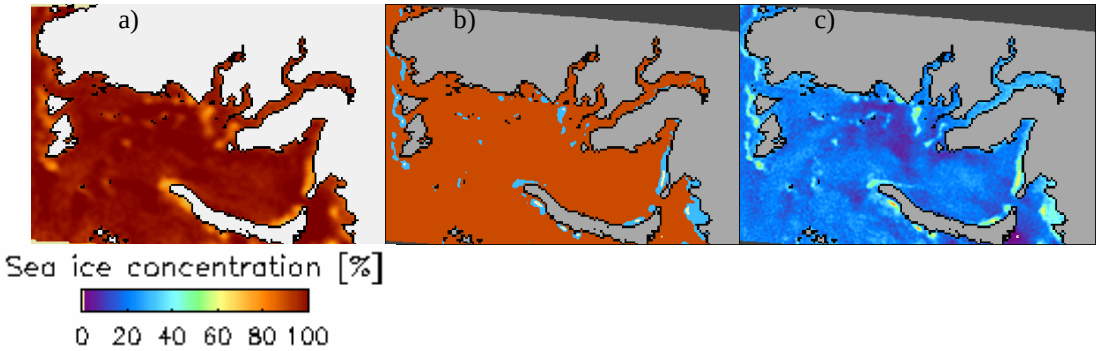

Fig. 6: Comparison of COMISO-Bootstrap ice concentration (a) with the result of the PSSM (b) and the used map of *P(85)* (c) for March 11, 4UTC. See figure 1 for colors in (b) and the legend below (a) for c): replace 100% by 0.12

The open water and thin ice areas obtained with the PSSM have been compared with NOAA (NOAA-16/17) AVHRR channel 4 infrared imagery. AVHRR data have been gridded and interpolated onto the same grid as was used for the PSSM. Figure 5 shows one example of this comparison for March 9. The polynyas in the vicinity of Nowaja Semlja can easily be identified; infrared temperatures decrease below 269K in these areas. More difficult to compare are the polynyas in the flaw-polynya region in the estuaries of Ob and Jenissej. However, high infrared temperatures (above 261K) in the AVHRR image agree with the polynyas shown in figure 5 b) – see arrows.

Figure 6 shows a comparison of the COMISO Bootstrap algorithm ice concentration with the coincident PSSM result and map of *P(85)* used for the PSSM. This comparison

reveals clearly that in almost all areas where the ice concentration map (a)) indicates lower ice concentrations, e.g., between 70 and 90%, the PSSM map indicates thin ice but almost no open water. The map of *P(85)* (c)) confirms location, size, and shape of all polynyas shown in figure 6 b) and puts confidence on the PSSM results.

This paper presents – to the authors best knowledge – for the first time, that SSM/I data of at least two DMSP spacecraft can be successfully used together to obtain a better view of the daily and sub-daily dynamics of polynyas in the Kara Sea. Location, size, and shape of the detected polynyas obtained with the PSSM from f13 SSM/I data agree with those inferred from f15 SSM/I data. Thin-ice areas obtained with the PSSM agree with areas revealing high infrared temperatures as inferred from NOAA AVHRR imagery. Unfortunately, the coverage of SSM/I overpasses during the day is not sufficient enough to have a PSSM map of the entire Kara Sea every six hours. However, the coverage between 2UTC and 16UTC is reasonably good to obtain one map every hour, and therefore to monitor the changes in the polynya extent which are obvious from the above results. It is intended to obtain polynya extent time series of the Kara Sea for at least the entire season 2002/2003 from f13, f14, and f15 SSM/I data in the near future. Evaluation of the obtained extents with NOAA AVHRR imagery will be continued. The usage of changing thick-ice tie points for *P(37)* will be verified.

ACKNOWLEDGEMENTS

The author thanks the Global Hydrology Resource Center (GHRC), Huntsville, AL, USA, and the Satellite Active Archive (SAA), NOAA, Washington D.C., USA, for provision of SSM/I and AVHRR data, respectively, and the German Science Foundation (DFG) for funding.

REFERENCES

Comiso, J.C., Cavalieri, D.J., Parkinson, C.L., and Gloersen, P. Passive microwave algorithms for sea ice concentration – a comparison of two techniques. *Remote Sensing of the Environment* 12: 357-384 (1997).

Dmitrenko, I., Hölemann, J.A., Tyshko, K., Churun, V., Kirillov, S., and Kassens, H. The Laptev Sea flaw polynya, Russian Arctic: effects on the mesoscale hydrography. *Annals of Glaciology* 33: 373-376 (2001).

Dokken, S.T., Winsor, P., Markus, T., Askne, J., and Björk, G. ERS SAR characterization of coastal polynyas in the Arctic and comparison with SSM/I and numerical investigations. *Remote Sensing of the Environment* 80: 321-335 (2002).

Hunewinkel, T., Markus, T., and Heygster, G. Improved determination of the sea ice edge with SSM/I data for small-scale analysis. *IEEE Transactions on Geoscience and Remote Sensing* 36: 1795-1808 (1998).

Kaleschke, L., Heygster, G., Lüpkes, L., Bochert, A., Hartmann, J., Haarpaintner, J., and Vihma, T. SSM/I sea ice remote sensing for mesoscale ocean-atmosphere interaction analysis. *Canadian Journal of Remote Sensing* 27(5): 526-537 (2001).

Markus, T. and Burns, B.A. A method to estimate subpixel-scale coastal polynyas with satellite passive microwave data. *Journal of Geophysical Research* 100(C3): 4473-4487 (1995).

Smith, S.D., Muench, R.D., and Pease, C.H. Polynyas and leads: An overview of physical processes and environment. *Journal of Geophysical Research* 95(C6): 9461-9479 (1990).

17th International Symposium on Ice
Saint Petersburg, Russia, 21 - 25 June 2004
International Association of Hydraulic Engineering and Research

WINTER OFFSHORE LOADING OPERABILITY RATE IN THE PECHORA SEA

Basile Bonnemaire[1]

ABSTRACT
Different concepts for arctic offshore loading of hydrocarbons will present different operability rates in the winter. The ice drift conditions at a particular location will influence these performances. Critical drift events that would interrupt a loading operation are defined for different loading systems. In this light, data collected from ARGOS-GPS buoys deployed in the drifting ice in the Pechora Sea during spring 1998 are analysed. Loading performances of the different concepts are estimated and compared. An average operability rate of 70 % is found varying upon the concept choice and design and the location in the Pechora Sea.

INTRODUCTION
Arctic offshore oil production will increase in the future. With regards to exploration and production, technology is rather up-to-date to cope with arctic environmental conditions. Experiences with year-round drilling and production platforms or vessel in ice-covered seas are sparser. The export of the produced hydrocarbons remains a major challenge in heavily ice-infested waters. This tends to penalise arctic offshore production activities.

Examples of arctic offshore production and oil export are not common. At the Northstar Production Island, a buried pipeline would transfer the oil to shore (Masterson, 2001). For oil production, direct offloading and shipping is often considered as pipeline transport to a shore terminal may cause operation problems linked to loading oil in ice covered harbours. In the Vityaz Complex, a standard Single Anchor Leg Mooring buoy is used to transfer oil from Molikpaq to a Floating Storage and Offloading (FSO) unit. Oil export is shut down during winter as the buoy cannot withstand ice forces. A Single Anchor Loading (SAL) system with a reinforced hawser was installed in the summer 2002 offshore Varandey in the Pechora Sea. This terminal is used to export a limited amount of oil (600 000 tons the first year) and the tankers (20 000 DWT) are assisted by icebreakers in the winter.

[1] NTNV, Norwegian University of Science and Technology, Trondheim, Norway

With the development of new arctic fields, other arctic offshore loading concepts may be used. The winter operability rate of one of these system is critical when establishing its profitability. This rate will highly depend on the ice drift conditions and properties in the area. In this light, ice drift data from ARGOS-GPS buoys are analysed in order to assess the operability rate of different arctic offshore loading concepts in different regions of the Pechora Sea.

WINTER LOADING OPERABILITY RATE OF DIFFERENT CONCEPTS

Many design solutions for arctic offshore loading have been presented in the literature in the past decades. In this study, four concepts that may be used with the next arctic offshore field developments were considered. A solution is to load directly from a structure. This structure can be the production platform itself equipped with loading arms. This technology is planned to be used on the Prirazlomnoye platform (Malyutin et al., 2003); the loading arms would be at the corners of a square Gravity Based Structure (GBS). The structure can also be a loading terminal, usually a narrow cylindrical structure around which the tanker can vane (see e.g. Gudmestad et al., 1999; Spencer et al., 1997). Minimizing interaction with ice, subsea concepts are also proposed. A Single Anchor Loading (SAL) system where the hawser for bow loading is protected in a "lobster" was proposed (Di Tella, 1996; Di Tella and Juurma, 1997). A SAL system with a non-protected reinforced hawser was built by APL (Advanced Production and Loading AS) and installed in the Pechora Sea offshore Varandey. These surface piercing concepts, though protected, will not be operational in very severe ice conditions unless effective ice management is performed. Finally, an adaptation of the Submerged Turret Loading (STL) system is presented in e.g Bonnemaire et al. (2003) and Bonnemaire (2004). The riser connected to the turret under the hull of the tanker is protected in a flexible armour. The riser will not interact directly with incoming ice that is broken by the vessel, but with ice fragments.

Few of the mentioned concepts have been used but some may be in the future. Economical considerations will drive the choice of a particular concept for a given project. Many parameters will interfere such as e.g. the location, the production stage (early or full), the vessel type or the environmental conditions. When year-round operations are considered, an important aspect is the operability rate in winter conditions.

The operability rate will vary depending on the chosen configuration, i.e. the manoeuvrability in ice of the chosen vessels (use of reamer, azipods), the size and the type of tankers, the use of ice management, the time needed for connecting and disconnecting the tanker or the loading rate. The ice conditions will also play a major role. Heavy ice conditions (e.g. high ridge concentration, high pressure in the ice cover or multiyear ice) may influence the operability rate. The changes in the ice drift will also determine most of the concept downtime. This problem is considered in the following.

Table 1 presents different critical drift events for some loading concepts. For example, a sudden shift of drift direction larger than 135º will tend to push the tanker against the loading structure. Each time one of these events will happen or is believed to happen, loading has to be stopped. So the operability rate depends on the frequency of appearance of these events. Disconnection, repositioning and reconnection will take some time. When loading in the vicinity of a structure in shallow waters, grounded

rubble might have to be cleared before reconnection is possible. Depending on the detailed design of the concept, the event characterisation in Table 1 might slightly vary; the diameter of the cylindrical narrow terminal for example will influence the forces in the mooring lines when drift direction is changing (Spencer et al., 1997).

Table 1. Critical drift events for different loading concepts

Concept	Drift event	Consequences	Risk
Loading from a platform corner	Over 90º change in drift direction	Change of loading arm corner	Collision tanker - platform
	Sudden important change in drift direction (e.g. > 135º)	Disconnection and manoeuvring around the platform	Collision tanker - platform
Loading from a narrow cylindrical terminal	Rapid change in drift direction (> 135º) and heavy ice conditions	Disconnection	Excessive mooring forces
	Sudden important change in drift direction (> 135º)	Disconnection	Collision tanker - terminal
Single Anchor Mooring*	Sudden important change in drift direction (e.g. > 135º) and heavy ice conditions	Disconnection	Loading line rupture; damage to mooring system
Submerged Turret Loading	Rapid change in drift direction and heavy ice conditions	Disconnection	Excessive mooring forces

* Ice management is mandatory with this concept in heavy ice conditions. Its performance will rely on the ice management.

ICE DRIFT IN THE PECHORA SEA

Arctic offshore loading is of high interest in the Pechora Sea. Export of inshore production and in the future export from the Prirazlomnoye field and other fields as the Dolginskaya field are of concern. The Pechora Sea presents shallow waters and severe ice conditions. Ice is found in the area 2/3 of the year with a maximum level ice thickness of 1.6 m and drift speeds up to 1.0 m/s. Icebergs are not present in this area but the ridging intensity can reach 5 balls in April and 12-18 m ridge keels are expected (Løset et al., 1997).

From March to May 1998, 4 ARGOS buoys (06640, 22435, 24050 and 24051) were deployed in the Pechora Sea. Løset and Onshuus (1999) and Løset and Økland (2000) present drift speed analysis derived from the ARGOS positions of these buoys. Partly based on these data, Voinov et al. (1999) present a method to process ARGOS buoy data and derive drift speeds trying to reduce errors due to the inaccuracy of the ARGOS positioning system.

Each of these buoys contained a GPS receiver, and the GPS position of the buoys was transmitted via the ARGOS satellite system. These GPS positions are not mentioned in the cited analysis. ARGOS positions present an accuracy of 150 m at best (Class 3 measurements). GPS positions, despite the signal degradation at that time, present a higher accuracy; Prinsenberg et al. (1998) tested the accuracy of such GPS-ARGOS ice beacons and found it to be less than 35 m. Nevertheless, the precision of the received

GPS coordinates data is 1/1000th of a degree, which corresponds to 60 m accuracy at that latitude (Løset and Onshuus, 1999).

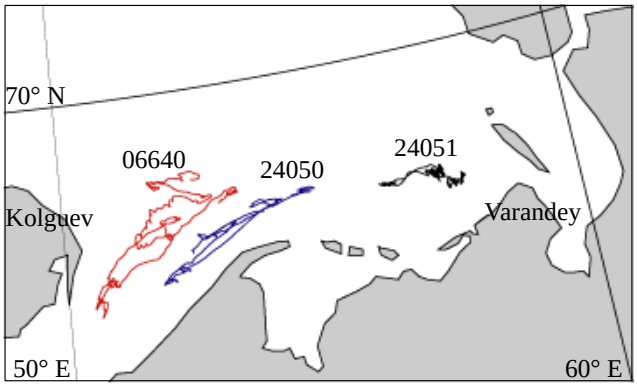

Fig. 1. Paths of the buoys in the Pechora Sea

The GPS positions of buoys 06640, 24050 and 24051 were then analysed (Fig. 1 presents the drift paths of these 3 buoys in the Pechora Sea). Erroneous and duplicate values of the positions were removed. The amount of GPS position data is then similar to the amount of ARGOS position data. A moving average with a 40 min window was run on the GPS longitude and latitude. A cubic spline interpolation was then applied to get positions estimates every 15 min.

Further analysis of the ice drift aimed at determining loading windows for different loading concepts. Each buoy drifted in a limited area (within a 60 km radius circle). It was assumed then that the ice drift was uniform in these areas; a loading system installed there would be subjected to the same drifting patterns.

To determine the critical drift events presented in Table 1, the ice drift heading and the curvature of the ice drift path were computed. If x and y are the longitude and latitude of a buoy, the curvature radius R is then defined as:

$$R = \frac{\left(\dot{x}^2 + \dot{y}^2\right)^{3/2}}{\left|\dot{x}\ddot{y} - \ddot{x}\dot{y}\right|} \qquad (1)$$

De Franco et al. (2001) presented distributions of beam accelerations of the ice drift. Though these values are related, the author believes that the curvature radius can more easily be related to manoeuvring capabilities of a vessel for example.

LOADING WINDOWS IN THE PECHORA SEA IN SPRING 1998

The loading windows for different loading concepts had to be characterised. Table 2 presents the criteria used (α_{15} and α_{30} are the drift heading variation within 15 and 30 min). A maximum value for α_{30} is believed to be 135º to avoid collision between the structure and the tanker. The minimum drift curvature radius will depend on the manoeuvring capabilities of the tanker, the size of the loading terminal or the ice conditions. The wake of the loading terminal may ease the manoeuvring capabilities of the connected tanker; the importance nevertheless depends on the loading terminal diameter (Spencer et al., 1997). Thus a shorter radius was chosen for this concept than for the STL concept.

Table 2. Suggested loading window characteristic for different concepts
(Note that a thorough risk analysis should be carried out to confirm these values)

Concept	Loading window characteristics
Loading from a platform corner	Drift heading within ± 45º of a corner direction
Loading from a narrow cylindrical terminal	R > 200 m and α_{30} < 135º
Submerged Turret Loading	R > 400 m

Fig. 2 shows the scenario and definitions used for the loading from a platform corner concept. For each location, the optimal platform heading was estimated in order to get a maximum of "long" loading windows (over 4 hours). For any concept, when the tanker has to connect or disconnect, time will be lost. Based on indications given by Jolles et al. (1997), a manoeuvring and connecting time of 2 h and a disconnection time of 15 min were considered. These durations will vary a lot depending on the concept, the vessel manoeuvring capabilities, the ice conditions and if there is ice management at the site. Loading windows for the single anchor mooring concept were not estimated. Full time ice management is necessary with this concept in heavy ice conditions, the loading operability rate will rely on the management efficiency.

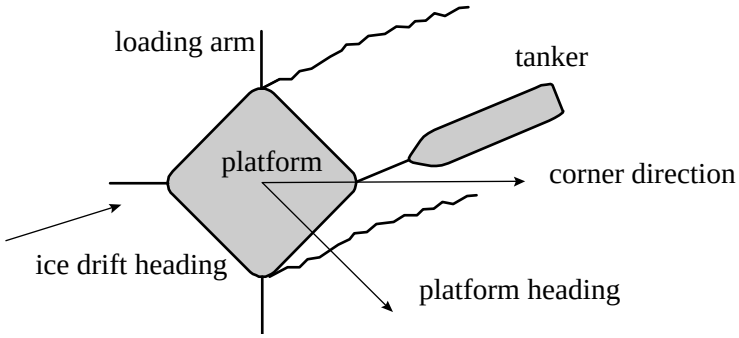

Fig. 2. Loading from a platform corner configuration

Table 3 presents results from the analysis of the 3 ARGOS buoys patterns. As shown in Fig. 1, buoys 06640 and 24050 were located in the West of Kolguev Island whereas buoy 24051 was drifting offshore Varandey. This explains why the optimal platform headings are close for the two first buoys. Offshore Varandey, the loading windows are shorter in average. This might favour the use of small tankers that need less time to load.

Loading from a narrow cylindrical terminal tends to present the highest operability rate and average loading window duration. Nevertheless care should be taken when reading these results. The operability rate for loading from the corner of a platform is a maximum value; even in light ice conditions the tanker will have to manoeuvre from corner to corner when drift heading changes. In light ice conditions, a tanker equipped with a STL system will be able to withstand rapid shift in ice drift directions (R < 400 m) without disconnecting; the operability rate presented here is then a minimum value. There will be the same effect when loading from a narrow cylindrical structure but still disconnection will be necessary if sudden important change in drift direction occur. The sensibility of the loading operability rate of these two concepts to

the minimum curvature radius was studied. In this range of curvature radius values (200 to 600 m), the operability rate varies almost linearly, decreasing of 2.8 % in average for a 100 m increase of *R*.

Table 3. Results from the analysis of drift patterns in the Pechora Sea, spring 1998

		ARGOS buoy		
		06640	24050	24051
Optimal platform heading (degrees)		80	70	35
Occurrences of $\alpha_{15} > 135^o$		25	32	38
Occurrences of $\alpha_{30} > 135^o$		71	102	139
Loading window average duration (h)	Loading from a platform corner	4.86	5.08	3.53
	Loading from a narrow cylindrical terminal	9.56	6.91	4.88
	Submerged Turret Loading	7.44	6.64	4.43
Loading operability rate for the season	Loading from a platform corner	74.4 %	74.5 %	67.5 %
	Loading from a narrow cylindrical terminal	81.2 %	70.1 %	66.1 %
	Submerged Turret Loading	> 73.7 %	> 63.9 %	> 60.7 %

Sudden changes in the drift direction happen often during the season (75 days of recording) as shown in Table 3. Structure – ship collision risks are higher each time one of these events happens. This favours the use of a subsea concept.

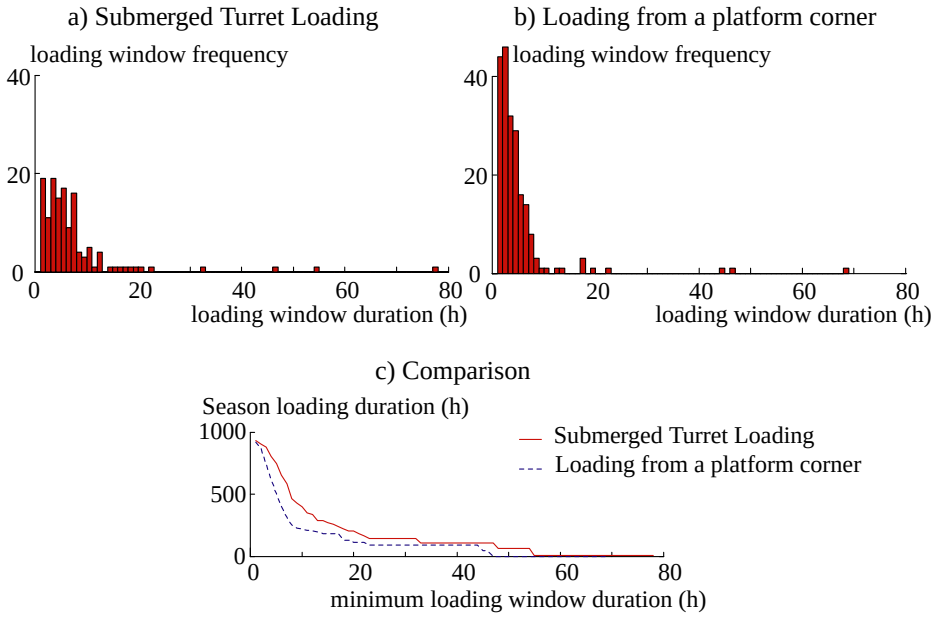

Fig. 3. Loading windows from buoy 06640; a) Loading window frequency for Submerged Turret Loading; b) Loading window frequency for loading from a platform corner; c) Season (75 days) total loading duration for a minimum loading window duration

Fig. 3 gives examples of results from analysis of the positions of buoy 06640. Loading from a platform corner present many short loading windows whereas STL loading present more longer loading windows. The use of STL would then favour using larger

tankers. If loading windows should have a minimum duration, the STL system will rapidly present a higher operability rate (Fig. 3c).

CONCLUSION

Though many concepts for arctic offshore loading have been presented, very few have practically been used. In seas presenting heavy ice conditions as the Pechora Sea, the ice drift patterns will influence the loading operability rate. The operability of three loading concepts is compared when analysing ice drift in the Pechora Sea recorded by ARGOS-GPS buoys in the spring 1998. It was seen that:

- Loading from a narrow cylindrical terminal seems to present the highest operability rate. Nevertheless, the frequency of sudden drastic change of drift direction is high and so is the collision risk between the tanker and the terminal.
- Loading from a platform corner presents the same risks and the average loading window is rather short.
- The found operability rate for the Submerged Turret Loading system is a minimum value; it will be larger when ice conditions are lighter.
- The results depend on the chosen loading window characteristics, these criteria will vary for different configurations of a same concept and with variable ice conditions along the winter.

ACKNOWLEDGEMENT

The financial support of Teekay Norway AS and the Research Council of Norway is gratefully acknowledged.

REFERENCES

Bonnemaire, B., S. Løset, , and O.T. Gudmestad (2003): Riser Armours for Subsea Offshore Loading of Hydrocarbons in Ice-Infested Waters. *Proceedings of the Russian Arctic Offshore Conference, RAO-03,* St. Petersburg, Russia, 2003.

Bonnemaire, B. (2004): Response of an Armoured Riser for Arctic Offshore Loading. *Proceedings of the International Society of Offshore and Polar Engineers (ISOPE) conference,* Toulon, 2004.

DeFranco, S., D. Blanchet, and R. Pritchard (2001): Pechora Sea Ice Motions. *Proceedings of the 16th International Conference on Port and Ocean Engineering under Arctic Conditions,* Ottawa, 2001.

Di Tella,V. (1996): Single Point Mooring and Off-loading System for Arctic Waters. *Proceedings of the Polartech'96 Conference,* St Petersburg 1996.

Di Tella, V. and K. Juurmaa (1997): A Single Mooring System for Tankers in Ice Infested Waters. *Third International Conference on Development of Russian Arctic Offshore (RAO),* St Petersburg, Russia, 1997, Volume II, pp. 257-274.

Gudmestad, O.T., A.B. Zolotukin, A.I. Ermakov, R.A. Jakobsen, I.T. Michtchenko, V.S. Vovk, S. Løset and K.N. Shkhinek, (1999): Basics of offshore petroleum engineering and development of marine facilities with emphasis on the Arctic Offshore. Stavanger, Moscow, St. Petersburg, Trondheim 1999, 344 p.

Jolles, W., R. Browne, and A. Keinonen (1997): Model development of vessel approach & mooring operations at arctic loading terminals. *Proceedings of the International Conference on Offshore Mechanics and Arctic Engineering,* Yokohama, 1997.

Løset, S., K. N. Shkhinek, O. T. Gudmestad, P. Strass, E. B. Michalenko, R. Frederking and T. Kärnä (1997): Comparison of Environmental Conditions of Some Arctic Seas. *Journal of Navigation and Hydrography,* Vol. 4, 1997, pp. 29-38 (English), pp. 39-49 (Russian).

Løset, S. and D.K. Onshuus (1999): Analysis of Speeds of Drift Ice in the Pechora Sea. *Proceedings of the Russian Arctic Offshore Conference,* St. Petersburg, 1999.

Løset,S. and J.K. Økland (2000): Ice Drift Speeds in the Pechora Sea. *15th International Symposium on Ice,* Gdansk, 2000.

Malyutin, A. A., A. R. Grintovt, E. E. Toropov and V. A. Chernestov (2003): Offshore Platforms for Oil and Gas Production on the Russian Arctic Shelf. *Proceedings of the 17th International Conference on Port and Ocean Engineering under Arctic Conditions (POAC),* Trondheim, June 2003, Volume I, pp. 13-22.

Masterson, D.M., 2001. Sheet pile design for offshore gravel islands. *The 16th Int. Conference on Port and Ocean Eng. under Arctic Conditions (POAC),* Ottawa, Canada 2001, pp 109-121.

Prinsenberg, S.J., G.A. Fowler and A. van der Baaren (1998): Pack Ice Convergence Measurements by GPS-ARGOS Ice Beacons. *Journal of Cold Regions Science and Technology*, vol. 28 pp.59-72, 1998.

Spencer,D., S.J. Jones and W. Jolles (1997): Effect of ice drift angle on a mooring hawser. *Proceedings of the International Conference on Offshore Mechanics and Arctic Engineering – OMAE,* Yokohama, 1997.

Voinov, G.N., N.Ye. Dmitriyev and G.K. Zubakin (1999): A Method of ARGOS Buoy Data Processing and Ice Drift Assessment in the Pechora Sea. *Proceedings of the 15th International Conference on Port and Ocean Engineering under Arctic Conditions,* Helsinski, 1999.

17th International Symposium on Ice
Saint Petersburg, Russia, 21 - 25 June 2004
International Association of Hydraulic Engineering and Research

PROBLEMS OF MATHEMATICAL MODELLING OF DYNAMICS OF SUB-ICE FLUXES

Elena Debolskaya, Vladimir Debolsky[1]

ABSTRACT

The problems of mathematical modelling of pollutant propagation in tidal ice-covered estuary and ice jams formation in river beds are presented. In the pollutant propagation model two plan directions are taken into account along and across of the flow with assumption of full mixing of the pollutant over the depth. The empirical relations for longitudinal and cross-sectional momentum transfer coefficients are used. The comparison of the calculation result with data of observations shows that the model is in satisfactory accordance with natural process. In the jam formation models water flows are described by one-dimensional Saint-Venan equations for narrow river beds and by two-dimensional equations for wide rivers with complex morphology. The ice destruction criteria were obtained and used at numerical calculating. The place and moment of ice cover destruction, speed of water level elevation caused by jam action and speed of jam propagation upstream may be calculated numerically used the model.

INTRODUCTION

Ice effects have strong impact on many spheres of human life. Besides a passive influence like impeding of navigation and exploitation of hydroengineering installations, decreasing of carrying capability of channels, changing of impurity transfer conditions and drift transport, they can turn to such disastrous forms like ice bulks during ice drift, ice jams, leading to catastrophical floods. Heavy liquidation cost of disastrous consequences as well as changing of operative conditions of hydraulic work is required almost every year.

There are lots of researches dedicated to tasks of forecast of ice breaks and ice jam levels. It is necessary to mention that in almost all methods of quantitative estimation of jam characteristics (power of the jam, magnitude and intensity of water level upsurge,

[1] Water Problem Institute of the RAS, Moscow

conditions of stable and critical state of the jam) analysis of inner processes was made via averaged characteristics of the system, including cross-section-averaged speed of flow and its depth directly before upper edge of the jam. Usually, certain dependences with many unjustified, empirical, hard to define parameters were acquired as a result of such researches. Significant disadvantage of many other works was their narrow, regional character. Dependences for defined parameters of flows and jam characteristics in these works most often can be assigned only to a certain water object. Mathematical modelling with its use of principal regularities of studied processes will allow to avoid many of these flaws and receive adequate overall evaluations for a wide class of water bodies. Main goal of the work is a construction of system of numerical models for calculation and forecast of ice jam formations, dynamics of jam-caused changes of level and discharge, mass exchange and impurity transfer mode. Vindications for one- and two-dimensional models of jam forming are given depending on geometric dimensions of riverbed and ice field. Use of mathematical modelling in study of dynamics of sub-ice fluxes brings forth series of strict requirements to problem definition and ability of legible determining of temporal and spatial scales of processes. These requirements are needed most of all for optimal choice of model dimensionality and applied equations. Only tasks with accounted additional resistance (it is a major difference between sub-ice and open fluxes) can be solved in the context of hydraulic or one-dimensional approximation. Variations of such integral characteristics like water discharges or section-averaged velocities and depths of fluxes can be acquired on solving of these tasks. Nevertheless, exactly this class of tasks allows to forecast dynamics of ice cover (its deformations and possible destructions), since spatial and temporal scales of mechanical changes of ice correspond to changing scales of integral characteristics of the flux. Within the bounds of one-dimensional approximation can be also solved tasks of ice jams origin. Solution of tasks that allow to trace change of sub-ice current character in horizontal plane can be rated as a next stage after hydraulic (one-dimensional) approximation. Event study with this approach can be directed to solution of tasks of the forecast of the jams and floods on wide rivers, curved reaches of channel and cross-sections of irregular shape, when account must be taken for dynamics of fluxes in scheme and use of two-dimensional equations is necessary.

THE MODEL OF POLLUTANT PROPAGATION UNDER ICE COVER IN THE TIDAL ESTUARY

The investigation of pollutant propagation in rivers of north regions acquires particular meaning in connection with accident discharge of sewage and accident in pipelines. The estimate of ecological consequences from these accidents is a serious problem. It is difficult to solve this problem without working out the corresponding mathematical models of pollutant spot propagation in the flow. The particularities of river flow in north regions make suppose that such models must take into account not only really morphology of river bed but two-dimensional character of pollutant propagation and existence of tidal wave and ice cover during long time of the year. The model of

pollutant propagation in tidal ice covered estuary was worked out in order to forecast the consequences of the accident discharge of sewage. The model based on enough strong hydrodynamics thesis permits us to obtain pollutant distribution at any studied reach of the river. The base equation of the model is the transfer equation with assumption of full mixing of the pollutant over the depth:

$$\frac{\partial c}{\partial t} + u\frac{\partial c}{\partial x} + v\frac{\partial c}{\partial y} = \gamma_1 \frac{\partial}{\partial x}(|u|h\frac{\partial c}{\partial x}) + \gamma_2 \frac{\partial}{\partial y}(|u|h\frac{\partial c}{\partial y}), \quad (1)$$

where c is pollutant concentration; t is time; u,v are averaged longitudinal and cross-sectional components of flow velocity; $|u|$ is module of averaged longitudinal velocity; h is flow depth; $\gamma_1 = 0.06$, $\gamma_2 = 0.024$ are empirical constants from relations for the longitudinal and cross-sectional momentum transfer coefficients: $D_x = \gamma_1|u|h$ and $D_y = \gamma_2|u|h$ respectively obtained by Dolgopolova and Orlov (1987). The values of the depth averaged longitudinal and cross-sectional components of flow velocity were calculated from the momentum equation for vertical axis z for gradiently-viscous regime of the flow, because as the preliminary investigations by Debolsky (1984) have shown this regime is characteristic for this region, when gradient of pressure and turbulent viscosity are balanced. After some transformation and estimation of members' values of the equation (1) with consideration of really significance of flow parameters we can write the equation (1) with enough accuracy in following form:

$$\frac{\partial c}{\partial t} + u\frac{\partial c}{\partial x} + (v - \frac{3}{2}\gamma_2 \frac{\partial h}{\partial x}|u|)\frac{\partial c}{\partial y} = \gamma_1|u|h\frac{\partial^2 c}{\partial x^2} + \gamma_2|u|h\frac{\partial^2 c}{\partial y^2}. \quad (2)$$

It may be shown that consideration of the different of the resistance on bottom and ice surfaces (i.e. non equality of flow parts sizes divided by the surface of zero shear stresses) for concrete task, when time of vertical turbulent mixing is considerably lesser than time of longitudinal mixing, not strongly defines more precisely but strongly makes difficulty the calculations. The equation (2) was solved numerically by splitting method on x and y. The boundary conditions of the second kind at left and right boundaries and at banks were assigned exempt point of output of pollutant where boundary condition of the first kind was assigned.

At first the cross-sectional averaged longitudinal velocity was calculated for conditions of the natural situation (river flow and tidal wave). Then we obtained the values of velocity depending on suite of calculated point in each cross-section and the time taking into consideration the depth changes over flow width. The following depends were used:

$$dh = \zeta = \zeta_0 e^{-kx}\sin(\omega t - kx), \quad (3)$$

$$\zeta_x = \frac{\partial \zeta}{\partial x} = -\sqrt{2}k\zeta_0 e^{-kx}\sin(\omega t - kx + \pi/4), \quad (4)$$

$$h = h_0 + dh,$$

where ζ_0 is amplitude of tidal wave in suite of river flowing in the sea, $k = 2\pi/L$ is wave number, L is length, $\omega = 2\pi/L$ is frequency and T is period of tidal wave, obtained from the measurements of flow velocity and directions. The values of the slope i and wave length L were obtained from the calculations with employment of formula (3) and famous significance of tidal wave characteristics in point of river flowing into the sea and in control station.

RESULT OF POLLUTANT PROPAGATION MODELING EXPERIMENT

The results of hydrodynamics calculations are demonstrated on figure 1, where change of surface level deviation and flow velocity module are shown in observe station. The results of the calculations show that the model sufficiently sensitive to the changes of parameter of the discharge of sewage, the duration and original pollutant concentration in output point (fig.2a) and in point situated at 15 km down stream at opposite bank (fig.4b), when the sewage was produced in 'steep' regime, i.e. during 8 hours with intervals during 16 hours for two values of pollutant concentration in sewage water $5\,g/m^3$ and 20. g/m^3.

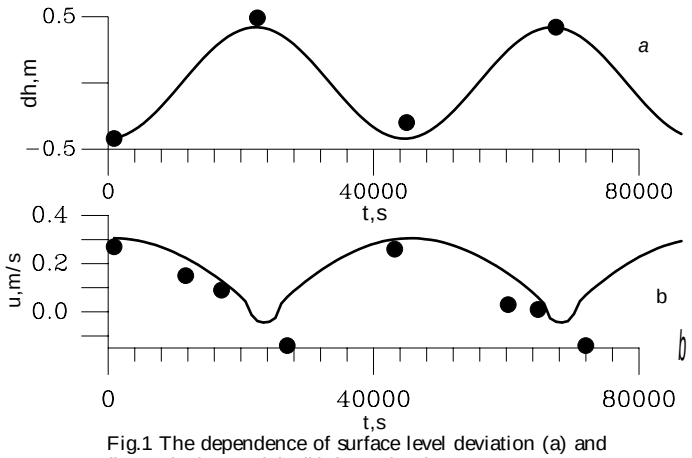

Fig.1 The dependence of surface level deviation (a) and flow velocity module (b) from the time
solid line - result of the calculation, dots - data of measurement

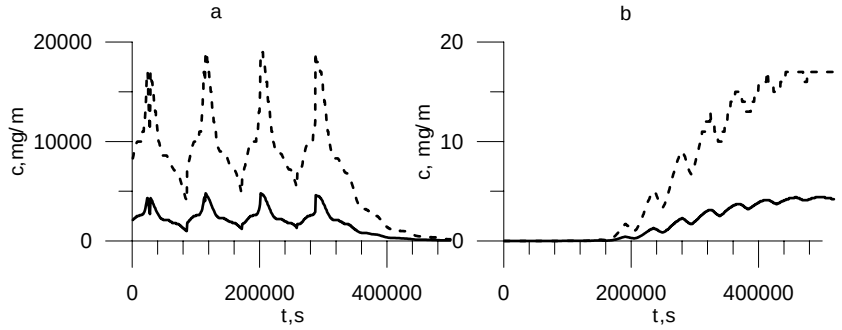

Fig.2 The dependence of the pollutant concentracion from the time
in output point (a) and in point at 15 km downstream at an oppoite bank (b)
solid line - pollutant concentration in sewage water 5 g/m
dush line - pollutant concentration in sewage water 20 g/m

THE 1-D ICE JAM MODEL

Model of interaction of long-wave disturbances with ice cover and criteria of destruction were used in development of one-dimensional model of ice jam. One-dimensional model can be used for rather narrow rivers. It allows to track the process from condition of undamaged ice field till appearance of bulks of broken ice, formed by incoming flood or drawdown wave, calculate change of water level and discharge in time and along the riverbed. Verification of destruction criteria allows determining location and time of ice cover destruction and size of broken away block of ice.

Following model of interaction of system of individual ice-floes with edge of a solid ice cover is proposed.

Let us suppose that solid, unbroken ice cover has a significant thickness, i.e. it can be considered as rigid. Stream with a mass of broken ice reaches the edge of such an ice field. This case is most interesting from a jam-forecasting point of view. In a proposed model we assume that width of ice blocks that reach the edge or summary width are closely approximated to the width of channel. One-dimensional system of Saint Venan equations is used to calculate characteristics of the flux, extending along the ice-free section of the channel. Method of definition of right boundary conditions where floating ice meets with the ice cover depends on a distance from lower edge of floating ice block to the edge of the ice cover, since possibility of ice block carry-over on a surface of the ice field is bound to this factor. Boundary condition is set in a place of meeting of solid ice cover with a flux that transports the broken ice. Assumption about complete ceasing of water level rising in the area occupied by approaching from above ice block is suggested. This suggestion may be justified by increased resistance to the flux on a lower surface of the ice block, friction of side edges and fluctuation energy consumptions. Right boundary condition for interaction of system of separate ice blocks with the ice cover is set using assumption that a separate ice block was a part of the solid ice field before break-up and has the same thickness. Rise of water level under the ice block directly contacting the edge of the ice cover occurs until coordinate of the lower edge of the ice block is not equal to a coordinate of upper surface of the ice field. Further it is supposed that part of the ice block which got atop the solid ice field is insignificant comparing with the size of the whole block. Further rise of water level will happen from a place where next ice block contacts with the first, i.e. right boundary point will move higher from a place of previous contact for a length of the first ice block. The process will go on in a similar manner, i.e. increasing of the water level will be represented with a piecewise continuous (stepwise) function. Such simplified schematization can be used for ice blocks of considerable sizes and for fluxes with small stream velocities, when part of the ice block carried out over a previous one is significantly lower than size of the entire ice block. Given one-dimensional schematization is regarded as hummocking jam type and can be used for forecasting on narrow rivers with straight riverbed and cross-section form close to rectangular.

RESULT OF 1-D MODELING EXPERIMENT

Series of numerical experiments were carried out on specific natural objects to demonstrate possibility of such schematization. Calculations were made for the Svir River. There were next initial values: width of riverbed on a level of ice freezing B = 300 m (in-situ measurements on Svir river), starting flow of preset disturbing hydrograph Q_0=1300 m^3/s and corresponding water level of the established flux z_n=4 m. Slope of Svir river on studied section $i_0 = 4 \cdot 10^{-5}$ was calculated using piezometric slope and known depths of the flux. Calculations were done for ice cover width $h_л$ = 0.5 m, 1 m, 2 m. Discharge rate on the left boundary (of disturbance) Q_p=6000; 9000 m^3/s. Lengths of ice-holes L_h=0; 500 m. Length of the entire section L=2.5 km; 25 km. Numerical experiment has shown that after 700 seconds from beginning of external disturbance right boundary of jamming moved on 50 m when ice thickness was 1 m, length of design section was 2,5 km and water discharge on left boundary was 6000 m^3/s. When ice thickness was 0.5 m, right boundary moved on 750 m.

THE 2-D ICE JAM MODEL

To forecast jams and floods on wide rivers, curved parts of riverbeds and on cross-sections of irregular shape it is necessary to take account of routine dynamics and use two-dimensional Saint Venan equations and equation of continuity, acquired after integration of motion equations by flux depth in the presence of ice and in the absence of wind:

$$\frac{\partial u}{\partial t} + u\frac{\partial u}{\partial x} + v\frac{\partial u}{\partial y} = -g\frac{\partial H}{\partial x} + \frac{\partial}{\partial x}\left(A_x\frac{\partial u}{\partial x}\right) + \frac{\partial}{\partial y}\left(A_y\frac{\partial u}{\partial y}\right) + \left(\frac{\tau_{ix} - \tau_{bx}}{\rho h}\right), \quad (5)$$

$$\frac{\partial v}{\partial t} + u\frac{\partial v}{\partial x} + v\frac{\partial v}{\partial y} = -g\frac{\partial H}{\partial y} + \frac{\partial}{\partial x}\left(A_x\frac{\partial v}{\partial x}\right) + \frac{\partial}{\partial y}\left(A_y\frac{\partial v}{\partial y}\right) + \left(\frac{\tau_{iy} - \tau_{by}}{\rho h}\right), \quad (6)$$

$$\frac{\partial H}{\partial t} + \frac{\partial Hu}{\partial x} + \frac{\partial Hv}{\partial y} = 0, \quad (7)$$

where x, y – rectangular coordinates; coordinate system is set in such a way that positive x axis is directed fluxward, while $0y$ axis is directed across; u, v – depth-averaged longitudinal and lateral water velocity components; g – acceleration of gravity; $H=h+h_0$ – level or mark of water surface; h_0 – bottom mark; h – depth of the flux; $\tau_{bx,ix}$ and $\tau_{by,iy}$ – components of tangential stress at the bottom and ice surface correspondingly; A_x and A_y – longitudinal and lateral coefficients of turbulent viscosity. To determine the coefficients of turbulent viscosity empirical correlation $A_x = \gamma_x hu$, $A_y = \gamma_y hv$ can be used, $\gamma_{x,y}$ – empirical constants. The relation between tangential stress at the solid surfaces $\tau_{bx,ix}$, $\tau_{by,iy}$ and other flow parameters is accepted using the dependences $\tau_{bi} - \tau_{ii} = \frac{\rho\lambda U_i|\vec{U}|}{2}$, $\lambda = \frac{2g}{C^2} \approx \frac{2gn^2}{h^{1/3}}$ – scalar coefficient of the hydraulic friction; C – Chesy coefficient, n – winter generalized coefficient of the

group roughness in the Manning formula, $\overset{\omega}{U}$ – velocity vector in the current plane, $U_1 = u,\ U_2 = v$.

The assignments of the different roughness coefficients in the riverbed and in the flood-lands, as well as the changing of the flood-lands cross slope in comparison with values of the bank slopes are provided in the model. The numerical experiments showed that these values were very largely affected the release wave propagation and jam formation.

The destruction criteria were assigned in the following way: if the inequality $\left|\frac{\partial^2 \xi}{\partial x^2}\right|_{\max} \geq \frac{2\sigma_{\text{пр}}}{Eh}$ holds true, the cross destruction is realized, if the inequality $\left|\xi_{y,\max}\right| \geq \frac{\sigma_{\text{пр}} B^2}{4Eh}$ holds true, the alongshore destruction is realized.

The condition of the block of ice diving under non-desolate ice cover is assigned in the following way:

$$U_{\text{crit}} = \sqrt{2gh_i \frac{\rho_w - \rho_i}{\rho_w}\left(1 - \frac{h_i}{h}\right)}, \qquad (8)$$

where h_i – ice thickness, ρ_i – ice density, ρ_w – water density.

If the destruction criteria and the block of ice diving condition are realized in the cell of the numerical area, the depth decreases by value of ice block thickness. If the depth becomes equal zero, the width will decrease by sell dimension, and the velocities will equal zero. Thus, the jam formation beginning condition is executed. Stationary solution of system of equation (5) – (7) is used as initial condition. Then a disturbance in a form of additional discharge is set on the left boundary. In a process of the solution of this nonstationary task the following parameters were checked: the criteria of destruction of the ice surface and beginning of ice block diving under undestroyed ice field; the degree of ice damming and forced by it rise of water level and change of velocity mode. In that way the modeling of diving jams was implemented. Such jams are typical for wide rivers taking into consideration river bends and changing of shape of cross-section along the riverbed. Width of riverbed remains unset and may vary according to the flood waves or increasing of water level due to ice jam, thus imitating process of overflow.

RESULT OF 2-D MODELING EXPERIMENT

As result of the modeling we can obtain the array of depth, longitudinal and cross-sectional velocities components, width of the flow, the coordinates and time of ice cover destruction, ice block diving and jam formation.

The fig. 3 demonstrates the momentary modeling realization of the flow plane. The wave propagates from left boundary. The velocities vectors are denoted by the arrows.

This figure is conformed to the scenario with following parameters: the length of the calculated river part is L=15 km; number of river stations n=15; initial maximal depth of the flow is h_0=3m; ice thickness h_l=1m; the width of the river bed:

$B = B_0 - (B_0 - B_1)\sin\left(\frac{\pi x}{L}\right)$, where B_0=200 m, B_1=100m; initial surge height h_{dop}=15 m.

a

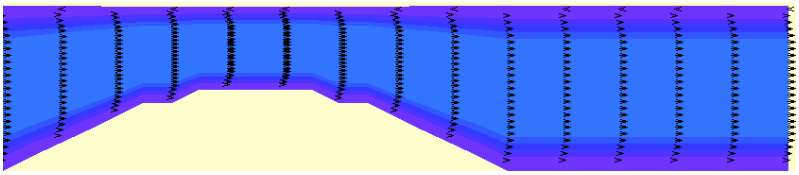

b

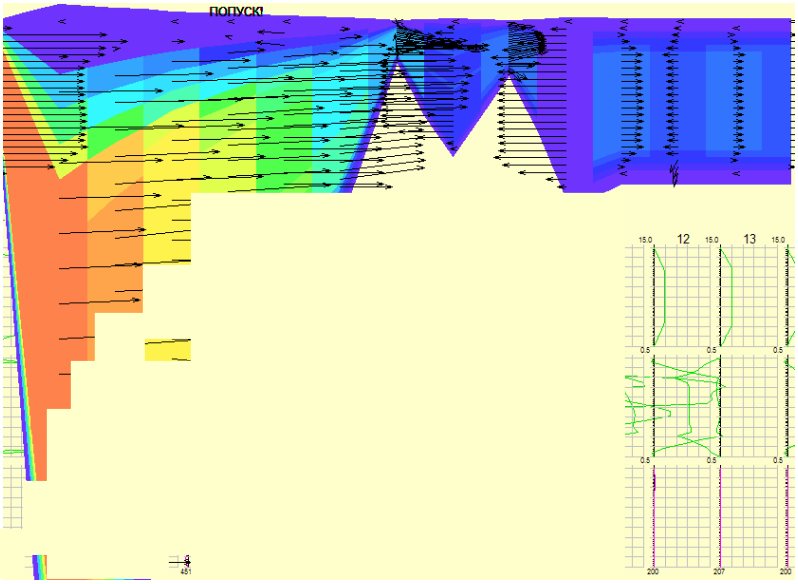

c

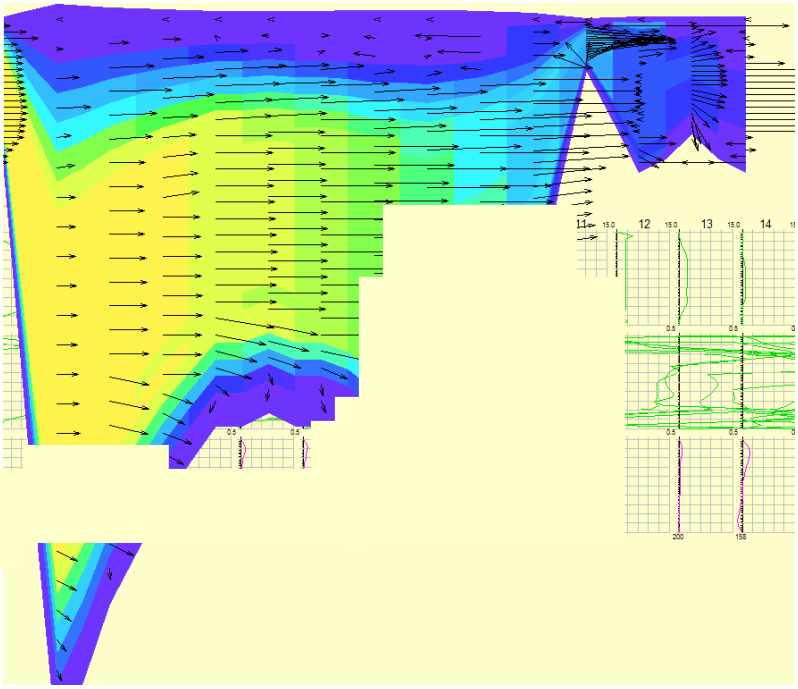

Fig.3. The momentary modeling realization of the flow plane

Figure 3a corresponds to an initial stationary regime. Figure 3b shows the situation of jam formation in the river stations N 8 and 10. These jams are found broken during posterior time under wave forcing, and the new jam forms in the river station N 11 (fig. 3c) after wave forcing finishes. The flood of the flood-lands was continued only under jam forcing, because the release wave forcing was stopped. After this moment the jam level growth velocity and flood region growth velocity could be estimated.

The figure 4 shows the change of flow width (a) and depth (b) along the riverbed in one hour after the beginning of release wave occurring. The dash lines show the change of flow width along the riverbed before beginning of the release wave occurring at stationary regime.

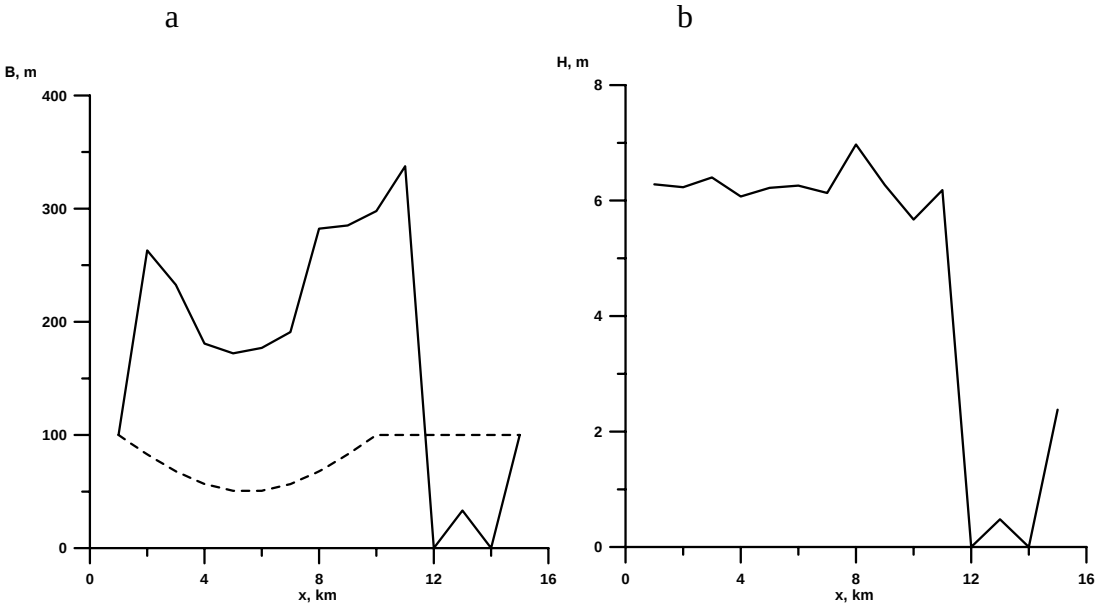

Fig.4. The change of flow width (a) and depth (b) along the riverbed in one hour after the beginning of release wave occurring

In this scenario the following parameters are used: the bottom slope is $i = 10^{-5}$, roughness coefficient in Manning formula in the river bed is 0.03 $s/m^{1/3}$, and in the flood-lands 0.07 $s/m^{1/3}$ the parameter of bank slope changes from 0.125 to 0.5 and cross-section slope changes from 0.0375 to 0.15.

RESUME

The results of the calculations by pollutant propagation model show that:

- model sufficiently sensitive to the changes of parameters of the discharge of sewage, the duration and original pollutant concentration in output point;
- the observation and numerical experiments demonstrate that the existence of ice cover during small discharges of water is the reason for more intensive mixing and rise of the pollutant stream in the transverse direction;

- pollutant stream width depend considerably on transverse gradients of the bed and flow lines curvatures due to the streamlines of banks and islands.

Thus we can suggest for cast estimation of water quality and ecological damage from accident discharge of sewage knowing the hydrodynamics characteristics and regime of water discharge and pollutant concentration.

The analysis of the numerical experiments by the 1-D and 2-D ice jam formation models allows to do some resume:

- the jam formation is depended on wave forcing power too much;
- the impact main factors on jam formation are height of wave, river bed curvature, the cross section slope. The ice thickness appeared to influence in a lesser extent.

ACKNOWLEDGEMENTS

This work has been conducted with financial support of the Russian Foundation for Basic Research grants 03-05-64327 and 03-05-64237.

REFERENCES

Debolsky, V.K., Zyryanov V.N. and Mordasov M.A. Turbulent exchange in tidel mouth under ice cover. *Dynamics and thermic regime of rivers and reservoirs*, Moscow, Nauka, (1984), 279-290.

Dolgopolova, E.N. and Orlov, A.S. River streams. Structure, propagation of impurities, transport of contact load. *Problem of research and employment of water resources*, Moscow, Nauka, (1987), 250-266.